Column Profile Maps:

A Tool for the Design and Analysis of Complex Distillation Systems

By

Simon Thornhill Holland

A thesis submitted for the degree of Doctor of Philosophy

To

The Department of Chemical and Metallurgical Engineering,

Faculty of Engineering, University of the Witwatersrand,

Johannesburg

Abstract

Techniques for the design and analysis of simple column separations are well established. Shortcut design techniques have been employed in the initial design of these "traditional" distillation systems for a number of years and these columns are well understood. However, few currently available techniques are useful in the design of novel or complex configurations. The techniques that are available tend to be configuration specific. An all inclusive or universal, design and analysis tool, that can be applied to any and all configurations, is required.

Tapp et al (2004) introduced Column Profile Maps (CPMS) as a means of addressing this issue. These are maps of composition profiles for column sections with defined net-molar-flow and reflux ratio. It is suggested that by producing CPMs for a configuration a designer can essentially superimpose these, determine feasible operating profiles and hence column operating parameters.

In this thesis we show that this technique can be used to, not only produce quick and easy complex column designs but gain a comprehensive understanding of the steady-state operation of these arrangements. We demonstrate this analytical potential first by application of the CPM technique to the two-product feed distribution problem. It is shown that feed distribution can lower the minimum required reflux ratio for non-sharp separations and in some cases produce feasible separations from previously infeasible product specifications. A composition region of operation for all distributed feed policies is also found.

The potential for detailed analysis, design and optimisation of complex configurations is demonstrated via application of the CPM procedure to the fully thermally coupled (Petlyuk) distillation column at both sharp and non-sharp split

conditions. A detailed design methodology for any configuration results from this. It is found that the Petlyuk column can operate under five possible bulk/net flow conditions and that very interesting and counter-intuitive net-molar-flows are possible. A feasible column parameter region equivalent to the optimality region (Halvorsen and Skogestad, 2001) is found for zeotropic systems. Importantly a minimum reflux condition for the Petlyuk column is found. This condition can be applied to all zeotropic systems for all product specifications. It is also demonstrated that the CPM technique can be used for design optimisation of separation systems.

Declaration

I declare that except where acknowledged, this thesis is my own un-aided work. It is being submitted for the degree of Doctor of Philosophy in the University of the Witwatersrand, Johannesburg. It has not been submitted before for any degree or examination in any other University.

18 July 2005

Acknowledgements

This thesis represents the culmination of almost five years of work. Throughout this period I have been fortunate enough to be exposed to a range of people who have offered me guidance, support and inspiration

First and foremost I would like to thank my supervisors Professor Diane Hildebrandt and Professor David Glasser who gave me the opportunity to begin this work at a time when I was lacking direction. Professor Hildebrandt's seemingly boundless imagination (with her "wacky" ideas) and Professor Glasser's vast knowledge and "feelings" about new ideas (which invariably proved correct) have been a constant source or inspiration. It has been a privilege working with two such talented researchers and I sincerely hope this thesis justifies the faith they showed in me.

I am also extremely grateful to Professor Steiner Hauan (Carnegie Mellon University) whose guidance and insight proved invaluable in the analysis of the Petlyuk column.

My friend and colleague Michaela Vrey (formerly Michaela Tapp) has been my single biggest influence on the content of this work. She and I have developed the Column Profile Map work together and regard it almost as parents regard a child; watching with concern as the work has grown since our input has diminished. The substance of this thesis is the product of hours of debate and at times outright argument. May our debates never become mundane.

A special thank you must go to Elitsa Mitova who during this period has served as friend, colleague and mathematical advisor. Her calming influence during heated debates is also much appreciated.

To T, thank you. Your friendship and support has meant the world to me.

Most importantly I wish to thank my family. Their love and unwavering belief in me at times when I have not believed in myself has meant more to me than they will ever know. Without their support this work would not have been possible. In addition to the love and support mentioned above my mothers nagging for me to finish can also not be underestimated.

Table of Contents

List of Figures

Chapter 2:

Chapter 3:

Chapter 4:

Chapter 5:

Chapter 6:

Chapter 7:

Chapter 8:

List of Tables

Nomenclature:

x_1 [-].....................................*Light component composition*

x_2 [-].....................................*Heavy component composition*

x_3 [-].....................................*Intermediate component composition*

i [-].....................................*Component index*

x_i [-].....................................*Composition of component i*

X [-] ....*Liquid composition vector*

$Y^*(X)$ [-].....................................*Equilibrium vapour composition vector*

$X^*(Y)$ [-].....................................*Equilibrium liquid composition vector*

Y [-].....................................*Vapour composition vector*

k [-].....................................*Column Section Index*

V_k [mol/s].............................*Vapour flow rate in column section k*

L_k [mol/s].............................*Liquid flow rate in column section k*

Δ_k [mol/s].............................*$(V_k - L_k)$ Net Flow in column section k*

$R_{\Delta k}$ [-].....................................*Reflux ratio(L_k/Δ_k) in column section k*

N [-].....................................*Stages*

Y^T [-].....................................*Top vapour composition vector*

X^T [-].....................................*Top liquid composition vector*

Y^B [-].....................................*Bottom vapour composition vector*

X^B [-].....................................*Bottom liquid composition vector*

X_F [-].....................................*Feed composition vector*

F [mol/s].............................*Feed flow rate*

X_S [mol/s].............................*Side-draw composition vector*

S [mol/s].............................*Side-draw flow rate*

D [mol/s].............................*Distillate flow rate = Δ_1*

B [mol/s].............................*Bottoms flow rate = Δ_6*

$X_{\Delta k}$ [-].....................................*Difference point = $(VY^T - LX^T)/(V-L)$ for column section k*

$X_{\Delta k-i}$ [-].................................... *Element i of difference point vector for*

....*column section k*

X_{Pk} [-].................................... *Composition vector of fixed point*

....*(Pinch Point)for column section k*

X_{Pk-i} [-].................................... *Element i of fixed point composition*

....*vector for column section k*

Y_{Pk} [-].................................... *Vapour composition vector of fixed*

....*point (pinch point) for column section k*

Y_{Pk-i} [-].................................... *Element i of vapour fixed point*

....*composition vector for column section k*

Φ_L [-].................................... *Liquid Split ratio(L_2/L_1)*

Φ_V [-].................................... *Vapour Split ratio(V_2/L_1)*

$\Phi_L{}'$ [-].................................... *Bottom Liquid Split ratio(L_4/L_6)*

$\Phi_V{}'$ [-].................................... *Bottom Vapour Split ratio(V_4/L_6)*

δ [-].................................... *Difference vector*

β_L [-].................................... *Coupled section liquid flowrate ratio*

....*(product side / feed side)*

β_V [-].................................... *Coupled section vapour flowrate ratio*

....*(product side / feed side)*

P_{tot} [bar].................................*Total vapour pressure*

$P_{Vap\,i}$ [bar].................................*Vapour pressure of component i*

α_i [-].................................... *Volatility of component i relative to micture*

....*heavy component*

T   [K].................................... *Temperature*

V [-].................................... *Eigenvector*

λ [-].................................... *Eigenvalue*

m [-].................................... *Stage count index (up CS)*

h [-].................................... *Differential stage count up CS*

n [-].................................... *Differential stage count down CS*

s [-].................................... *Separation vector (X-Y(X))*

s_i [-].................................... *Component i of the separation vector*

Chapter 1:

Introduction

Distillation is one of the most utilised large scale industrial methods of mixture separation. It is a very energy intensive process and accounts for a significant percentage of plant utility costs. A survey (Ognisty, 1995) conducted in the mid 1990's estimates that energy inputs to distillation columns in the United States accounts for approximately 3% of the countries entire energy consumption. It is clear that the efficiency of the separation can have a substantial influence on the profitability of a process and methods of improving the energy efficiency of distillation systems are, therefore, constantly sought.

Recently, much interest has been shown in complex distillation configurations for their potential to reduce the energy requirements of separations. The term complex is often used in connection with configurations that involve some degree of thermal coupling. These configurations include side-rectifiers, side-strippers, dividing wall columns, Petlyuk columns and Kaibel columns (Kaibel, 1987).

Despite the significant advantages that complex configurations offer, simple (one feed two product) distillation columns are overwhelmingly more utilised. One factor contributing to the under-utilisation of the complex arrangements is, possibly, a lack of understanding of these columns. Simple columns, by comparison, are extremely well understood. The graphical separation synthesis methodologies, in particular, have been very successful in providing insight into simple column operation. Extensive work on residue curve and distillation line maps (Schreinemakers (1902), Ostwald (1902), Doherty and Perkins (1978a), Hausen (1952) and Rishe (1955), Zharov (1967; 1968c), Stichlmair (1989), Widago and Seider (1996), Serafimov (1968a; 1968d)) as well as operation leaves (Wahnschafft et al. (1992); Castillo et al. (1998)) has led to a comprehensive understanding of these columns and the feasibility of simple separations. Synthesis methodologies for complex arrangements, on the other hand, can not be

generalised for all configurations and graphical methodologies, which comprehensively cover simple separation synthesis, have not been extended adequately to include all complex configurations.

The advent of powerful chemical engineering design packages such as ASPEN Plus^{TM} and Pro 2^{TM} despite their unquestioned modelling capabilities have not aided in the general understanding of complex configurations, much, either. Separation synthesis too often reverts to a trial and error procedure using these tools. For some configurations, such as the Petlyuk column, advance knowledge of the solution is required for simulation initialisation. This cannot possibly be done effectively without understanding the nature of the column dynamics and solution.

An all inclusive, graphical, design and analytical tool is required for application to the complex configuration problem. This tool should extend the existing graphical, simple distillation, design and analysis methodologies. The graphical nature of such a tool would allow insight into the operation of any distillation structure and remove the necessity for trial and error design procedures.

This thesis will illustrate the use of Column Profile Maps (CPMs) as a comprehensive analytical and synthesis tool for all distillation column configurations. We will initially present the derivation of and theory relating to, CPMs. This work was introduced by Tapp et al (2004) and Holland et al (2004a). We will then illustrate the potential of CPMs for column analysis by investigating the pros and cons of distributed feed addition. Finally, a detailed design methodology will be produced, through an investigation into the operation of the Petlyuk/thermally-coupled column. Through this investigation a thorough understanding of the operation of these columns will be gleaned.

An outline of the material covered in each chapter is discussed in the overview below.

Thesis overview:

Most of the chapters of this thesis have either been published as journal articles or prepared as papers for future publication. Because CPMs are not a well established distillation tool yet, there is a degree of repetition in the introductions to each chapter. This repetition specifically covers the derivation of column profile maps, but should serve to strengthen the readers understanding.

Chapter 2 covers the detailed derivation of column profile maps (CPMs). This work was done together with Michaela Tapp and was published as the first part of a CPM series, in *Industrial and Engineering Chemistry Research* (see Tapp et al, 2004). I was involved in the preliminary fundamentals, but she is responsible for all the pinch point loci analyses and classifications which constitute the major portion of the work.

Chapter 3 deals with the underlying mathematics and topology of both ideal and non-ideal CPMs. The use of singular point eigenvectors and eigenvalues for further understanding the thermodynamics of vapour-liquid-equilibrium systems and CPMs is explored. This work was published as the second part of a CPM series, in *Industrial and Engineering Chemistry Research* (see Holland et al, 2004 a). Although my name appears as first author on this paper, the work is almost exclusively Michaela Tapp's.

Chapter 4 presents the first application of CPMs for distillation configuration analysis. This work is unpublished and details the topological effects of feed distribution in two product distillation columns. Attainable composition regions are found and the pros and cons of feed distribution are discussed. Both Michaela Tapp and I have tackled this problem, but from different perspectives. This approach is my own.

Chapter 5 presents the first application of CPMs for complex distillation column modelling and design. The work was published in *Computers and Chemical*

Engineering in 2004 (see Holland et al, 2004 b). A coupled column section system is used to gain insight into possible design approaches for and operation of the Petlyuk column. Composition regions of feasible operation at overall infinite reflux are found. Michaela Tapp offered valuable insight in the development of this work, but it is almost exclusively my own.

Chapter 6 presents a comprehensive analysis and design methodology for the Petlyuk column at sharp-split conditions and ideal thermodynamics using CPMs. The purpose of the work is to illustrate the use of the CPM technique for the comprehensive analysis and design of complex distillation configurations. Parameter regions containing all column solutions for a given feed composition are found for the Petlyuk column. This chapter is as yet unpublished. Much of the guidance in this work was offered by Prof Steiner Hauan, of Carnegie Mellon University, for which I am extremely grateful.

Chapter 7 expands on the sharp-split Petlyuk results of chapter 6 to incorporate general product specifications. A general minimum reflux ratio condition is found for the Petlyuk column. It is shown that very interseting and counter-intuitive component net-molar-flows are possible. Parameter regions containing column solutions are also found. This work, also, is as yet unpublished.

Chapter 2:

Column Profile Maps

1. Derivation and Interpretation

This work was done together with Michaela Tapp and was published as the first part of a CPM series, in Industrial and Engineering Chemistry Research (see Tapp et al, 2004). I was involved in the preliminary fundamentals, but she is responsible for all the pinch point loci analyses and classifications which constitute the major portion of the work.

Abstract

The use of ordinary differential equations (ODE) as a short – cut technique for the description of distillation columns has been well established over the last three decades. Residue curve maps (RCM) have been employed as a graphical representation tool in the analysis and interpretation of the behaviour of distillation systems. However, RCM's enable one to gain insight into infinite reflux column behaviour only. This paper will be the first part of a series that looks at column profile maps (CPM) obtained by using the difference point equation (DPE). CPM's represent the finite reflux case, and the map depends on the values of the difference point and the net flowrate. This paper focuses on analysing the behaviour of distillation systems for ideal thermo and shows how using CPM's one can devise more creative designs. The focus of the second part lies in analysing systems with non-ideal behaviour and develops tools for synthesis of distillation.

2.1 Introduction

Graphical representation is an extremely useful tool in the analysis and interpretation of the behaviour of distillation systems. The thermodynamic topological analysis is based on the classical works of Schreinemakers (1902) and Ostwald (1902), where the relationship between the vapour-liquid equilibrium of a mixture and the behaviour of open evaporation residue curves for ternary mixtures was established. The residue curve (Doherty and Perkins (1978a)) is defined as the locus of liquid compositions remaining un-evaporated from a simple distillation process. Schreinemakers established that the interior of the composition space is filled with residue curves to form a residue curve map (RCM). The pure components and azeotropes are end and starting points of the residue curves and the edges of the composition space between the singular points are also residue curves. Residue curve maps provided one of the first graphical methods of understanding the volatility and compositional changes of (3 component) batch evaporative systems. Residue curve maps are not restricted in their usefulness to simple boiling experiments. Hausen (1952) and Rishe (1955) showed that the residue curve can represent the composition profile of a packed distillation column at infinite reflux. A residue curve map therefore represents all possible operational composition profiles in a packed column at infinite reflux. Although only directly useful in ternary and quaternary systems, great insights into higher order systems can be gleaned by the analysis of various groups of ternary (or quaternary) mixtures comprising the system. In the late 1960s Zharov (1967; 1968c) gave a more rigorous mathematical foundation of the residue curve map analysis and expanded it to multicomponent mixtures. Similar maps, termed distillation line maps, were produced for staged columns (Stichlmair (1989), Widago and Seider (1996)). The distillation line maps and residue curve maps have slightly different curvature. Unlike the residue curves, the distillation lines are not continuous, but defined at discreet points or stages. The overall topology of the maps is the same however.

Serafimov (1968a; 1968d) proposed to use structural information of VLE diagrams to predict feasible separations. Residue curve maps are useful in the determination of infinite reflux split feasibility and provide an understanding of the thermodynamics of the vapour-liquid-equilibrium; however, they are less useful when applied to finite reflux separations. Finite reflux split feasibility has been addressed through the use of operation leaves (Wahnschafft et al. (1992); Castillo et al. (1998)). The operation leaves, defined as the total attainable composition region in a column section (for a defined product composition), are useful not only for feasibility tests, but the determination of minimum reflux as well. The limitation of the operation leaf method is that it is essentially limited to simple one feed two product distillation columns. It, also, is limited to a maximum of, 4 component mixtures.

Tapp et al. (2003) addressed this problem with the use of the difference point equation (DPE), an adaptation of Doherty's (1978) original rectifying and stripping differential equations (DE's). The use of difference points in the design of non-reactive and extractive cascades has been presented in textbooks and papers over several decades, i.e. Hoffmann (1964), Hauan (1998). In accordance with the definition of the difference point presented in Hauan's work, Tapp et al. defined the difference point as a pseudo net-molar-flow composition within a column section. The difference point was not restricted to product compositions or indeed values within the Gibbs or mass balance triangle (MBT). The column section was redefined as a length of column between points of addition or removal of material or heat. This definition includes the rectifying and stripping column sections, but is not limited to them. New operation leaves were defined, all extended from a chosen composition within the column section (X_T), with a set net-molar-flow (difference point). These operation leaves extended to areas untouched by the original operating leaves. Because the net fluxes have a direction associated with them, internal mass balances for a series of column sections can be achieved by simple addition (or subtraction) of the net fluxes within the column sections. Any distillation process can therefore be modelled

including multiple feed addition, side-stream withdrawal (Tapp et al. (2003)) and column coupling.

The idea of producing composition trajectories from points other than the product point was first introduced by Franklin (1986). Franklin used Underwood's (1948) Z –transformation method to transform the total reflux composition trajectories (distillation lines) for partial/finite reflux conditions. He showed that the composition space could be populated with trajectories and that these trajectories all had a common "fixed point" for a defined reflux. This "fixed point" is analogous to the difference point. Petlyuk (2001) put forward a concept very similar to Franklins when he proposed the use of "trajectory bundles" for the design of sharp split separations.

This work, although developed independently, will essentially be an extension of Franklin's work. It will be shown that the entire composition space can be populated with composition profiles using the difference point equation. These sets of trajectories with common difference points and reflux ratios will be referred to as column profile maps (CPMs). It will be shown that the CPM is simply a transformation of the residue curve map as the DPE is a linear transform of the residue curve equation apparently. Physically irrelevant residue curves (outside the MBT) can be shifted into the "real" space (MBT) when transformed with certain parameters.

This paper will be the first in a series of papers that outlines the nature of and theory behind column profile maps as well as their potential use in distillation column design.

2.2 Derivation of column profile maps

2.2.1 The difference point equation

The difference point equation (see Equation 2.1) was introduced by Tapp et al (2003) for the modelling of the generalised column section (See Figure 2.1). Instead of being limited to rectifying or stripping column sections it can model

any vapour liquid equilibrium cascades, including absorption and stripping columns. A detailed derivation is given in Appendix I.

$$\frac{dx}{dn} = \left(\frac{1}{R_\Delta} + 1\right)(x - y^*) + \frac{1}{R_\Delta}(X_\Delta - x)$$

_(2.1)

where

$$x_\Delta = \left(\frac{V \cdot Y_T - L \cdot X_T}{\Delta}\right) ; \quad R_\Delta = \frac{L}{\Delta} \quad and \quad \Delta = (V - L) \neq 0$$

with X_Δ being the difference point. The limits on the value of R_Δ and its physical relevance will be discussed later. The mathematical properties of the equation can be analysed further.
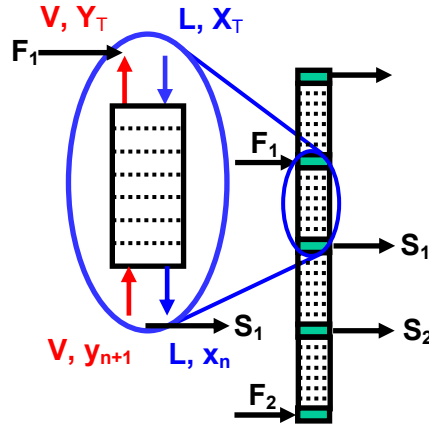
Figure 2.1: Generalised column section

2.2.2 Infinite reflux

Positive integration

Under the conditions of L = V and X_T = Y_T (Total reflux), the equation collapses to the following:

$$\frac{dx}{dn} = (x - Y(x))$$

(2.2)

This form of the DE is mathematically identical to the residue curve equation:

$$\frac{dx}{d\xi} = (x - Y(x))$$

<div align="right">(2.3)</div>

Note: All composition profiles and residue curves will be generated for a system with constant relative volatility with $\alpha_{12} = 3$, $\alpha_{22} = 1$ and $\alpha_{32} = 1.5$. Subscript 1 refers to the lowest boiling component, subscript 2 to the highest boiling component and subscript 3 to the intermediate boiling component throughout the thesis.

The only difference between Equation 2.2 and Equation 2.3 is that the residue curve equation differentiation variable is time dependent while in the DPE it is a variable representing stages. They are in fact identical in x_1 vs. x_2 space. It is therefore evident that profiles can be generated from any point in the space in the same way that residue curve trajectories are modelled. i.e. integration can be performed from arbitrary initial conditions from n = 0 to values of n > 0. See Figure 2.2.
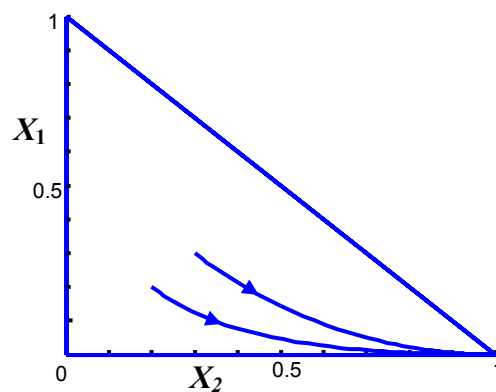
**Figure 2.2: Solutions of the difference point equation
at arbitrary initial conditions as n → + ∞.**

For ideal thermodynamics, these column section profiles pinch at the high boiling (heavy) pure component composition (for n → + ∞).

Negative integration

The DE can be integrated in the negative direction as well. (i.e. integration can be performed from arbitrary initial conditions from n = 0 to values of n < 0). This

process is equivalent to determining the composition profile in a column section from the bottom to the top. See Figure 2.3.
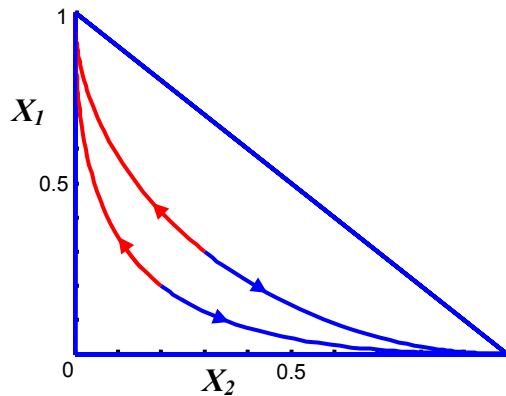
**Figure 2.3: Solutions of the difference point equation
at arbitrary initial conditions as n → - ∞ and n → + ∞.**

For ideal thermodynamics the column section profiles pinch at the lowest boiling (light) pure component composition as n → - ∞.

Negative initial conditions

The mathematics, of the DPE at infinite reflux (or residue curve equation), is not bound by any physically relevant initial conditions. It is possible to evaluate the DE at initial values of x_1, x_2 and x_3 greater than 1 and less than 0 (see Appendix J for a discussion of the validity of this). Any point in x_1-x_2-x_3 space can be populated with trajectories arising from the DPE. If an arbitrary initial condition of X_o = [0.6; -0.2; 0.6][*] is chosen and integration is performed in both the positive and negative directions, (as demonstrated above) the additional profile of Figure 2.4 results. In this case, the profiles again terminate at the pure heavy component composition (as n → + ∞) and the light pure component composition (as n → - ∞).

---

[*] It should be noted that all vectors are of the form [x_1 , x_2 , x_3]. Subscript 1, 2 and 3 represent the light, heavy and intermediate components respectively.
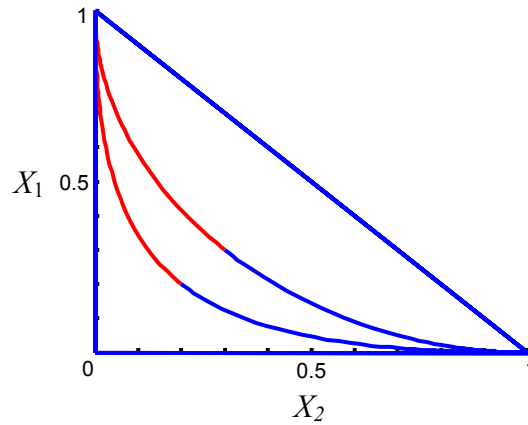
Figure 2.4: Solutions of the difference point equation at arbitrary initial conditions inside and outside the MBT.

If the entire space surrounding physically relevant compositions ($0 \leq x_1, x_2, x_3 \leq 1$ - the Gibbs or Mass Balance Triangle (MBT)) is populated in this way, integrating both in the positive and negative directions, Figure 2.5 results (for the constant relative volatility system).
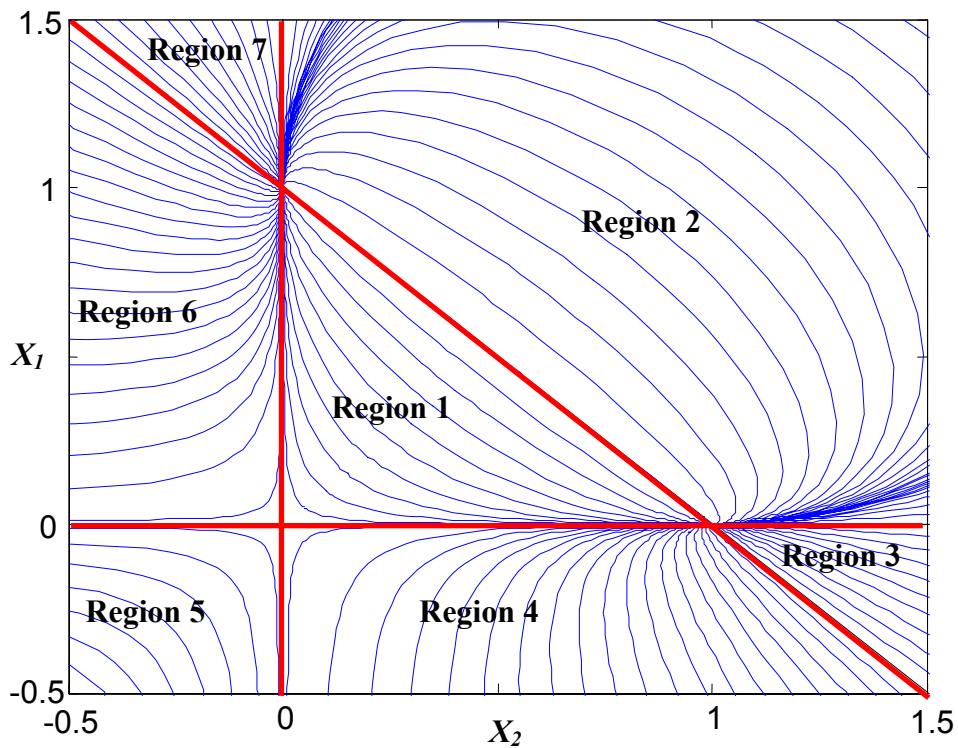
Figure 2.5: Entire Residue curve map for an ideal system.

Figure 2.5 can be divided into a number of different regions. The behaviour in these regions represents all possible profile solutions for a constant relative volatility system. Table 2.1 below summarises some of the properties of these regions.

	X_1	X_2	X_3	Termination $n \to + \infty$ [x_1,x_2,x_3]	Termination $n \to - \infty$ [x_1,x_2,x_3]
Region 1	$0 \leq x_1 \leq 1$	$0 \leq x_2 \leq 1$	$0 \leq x_3 \leq 1$	[0,1,0]	[1,0,0]
Region 2	$0 < x_1 <+\infty$	$0 < x_2 <+\infty$	$-\infty < x_3 < 0$	[0,1,0]	[1,0,0]
Region 3	$-\infty < x_1 < 0$	$1 < x_2 <+\infty$	$-\infty < x_3 < 0$	[0,1,0]	*Discontinuity
Region 4	$-\infty < x_1 < 0$	$0 < x_2 <+\infty$	$0 < x_3 <+\infty$	[0,1,0]	*Discontinuity
Region 5	$-\infty < x_1 < 0$	$-\infty < x_2 < 0$	$1 < x_3 <+\infty$	[-∞,-∞,∞]	*Discontinuity
Region 6	$0 < x_1 <+\infty$	$-\infty < x_2 < 0$	$0 < x_3 <+\infty$	[∞,-∞,∞]	[1,0,0]
Region 7	$1 < x_1 <+\infty$	$-\infty < x_2 < 0$	$-\infty < x_3 < 0$	[∞,-∞,-∞]	[1,0,0]

Table 2.1: Summary of Residue Curve Map regional behaviour on the MBT side of the discontinuity.

Solutions of the difference point equation (Equation 2.1), generated in this way will be referred to as column profile maps (CPMs). The pinch points or nodes of the CPM can be categorised in the same way as the residue curve map. At infinite reflux the pure light component corresponds to an unstable node, the pure heavy component to a stable node; and the intermediate pure component to a saddle point.

Note: the behaviour of the trajectories outside the MBT shown in Figure 2.5 is unique to the constant relative volatility system. Non-constant relative volatility systems result in different topologies in the same way, as the RCM for an ideal system shows different behaviour than the RCM for non - ideal systems. In non-ideal systems stationary points occur inside and outside the MBT, this leads to very interesting topologies (see chapter 3.3).

A discontinuity arises from the equilibrium function and will be discussed in more detail later.

Different thermodynamic models (i.e. Wilson, NRTL) predict the same number of stationary points occurring in the topology of the system, although the predicted curvature differs and the exact position of the stationary points within the topology outside the MBT differs as well. It might be possible to determine the best model for a particular system by looking at their prediction of the position of the stationary points outside the MBT. But this is beyond the scope of this thesis.

Discontinuity

A discontinuity in the constant relative volatility system arises from the structure of the function describing the vapour-liquid equilibrium.

$$y_i(x) = \frac{\alpha_{i2} x_i}{\alpha_{12} x_1 + \alpha_{22} x_2 + \alpha_{32} x_3} \qquad (2.4)$$

We can see from Equation 2.4 that this function is indeterminate when the denominator is zero. It is therefore possible to determine the discontinuity by setting this denominator to zero.

$$\alpha_{12} x_1 + \alpha_{22} x_2 + \alpha_{32} x_3 = 0$$

But $x_3 = 1 - x_1 - x_2$

$$\therefore \quad \alpha_{12} x_1 + \alpha_{22} x_2 + \alpha_{32}(1 - x_1 - x_2) = 0$$

$$x_1 = \frac{(\alpha_{32} - \alpha_{22}) x_2 - \alpha_{32}}{(\alpha_{12} - \alpha_{32})} \qquad (2.5)$$

The discontinuity for this system is a straight line intersecting the x_1-axis at $-\alpha_{32}/(\alpha_{12} - \alpha_{32})$ and the x_2-axis at $\alpha_{32}/(\alpha_{32} - \alpha_{22})$. Because α_{32} (the volatility of the intermediate) is always larger than α_{22} (the volatility of the heavy) the x_2 intercept is always positive and larger than 1, hence, only profiles of region 2, 3, 4 and 5 will be affected by the discontinuity. See Figure 2.6.

In general, because of the models describing the VLE, most if not, all real systems will contain discontinuous regions. Models such as Wilson, NRTL and Unifac are indeterminate at certain values of x_1, x_2 and x_3. These discontinuities are inherent

to the thermodynamic model and their position depends on the model used. Discontinuous regions can not be moved and they always occur outside the MBT.
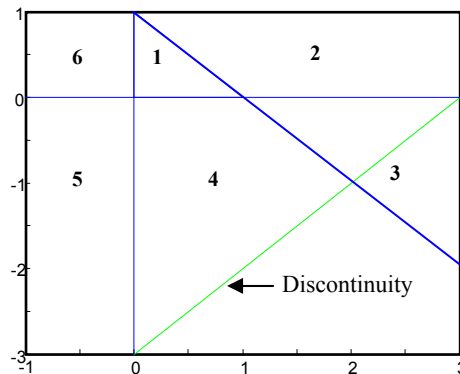
**Figure 2.6: Discontinuity for constant relative volatility
system $\alpha_{12} = 2$, $\alpha_{22} = 1$ and $\alpha_{32} = 1.5$.**

2.2.3   Finite reflux

If the difference point and reflux, are arbitrarily set (say [0.9; 0.05; 0.05] and 9), the space can be populated with composition profiles or trajectories, in exactly the same way that the residue curve map was produced, by integrating the difference point equation at arbitrary initial conditions (as n $\rightarrow +\infty$ and n $\rightarrow -\infty$). Both MBT and "outside"/negative space can be populated with profiles.
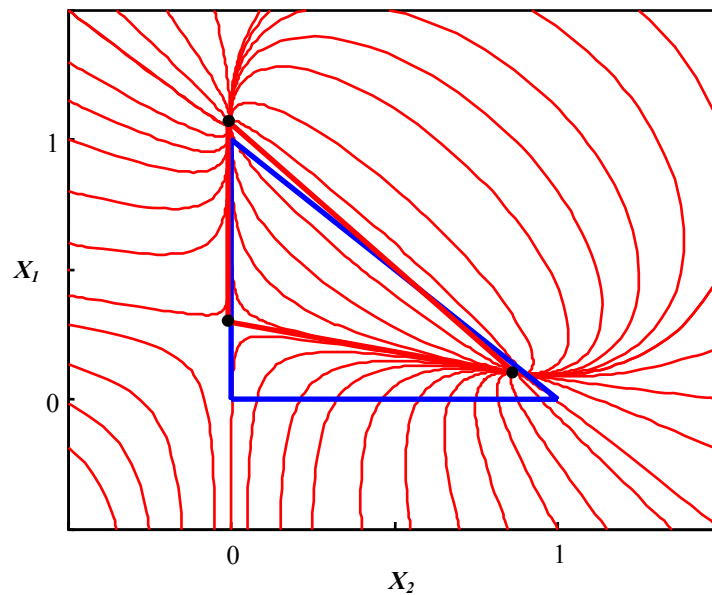
Figure 2.7: Column Profile Map $X_\Delta = [0.9; 0.05; 0.05]$, $R_\Delta = 9$.

From Figure 2.7 it is apparent that the CPM solutions have the same geometry as the residue curve map (Figure 2.5).All the original singularities are present but have been shifted in the composition space. A section of the topology from region 4 (see Figure 2.6) representing physically irrelevant composition profiles (at infinite reflux) has been shifted into the MBT and these solutions are valid composition profiles. That is to say that any column section operating at a reflux ratio of 9 with this difference point (or net-molar-flow) could in fact operate on one of these trajectories. The CPM is in fact a simple transform of the RCM. For constant relative volatility systems, the boundaries of the mass balance triangle (representing particular residue curve solutions) are also transformed at finite reflux maintaining their straightness to form a "transformed" triangle. This fact has led to the phenomenon being described as "transformed" or "moving" triangles, this will be discussed in more detail in section 3.3.1.2. Under very extreme conditions, however, the singularities of the system merge and the transformed triangle collapses. Under these conditions the entire topology of the system changes. Figure 2.8 to Figure 2.13 illustrate CPM solutions for difference points in each of the remaining 6 regions at a reflux of 9. It is interesting to note, that the resulting trajectories inside the MBT follow very different paths, depending on the position of the difference point. The X_Δ in Figure 2.12 for instance shifts a saddle and an unstable node inside the MBT, this changes the path and the directions of the profiles dramatically. All profiles around the singularities are either running towards the node (stable node in the bottom right corner) or away from it (saddle node in the bottom left corner).

It is important to note that the discontinuity present in the residue curve map does not move and is still fixed in its original position. This is due to the fact that, at the discontinuity, the thermodynamics of the system are not defined and the thermodynamics are not changed by the linear transformation of the DE. In principle the topology from all 7 original regions may be utilised in the design of both simple and complex distillation columns. In this paper we discuss constant relative volatility systems only. This has been done for illustrative purposes. The objective of this paper is to present a new approach for designing separation

systems by looking at the theory and nature of CPM's. Non-constant relative volatility systems show a much more complex behaviour, i.e. the transformed boundaries of the MBT are no longer straight, azeotropes occur outside the MBT changing the topology. The technique to analyse the behaviour is not analytic anymore, as the temperature is not obtainable as an explicit function. However, non-ideal systems have been analyzed (i.e. methanol/ethanol/acetone-system, chloroform/benzene/acetone-system) and these results agree in principle with the results obtain for the ideal system (see chapter 3.3).
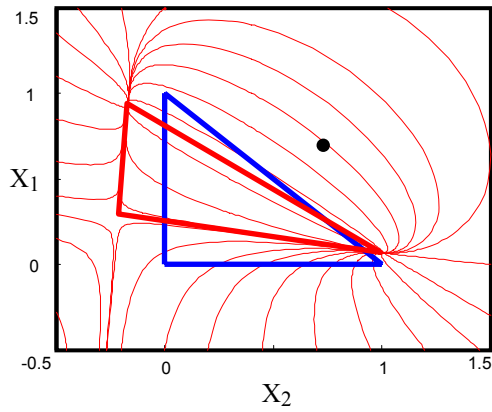
Figure 2.8: Column profile map
X_Δ = [0.7; 0.7; -0.4], R_Δ = 9, region 2.
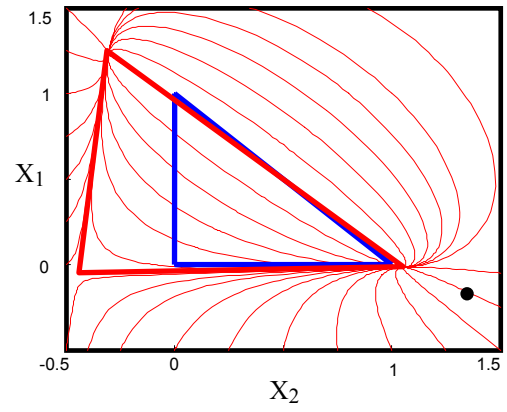
Figure 2.9: Column profile map
X_Δ =[-0.2; 1.4, -0.2], R_Δ = 9, region 3.
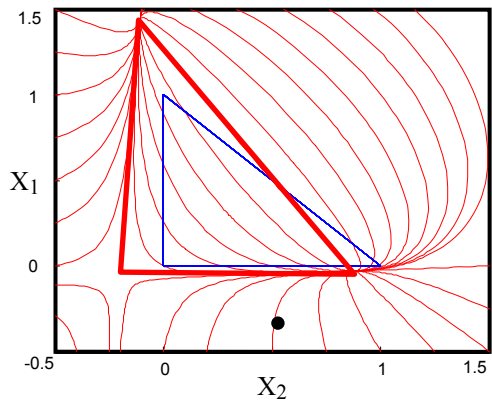
Figure 2.10: Column profile map
X_Δ =[-0.3; 0.5; 0.8], R_Δ = 9, region 4.
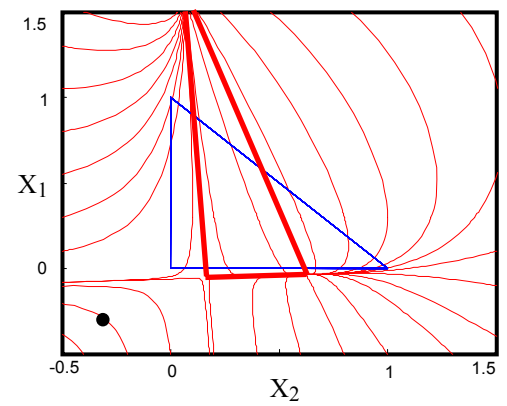
Figure 2.11: Column profile map
X_Δ = [-0.3;- 0.3; 1.6], R_Δ = 9, region 5.
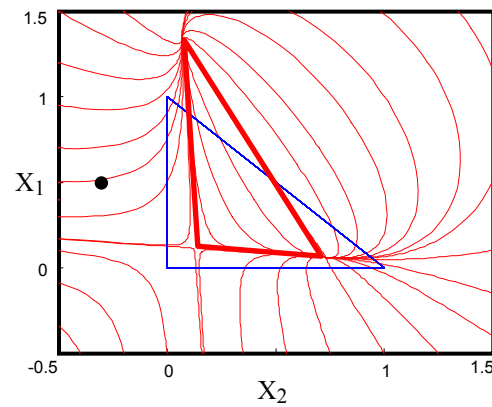
Figure 2.12: Column profile map
X_Δ = [0.5;-0.3; 0.8], R_Δ = 9, region 6.
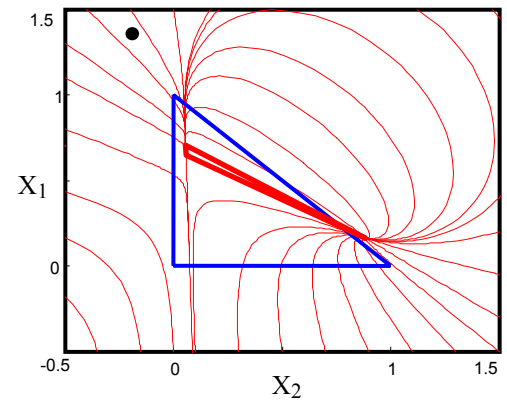
Figure 2.13: Column profile map
X_Δ = [1.4;-0.2; -0.2], R_Δ = 9, region 7.

2.3 Column profile map pinch locus

Pinch point loci have been defined as the locus of all pinch points obtained by varying the reflux ratio R. They are unique for a fixed distillate composition X_D. Pinch points can be determined mathematically by solving the differential equation for $dx/dn = 0$ or graphically by finding the line from either the distillate X_D or bottoms composition X_B tangent to the residue curves. The difference point equation is mathematically identical to the differential equations describing the rectifying or stripping sections in a distillation column (Doherty 1978) hence for a fixed X_Δ there is a unique pinch point locus obtainable by varying R_Δ. As X_Δ does not need to lie inside the MBT, pinch point loci show vastly different behaviour depending on the position of the difference point in the x_1-x_2-space. Pinch loci help describe the path that the triangles take as R_Δ is varied as the nodes for every CPM have to lie on the respective pinch curve. In this section we will show how the behaviour of the pinch point loci affects the topology of CPM's. This will be shown again for a constant relative volatility system. However the overall theory holds for real systems as well. See chapter 3.3.

2.3.1   Pinch loci for difference points inside the MBT

A difference point inside the MBT has only positive values, i.e. $X_\Delta = [0.2\ 0.5\ 0.3]$, which have to sum up to 1. However, if the flowrate difference point Δ is negative, the net-molar flowrate ΔX_Δ, can become negative. Some typical pinch point loci for different X_Δ inside the MBT are shown in Figure 2.14. Remember that one can find a pinch point by finding a point on a residue curve such that the line from the initial point is tangent to the residue curve. This is equivalent to saying that the separation vector $(x-y^*)$ is collinear to the mixing vector $(X_D - x)$.

Highest boiling component

Intermediate boiler component   Lowest boiling component
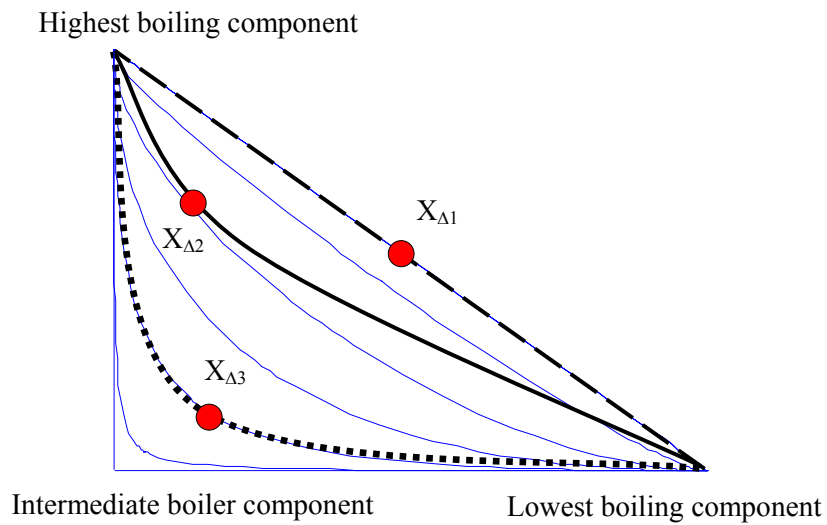
Figure 2.14: Pinch point loci inside the MBT for different X_Δ

The position of X_Δ determines the path of the pinch point loci, see Figure 2.14. Pinch loci do not stop at the pure components as there are composition profiles outside the MBT (see Figure 2.5) and one can find tangents that meet the collinearity condition. This is shown in Figure 2.15.
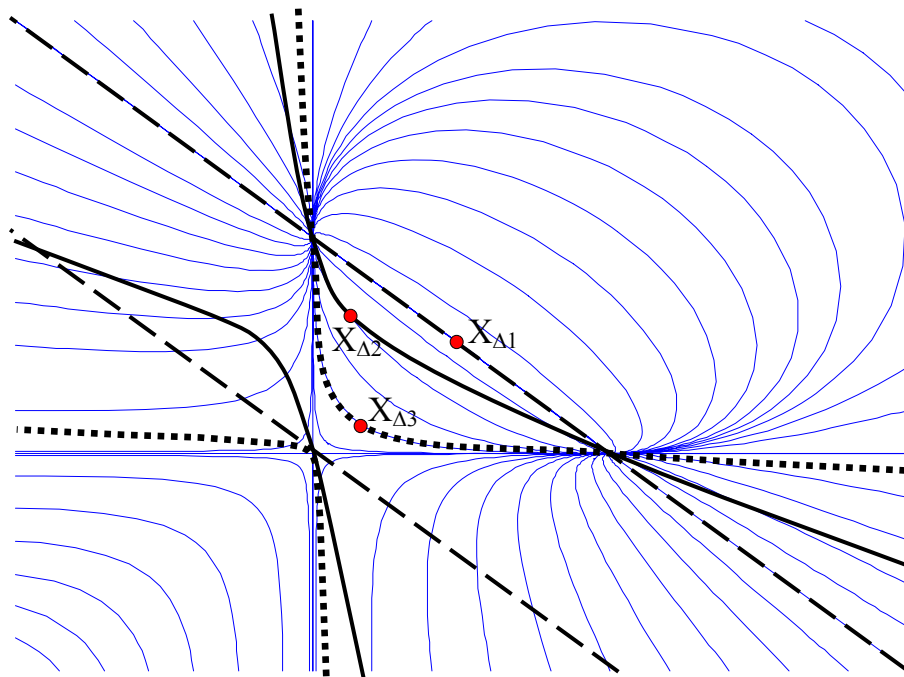
Figure 2.15: Pinch point loci in the expanded space for different X_Δ.

Figure 2.15 shows that the pinch point loci determined by x_Δ consists of two branches. Any choice of X_Δ inside the MBT results in two pinch point loci branches with one branch connecting the highest and lowest boiling component and one branch running through the intermediate boiler.

Pinch loci and the reflux ratio R_Δ

Now where do pinch point loci start and end? To answer this question we have to look at the effect of the reflux ratio R_Δ in more detail. Every point of the pinch point locus has a unique R_Δ. For $R_\Delta \rightarrow +\infty$ the difference point equation reduces to the residue curve equation. The resulting pinch points are the pure components and form the MBT. Hence every set of pinch point loci must run through the vertices as the residue curve equation is independent of X_Δ, see Figure 2.15. Different values of R_Δ result in different positions of the singularities on the pinch locus. Figure 2.16 shows the position of singularities for $R_\Delta \rightarrow +\infty$, $R_\Delta = 2$ and $R_\Delta \rightarrow 0$.
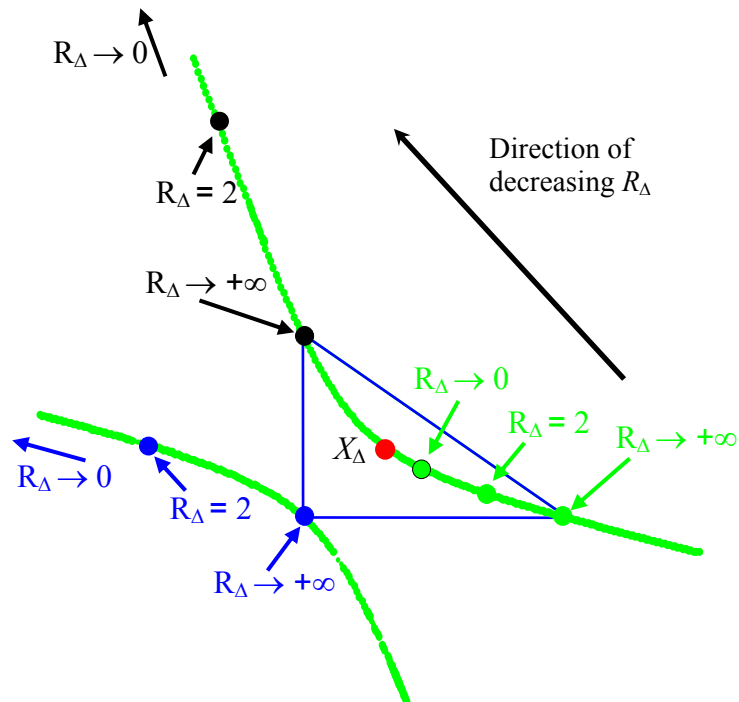
Figure 2.16: Position of singularities on the pinch point locus for positive R_Δ in the range from $R_\Delta \rightarrow +\infty$ to $R_\Delta \rightarrow 0$.

From Figure 2.16 one can deduce, the smaller the reflux, the further away the singularities move from the MBT. The limiting case $R_\Delta \to 0$ moves two of the singularities to positive infinity values in the x_1,x_2-space along the pinch curve while the third one reaches a boundary value, as shown in Figure 2.16. $R_\Delta \to 0$ represents a "switching over" point, as a further decrease in R_Δ makes it become negative. This change of sign can be interpreted as changing from rectifying into stripping mode, ΔX_Δ changes from being all positive to all negative due to the fact that negative R_Δ changes the sign in the differential equations. In analogy to the above, Figure 2.17 shows the movement of the singularities along the pinch point locus for negative R_Δ ranging from $R_\Delta \to 0$ to $R_\Delta \to -\infty$.
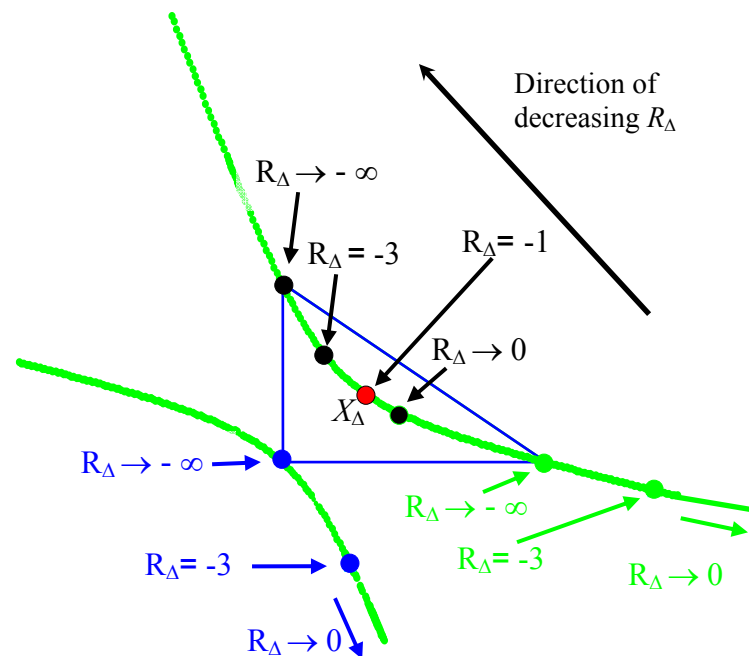
Figure 2.17: Position of singularities on the pinch point locus for negative R_Δ in the range from $R_\Delta \to 0$ to $R_\Delta \to -\infty$.

Approaching $R_\Delta \to 0$ from the negative side moves the two singularities to negative infinity values in the x_1,x_2-space while the third one reaches the boundary value. It is interesting to note that at $R_\Delta = -1$, X_Δ becomes the only singularity that occurs, as the differential equation reduces to x- $X_\Delta = 0$. Hence X_Δ always lies on the pinch point locus. The pinch locus region between $R_\Delta \to 0$ and $R_\Delta = -1$ is for counter-current flow patterns is only of mathematical interest, as the

V/L ratio has to be negative in order to attain reflux ratios in that range. However if one would adopt that negative values of the V/L ratio correspond to co-current flows this methodology could be applied to both counter current and co-current cascades. We can now interpret the pinch point locus with respect to the sign of the reflux ratio. This is shown in Figure 2.18.
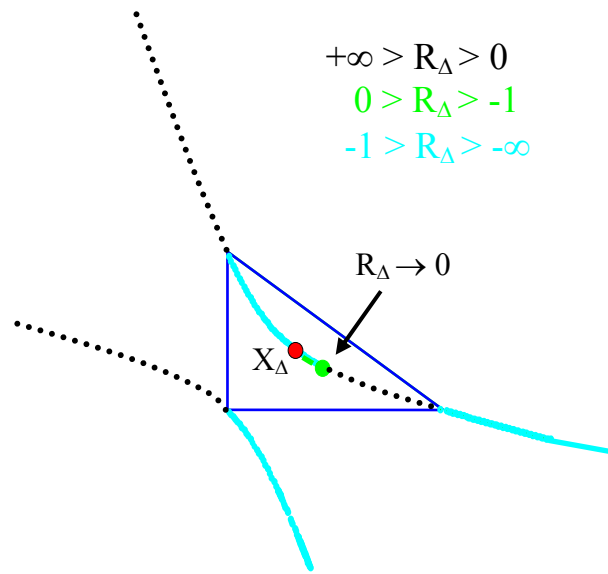
Figure 2.18: Classifying the pinch point locus with respect to the sign of the reflux ratio.

Positive values of R_Δ result in all pinch points being positioned somewhere on the dotted part of the pinch curve, see Figure 2.18, and negative values of R_Δ positions all the pinch points on the solid part of the pinch locus. We can conclude now, that pinch loci have no start or end point. They describe a circular path as they switch from $+\infty$ to $-\infty$ in the x_1, x_2-space as $R_\Delta \rightarrow 0$.

Note: The statement, that pinch curves follow a circular path seems to be incorrect, as there is a discontinuity in the form of a straight line apparent in the system, see Figure 2.6. What happens to the pinch locus if it meets the discontinuity? Pinch points exist for $-1 < R_\Delta < 0$ (although they are only attainable for negative V/L ratios). This implies that the triangles do move from $-\infty$ in the x_1, x_2-space for $R_\Delta \rightarrow 0$ towards the MBT by decreasing R_Δ. As mentioned earlier, $R_\Delta = -1$ results in only one pinch point. The reason for this lies in the existence of the

discontinuity. By approaching the value of -1, the triangle moves closer to the discontinuity until, for $R_\Delta = -1$, the triangle collapses into $X_P = X_\Delta$. In conclusion, we might restate that the pinch locus follows a closed circular path as long as its path does not cross the discontinuity in the system. If it crosses the discontinuity there is an undefined point on the pinch curve for $R_\Delta = -1$. The collapsing of the triangle can also explained by looking at the flowrates. At $R_\Delta = -1$ the internal vapour flow rate V goes to zero. Obviously nothing happens with the liquid flowing through an empty tube without contact with the vapour. Similarly if $R_\Delta = 0$ the internal liquid flowrate L goes to zero and nothing happens with the vapour rising up through an empty tube. Thus the difference point has to be the only singularity in both cases leading to the collapsing triangle for these conditions.

Moving triangles

To understand how pinch loci are helpful in understanding the topology of systems we have to look at the pinch loci in terms of the kind of singularity (pinch point) that occurs. As mentioned earlier, the nodes of the MBT (pure components) can be classified as an unstable node (highest boiler), stable node (lowest boiler) and a saddle point (intermediate boiler). Now by fixing X_Δ we can investigate the kind of node that occurs for different R_Δ and split the pinch loci into an unstable/stable node branch and a saddle branch.
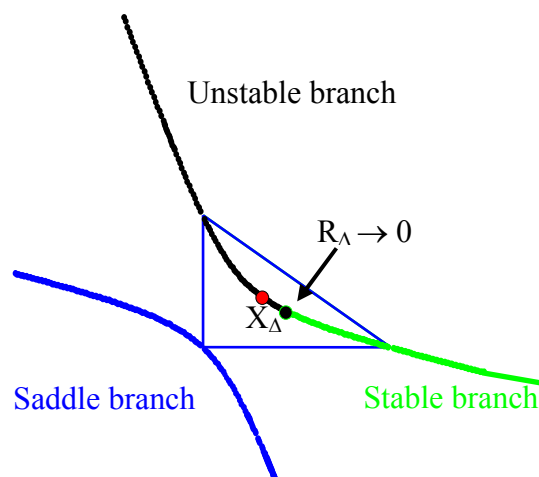
Figure 2.19: **Classifying the pinch point locus with respect to kind of singularities that occur.**

To understand the usefulness of this for understanding the topology, we will look at an example. Let us pick a reflux ratio, i.e. $R_\Delta=2$ and plot the nodes, as done in Figure 2.20a.
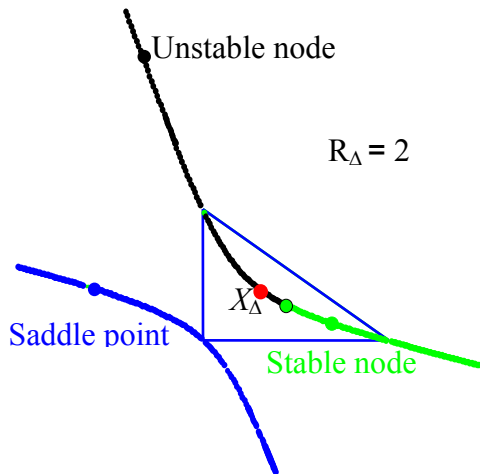
Figure 2.20a: Singularities for $R_\Delta=2$ and their position on the pinch locus.
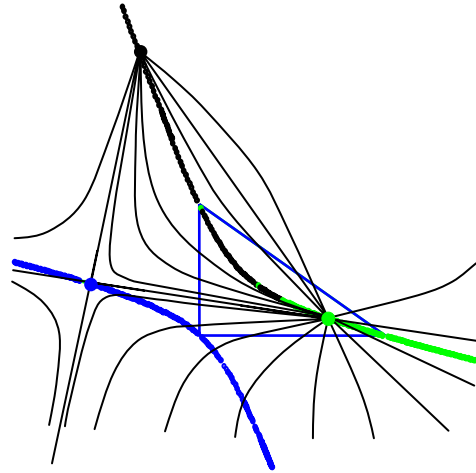
Figure 2.20b: The triangular region for $R_\Delta=2$ and the respective CPM.

By looking at the position of the nodes on the pinch locus, we can classify the nodes as stable, unstable and saddle point. As the profiles connecting the nodes are straight lines, we can construct a triangular region and draw the CPM for $R_\Delta=2$, as shown in Figure 2.20b. Different R_Δ result in different triangular regions; Figure 2.21 shows the movement of the triangular regions for $R_\Delta=8$, $R_\Delta=2$, $R_\Delta=-3$ and $R_\Delta=-7$. Decreasing R_Δ from $+\infty$ moves the triangle away from the MBT as indicated in Figure 2.21a. As R_Δ becomes negative, the triangles appear from negative infinity values in the x_1,x_2-space and with further decrease move towards the MBT until $R_\Delta = -\infty$, see Figure 2.21b. We can conclude that, the higher the absolute value of R_Δ, the closer the triangle to the MBT.
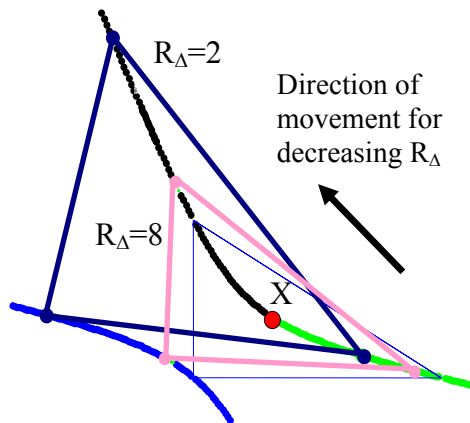
Figure 2.21a: Moving of the triangles for $R_\Delta=2$ and $R_\Delta=8$.
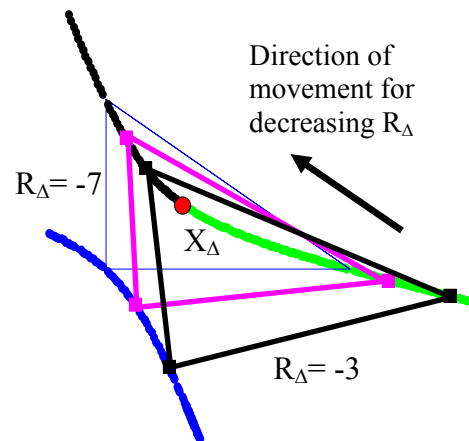
Figure 2.21b: Moving of the triangles for $R_\Delta=-3$ and $R_\Delta=-7$.

Summary

Difference points inside the MBT have only positive values. The path of the pinch locus depends on the position of X_Δ. They can be extended outside the MBT and they do not have a start or end point as they describe a circular path. Pinch loci for this case consist always of two branches with one branch connecting the highest and lowest boiling component and the other running through the intermediate boiler. Every set of pinch loci has the vertices as a common pinch point as for $R_\Delta \to \pm\infty$ the difference point equation reduces to the residue curve equation and the only singularities are the vertices. X_Δ is a singularity on the pinch locus. The branches of pinch loci can be classified in regions of positive and negative reflux, with $R_\Delta \to 0$ as the "switching over" point. The branches of the pinch locus can also be classified with respect to the kind of singularity occurring. This allows predicting the topology of the system by determining the position of the nodes on the pinch locus. The pinch loci trace the path the triangles move for a fixed X_Δ by varying R_Δ.

2.3.2   Pinch loci for difference points outside the MBT

To be able to examine the behaviour of the pinch loci for difference points outside the MBT, we have to define regions of similar behaviour. These regions are characterised by regions in which the values of difference point have the same sign.

Pinch loci for regions of similar X_Δ

In section 2.2.2 we introduced seven regions, see Figure 2.5. One of these regions has been discussed in the previous section (all values of X_Δ are positive). What about the other cases? Figure 2.22a-f each show one set of pinch loci for an arbitrarily chosen X_Δ in the remaining six different regions. The notation of the respective difference point is as follows: $X_\Delta = [- + +]$. This represents a difference point with the lowest boiling component having a negative sign, while the highest boiling and the intermediate component have positive signs.

a) $X_\Delta = [+ + -]$:

$X_\Delta = [1.2\ 0.5\ -1.7]$

2

b) $X_\Delta = [+ - +]$:

$X_\Delta = [1.2\ -0.1\ -0.1]$

3

c) $X_\Delta = [+ - +]$:

$X_\Delta = [0.3\ -0.3\ 1]$

4

d) $X_\Delta = [- - +]$:

$X_\Delta = [-0.3\ -0.3\ 1.6]$

5

e) $X_\Delta = [- + +]$:

$X_\Delta = [-0.4\ 0.5\ 0.9]$

6

f) $X_\Delta = [- + -]$:

7

$X_\Delta = [-0.1\ 1.2\ -0.1]$
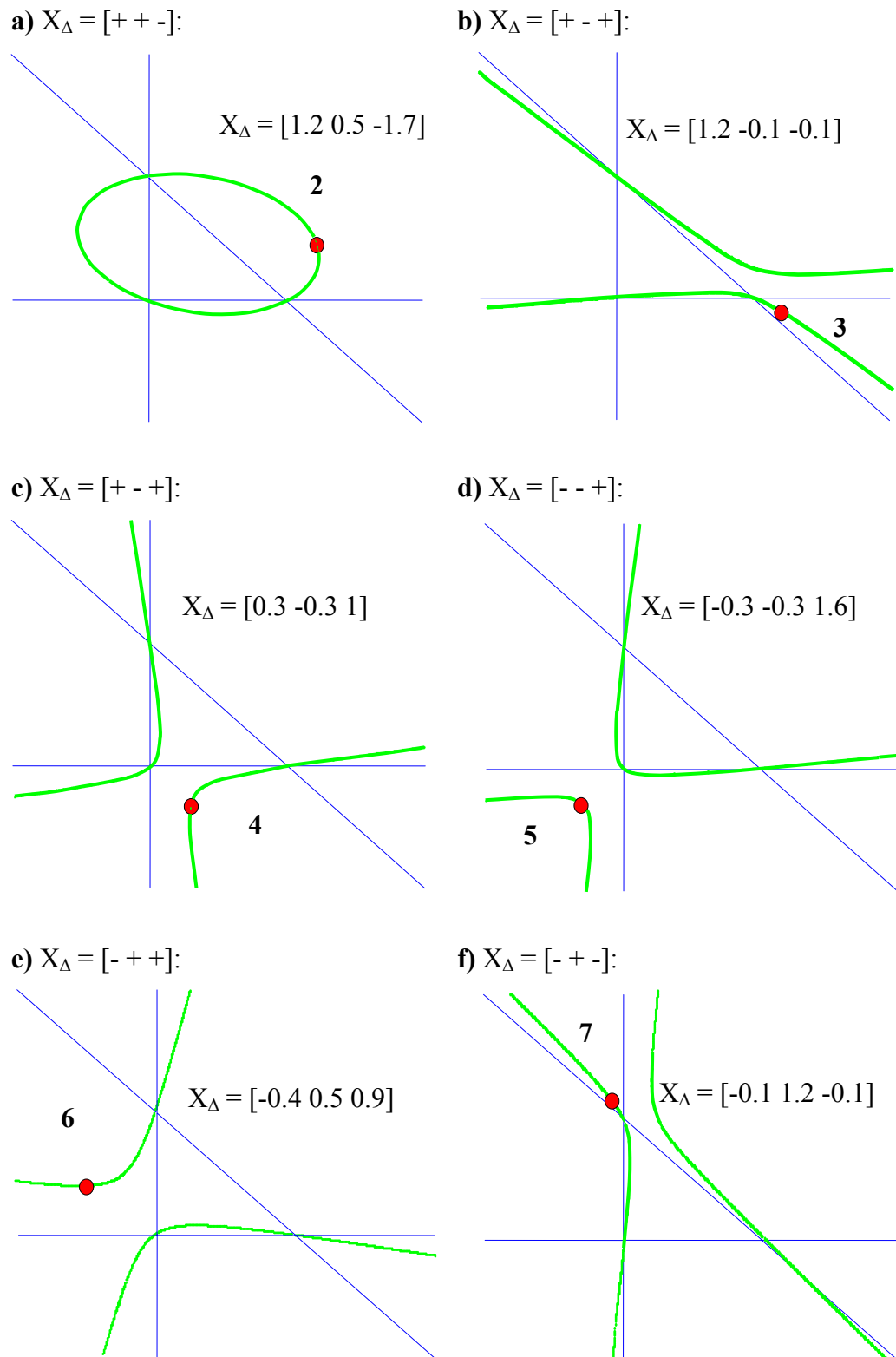
Figure 2.22a-f: All sets of different pinch loci for fixed X_Δ in the six different regions.

Figure 2.22a-f show vastly different behaviour of pinch loci depending on the region in which the X_Δ is. Looking at Figure 2.22a we can see the one branch runs through the unstable node, whereas the other branch connects the stable and the saddle point. However there are cases, such as Figure 2.22c and Figure 2.22f with one pinch locus going through all three nodes. Figure 2.22c also shows that it is possible that there is only one branch in the system. Any other choice of X_Δ within these regions only changes the curvature of the pinch loci. The overall pattern (the way the branches connect the nodes and the number thereof) of the pinch loci remain. In other words: choosing a different X_Δ within the region shown in Figure 2.22c, always results in an elliptic pinch locus although their position and size differs from the one shown in Figure 2.22c. As there is such a variety of pinch loci, one might ask, what is actually happening to the pinch loci as X_Δ moves through the regions?
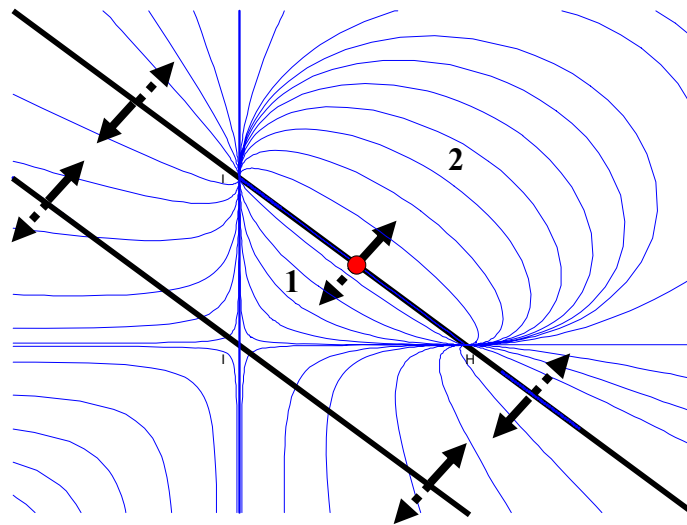
Figure 2.23a: Shifting of the pinch curve branches by moving x_Δ from region 1 to region 2.

Figure 2.23a shows the residue curve map and the pinch loci defined by $X_\Delta = [0.6\ 0.4\ 0]$. Now moving X_Δ inside the MBT shifts the branches of the pinch locus as indicated by the dashed line arrows in Figure 2.23a. This results in pinch loci as discussed in the previous section. Moving X_Δ into region **2** shifts the pinch loci in exactly the opposite direction, shown as the full line arrows in Figure 2.23a, this

result in pinch loci shown in Figure 2.22c. To understand the shifting of the branches for the other regions, we have to look at a few more figures.
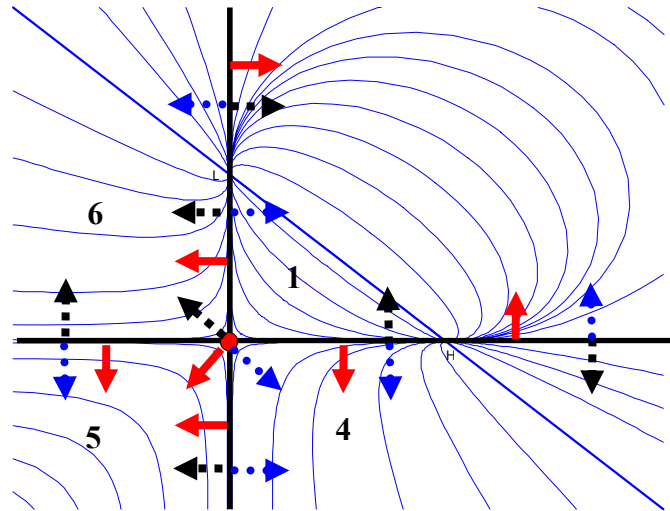
Figure 2.23b: Shifting of the pinch locus branches by moving X_Δ from region 1 to the regions 4, 5 and 6.
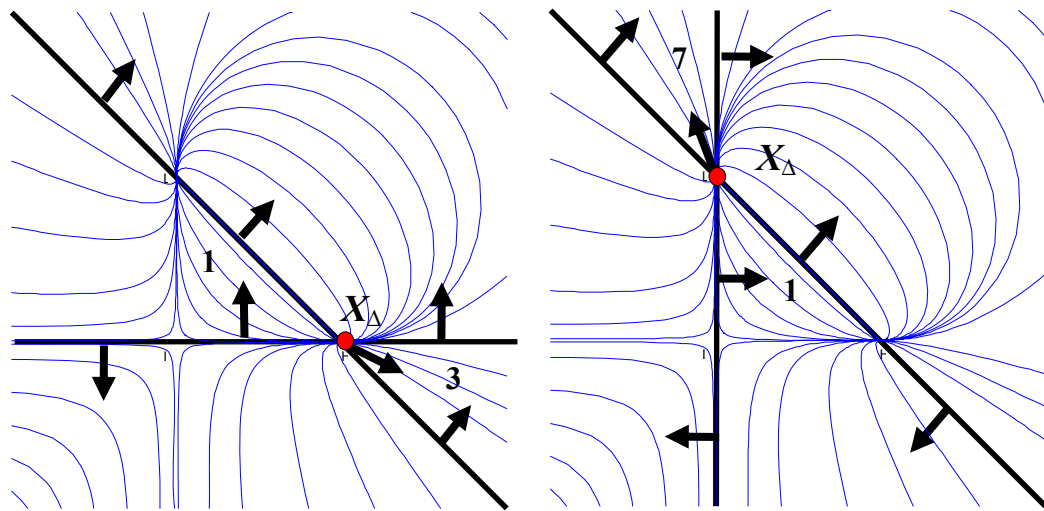
Figure 2.23c: Shifting of the pinch locus branches by moving X_Δ from region 1 to region 3 and from region 1 to region 7.

In analogy to the above, Figure 2.23b shows the shifting of the pinch curve branches defined by $X_\Delta = [0\ 0\ 1]$ by moving x_Δ from region **1** to regions **4, 5** and **6**, which results in pinch loci shown in Figure 2.22a, Figure 2.22e and Figure 2.22f. Finally we are left with moving X_Δ from region **1** to the regions **3** and **7**. This is shown in Figure 2.23c with $X_{\Delta 1} = [1\ 0\ 0]$ and $X_{\Delta 2} = [0\ 1\ 0]$; the respective pinch loci are shown in Figure 2.22b and Figure 2.22d.

Effect of pinch loci on the topology of the system

So what is the effect of the position of the pinch loci on the topology of the system? Figure 2.24a shows an example of how the triangles can be situated on the pinch locus defined by $X_\Delta = [-0.3\ -0.3\ 1.6]$ for $R_\Delta = 8$ and $R_\Delta = -1.5$.
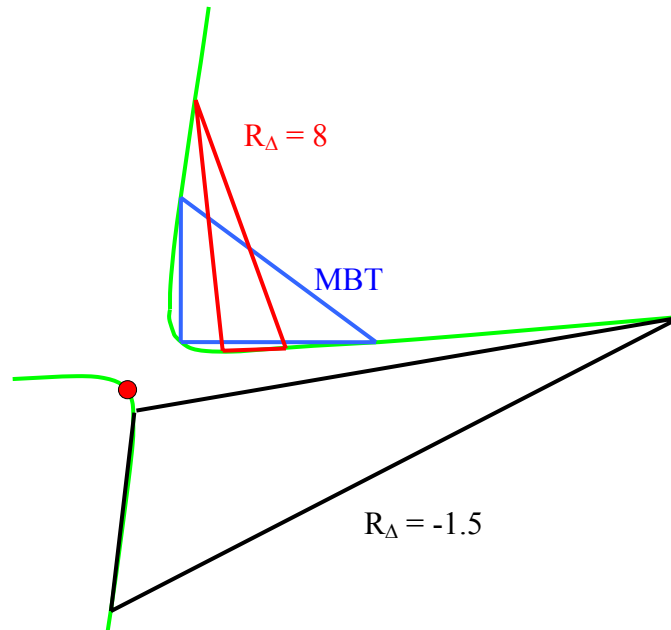
Figure 2.24a: Position of triangular regions on a pinch point locus defined by $X_\Delta = [-0.3\ -0.3\ 1.6]$, for $R_\Delta = 8$ and $R_\Delta = -1.5$.

The respective topology of the CPM's is shown in Figure 2.24b and Figure 2.24c.
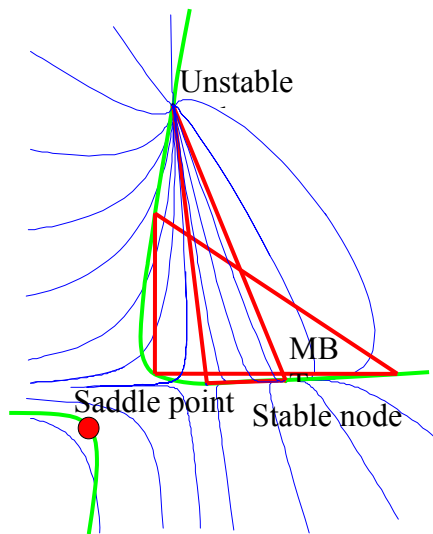
Figure 2.24b: CPM for R_Δ=8 and X_Δ = [-0.3 -0.3 1.6].
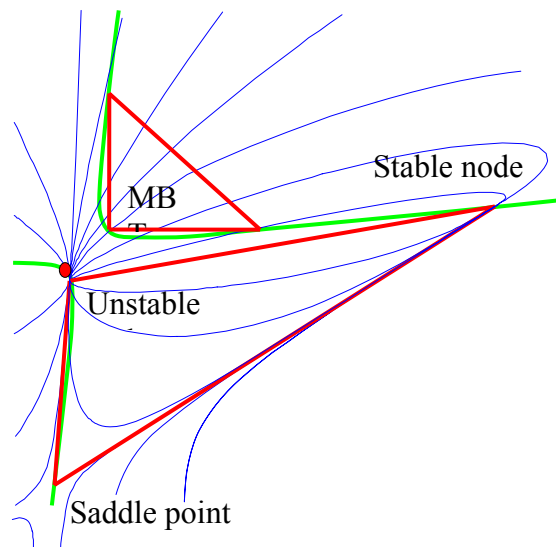
Figure 2.24c: CPM for R_Δ=-1.5 and X_Δ = [-0.3 -0.3 1.6].

The implication of the movement of the triangles along the pinch locus shown in Figure 2.24a is not immediately obvious, but extremely important as the resulting topologies show vastly different behaviour, see Figure 2.24b and Figure 2.24c. These figures show no singularity inside the MBT is that a problem? What happens if the two feeds X_T and y to the column sections are controlled and the column section height would be enlarged up to infinity in a system where all singularities are situated outside the MBT? For a constant X_Δ there is a set number of stages to achieve the two wanted compositions (X_T and y). Adding more and more stages changes the composition of the passing streams Y_T and x. This results in a change of X_Δ and therefore changes the entire CPM and the position of the singularities as well. In other words adding more stages moves the singularity until they are shifted inside the MBT. This also means that CPM's without a singularity inside the MBT produce feasible profiles.

To be able to understand how the singularities move for a fixed X_Δ outside the MBT we have to look at the mathematics involved on how to determine the kind of singularity occurring. As this is quite complex, we shall devote an entire paper looking at how the system behaviour can be characterized by the study of singular points (stationary points). However the purpose of this paper is to create an

understanding of the behaviour of CPM's. Through novel and creative design these topologies can be used in order to achieve a desired separation initially thought impossible.

In honour of Reuel Shinnar we have used these ideas to generate a column section configuration that writes "Reuel". In this case we assumed any needed feedstream to be available. The first column section needs to operate as a rectifying section with $X_{\Delta 1} = X_D$ thus the profile has to start at the difference point composition this is represented as the dashed red line in Figure 2.25a.
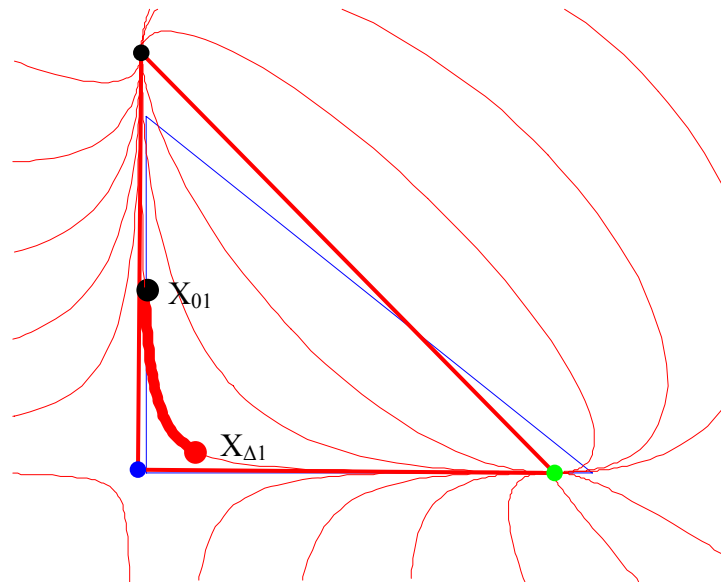
Figure 2.25a: First profile of the sequence of column profiles that show the word "Reuel".

The second column section needed to have a profile that runs at a 90° angle to the first profile starting at the composition X_{01}. This has been realized by using a difference point $X_{\Delta 2}$ in region 7 with a high reflux ratio of $R_{\Delta} = 10.2$. This results in a CPM shown in Figure 2.25b. The bold line in Figure 2.25b represents the second part of the letter "R".
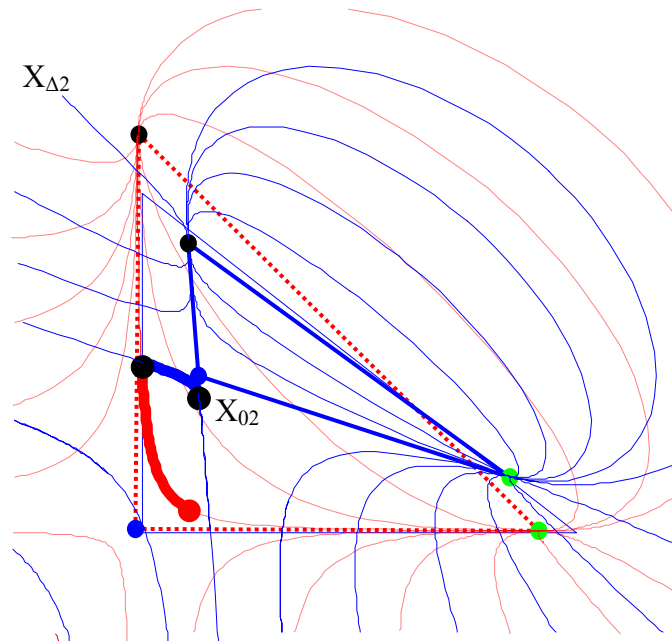
Figure 2.25b: First and second profile of the sequence of column profiles that show the word "Reuel".

In analogy to the above it is possible to assemble the whole word "Reuel" with column profiles, see Figure 2.25c. The entire column section configuration with the respective X_Δ and R_Δ is shown in Figure A.1 in Appendix A. The colours used for the column sections matches the column profiles in Figure 2.25c.
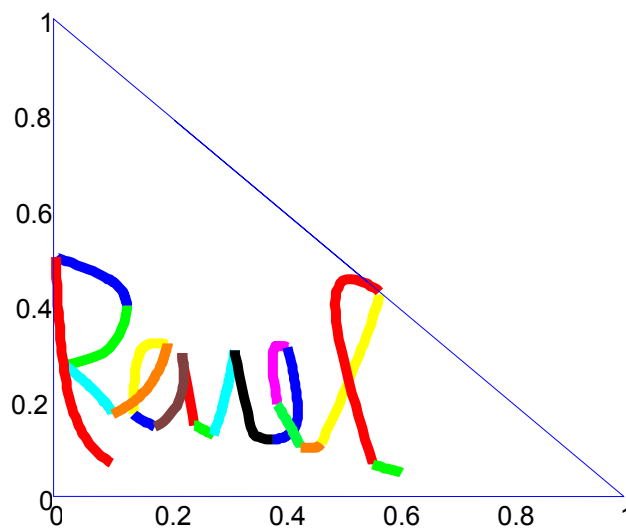
Figure 2.25c: Sequence of column profiles that show the word "Reuel".

2.4 Discussion and Conclusions

The development of graphical tools to gain insight into simulation procedures is always of great interest. In this paper we showed how to generate CPM's for constant relative volatility systems by using the difference point equation. CPM's give great insight into the system behaviour, as they are the plot of all possible profiles achievable in a column section, defined by the difference point X_Δ and the reflux ratio R_Δ. This is a great advantage over the traditional approach, which results in just a single profile (stripping or rectifying profile). The designer can now for instance choose the optimal profile for the desired separation, by having an understanding of the overall behaviour of the system, from the topology of the CPM's. Once the determination of the optimal profile has been done by the designers, this technique enables them to choose the right operating parameters and the column configuration to achieve the desired separation i.e. if the designer decides to build a column network that writes "Reuel" in the form of concentration profiles, this approach makes it possible.

The knowledge of the behaviour of the overall system can also be very useful in terms of the stability in a column section. CPM's are defined by their stationary points (singularities, pinch points, nodes) and it is relatively quick and cheap to determine the topology qualitatively and classify regions of instability, such as operating the column close to the triangular region. This might result in profiles going in the opposite direction from that desired.

Mathematically CPM's as well as RCM's are not bounded by the MBT, although only profiles inside the MBT are realistic concentration profiles. However the knowledge of the behaviour of the outside topology can be of great use. We have shown that transforming the space by changing the transformation parameters X_Δ and R_Δ outside profiles can be shifted inside the MBT, to become realistic concentration profiles. We also showed that the vertices of the triangles move along the pinch locus and how this is a powerful tool for understanding the shifting of the topology. It is now up to the designer to transform the space such

that the separation becomes optimal. This could revolutionise the way separation processes are designed. The designer now has the freedom to dictate the system behaviour as opposed to being constrained by it. There are of course limitations for the designing of separation processes. These include mass balance constraints and energy requirements. However we have shown that there are vastly different topologies attainable even for constant relative volatility systems, by choosing the respective transformation parameters. One can expect a lot more diversity for azeotropic systems, but this is beyond the scope of this paper.

Chapter 3:

Column Profile Maps

2. Singular Points and Phase Diagram

Behaviour in Ideal and Non-Ideal Systems

This work was published as the second part of a CPM series, in Industrial and Engineering Chemistry Research (see Holland et al, 2004 a). Although my name appears as first author on this paper, the work is almost exclusively Michaela Tapp's.

Abstract

Column Profile Maps.1. Derivation and Interpretation, (see chapter 2) analysed the behaviour of distillation systems by using column profile maps which are generated by using the difference point equation. Ideal thermo was assumed and it has been shown how using CPM's one can devise more creative designs. Part B focuses on extending the ideas to non – ideal thermo and develops tools for synthesis of distillation for ideal and non – ideal systems by looking at eigenvalues and eigenvectors and how one can characterize, explain and manipulate the behaviour of systems by moving the singular points.

3.1 Introduction

Early attempts to explain the nature of separation processes began in the 1900's when Schreinemakers (1902) developed an experimental technique to measure residue curves. He formally defined the residue curve as the locus of the liquid composition remaining from a simple distillation process. By starting with different liquid compositions, a set of unique residue curves is formed. This set of residue curves that falls in the mass balance constraint space is called a *residue curve map.* For ternary mixtures, these features can be represented by means of a ternary diagram. Hausen (1952) and Rishe (1955) showed that the residue curve can represent the composition profile of a packed distillation column at infinite reflux. A residue curve map therefore represents all possible operational composition profiles in a packed column at infinite reflux. Although only directly useful in ternary and quaternary systems, great insights into higher order systems can be gleaned by the analysis of various groups of ternary (or quaternary) mixtures of which the system comprises. In the late 1960s Zharov (1967; 1968c) gave a more rigorous mathematical foundation for the residue curve map analysis and expanded it to multicomponent mixtures.

In the 1980's Van Dongen & Doherty (1985) introduced the concept of nonlinear autonomous ordinary differential equations (ODE's) as a shortcut design tool to determine the composition profiles along the length of a distillation column. The differential approximation models the liquid phase composition profile in both the rectifying and the stripping sections of the column. Vogelpohl (1964) showed that the set of differential equations describing the simple distillation process is identical to the one for the concentration profiles of packed columns operated at total (infinite) reflux when the mass transfer coefficient is unity. Van Dongen and Doherty (1985) also demonstrated that the results yielded by a differential column model and by stage by stage calculation are very similar. Moreover, the simplicity and the accuracy of the first order differential approximation make it the preferred model for design calculations. While these ODE's model the rectifying and the stripping sections of a distillation column, they do not describe the transition from

the rectifying to stripping sections and are therefore no longer valid at the feed stage. (Doherty (1977) used the mathematical approach on ODE's to determine the occurrence of singularities in ideal and azeotropic RCM's.)

The use of the stage by stage or the differential approximation model helps to solve specific design problems involving multi-component separation, by numerical calculation. Such calculations usually involve rigorous iteration. They do not contribute very much to our ability to produce generalisations or an analytical theory of multi-component separation neither do they provide an intellectual framework to better understand the options in designing separation processes. In this paper we will use original ideas developed by Franklin (1986). He interpreted the z-transformation method used by Underwood (1948). Based on Underwood's equations and the assumptions of constant relative volatility and constant molar flows he analysed counter-current cascades. He showed that composition profile maps for finite reflux columns are transforms of the infinite case.

This paper is the second of the series Column Profile Maps (CPM's). The objective of the first part: Column Profile Maps Part. 1. Derivation and Interpretation, (see chapter 2) was to analyze the behaviour of column profile maps for ideal systems and to show that CPM's are maps describing the topology for finite reflux conditions and they are in fact transforms of the residue curve map as the difference point equation (DPE) is a linear transform of the residue curve equation. In this paper we will explore ODE's, and in particular the difference point equation, and develop synthesis tools for ideal and non-ideal systems which can be of great use for column design. This approach will enable us to characterize, explain and manipulate the behaviour of systems by moving the singular points. It will create a better understanding of multi-component separation, i.e. systematic finding of operating conditions corresponding to a specific behaviour of the mathematical model. Vogelpohl (1999) mentioned composition profiles which extend beyond the composition triangle (Gibbs triangle or mass balance triangle). These profiles have no physical meaning, but we will show how they can be used in order to achieve a desired separation.

3.2 Ideal systems

The objective of this paper is to show that system behaviour can be characterized by the study of singular points (stationary points) - see Doherty (1977). Therefore, it is necessary to look at these points in more detail. Singular points in distillation are pure components, azeotropes and pinch points. These points are defined by $dx/dn = 0$. It has been shown in Appendix B that at every point in the space X_S, one can calculate a set of eigenvalues and eigenvectors. The eigenvalues characterise the type of singularity that can occur at that point in space while the eigenvectors characterise the asymptotic direction of the trajectories in the neighbourhood of the singularity.

Assuming constant relative volatilities α_i and equimolar overflow, $y_i(x)$ can be expressed as:

$$y_i(x) = \frac{x_i \alpha_{iN}}{\displaystyle\sum_{i=1}^{N} x_i \alpha_{iN}}$$

(3.1)

where N is the index of the heavy component

There exists a unique eigenvector map for each system i.e. in this case for a particular set of α_I (for detailed information see Appendix B). The eigenvector map can be obtained by plotting the eigenvectors over a range of x, as shown in Figure 3.1 with $\alpha_{12} = 2$, $\alpha_{22} = 1$ and $\alpha_{32} = 1.5$.
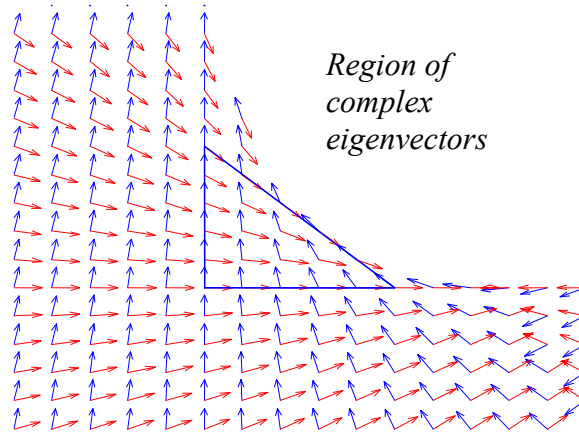
Figure 3.1: Eigenvector map for an ideal system.
The compositions x_1 and x_2 range from $x_i = [-1..2]$.

The region of complex eigenvectors in Figure 3.1 is a result of complex roots of the characteristic equation. There is no determinable asymptotic direction in the real space. Hence this region has stationary points that comprise of midpoints and stable/unstable foci only, whereas in the region of determinable eigenvectors in the real space there are stable/unstable nodes, saddles and half nodes. To make use of the eigenvectors we have to determine the number, position and the kind of the singularities occurring. Singular points are defined by $dx/dn = 0$ hence the number of singularities is defined by the order of the thermodynamic model used. Ideal systems are modelled by a cubic function (see Equation 3.1) thus the number of singularities is always three. The kind and the positions of these three singularities depend on the choice of the parameters X_Δ and R_Δ in the difference point equation (Equation 2.1).

3.2.1 Infinite reflux

We will start with the case $R_\Delta \rightarrow \pm \infty$. In analogy to the eigenvector map there exists an eigenvalue map, as shown in Figure 3.2.
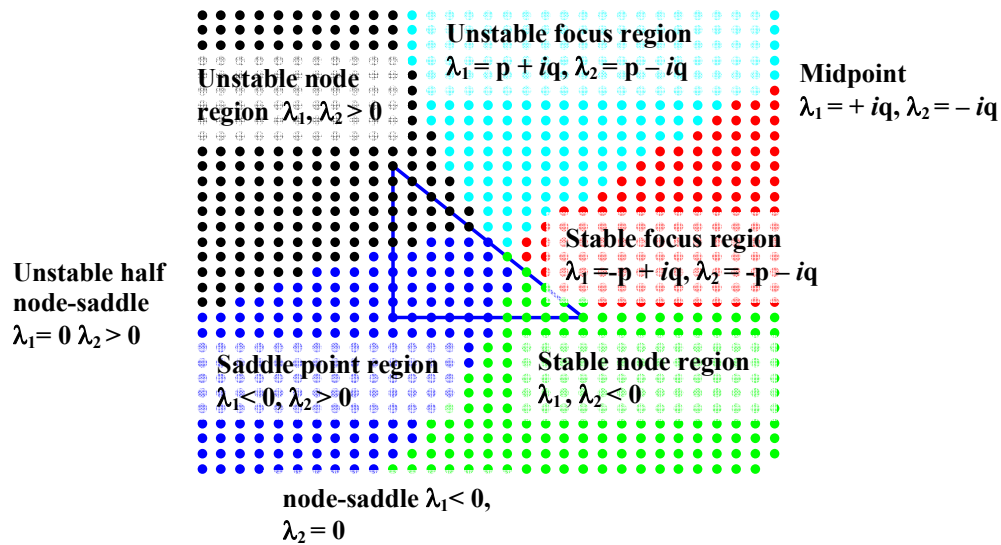
Figure 3.2: **Eigenvalue map for an ideal system for $R_\Delta \to \pm\infty$.**
The compositions x_1 and x_2 range from $x_i = [-1..2]$.

The eigenvalue map in Figure 3.2 shows discrete regions of node types in the x_1, x_2-space. A singularity occurring at $x_1=1$, $x_2=0$ would be of the stable node kind, while a singularity at $x_1=0$, $x_2=0$ results in a saddle point. The eigenvalues in the x_1 - x_2 space are continuous, hence the border between these regions is uniquely defined. The border between the unstable and the saddle point region is characterized by $\lambda_1 = 0$, $\lambda_2 > 0$. This describes an unstable half node-saddle. In analogy to the above, a singularity appearing at the saddle point/stable node border would be of the stable half node-saddle kind, with $\lambda_1 < 0$, $\lambda_2 = 0$ These points can be calculated for the condition that for the entries of the n x n matrix $J(X_S) = [a_{ij}]$ holds: $a_{11} \ a_{22} = a_{12} \ a_{21}$. The border between the unstable and the stable focus region shows interesting behaviour as well. A singularity in the unstable/stable focus region is defined by $p + iq$, $\lambda_2 = p - iq$, with $p > 0$, $q \neq 0$ (unstable) or $p < 0$, $q \neq 0$ (stable). A continuous change of eigenvalues leads to a border region, that is defined by $p = 0$, $q \neq 0$ this classifies the singularity occurring at the border between the two complex regions as a midpoint. These points can be calculated for the condition that for the entries of the n x n matrix $J(X_S) = [a_{ij}]$ as defined in Appendix B holds: $a_{11} = -a_{22}$.

Solving Equation 3.2 for $R_\Delta \to \infty$ leads to leads to three distinct and real solutions

$X_s = \{\mathbb{R}_1 \neq \mathbb{R}_2 \neq \mathbb{R}_3\}$. This is not surprising, as these solutions represent the three

pure components however, it is interesting to note, that this applies for the entire

space $x \in \mathbb{R}$. By entire space we refer to profiles outside the mass balance triangle;

see Figure 3.3.
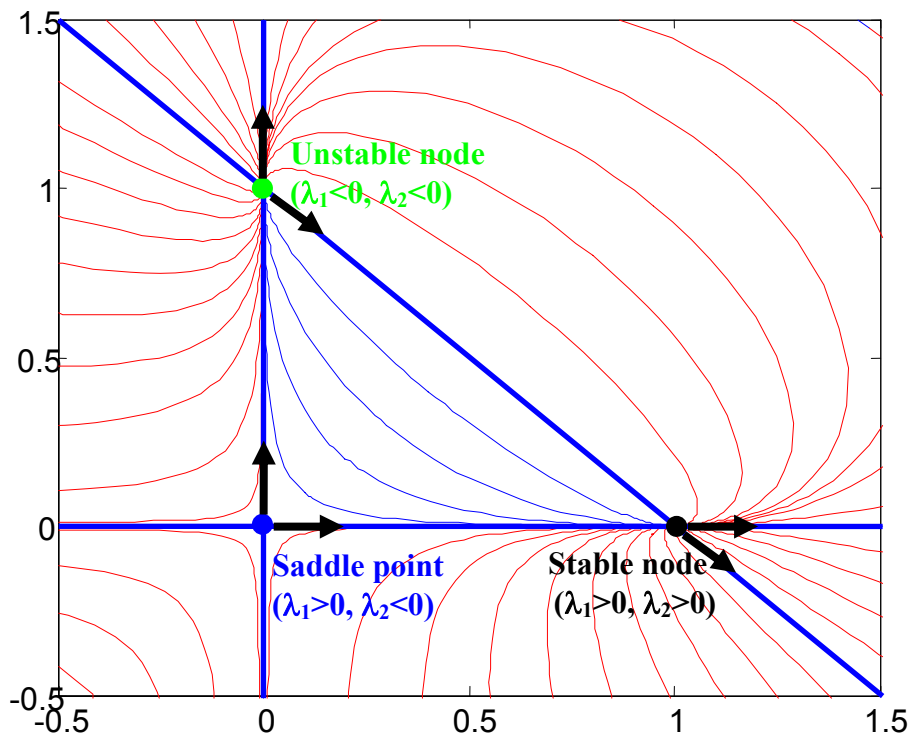
Figure 3.3: Entire Residue curve map for ideal systems with the respective classification of the nodes.

As mentioned in the introduction, these profiles have been introduced by Vogelpohl (1964). They have no physical meaning, however they play an important role in understanding the system behaviour, as parts of it can be shifted inside the MBT, but this will be discussed at a later stage.

Doherty and Perkins (1977), showed, that for ideal c–component mixtures there are exactly c singular points. Evaluating $J(X_s)$ and solving the roots of the characteristic equation lead to a stable, unstable node and a saddle, with the respective eigenvectors pointing along the axes of the composition triangle; see

Figure 3.3. Extending the axis of the mass balance triangle shows, that there exist two eigenvectors that are collinear on each axis and we therefore can conclude, that the axes are straight. This appears as a natural observation due to the mass balance constraint. However the lines connecting the singularities are straight for ideal systems. Knowing the direction of the eigenvectors, the kind, number and position of the singularities enables us to draw any ideal system CPM qualitatively. Doherty and Perkins (1977) also stated that there is exactly one stable node (corresponding to the least volatile component) one unstable node (corresponding to the most volatile component) and (c-2) saddles. This is not always true, as we will now show.

3.2.2 Finite reflux

Solving the difference point equation for an ideal ternary mixture, with a specified R_Δ and X_Δ, leads to three solutions. However depending on the choice of R_Δ and X_Δ there are certain types of solutions that occur. The cases of singularities X_s with the resulting roots λ_1, λ_2 for ideal ternary mixtures are listed in Table 3.1:

	Nature of solutions	*Type of Nodes occurring*	*No of nodes*	
Case 1	$X_s = \{\mathbb{R}_1 \neq \mathbb{R}_2 \neq \mathbb{R}_3\}$	Unstable ($\lambda_1 < 0$, $\lambda_2 < 0$)	1	3
		Stable ($\lambda_1 > 0$, $\lambda_2 > 0$)	1	
		Saddle point ($\lambda_1 > 0$, $\lambda_2 < 0$)	1	
Case 2	$X_s = \{\mathbb{R}_1 \neq \mathbb{R}_2 = \mathbb{R}_3\}$	stable/unstable ($\lambda_1 = \lambda_2 > / <0$)	1	2
		half unstable-saddle/ half stable- saddle ($\lambda_1 = 0$, $\lambda_2 < 0 / \lambda_2 > 0$)	1	
Case 3	$X_s = \{\mathbb{R}_1, \mathbb{C}_2, \mathbb{C}_3^*\}$	stable/ unstable focus ($p < 0$, $q \neq 0$ / $p > 0$, $q \neq 0$) or midpoint ($p = 0$, $q \neq 0$)	1	1

Table 3.1: The three different cases of solutions for an ideal ternary system and the resulting type and number of nodes occurring in the phase diagram.

The phase diagrams for finite reflux ratios are called column profile maps (CPM's). They are linear transforms of the RCM and thus consist of a triangular region if singularities of case 1 occur. The triangular region is determined by the direction of the eigenvectors at X_s. Examples of the phase diagrams for the different cases with the respective R_Δ, X_Δ and the eigenvectors are shown in Figure 3.4 to Figure 3.6.
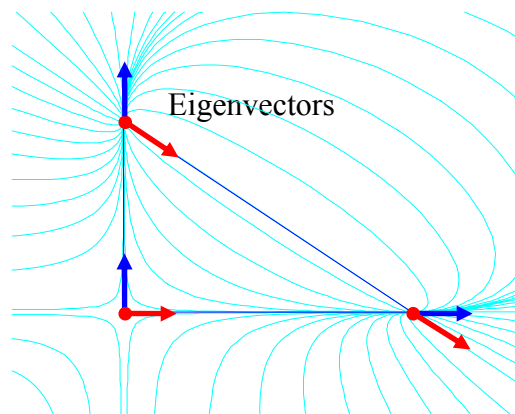
Figure 3.4: Example for case 1 singularities with the respective eigenvectors for $R_\Delta \rightarrow \infty$.
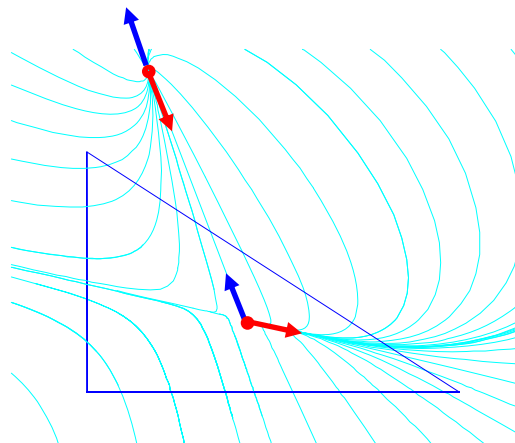
Figure 3.5: Example for case 2 singularities with the respective eigenvectors for $R_\Delta = 5$ and $X_\Delta = [-0.35\ 1.00]$.
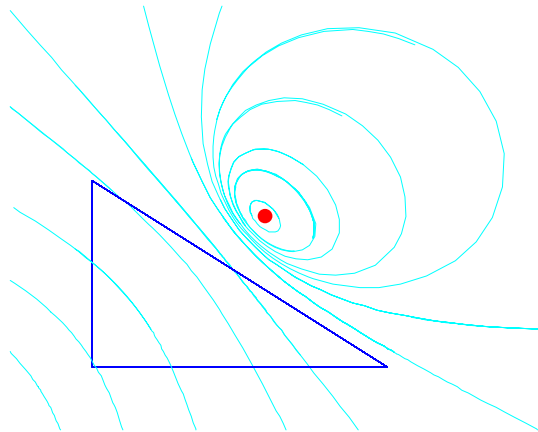
Figure 3.6: Example for case 3 (midpoint)
singularities with $R_\Delta = 5$ and $X_\Delta = [-0.74\ 2]$.

The design parameters R_Δ and X_Δ in ideal systems

The parameters R_Δ and X_Δ play an important role in determining the occurrence and the type of singularities and therefore the behaviour of the system. In addition, they are design parameters for separation processes. By varying the flowrate ratio R_Δ in column sections, the designer shifts the eigenvalues of the system independently of the difference point composition X_Δ. This is because the eigenvalues are a function of the thermodynamic data and R_Δ only. Let us look at the eigenvalue map changes for different R_Δ. Figure 3.7 and Figure 3.8 show eigenvalue maps for $R_\Delta = 4$ and $R_\Delta = -2$.

Eigenvalue maps apply for every column that runs at that particular reflux ratio R_Δ, hence there are an infinite number of difference points X_Δ available for the eigenvalue maps shown in Figure 3.7 and Figure 3.8. Figure 3.7a and Figure 3.8a each show one possible CPM for a specific X_Δ.
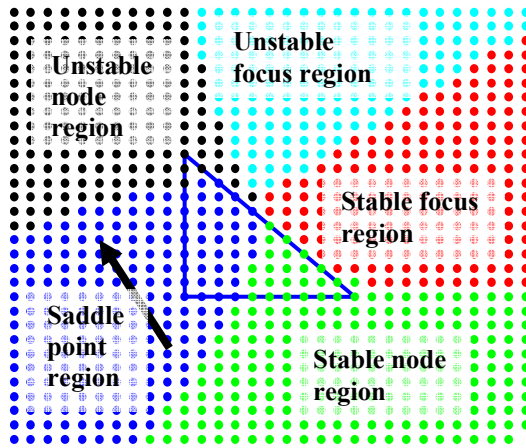
Figure 3.7: Eigenvalue map for $R_\Delta = 4$ and x = [-1..2].
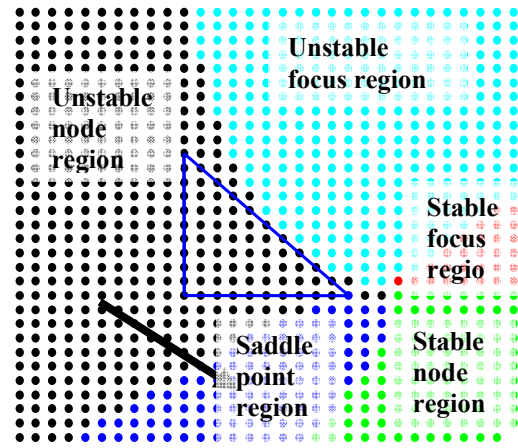
Figure 3.8: Eigenvalue map for $R_\Delta = -2$ and x = [-1..2].
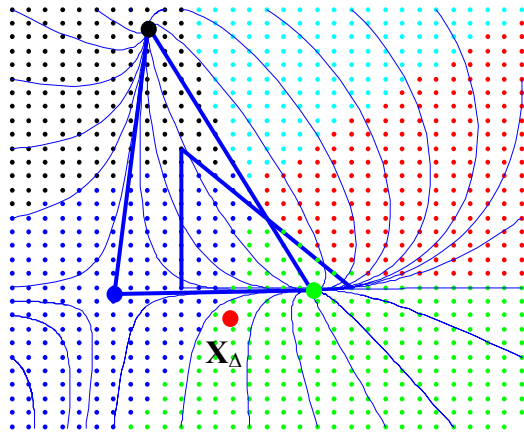
Figure 3.7a: CPM for $R_\Delta = 4$, $X_\Delta = [0.4\ -0.1]$ and x = [-1..2].
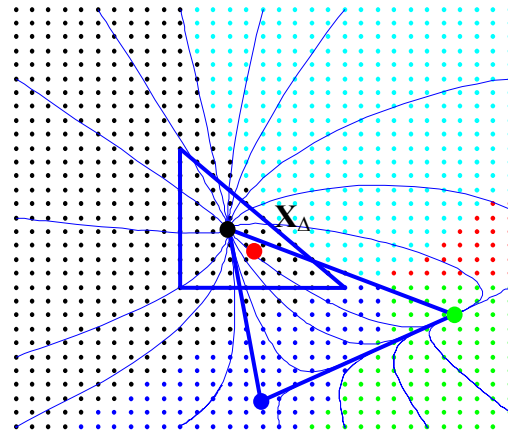
Figure 3.8a: CPM for $R_\Delta = -2$, $X_\Delta = [0.4\ -0.1]$ and x = [-1..2].

$R_\Delta = 4$ shifts the whole eigenvalue map "upwards" with respect to the eigenvalue map for $R_\Delta = \infty$, as indicated by the arrow in Figure 3.7. It is important to note, that the regions shift as a whole and the neighbouring relationships remain. The area inside the mass balance triangle still consists of an unstable, stable and saddle point region, however the size of the stable node region has increased, whereas the size of the unstable node region has decreased. $R_\Delta = -2$ shifts the map "downwards", see Figure 3.8. In this case the mass balance triangle is almost covered completely by the stable node region. In conclusion, a positive R_Δ shifts the map upwards, while a negative R_Δ shifts it downwards. Due to mass balance constraints and the thermodynamic models it is not possible to shift the complex region of eigenvalues into the mass balance triangle. Thus no midpoint or spiral

can be placed inside the MBT, although the profiles do get affected by singular points outside the MBT. However saddle points, nodes and half-nodes can be placed inside the MBT which results in a great variety of different CPM's.

Consider placing a saddle point at $X_S = [0.1\ 0.2]$. This would require a reflux ratio of approximately 4. To operate a column section the designer has to specify the second design parameter X_Δ. What impact does the choice of the difference point have on the above requirement and how can one manipulate it?

In chapter 2 we showed that the pinch point curve solely depends on the value of X_Δ. The pinch curve is the path that the singularities move in the space (inside and outside the MBT) and we established eight regions of different pinch point curve behaviour, depending on the position of X_Δ (see Figures 2.22a-f in chapter 2.3.2). By varying the difference point X_Δ, the difference in composition on top of the column section changes and the designer shifts the pinch point curve without changing the flowrate ratio necessarily inside the column section. In order to meet the above requirement, the designer has now to find the right pinch curve by choosing the appropriate X_Δ. According to the Figures 2.22a-f in chapter 2.3.2 pinch curve behaviour of the regions 3, 4, 6 and 7 would meet the requirements. (Only these pinch curves ran inside the MBT and connect the saddle point with either a stable or unstable node.) Figure 3.9 shows a difference point in region 6 that met the requirement.
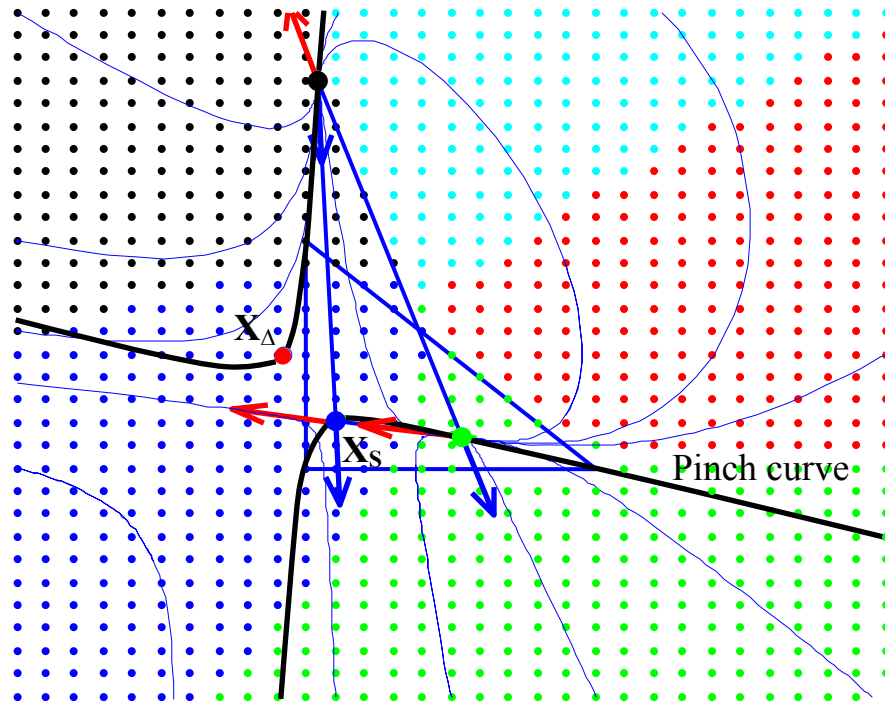
**Figure 3.9: CPM with a saddle point at X_S = [0.1 0.2] and the
design parameters R_Δ = 4 and X_Δ= [-0.08 0.5].**

Once the composition of one singularity and the pinch curve is known, the CPM
can be easily and quickly drawn qualitatively by determining the eigenvectors at
the singularities and extending their directions until they cross the pinch curve.
This determines the triangular region and therefore the CPM.

How is this helpful for design? The designers are in principle able to generate any
profile they want. As they can influence the type of singularity occurring by the
flowrate ratio and they can shift the pinch curves such that the position of the
singularity suits their design. We are going to demonstrate this on two examples.
Example 1 is a problem to sample the intermediate boiler in ideal systems. As the
node is described as a saddle point traditional design techniques require an infinite
number of stages for 100% purity. The objective is to generate a profile that runs
straight into the corner. This can be performed by transforming the system such,
that the resulting singularities offer a column profile map that achieves the desired
separation. This is shown in Figure 3.10.
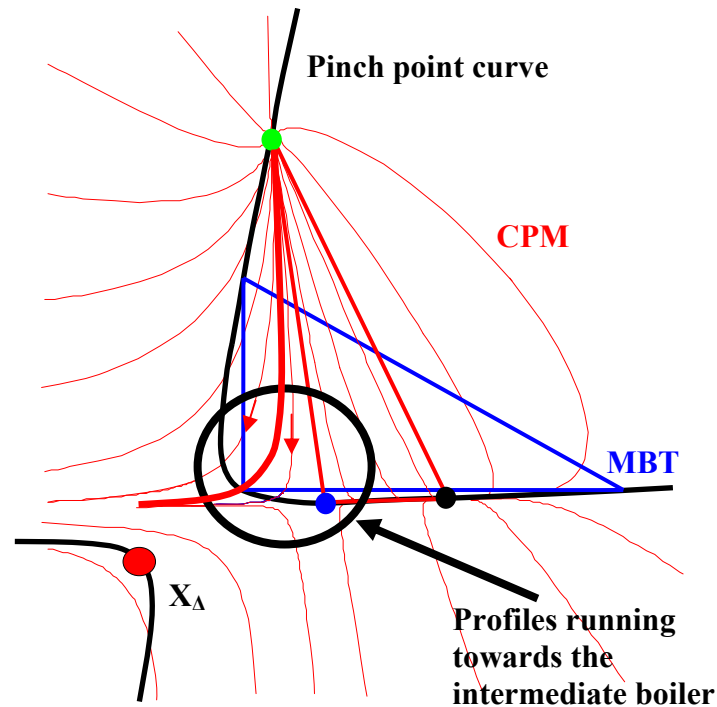
Figure 3.10: CPM with the parameters $R_\Delta = 8$ and $X_\Delta = [-0.3 \ -0.3]$.
The bold profile inside the circle runs direct into the intermediate boiler.

The bold line in Figure 3.10 represents the one profile that runs directly into the corner. In other words, looking at the liquid profiles only it seems to be possible to sample the intermediate component with a finite number of stages and 100% purity. However a feasible design needs to be checked with respect to the vapour phase as well and in this particular case the corresponding vapour profile runs outside the MBT. Is this specific for this case or is it in principal impossible because of thermodynamic limitations? We do not know the answer to this question yet although using this technique almost everything seems to be possible.

Example 2: For illustrative purposes we were asked to put a column section configuration together where the profiles show the word "Wits". In this case we could assume any needed feedstream to be available. The first column section needs to operate as a rectifying section with $X_{\Delta 1} = X_D$ thus the profile has to start at the difference point composition while the profile is represented by the dashed blue line in Figure 3.11.
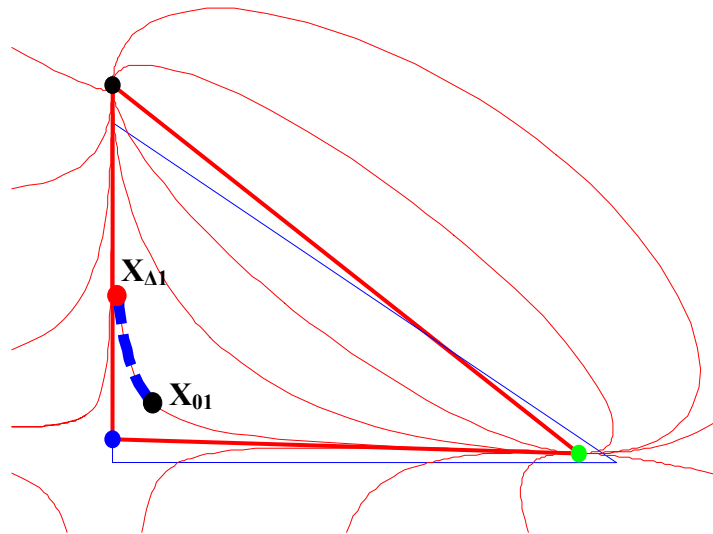
Figure 3.11: First profile of the sequence of column profiles that show the word "Wits".

The second column section needs to have a profile that runs in the opposite direction this has been realized by placing a saddle node close to the composition X_{01} (the difference point $X_{\Delta 2}$ for this CPM lies in region 6). The profile starting at X_{01} shows the second part of the "W", this is represented as the dashed blue line in Figure 3.12.
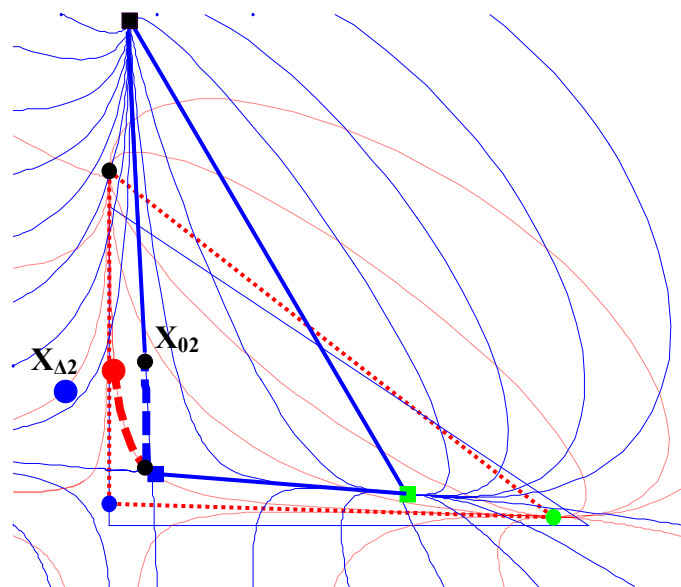
Figure 3.12: First and second profile of the sequence of column profiles that show the word "Wits".

In analogy to the above it is possible to assemble to whole word "Wits" with column profiles, see Figure 3.13. The entire column section configuration with the respective X_Δ and R_Δ is shown in Figure C.1 in Appendix C. The colours used for the column sections match the column profiles in Figure 3.13.
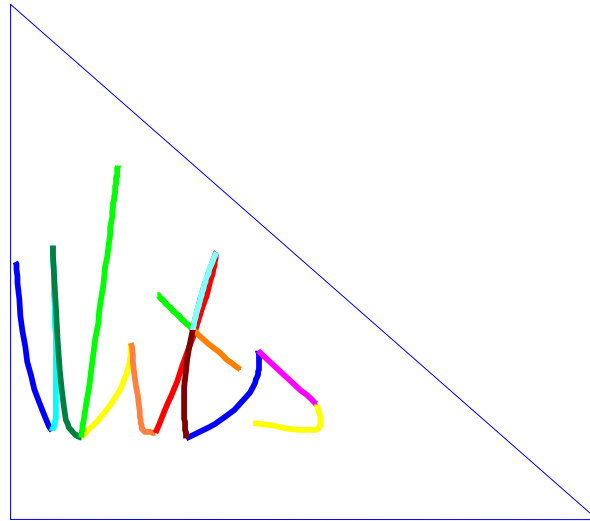
Figure 3.13: Sequence of column profiles that show the word "Wits".

3.3 Non-ideal systems

For non-constant relative volatility systems $y_i(x)$ can be expressed as:

$$y_i(x) = \frac{\gamma_i \, x_i \, P_{vap\,i}}{P_{tot}}$$

(3.2)

The total pressure P_{tot} of the system was set to one bar for all examples. The vapour pressure P_{vap} for each pure component can be calculated by using the Antoine equation:

$$P_{vap\,i} = \frac{\exp\left(A_i - \dfrac{B_i}{T + C_i + 273} \right)}{P_{tot} \, 760}$$

(3.3)

The NRTL (Non Random Two Liquid) model has been used to determine the liquid activity coefficient γ:

$$\gamma_i = \exp\left(\frac{\sum_j x_j \tau_{ji} G_{ji}}{\sum_k x_k G_{ki}} + \sum_j \frac{x_j G_{ij}}{\sum_k x_k G_{kj}} \left(\tau_{ij} - \frac{\sum_m x_m \tau_{mj} G_{mj}}{\sum_k x_k G_{kj}} \right) \right)$$

(3.4)

Where $G_{ij} = \exp\left(-c_{ij} + d_{ij}(T - 273.15K)\tau_{ij} \right)$ and $\tau_{ij} = a_{ij} + \dfrac{b_{ij}}{T} + e_{ij} \ln T + f_{ij} T$

The binary parameters a_{ij}, b_{ij}, c_{ij}, d_{ij}, e_{ij} and f_{ij} for the NRTL model can be determined from VLE and/or LLE data regression. ASPEN PLUS has a large number of built-in binary parameters. They have been regressed using the data from the Dortmund Databank.

Although the determination of the vapour composition in equilibrium with the liquid composition $y_i(x)$ for non-ideal systems is not as easy as for the ideal case, the eigenvectors for non-ideal systems are still a function of the thermodynamics only ($v = f(y_i(x))$) whereas the eigenvalues are a function of the thermodynamics and the reflux ratio ($\lambda = f(y_i(x), R_\Delta)$). In this paper we look at the acetone / benzene / chloroform system.

3.3.1   The benzene / chloroform / acetone system

Figure 3.14 shows the eigenvector map for the benzene / chloroform / acetone system.
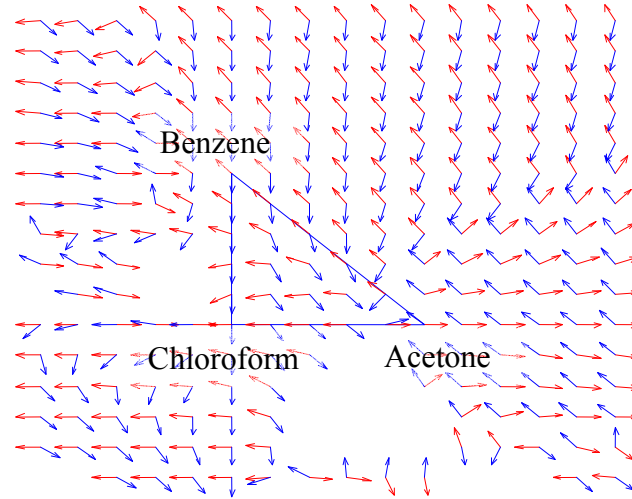
Figure 3.14: Eigenvector map for the benzene/chloroform/acetone system. The compositions x_1 and x_2 range from $x_i = [-1..2]$.

The empty spaces in Figure 3.14 correspond to region of complex eigenvectors and the resulting singularities are foci and midpoints. As a result of the thermodynamics, there is a great change in direction of the eigenvectors in some areas along the x_1 − axis. Hence changing the position of the nodes by transforming the space will result in a great variety of phase diagrams. The number of singularities in ideal systems is three, as the vapour in equilibrium is expressed by a cubic function. The determination of the order of the thermodynamic model used for non-ideal systems is not as easy, as this equation can not be solved algebraically.

Infinite reflux

The eigenvalue map for this system is shown in Figure 3.15. This system has three pure component singularities and one azeotrope on the chloroform acetone axis inside the MBT. The eigenvalue map shows that these are one unstable, one stable and two saddle points. And again the only possible singularities occurring inside the MBT are nodes, saddle points and half nodes as the complex regions can not be shifted inside the MBT.
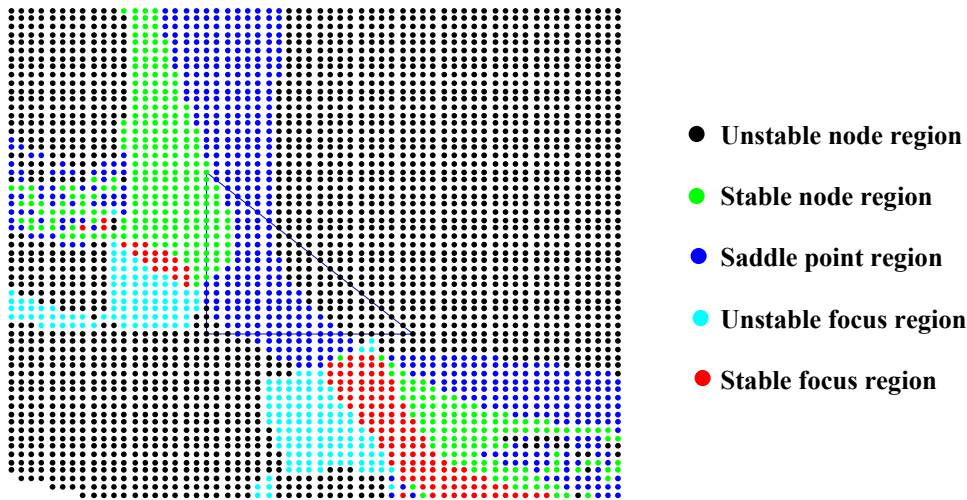
Figure 3.15: Eigenvalue map for the benzene/chloroform/acetone system for $R_\Delta \to \pm \infty$. The compositions x_1 and x_2 range from $x_i = [-1..2]$.

Superimposing the eigenvector and the eigenvalue map would show that the empty spaces in Figure 3.14 are filled with complex eigenvalues. It is also interesting to note, that the regions of great change in direction of the eigenvectors in Figure 3.14 correspond to regions in Figure 3.15 where small changes of x_1 creates large changes in eigenvalues. This is an indication of highly unstable regions. Comparing the eigenvalue map of Figure 3.15, with the eigenvalue map for ideal systems shown in Figure 3.2 shows that the maps can look quite different. However similar conclusions can be drawn. Singularities can be characterized with respect to the region in which they occur. The bordering regions indicate half nodes and midpoints occurring in the system. The border between the unstable (λ_1, $\lambda_2 > 0$) and the stable (λ_1, $\lambda_2 < 0$) region does not introduce a new singularity as both eigenvalues λ_1 and λ_2 have to be zero. The RCM of the benzene / chloroform / acetone system consists of three pure component nodes and a binary maximum boiling azeotrope node on the chloroform / acetone axis that are situated inside the MBT. However solving the differential equation for $dX/dn = 0$ gives more than four solutions. For x_1 and x_2 ranging from -1 to 2 seven solutions can be found. The eigenvalues and eigenvectors can be calculated and the phase diagram drawn; see Figure 3.16.
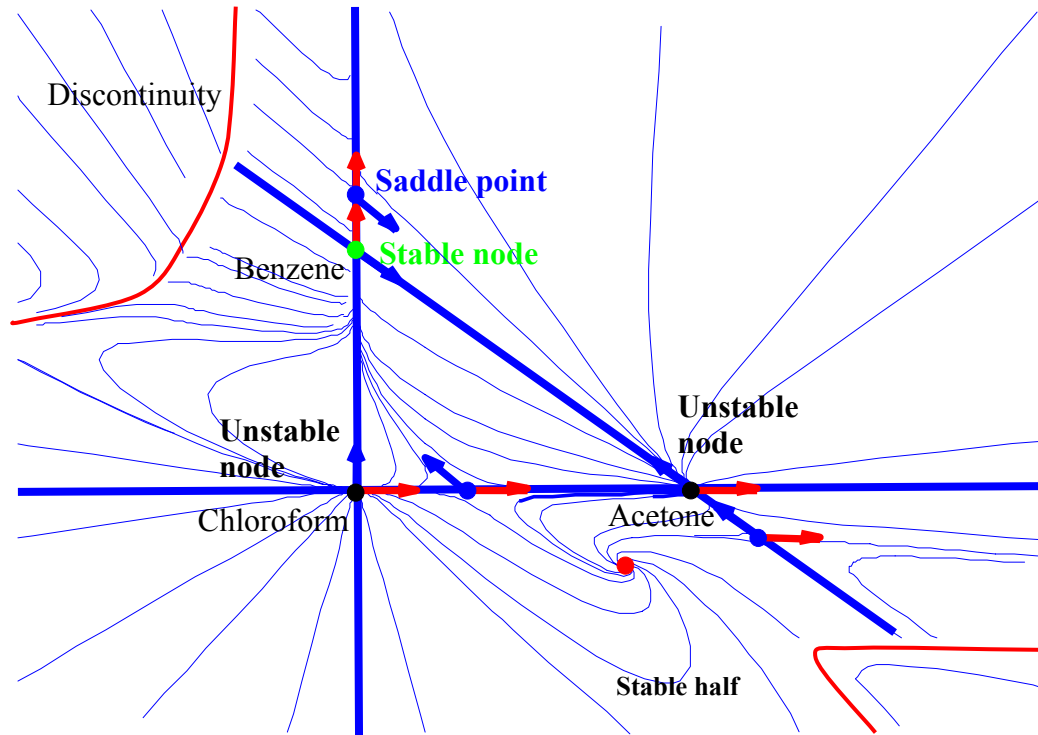
Figure 3.16: RCM for x_1 and x_2 ranging from -1 to 2 for the benzene/chloroform/acetone system with the eigenvectors and the eigenvalues at the nodes.

Figure 3.16 shows two regions in the phase diagram where the profiles are discontinuous. These regions correspond to the border region of stable and unstable singularities on the eigenvalue map. They also seem to affect the regions around it, as that is where the highly unstable regions occur. Discontinuities are inherent to the thermodynamic model. However they can not be moved by changing the parameters. This gives a limitation on what areas of the outside phase diagram can be shifted inside the MBT. It is also important to note, that the lines connecting the singularities are no longer straight. The only exceptions are the connectors of singularities that lie on the MBT or the extensions of the MBT.

Finite reflux

The ideal thermodynamic data dictated three singularities for every choice of X_Δ and R_Δ. Based on that, these singularities could be classified into three types of solutions, depending on the choice of X_Δ and R_Δ. The benzene/chloroform/acetone system has seven singularities, of which three are saddle points, two unstable nodes, one stable node and one stable focus; see Figure 3.16. As the differential

equation cannot be solved algebraically for dx/dn = 0, the different cases occurring in this system have been established by looking at the phase diagrams by varying R_Δ. These cases are listed in Table 3.2.

	Nature of solutions	*Type of Nodes occurring*	*No of nodes*	
Case 1	$X_s = \{\mathbb{R}_1{\neq}\mathbb{R}_2{\neq}\mathbb{R}_3{\neq}\mathbb{R}_4{\neq}\mathbb{R}_5{\neq}\mathbb{R}_6{\neq}\mathbb{R}_7\}$	Unstable	2	7
		Stable	1	
		Saddle point	3	
		Stable focus	1	
Case 2	$X_s = \{\mathbb{R}_1{\neq}\mathbb{R}_2{\neq}\mathbb{R}_3{\neq}\mathbb{R}_4{\neq}\mathbb{R}_5{\neq}\mathbb{R}_6{=}\mathbb{R}_7\}$	Unstable	1 (2)	6
		Stable	1 (0)	
		Saddle point	2	
		Stable focus	1	
		Unstable(Stable) half node saddle	1	
Case 3	$X_s = \{\mathbb{R}_1{\neq}\mathbb{R}_2{\neq}\mathbb{R}_3{\neq}\mathbb{R}_4{\neq}\mathbb{R}_5, \mathbb{C}_6, \mathbb{C}_7{}^*\}$	Unstable	1 (2)	5
		Stable	1 (0)	
		Saddle point	2	
		Stable focus	1	
Case 4	$X_s = \{\mathbb{R}_1{\neq}\mathbb{R}_2{\neq}\mathbb{R}_3{\neq}\mathbb{R}_4{=}\mathbb{R}_5, \mathbb{C}_6, \mathbb{C}_7{}^*\}$	Unstable	1	4
		Stable (focus)	1	
		Saddle point	1	
		Stable(Unstable) half node saddle	1	
Case 5	$X_s = \{\mathbb{R}_1{\neq}\mathbb{R}_2{\neq}\mathbb{R}_3, \mathbb{C}_4\,\mathbb{C}_5{}^*, \mathbb{C}_6, \mathbb{C}_7{}^*\}$	Unstable (focus)	1	3
		Stable	1	
		Saddle point	1	
Case 6	$X_s = \{\mathbb{R}_1{\neq}\mathbb{R}_2{=}\mathbb{R}_3, \mathbb{C}_4\,\mathbb{C}_5{}^*, \mathbb{C}_6, \mathbb{C}_7{}^*\}$	Unstable	1	2
		Stable half node saddle	1	
Case 7	$X_s = \{\mathbb{R}_1, \mathbb{C}_2\,\mathbb{C}_3{}^*, \mathbb{C}_4\,\mathbb{C}_5{}^*, \mathbb{C}_6, \mathbb{C}_7{}^*\}$	Unstable	1	1

Table 3.2: Cases of nodes occurring in the benzene/chloroform/acetone system.

A fixed X_Δ results in a unique pinch curve this is shown in Figure 3.17. Every point on the pinch curve is associated with a particular R_Δ and a certain eigenvalue and hence a certain node type. This is represented by the different colours in Figure 3.17. The RCM shown in Figure 3.17 would be an example of a phase diagram for case 1 in Table 3.2. All seven singularities are real and distinct.
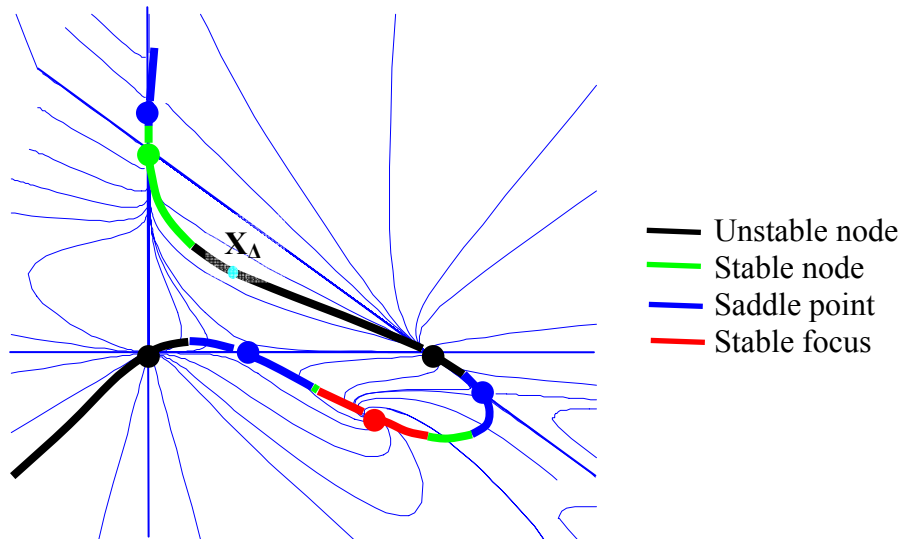
Figure 3.17: RCM with the respective singularities and pinch curve defined by $X_\Delta = [0.3\ 0.4]$ for the benzene/chloroform/acetone system.

Decreasing the reflux ratio moves the nodes along the directions indicated by the red arrow in Figure 3.18. Note: not all the nodes move in the same direction. At $R_\Delta = R_{\Delta 1}$ one unstable node merges with one saddle point to form an unstable half node saddle (Case 2).
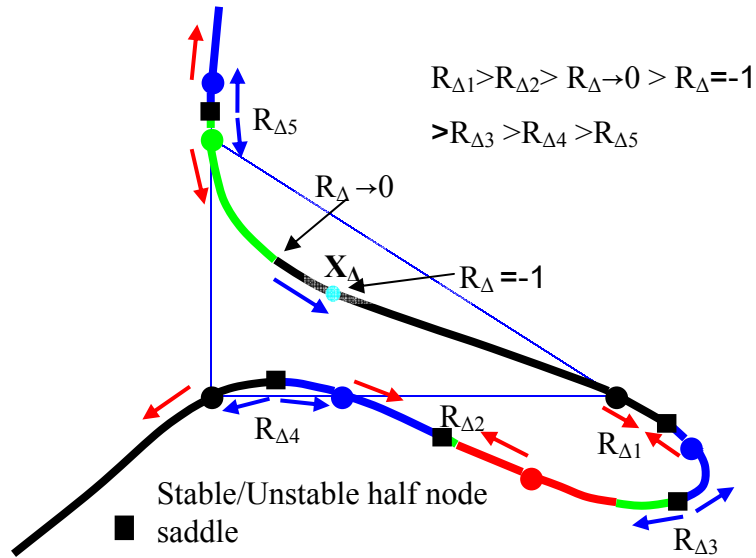
Figure 3.18: **The movement of the singularities by decreasing the reflux ratio from $R_\Delta \to +\infty$ to $R_\Delta \to -\infty$.**

Decreasing R_Δ further causes the non-elementary singularity to disappear into the complex space and Case 3 solutions occur until $R_\Delta = R_{\Delta 2}$ another saddle point merges with a stable node to form a stable half node saddle (Case 4). (In this example the stable focus changed into a stable node to merge with the saddle point. Further decrease to $R_{\Delta 2} > R_\Delta > 0$ results in solutions of case 5, the system consists of one unstable, one stable and one saddle point. At $R_\Delta \to 0$ the saddle point and the unstable node moved to infinity in the x_1-x_2 *space* and further movement changes the nature of the unstable node into a stable node and vice versa. $R_\Delta = -1$ results in X_Δ being the only solution. Further decrease shows one singularity moving along the unstable branch, this is captured as case 7 in Table 3.2. At $R_\Delta = R_{\Delta 3}$ a stable half node saddle emerges and two nodes determine the system (Case 6). The half node saddle separates by further reducing the reflux (Case 5). For $R_\Delta = R_{\Delta 4}$ another unstable half node saddle emerges (Case 4) and separates (Case 3). Finally for $R_\Delta = R_{\Delta 5}$ the last node emerges (Case 2) and separates (Case 1) until $R_\Delta \to -\infty$. Cases 5, 6 and 7 correspond to the three cases introduced for ideal systems. Examples of phase diagrams for cases 2-7 with the respective X_Δ and R_Δ are shown in Figures 3.19a-d and Figures 3.19e-f.

a) Case 2:

X_Δ=[0.54 -0.1 0.54], R_Δ=2.74 **System with six singularities**
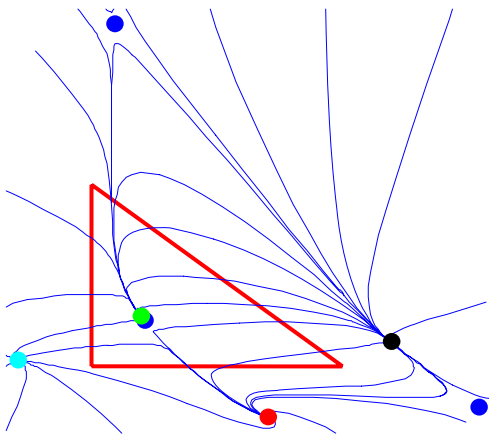
b) Case 3:

X_Δ = [0.3 0.4 0.3], R_Δ =10.9

System with five singularities
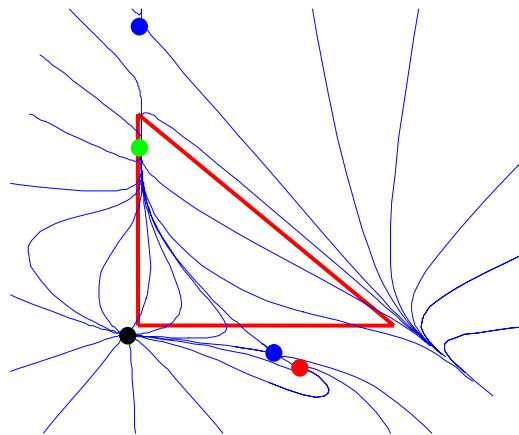
c) Case 4:

X_Δ = [0.3 0.4 0.3], R_Δ =-11.7

System with four singularities
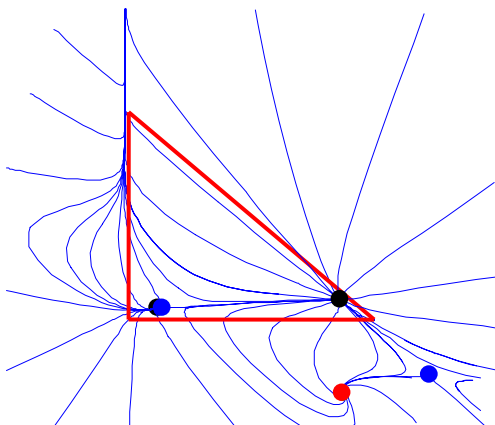
d) Case 5:

X_Δ = [1.2 -0.1 -0.1], R_Δ =3

System with three singularities
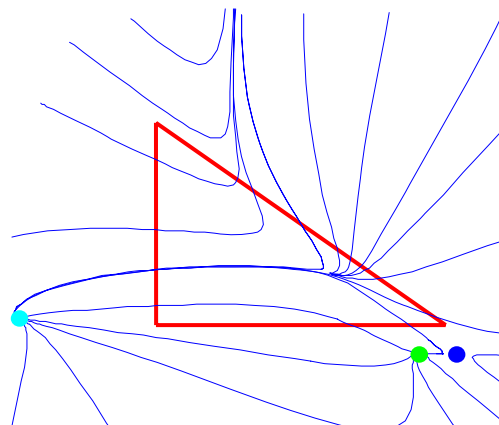
Figures 3.19a-d: Examples of phase diagrams for cases 2-5.

e) Case 6:

$X_\Delta = [0.54\ -0.1\ 0.54]$, $R_\Delta = 2.74$

System with two singularities
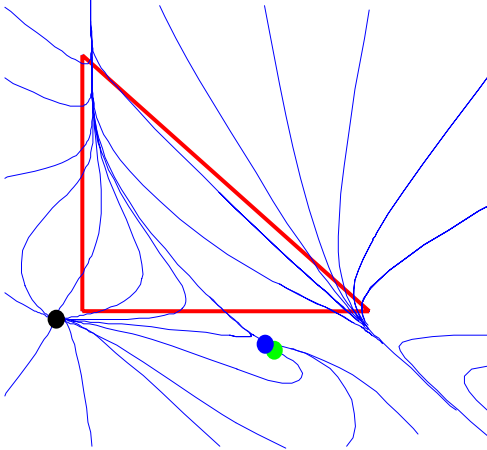
f) Case 7:

$X_\Delta = [1.2\ 0.5\ -0.7]$, $R_\Delta = 3$

System with one singularity
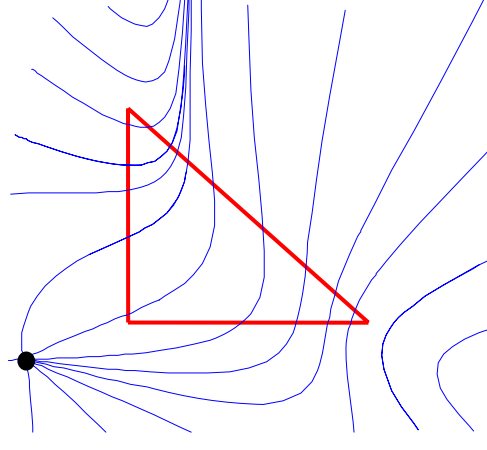
Figures 3.19 e-f: Examples of phase diagrams for cases 6 and 7.

All systems which comprise seven singularities can be divided into seven cases, however the types of nodes occurring is unique to the particular system being studied.

The design parameters R_Δ and X_Δ in non-ideal systems

Changing the flowrate ratio of a column section changes the value of R_Δ. As demonstrated for ideal systems, negative values of R_Δ shift the eigenvalue map downwards, whereas the eigenvalue map gets shifted upwards by positive values of R_Δ. This is shown in Figure 3.20a and Figure 3.20b. Placing a half node saddle inside the MBT would require a R_Δ of the order of two. Now to be able to create this singularity there the designer has to find an appropriate X_Δ in other words a pinch point curve that runs through that area.

● Unstable node region
● Stable node region
● Saddle point region

● Unstable focus region
● Stable focus region
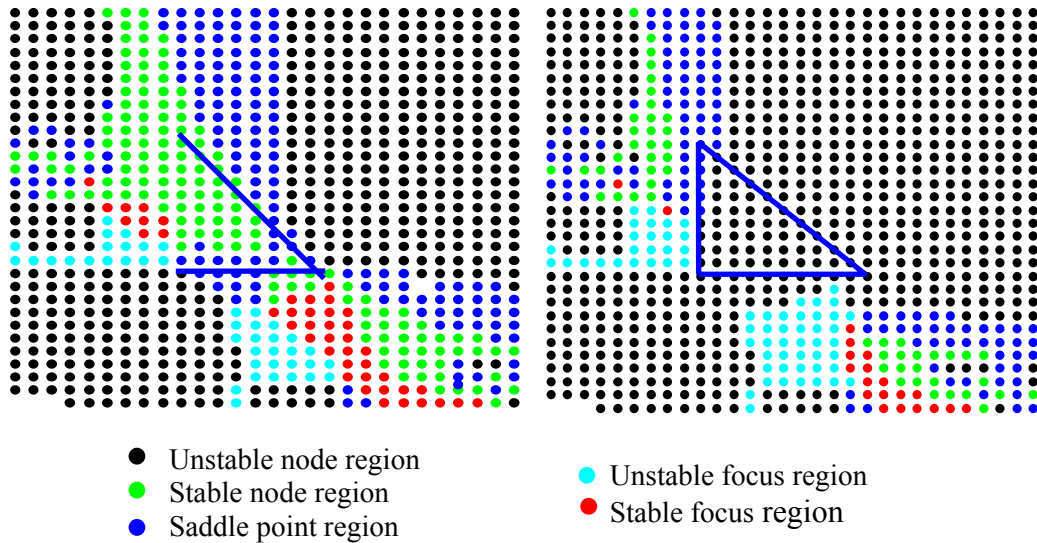
Figure 3.20a: Eigenvalue map for
$R_\Delta = 2$ and x = [-1..2].

Figure 3.20b: Eigenvalue map for
$R_\Delta = -2$ and x = [-1..2].

Ideal systems could be divided into eight regions of different X_Δ each of which show similar behaviour of the pinch point curves. These regions could be easily determined as they depend on the signs of X_Δ only and X_Δ changes sign as it crosses the lines obtained by connecting the singularities along the direction of the eigenvectors. This could be done, as all the profiles connecting the singularities are in fact straight lines, see Figure 3.4. We will refer to them as X_Δ - boundaries. X_Δ - boundaries divide regions of similar pinch curve behaviour, they cannot be crossed by pinch curves.

Non-ideal systems have lines and curves connecting singularities. These curves are called distillation boundaries. The benzene/chloroform/acetone system has five distillation boundaries, see Figure 3.21. Distillation boundaries are not X_Δ - boundaries as pinch curves can cross them. Current research is looking for ways to determine X_Δ - boundaries. Up to now these boundaries can only be determined by a parametric trial and error procedure which finds that X_Δ which results in a different pinch curve behaviour.

15 regions of similar pinch curve behaviour could be established for the benzene/chloroform/acetone system, this is shown in Figure 3.21.
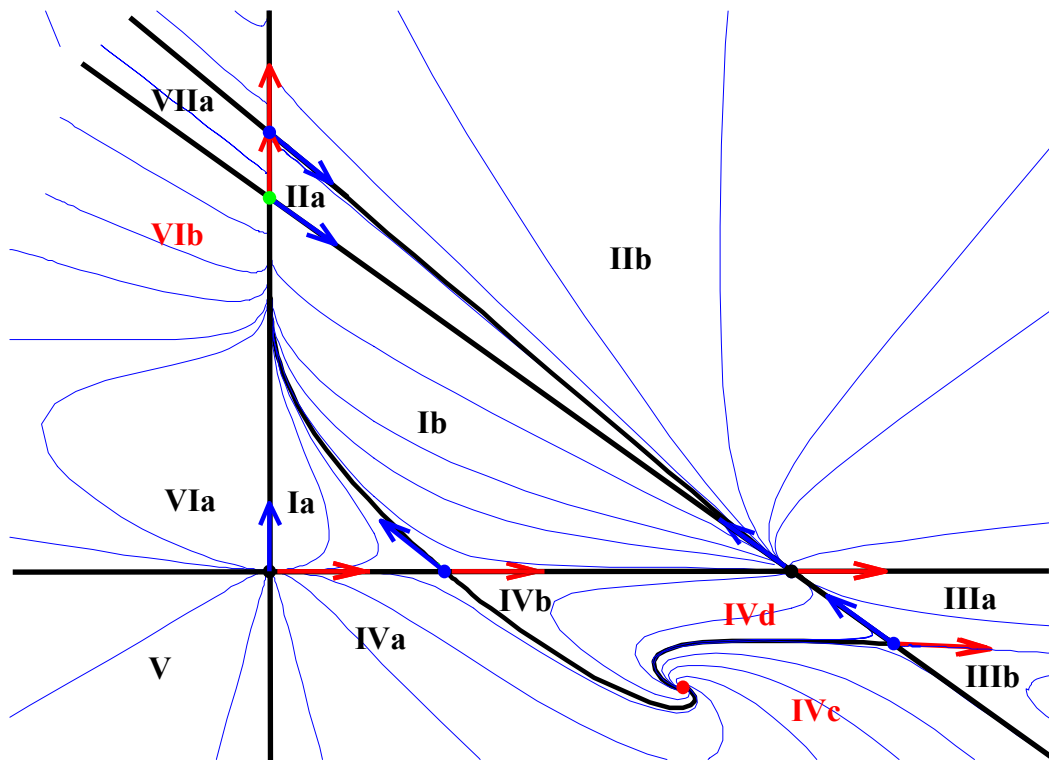
Figure 3.21: **The 15 regions of similar X_Δ for the benzene/chloroform/acetone system.**

The resulting pinch curves in these regions are shown in Figures 3.22a-o. The different colours show the kind of singularity occurring on the pinch point curve.

a) Region Ia : $X_\Delta = [0.1\ 0.2\ 0.7]$
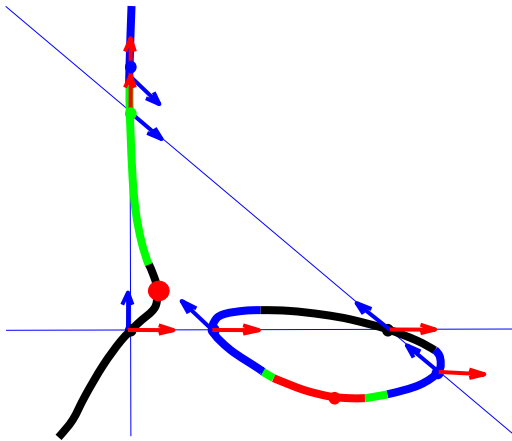
b) Region Ib : $X_\Delta = [0.3\ 0.4\ 0.3]$
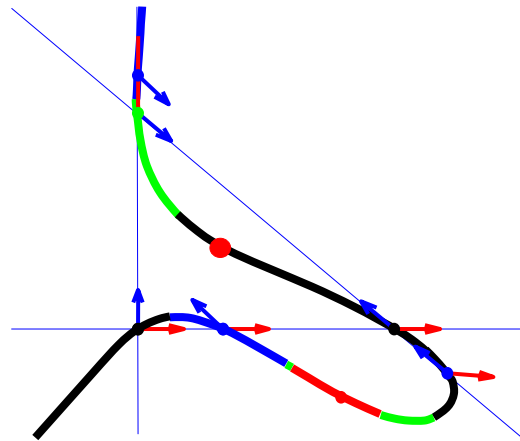
c) Region IIa : $X_\Delta = [0.05\ 1.05\ -0.1]$
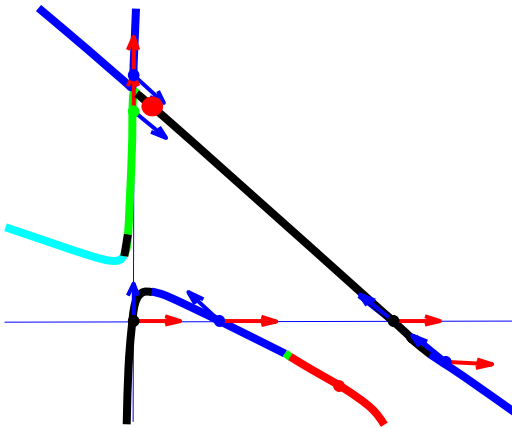
d) Region IIb : $X_\Delta = [1.2\ 0.5\ -0.7]$
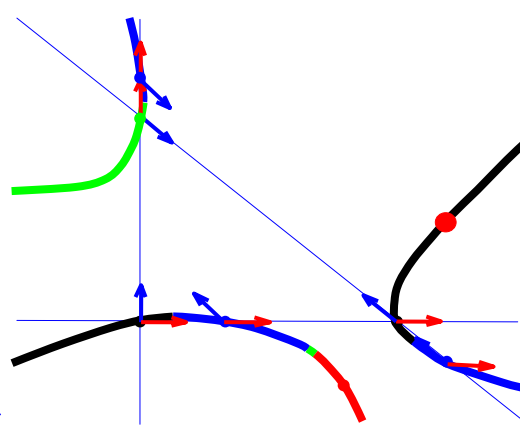
e) Region IIIa : $X_\Delta = [1.2\ -0.1\ -0.1]$
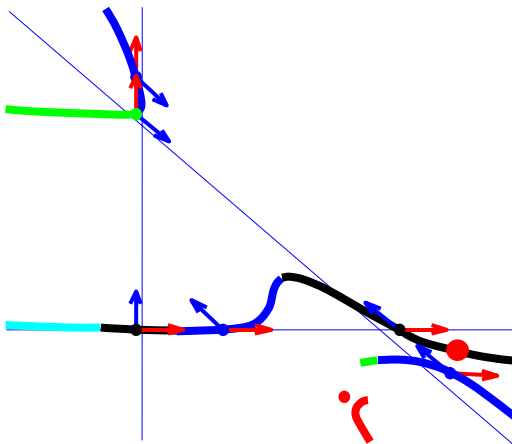
f) Region IIIb : $X_\Delta = [1.4\ -0.3\ -0.1]$
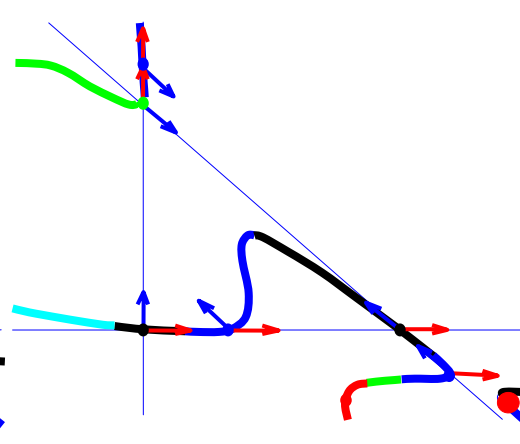
Figures 3.22a-f: All sets of different pinch loci for fixed X_Δ in the 15 different regions.

g) Region IVa : $X_\Delta = [0.1\ -0.2\ 1.1]$

h) Region IVb : $X_\Delta = [0.54\ -0.1\ 0.56]$

i) Region IVc : $X_\Delta = [1.1\ -0.4\ 0.3]$

j) Region IVd : $X_\Delta = [0.97\ -0.15\ 0.18]$

k) Region V : $X_\Delta = [-0.1\ -0.1\ 1.2]$

l) Region VIa : $X_\Delta = [-0.2\ 0.2\ 1]$
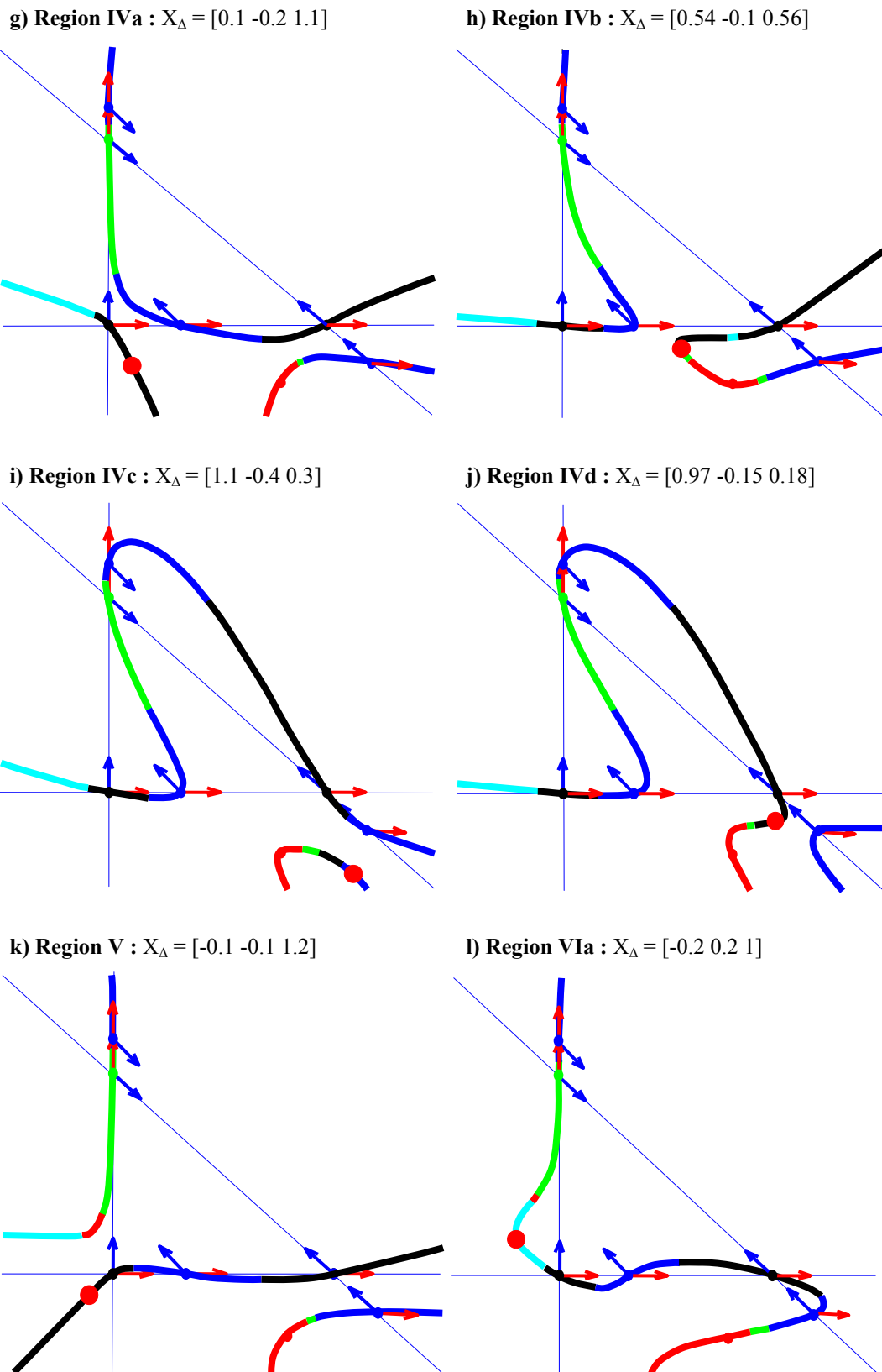
Figures 3.22 g-l: All sets of different pinch loci for fixed X_Δ in the 15 different regions

m) Region VIb:X_Δ=[-0.14 0.9 0.24]   **n) Region VIIa** : X_Δ = [-0.1 1.2 -0.1]

o) Region VIIb : X_Δ = [-0.2 1.7 -0.5]
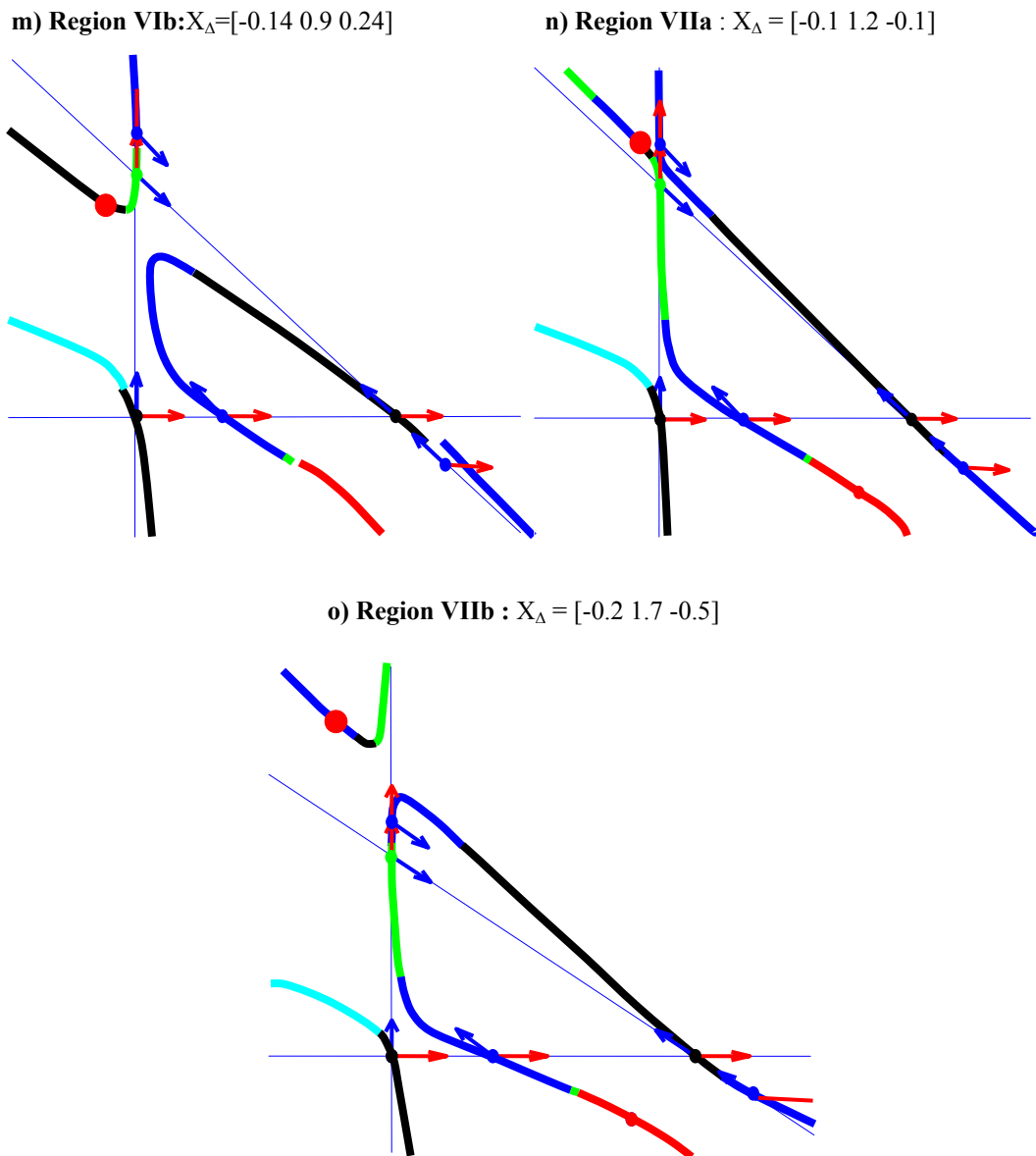
Figures 3.22m-o: All sets of different pinch loci for fixed X_Δ in the 15 different regions.

What importance do X_Δ - boundaries have and how can they be used for a better understanding of the system and for designing separation processes? These questions will be answered in the next section.

Crossing distillation boundaries

Let us first understand how this knowledge can be used to get a greater understanding for designing separation processes. There has been much discussion in the literature regarding whether column profiles can cross distillation boundaries and by how much. Wahnschafft (1992) showed that it was

possible to cross distillation boundaries for infinite and finite reflux ratios. Crossing boundaries at infinite reflux requires a sequence of columns and a curved distillation boundary. Crossing boundaries at finite reflux can be done in a single rectifying or stripping section of a column, but it is only possible, if the boundary is sufficiently curved, the distillate or bottoms composition lies close and on the convex side of it and the distillation column operates over a certain range of reflux ratios. If these criteria are met the profiles "flip over" the distillation boundary; see Figure 3.23. This phenomenon has been known for more than a decade, but there is now explanation on why it happens and on how to determine the critical reflux ratio that makes the profiles flip over.
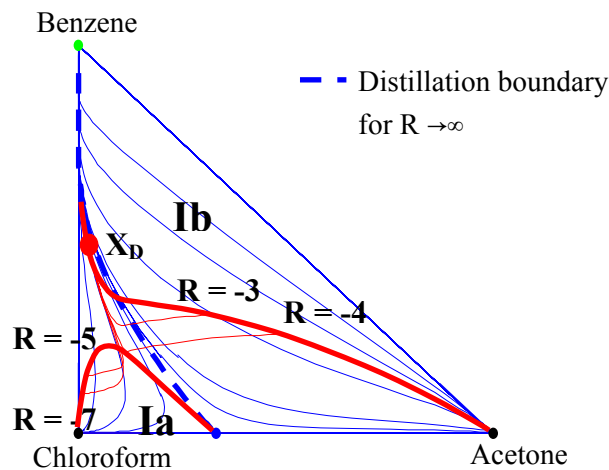
Figure 3.23: **"Flipping over" of profiles for certain reflux ratios which cross the distillation boundary from region** Ib **to region** Ia.

How can we explain this phenomenon? X_D lies close to the boundary on the concave side. The pinch curve shows pinch curve behaviour of type Ib (the pinch curve crossed the distillation boundary). The residue curve through X_D pinches at the pure chloroform node. Decreasing the reflux ratio moves the unstable chloroform node and the saddle node (azeotrope on the chloroform-acetone axis) towards each other along the pinch curve. At R = -4 the CPM has shifted so far up the pinch point curve, that the distillation boundary for the CPM runs through the distillate composition X_D. Figure 3.24 shows the column profile map for R = -4 (X_D = [0.02 0.5]).
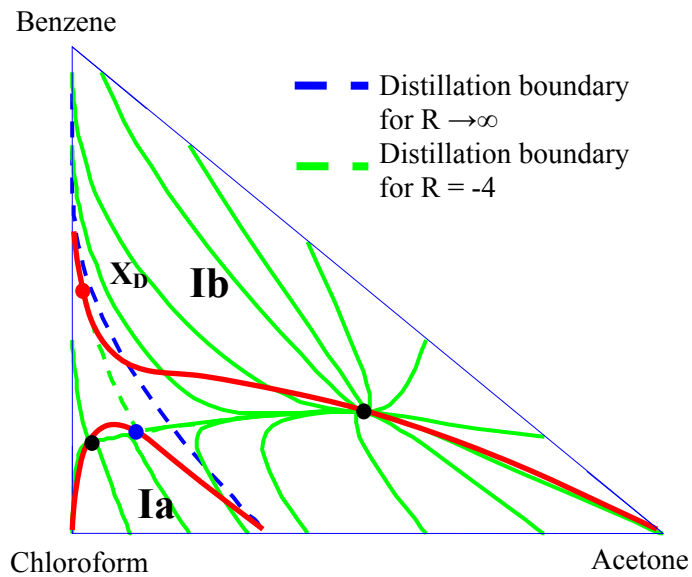
Figure 3.24: **Column profile map inside the MBT for X_D/X_B = [0.02 0.5] and R = -4. The respective pinch curve is shown as the red line. The dashed lines represent the distillation boundaries for R →∞ (blue) and R = -7 (green).**

This represents the last reflux ratio that crosses the distillation boundary for R →∞.Every smaller R results in profiles that pinch in region Ia. What happens if X_{D2} moves further away from the distillation boundary for R →∞.? An X_{D2} of [0.01 0.5] results in a type Ia pinch curve behaviour, this is shown as the green line in Figure 3.25.
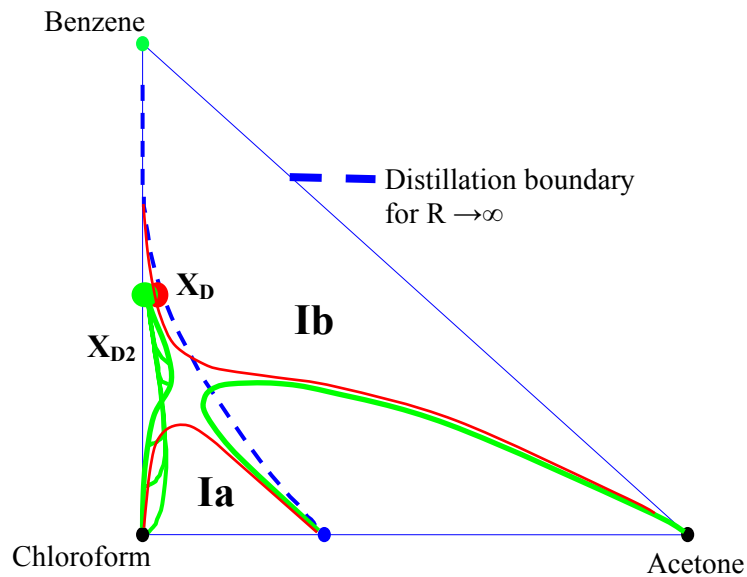
Figure 3.25: **Pinch curves inside the MBT for X_D = [0.01 0.5] (type Ia)
and X_{D2} = [0.02 0.5] (type Ib).**

An X_Δ - boundary has been crossed. This case shows a flipping over of the profiles as well, although they do not cross the distillation boundary for R →∞. A distillate composition on the X_Δ - boundary is the last one where a flipping over to region Ib of the profiles could occur. A flipping over of profiles through X_D occurs if the residue curve through the distillate or bottoms composition intersects the pinch curve.

In summary: Distillation boundaries for R →∞ are not boundaries for the transformed system defined by the parameters X_Δ and R_Δ. If $X_D/X_B = X_\Delta$ the difference point equation is mathematically identical to the traditional rectifying or stripping equation. For this case distillation boundaries can only be crossed if:

- the distillation boundary is sufficiently curved
- the top or bottom composition and the X_Δ - boundary lie on the concave side of the distillation boundary
- the top or bottom composition lies close to the distillation boundary between the distillation boundary for R →∞ and the X_Δ - boundary.

- the distillation column runs with reflux ratios low enough to shift the distillation boundary for the transformed system past the top or bottoms composition.

The operating region for columns where this flipping over occurs is small, as a result this phenomenon was more of academic interest. However the case discussed is a very constrained case of crossing distillation boundaries, as the difference point equation (Equation 2.1) has been reduced to a rectifying or stripping equation, with $X_T = Y_T$ or $X_D = X_\Delta$. This means the difference point has to lie inside the mass balance triangle, as it represents real compositions and the column profile has to start from this composition. These constraints do not exist if the idea of the difference point is employed. Thus many more profiles of various column profile maps can be used. An example is shown in Figure 3.26.
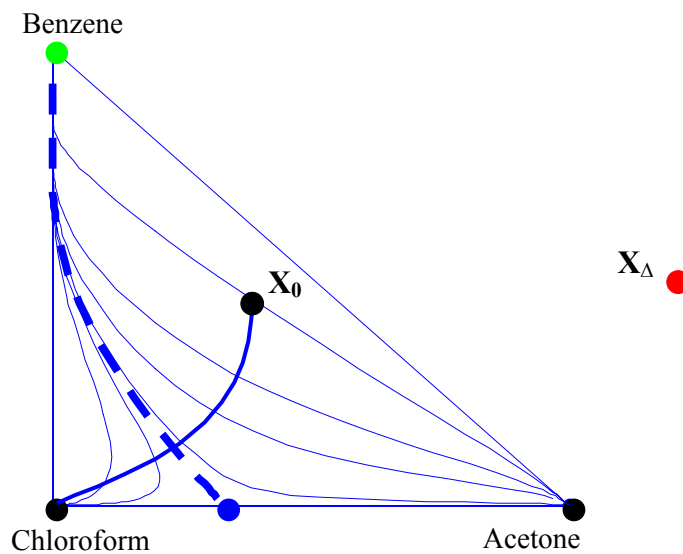
Figure 3.26: **Column profile that crosses the distillation boundary for**
R →∞ from an initial condition X_0 = [0.39 0.45] with X_Δ = [1.2 0.5]
(type IIb pinch curve) and R_Δ = 3.

The difference point in this example lies in region IIb. The composition X_0 lies far from the distillation boundary and the resulting profile still crosses the boundary and terminates close to the pure chloroform node.

3.4 Conclusions

The design of distillation systems can be based on differential equations and column profiles. The knowledge of the curvature and the path of the trajectories on phase diagrams is essential for every successful design. In this paper we have shown, based on the difference point equation, that the phase diagram behaviour can be described by the singular points occurring in the system. To determine the phase diagram one needs to know the position of the singularities occurring in the x_1- x_2 space and the type thereof. The type of singularity can be expressed in terms of the eigenvalue and be manipulated by the flowrate difference point R_Δ. Changing the value of R_Δ shifts entire regions up and down the x_1- x_2 space. The position of the singularities depends solely on the difference point X_Δ itself. Hence pinch point curves can be used to determine the path that singularities move in the space. As X_Δ does not need to lie inside the MBT we have shown that depending on the position of X_Δ in the space there exist regions of similar pinch curve behaviour. It has been shown previously that ideal systems comprise seven regions of different X_Δ whereas the non – ideal system acetone-benzene-chloroform comprises 15 regions. The number of regions and the resulting pinch point curve behaviour is unique for each system. The more variety there is the more options there are for designing the optimal process.

Eigenvalue maps, pinch point curves and eigenvector maps introduced in this paper for distillation are powerful tools for synthesis of distillation as the use of the whole variety of pinch point curves as well as eigenvalue maps, enables the designer in principle to create an optimal system behaviour (phase diagram, column profile) as the type of singularities can be manipulated and placed in space. I.e. sampling the intermediate boiler in ideal systems requires an infinite number of stages, as this node is of the saddle point type. With our approach profiles can be generated that run straight into the intermediate boiler. We also showed that distillation boundaries in non – ideal systems can be crossed from far off the boundary by choosing the appropriate X_Δ and R_Δ.

The determination of the optimal system behaviour is up to the designer. This approach just enables the determination of the design parameters X_Δ and R_Δ for a specific purpose.

The tools presented in this paper are in addition extremely helpful for the design of complex distillation configurations such as Petlyuk, divided wall columns, columns with multiple feeds and side rectifiers etc. Every complex column can be broken down into column sections and CPMs can be used to describe the change of composition within each of these. This will be discussed in the following chapters.

Chapter 4:

The Topological Effects and Advantages of

Distributed Feed Addition

This chapter covers the analysis of feed distribution from a CPM perspective. Both Michaela Tapp and I have tackled this problem from different perspectives. This approach is my own

---

Abstract

Despite the apparent maturity of distillation research, relatively little work has been focused on the effect of feed distribution on a separation. In this work we demonstrate the potential of column profile maps (CPMs) for analysing and understanding distillation configurations by applying the CPM technique to the feed distribution problem. It is shown that feed distribution can produce feasible separations from infeasible non-sharp (simple column) product compositions if the transformed triangles (TTs) of the rectifying and stripping CPMs overlap. This is analogous to reducing the minimum reflux ratio for these non-sharp splits. It is also shown that, from a topological perspective, feed distribution offers no advantages for two-product sharp-split separations.

4.1 Introduction

In distillation column design a significant amount of time is put aside for design optimisation. The most obvious optimisation variables are the reflux ratio and the total number of required stages as these variables impact directly on the cost and feasibility of a separation. Another important factor to consider, however, is the column feed policy. This includes not only the feed quality and placement but also the use of a single feed tray or distributed feed addition.

The first significant work done addressing the feed placement and quality issue was done by McCabe and Thiele (1925) for binary systems. This work showed that, from a total stages perspective, for saturated vapour or saturated liquid feeds, the optimal point at which to introduce this material is on the tray at which the composition is most similar to that of the feed. Adding feed at a different stage increases the total number of required stages for the separation.

The McCabe-Thiele construction has been very successful in designing and understanding binary separation systems. For multi-component systems, however, the column tray compositions need not be at all similar to the feed material composition and hence this placement strategy no longer holds. Most of the current design rules for the placement of the feed tray are based on heuristics (Akashah et al. (1979), Fenske (1932), Hengstebeck (1961), Kirkbridge (1944)). None of these rules even address the distributed feed case.

Despite the "maturity" of the field of distillation, relatively little is understood about the effects of distributing feed over a number of stages. The topological implications, in particular, have received very little attention by researchers. In this work we will address the effects of feed distribution on the column composition profiles by making use of column profiles maps (CPM). The effect on feasibility and (for certain cases) total required stages will also be studied. It will be shown that in certain situations feed material distribution can reduce the number of required stages and in others make infeasible separations feasible. It

will be shown that an attainable composition region exists for a set of specified products and column reflux ratio. This attainable region contains all solutions for all feed distribution policies. The optimal point at which to add feed, for single feed point columns, will also be found. A comprehensive understanding of the effects on all major column parameters will be gleaned.

Assumptions:

We will address the three component problem in this work, although the results can be generalised for any number of components. Constant molar overflow is assumed for all distillation modelling. An assumption of constant relative volatility is also made. The results are, however, applicable to all three component zeotropic thermodynamics. For convenience feed material is assumed to be saturated vapour. The results are, however, applicable to any feed quality. Perfect mixing is assumed over all mixing points.

4.2 Column Profile Maps as a Tool for Modelling and Design

The analysis of distributed feed addition and feed location, in this work, relies completely on the use of Column Profile Maps (CPM). It is therefore useful to summaries/emphasise some of the important properties of CPMs and outline the general CPM design procedure.

Tapp et al (2004) introduced the CPM, which is a map of column section (CS) composition trajectories. They defined a column section as a length of column between points of addition or removal of material and/or energy. These CPMs are generated using the difference point equation - Equation 2.1 - (Tapp et al, 2004) and are therefore defined for a single difference point (X_Δ) and reflux ratio (R_Δ). X_Δ is the pseudo composition of the net flow through a column section. For a rectifying section $X_\Delta = X_D$, while for a stripping section $X_\Delta = X_B$.

Holland et al (2004 b) showed that a full distillation configuration can be designed by simply overlaying the CPMs of each column section of a configuration and choosing appropriate operating profiles. For synthesis purposes only the liquid profiles need be tracked as the vapour profiles can be determined by material balance.

Tapp et al (2004) showed that the qualitative form of the CPM is dependent on the position of X_Δ in composition space. They identified seven regions of X_Δ placement that resulted in qualitatively different CPMs. These regions can be seen in Figure 4.1 below. The CPM was also shown to be a simple transform of the residue curve map. The topology present in each of the seven regions of qualitatively different X_Δ placement is simply shifted around the composition space when a column section is operated at finite reflux (Figure 4.2).

Because the different topology of the residue curve map corresponds to the regions of X_Δ placement we can track the shifted topology by referring to "transformed regions". A transformed region (TR) simply represents topology that is qualitatively similar to topology present in the residue curve map within a particular X_Δ region.
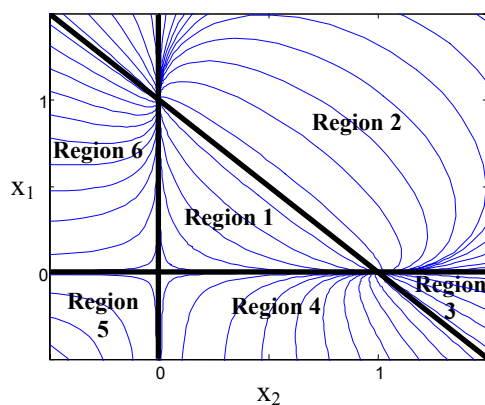
Figure 4.1: Difference point regions of Residue Curve Map
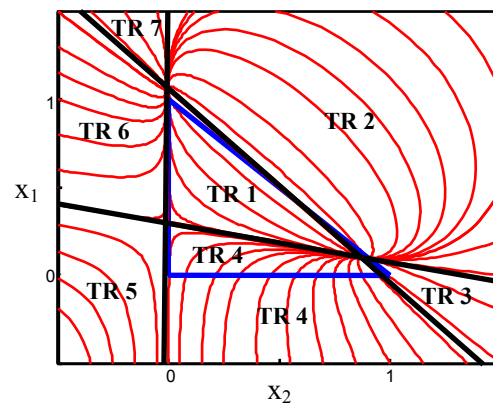
Figure 4.2: Transformed regions of Column Profile Map

The transformed triangle (TT) is the triangle produced by straight lines between the stationary points of the CPM. It is defined by the set of boundaries which, at

infinite reflux, define the MBT and it forms the boundary of TR1. TTs retain all the qualitative topological information of the CPM because straight lines through the stationary points divide regions of qualitatively different CPM topology. We can, therefore, understand topological changes in a CPM (for varying reflux or difference point) by simply producing a TT instead of an entire CPM.

4.3 Column Section Breakdown for Distributed Feed Column

Before CPMs can be produced and an analysis of the distributed feed column performed, we need to break the configuration into column sections.

Consider a two product distillation column terminated at the top by a condenser and at the bottom by a reboiler (see Figure 4.3). If the feed stream to this column is of flow rate F_T and is divided among N feed points we can – using the column section breakdown approach of Tapp et al (2004) – identify N+1 individual column sections. The uppermost column section, terminated by the condenser, is a standard rectifying section while the bottommost CS, terminated by the reboiler, is a standard stripping section. The column sections between these are neither rectifying nor stripping sections but can operate in rectifying-like mode or stripping-like mode.
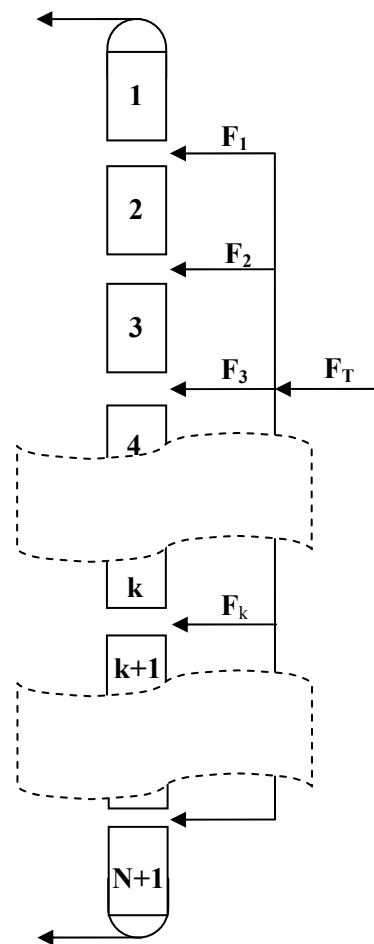
Figure 4.3: Distributed Feed Column Sectional Breakdown

4.4 The Effect of Distributing Feed on the Net Flow and Reflux Ratio

4.4.1 Net Flow

The net flow of the rectifying section is equal to the distillate product flow rate. Addition of feed material reduces the magnitude of the net flow from one CS to another down the column. See Equation 4.1.

$$\Delta_{k+1} = \Delta_k - F_k \tag{4.1}$$

While the total addition of feed material ($\sum_1^k F_k$) is smaller than Δ_1 (the rectifying section net flow), Δ_k is greater than zero and we can say that the CS operates in a rectifying-like mode. If $\sum_1^k F_k = \Delta_1$ then $\Delta_{k+1}=0$. In this case, there is no bulk flow of material in CS_{k+1}. Once $\sum_1^k F_k$ exceeds Δ_1 the net flow of subsequent column sections changes sign and the bulk flow of material is down the CS. At these conditions we can say that the CS operates in a stripping-like mode. The CS below the last feed point is a standard stripping section and the magnitude of the net flow is equal to the bottoms flow rate.

4.4.2 Reflux Ratio

The reflux ratio of a CS is defined as:

$$R_{\Delta k} = \frac{L_k}{\Delta_k} \tag{4.2}$$

Its magnitude is inversely proportional to the net flow in the column section. When the net flow is positive the reflux ratio is positive and similarly when the net flow is negative, the reflux ratio is also negative. The reflux ratio of CS_{k+1} can also be described in terms of the conditions of CS_k and the quantity of feed material added between these column sections. Below is a, feed-phase independent, expression for the reflux ratio of CS_{k+1}; Equation 4.3.

$$R_{\Delta k+1} = \frac{R_{\Delta k} L_{k+1}^{2}}{L_k L_{k+1} - F_k R_{\Delta k} L_{k+1}} \tag{4.3}$$

The reflux ratio is increased from one section to another, down the column, as more feed is added. While $\sum_{1}^{k} F_k < \Delta_1$, the reflux ratio is positive. When $\sum_{1}^{k} F_k = \Delta_1$ and $\Delta_{k+1}=0$ the reflux ratio of CS_{k+1} is infinite. Further addition of feed material now results in negative reflux ratios as Δ_k becomes negative. The magnitudes of these negative reflux ratios then decrease as more feed is added until $R_{\Delta k+1} = R_B$ when $\sum_{1}^{N} F_k = F_T$.

4.5 The Effect of Distributing Feed on the Difference Point

Each CS difference point ($X_{\Delta k}$) must obey linear mixing rules with respect to the feed composition and the difference point, of the CS, above or below it. See (Equation 4.4) below.

$$\Delta_k X_{\Delta k} = \Delta_{k+1} X_{\Delta k+1} + F_k X_F \tag{4.4}$$

This means that adjacent CS difference points represented in composition space must exist on a straight line running through the feed composition added between the column sections. For a column with a single feed composition every difference point will exist on a single straight line. See Figure 4.4.

For two sections operating at positive net flow, material balance dictates that the upper column section difference point lies between the lower section difference point and the feed composition. The uppermost column section is of course the rectifying section. The difference point for this section is a specified variable – it is a product composition. The difference points for sections below the rectifying section must exist on the opposite side of the distillate composition to the feed (in composition space) while the net flow is positive. As incremental amounts of feed are added to the column the difference points, for positive net flow sections, will move towards the boundaries of the mass balance triangle (MBT). The net-molar-

flow of individual components, in the corresponding column sections, is up because the net flow is positive and the difference points are within the MBT. After a sufficient quantity of feed has been added the resulting difference points will move outside the MBT. These feed requirements can be calculated using Equation 4.5 below.

$$F^{X2Boundary} = \sum F_k = \frac{DX_{D-2}}{X_{F-2}} \qquad \text{(4.5)}$$

Beyond this point the heavy component net-molar-flow will change sign and it will effectively move down the column. If the orientation, of the material balance line (in composition space), is such that it intersects the $x_3=0$ line (zero intermediate axis), between regions 6 and 7, the net-molar-flow direction of the intermediate component will change while the net flow is positive and it too will flow down the column after sufficient addition of feed material. This feed quantity can be calculated using Equation 4.6.

$$F^{X3Boundary} = \sum F_k = \frac{D(1 - X_{D-1} - X_{D-2})}{(1 - X_{F-1} - X_{F-2})} \qquad \text{(4.6)}$$

Subsequent addition of feed material will shift the difference points ever further from the MBT such that the elements of the difference point ($X_{\Delta k-i}$) tend to positive or negative infinity. (See Figure 4.4). Once the total feed addition exceeds the distillate flow rate the net flow, of subsequent column sections, changes sign. The elements of the difference point ($X_{\Delta k-i}$) also change sign and "appear from infinity", at the opposite end of the material balance line, moving closer to the MBT as further feed material is added to the column. If the intermediate component net-molar-flow direction does not changed while the net flow of column sections is up, it will change at some point after sufficient feed material is added to change the direction of the net flow. At this point in the column the net-molar-flow of the intermediate and heavy components is down and the light component net-molar-flow is up. The difference points of lower sections can now enter the MBT. This occurs when:

$$F^{X1Boundary} = \sum F_k = \frac{DX_{D-1}}{X_{F-1}} \qquad \text{(4.7)}$$

These column sections exhibit net-molar-flow of all components down the column. When the total feed addition is equal to F_T, the resulting difference point

is the bottoms product composition and the associated column section is a standard stripping section.
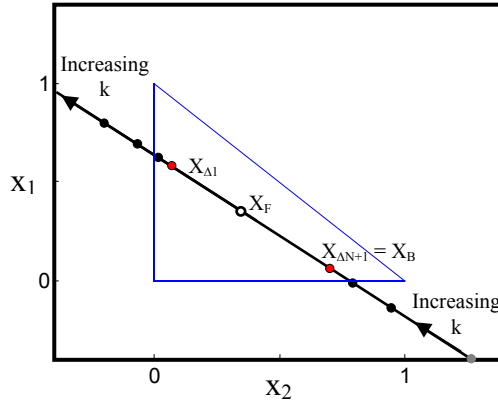
**Figure 4.4: Distributed difference points obey
linear mixing rules –hence they lie on a straight line.**

There are two net-molar-flow change sequences that summarise all possibilities in the distributed feed column. These are associated with the value of $F^{X3Boundary}$. If $F^{X3Boundary} > D$, the difference point locus will cross the intermediate component axis in positive heavy component space and the case in Figure 4.5 will result, while if $F^{X3Boundary} < D$, it will cross the intermediate axis in negative heavy component space and the case in Figure 4.6 will be obtained. In both Figure 4.5 and Figure 4.6 the direction of change of the difference points down the column is represented by the directions of the arrows along material balance lines. Both cases are summarised in the Table 4.1 and Table 4.2 below. The Δ_k column of Table 4.1 and Table 4.2 represents the direction of the net-molar-flow at various points on these lines corresponding to qualitatively different X_Δ regions. The component net-molar flow directions are represented in the $\Delta X_{\Delta k-i}$ column. The corresponding difference point placement is represented by the region of its occurrence.
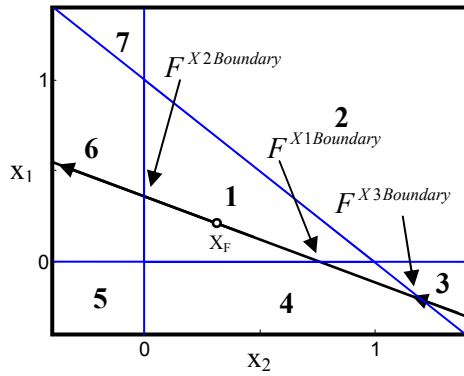
Figure 4.5: Line of possible difference point change - $F^{X3Boundary} > D$
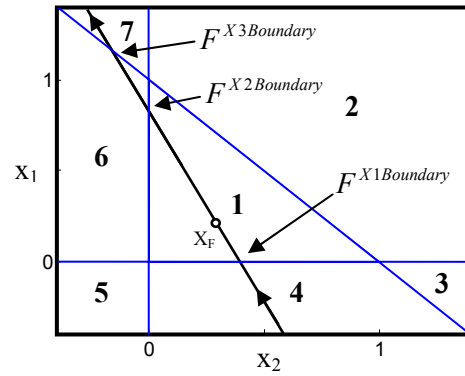
Figure 4.6: Line of possible difference point change - $F^{X3Boundary} < D$

Table 4.1: Summary of Net-Molar Flow Change ($F^{X3Boundary} > D$) Figure 4.5						
Δ	$\mathbf{R_\Delta}$	$\mathbf{\Delta X_{\Delta k\text{-}i}}$	$\mathbf{X_\Delta}$ **Region**	**Unstable Node Region**	**Saddle Point Region**	**Stable Node Region**
↑	+ve	↑ ↑ ↑	1	7	6	1
↑	+ve	↑ ↑ ↓	6	2	1	1
↓	-ve	↑ ↑ ↓	3	2	1	1
↓	-ve	↑ ↓ ↓	4	1	1	2
↓	-ve	↓ ↓ ↓	1	1	3	4

Table 4.2: Summary of Net-Molar Flow Change ($F^{X3Boundary} < D$) Figure 4.6						
Δ	$\mathbf{R_\Delta}$	$\mathbf{\Delta X_{\Delta k\text{-}i}}$	$\mathbf{X_\Delta}$ **Region**	**Unstable Node Region**	**Saddle Point Region**	**Stable Node Region**
↑	+ve	↑ ↑ ↑	1	7	6	1
↑	+ve	↑ ↑ ↓	6	2	1	1
↑	+ve	↑ ↓ ↓	7	1	1	2
↓	-ve	↑ ↓ ↓	4	1	1	2
↓	-ve	↓ ↓ ↓	1	1	3	4

|	Net Flow Direction
|	Light Component Net – Molar-Flow Direction
|	Intermediate Component Net –Molar-Flow Direction
|	Heavy Component Net – Molar-Flow Direction
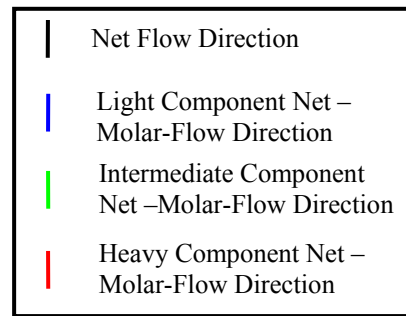
4.6 Topological Effects of Feed Distribution

We have discussed the effect of distributing feed on the net-molar-flow, reflux ratio and difference point. However, we have not discussed the topological implications of the shifting difference points and varying reflux ratio. The form of the CPM is dependent on both of these variable – reflux ratio and difference point. If we are to fully understand the effect of feed distribution we need to understand the qualitative form of distributed feed solutions. This essentially means that we need to understand the regions of each CPM that can be sampled in each column section.

<u>Note:</u> Transformed Triangle Boundary Definitions

For the following sections it will be convenient to label the boundaries of the TTs. A boundary defined between an unstable node and a saddle point of TT "k" will be referred to as boundary "A_k". A boundary defined between a stable node and a saddle point of TT "k" will be referred to as boundary "B_k". The final boundary defined between an unstable node and a stable node will be referred to as boundary "C_k" of the TT. Figure 4.7 below illustrates these boundary definitions. Unless otherwise stated this will always refer to liquid TT boundaries. Vapour TT boundaries will be referred to as "vapour boundary A_k", ... etc.
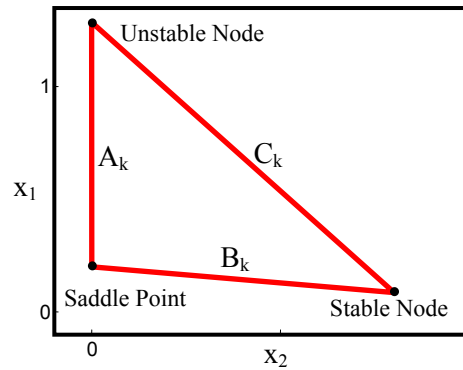
Figure 4.7: Transformed triangle boundary definitions

Distributed Feed Pinch Point Curves

The potential to sample the various regions of a CPM depends on the feasibility of producing a continuous (composition profile) path - for either the vapour or liquid profiles - from the rectifying composition to the stripping composition through these regions. This ultimately depends on the "movement" of the stationary points from one section to another because the stationary points dictate the positioning of all topological regions. By "movement" we are referring to the relative position of the nodes of column sections when we add feed material between them. The nodes appear to move as we shift our attention from one section to another.

The simplest way to analyse this "movement" is to produce a pinch point curve. This pinch point curve will not be produced in the conventional way - varying the reflux ratio at a set difference point value - but will be the loci of stationary points produced by varying the difference point and reflux ratio in a manner consistent with differential feed addition along the length of a distributed feed column. This means that each difference point will lie on a material balance line through the feed composition and the chosen product compositions and that the reflux ratio will be varied differentially from the rectifying reflux ratio to the stripping reflux ratio. Each point on the (pinch point) curve will be associated with a different column section, reflux ratio and difference point value.

Figure 4.8 shows a distributed feed pinch point curve produced – for a feasible separation - in this manner. The pinch point curve has three branches

corresponding to the three stationary points of constant-relative-volatility CPMs. Each branch has finite length with a "starting" point corresponding to the rectifying CPM stationary points and an "end" point corresponding to the stripping CPM stationary points. Notice that the pinch points "move" in a direction of increasing heavy component and decreasing light component composition, from section 1 to section N+1. This means that the B_k boundaries of the TTs shift in a direction of decreasing light component value, while the A_k boundaries move in a direction of increasing heavy component value down the length of the column.

The pinch point curves span multiple difference point regions. The unstable node "moves" from region 7 through region 2 to region 1. The saddle point "moves" from region 6 through region 1 to region 4. The stable node "moves" from region 1 through region 2 to region 3. This "movement" from one region to another is dictated by the "movement" of the X_Δ, along the material balance line through each difference point region. While X_Δ is inside the MBT and the reflux is positive, the forms of the CPMs are similar to the rectifying CPM; the stationary points of the TT are in the same regions - the saddle point is in region 6, the unstable node is in region 7 and the stable node is in region 1. When the difference points shift into region 6, the unstable node and saddle points of subsequent column sections cross over the light-intermediate axis. The saddle moves into region 1 and the unstable node shifts into region 2, while the stable node remains within region 1. A comprehensive summary of all possible stationary point placements is presented in Table 4.1 and Table 4.2.

Feasible Topology

The "movement" of the TTs in this way brings very different topology into the MBT. However, only a very limited area of this topology can be sampled. From the pinch point curve in Figure 4.8, we see that because the B_k boundaries decrease in light component value, the composition profile of column section k can only ever sample transformed regions 1 and 6 of column section k+1. This is illustrated in Figure 4.9. All seven transformed regions, for a column section

(below the rectifying section) with a difference point in region 6, have been superimposed over a rectifying profile. The rectifying profile is only able to sample transformed regions 1 and 6.

Similarly, if we analyse the movement of the A_k boundaries from the stripping TT up the column, we notice that CS k+1 can only sample TR 1 and 4 of CS k.
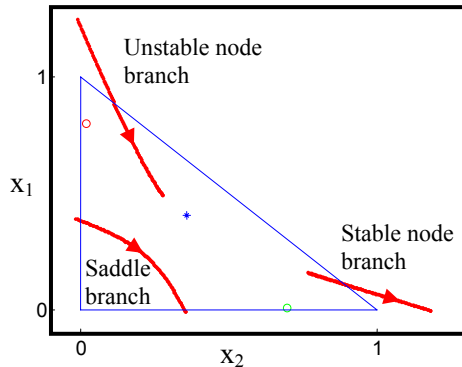
Figure 4.8: Distributed feed pinch point curves
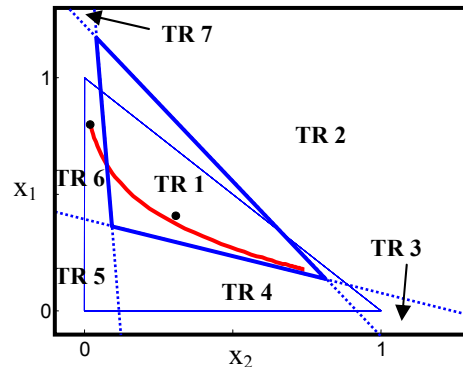
Figure 4.9: Transformed regions for X_Δ in difference point region 6 at positive reflux with superimposed rectifying profile

A CS operating on a profile within TR 6 can intersect the rectifying profile but not the stripping profile, while a CS operating on a profile within TR 4 can intersect the stripping profile but not the rectifying profile. Because TR 1 is the only common region sampled, from one section to another, up and down the column, we can conclude that it is the only feasible region of operation for distributed feed columns.

The TTs for a distributed feed column with five feed points of equal magnitude are illustrated in Figure 4.10. Notice how each corner of the TTs correspond to points along distributed feed pinch point curves.
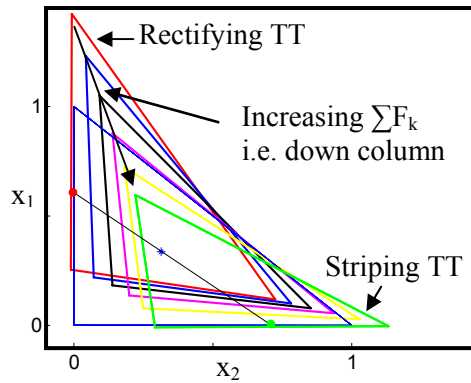
Figure 4.10: Distributed feed column with five feed points of equal magnitude
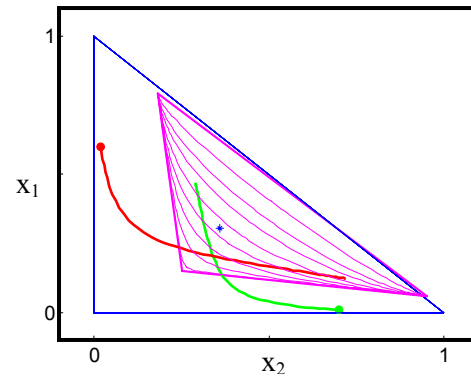
Figure 4.11: Choosing operating profiles from CPM/TT

We can easily choose operating profiles for each column section from the transformed triangles as we know the form of the topology within TR 1. This process is illustrated by Figure 4.11, where we can choose a number of operating profiles from within the pink TT along which to run the column.

4.7 Operating Regions

Five feed points have been used to generate the TTs for the example in Figure 4.10. Depending on the feed point placement in the column, an infinite number of different operating profiles within the blue, black, pink and yellow TTs could be sampled. It is theoretically possible for a column to be designed such that the operating profile ran from the rectifying profile along the boundaries of the blue, black, pink and yellow TTs (through the saddle points) to the stripping profile. This would require an infinite number of stages in all sections other than the rectifying and stripping sections.

What operating profiles could be sampled if, instead of a finite feed policy, we added infinitesimal quantities of feed at infinitely many feed points? As in the previous example an infinite number of solutions exist. Also, as in the previous example, we can choose profiles that run through the saddle points of TTs. However, as there are infinitely many TTs, in this case, the profile could run continuously along the saddle branch of a distributed feed column pinch point

curve. Such an operating profile could actually run along a TT boundary passing through the distillate composition, then along the saddle branch of a pinch point curve and finally along a TT boundary through the bottoms composition. An example of such a profile is seen in Figure 4.12 below. The column sections corresponding to the pinch point curve would all require infinitely many stages.

This composition profile is of more than just academic interest. Because only TR 1 can be sampled in distributed feed columns, *this profile represents a bound on attainable compositions within the composition space*. It represents the highest intermediate component compositions that can be achieved, at any particular light or any particular heavy composition, using distributed feed.
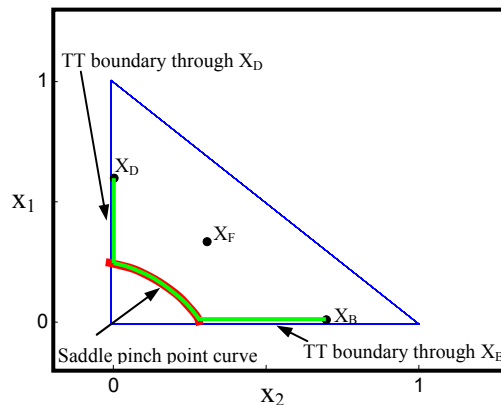
Figure 4.12: Composition profile path running along pinch point curve

It is interesting to notice that the intermediate compositions, achievable along this boundary can be significantly higher than any composition achievable along the rectifying and stripping profiles. In fact, if we consider the movement of the TT boundaries (from column section to column section) discussed in section 4.6 and Figure 4.11, it would appear that no path exists, between the rectifying and stripping profiles, that can sample a lower intermediate composition (at given heavy or light compositions) than these profiles. Rate vectors along profiles, for column sections between the rectifying and stripping sections, seem to point in directions that increase the intermediate composition (see Figure 4.13). *It is postulated that the rectifying and stripping profiles represent lower bounds (for*

feed distribution) on achievable intermediate compositions at any particular light or any particular heavy composition.

If the two above mentioned boundaries are superimposed a region containing all attainable solutions can be found. Figure 4.14 illustrates such an attainable or feasible composition region. *This region contains the solutions for distributed feed columns at a set reflux ratio and for set product specifications with any (saturated vapour) feed policy.*

The two composition profiles forming the attainable region boundaries can be deconstructed into five qualitatively different boundaries in this case. These are:

- saddle pinch point curve boundary
- rectifying profile boundary
- stripping profile boundary
- TT boundary through X_D
- TT boundary through X_B
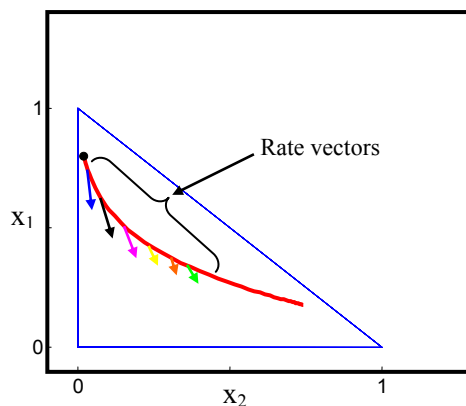
Figure 4.13: Rate vectors of trajectories from CPMs for CSs below the rectifying section
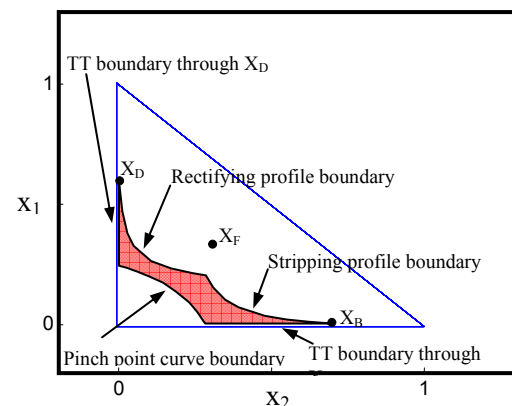
Figure 4.14: Feasible operating region for all feed policies

4.8 The Benefits of Distributed Feed Addition

4.8.1 Stage Reduction

It is well known that distributing feed material of a single composition does not hold any particular advantages for binary separations. The number of required stages for a binary distributed feed column is actually larger than that of a single feed column. Figure 4.15 and Figure 4.16 illustrate this using the McCabe-Thiele constructions. The distributed feed construction in Figure 4.16 requires 7 stages while the single feed construction in Figure 4.15 requires only 6. Are distributed feed columns for multi-component systems similarly limited?

Because the stage requirement is a hidden variable in a CPM this is a little more difficult to ascertain using the CPM technique than it was using the McCabe-Thiele construction. There are points on the CPM where the total stages required are known, however. Near the stationary points (corners of the TT) the number of stages required approaches infinity. If a, single feed point, separation initially requiring infinite stages can be effected with distributed feed without pinching we can conclude that feed distribution can, depending on the feed policy, lower the number of required stages for multi-component separations.
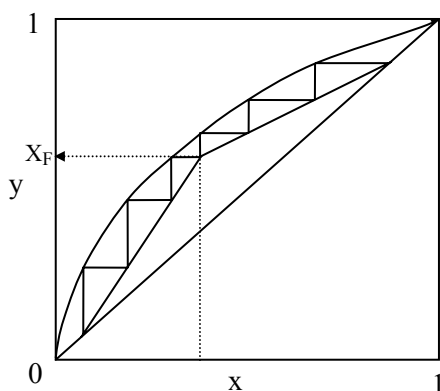
**Figure 4.15: McCabe-Thiele construction
for single feed point**
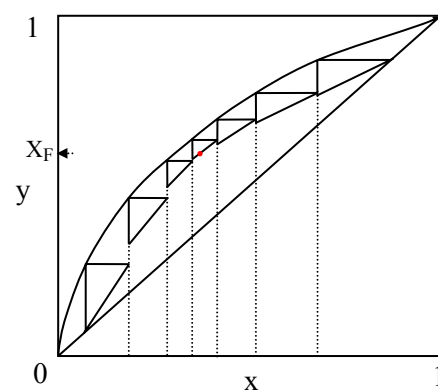
**Figure 4.16: McCabe-Thiele construction
for six feed points**

Figure 4.17 illustrates a non-sharp separation with a single feed point. From the position of the stripping section TT we can see that the stripping profile reaches a

pinch point. The pinch point intersects the rectifying profile so this is, in fact, a minimum reflux separation for the chosen products. By distributing the feed over two or three feed points we can produce profiles which "bypass" this pinch point.

Figure 4.18 shows the TTs for the same separation in a distributed feed column with three feed points. Profiles for the blue TT of Figure 4.18 can be initiated from any point along the rectifying profile between point "A" (intersection with the blue unstable-node/saddle-point TT boundary) and point "B" (intersection with the stripping profile pinch composition). A profile initialised at point "A" would still require infinite stages as it would have to pass through the saddle point. Clearly, profiles initialised at the stripping pinch composition would also require infinite stages. However, profiles started between these points (say point "C") would require finite stages and would intersect the stripping profile well away from the pinch composition. If the third feed point was incorporated and profiles of the black TT were sampled, these would intersect the stripping profile even further from the (stripping profile) pinch composition.

It is clear, therefore, that distributing feed in multi-component separations can reduce the number of required stages. In some cases, such as this, the stage saving can be quite significant.
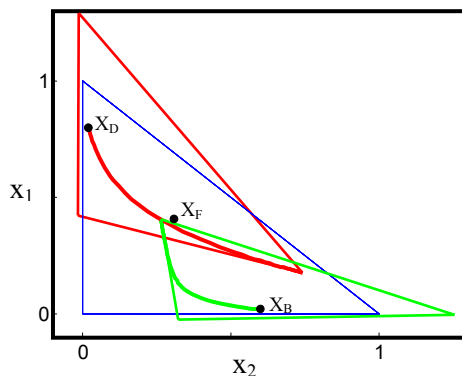
Figure 4.17: Non-sharp separation with single feed point requiring infinite stages.
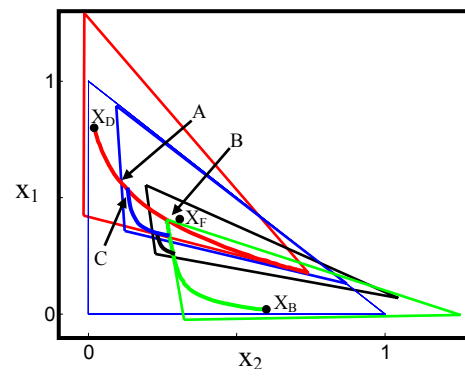
Figure 4.18: Distributed feed reducing number of required stages for non-sharp split

4.8.2   Separation Feasibility

It is interesting to note that in the previous example the unstable-node/saddle-point and saddle-point/stable-node boundaries of both the blue and black TTs extend quite far beyond the rectifying and stripping profiles respectively i.e. large sections of these boundaries extend into the feasible operating region. It would be useful if this fact could be put to some practical purpose.

Figure 4.19 depicts an infeasible non-sharp separation. The rectifying and stripping profiles do not intersect at the chosen reflux ratio; hence this (single feed point) separation is not possible at these conditions. The obvious way to produce a feasible split from this set of product compositions is to increase the reflux ratio. *If the feed addition is changed from a single feed point to a distributed feed policy, however, this infeasible separation can be made feasible at the current value of the reflux ratio.*

This is clearly illustrated in Figure 4.20 where a three feed point column provides profiles that allow a path between the non-intersecting rectifying and stripping profiles. A first feed point allows a transition from the rectifying profile to a profile within the blue TT. A second feed point allows a transition from the blue TT to a profile within the black TT. This black profile intersects the stripping profile where the final feed addition is made. This separation could actually have been performed with only two feed points. If enough feed had been added further down the rectifying section to produce the black TT, one of these profiles could have been sampled directly without introducing the blue TT.
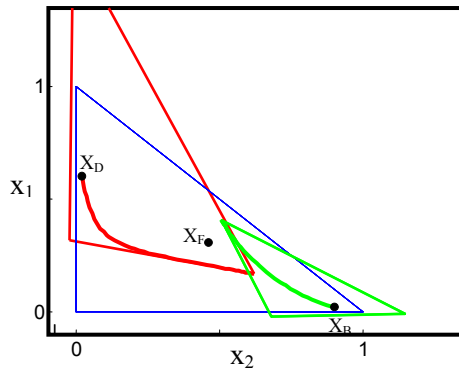
Figure 4.19: Infeasible non-sharp separation
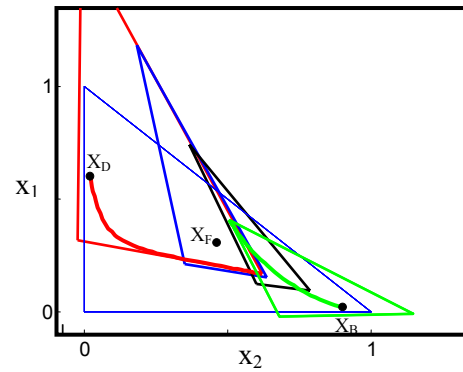
Figure 4.20: Distributed feed makes non-sharp infeasible separation feasible

An analogous result of producing feasible splits in this way, from non-intersecting non-sharp rectifying and stripping profiles is that the minimum reflux ratio, for these splits, using one feed point, can be reduced by distributing the feed material over a number of trays. This is only possible for non-sharp separations under very specific conditions as we will see later.

Producing a feasible separation through distributed feed, from a previously infeasible set of products, we introduce another boundary in the feasible operating region. This boundary is comprised of a *stable-node pinch point curve* extending from the rectifying TT stable node to the stripping profile (see Figure 4.21). In other circumstances it is possible to introduce an *unstable-node pinch point curve boundary* between the stripping section TT unstable-node and the rectifying profile.
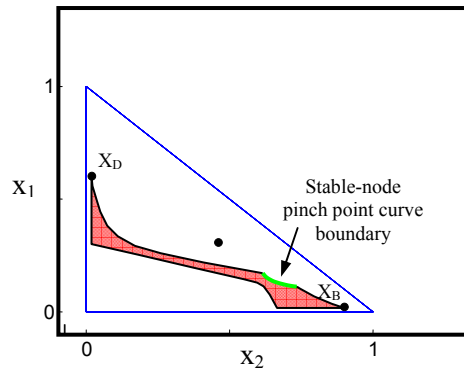
Figure 4.21: Feasible operating region for distributed feed column with non-intersecting rectifying and stripping profiles

4.9 The Benefits of Distributed Feed Addition – Limiting Conditions

There are two separate conditions that limit the potential benefits of feed distribution. The first condition is a sharp product split specification. The closer the distillate or bottoms compositions are to the boundaries of the MBT, the closer one of the boundaries of their respective TTs is to these axes. In the limit, *when the product point is essentially on an axis, the corresponding composition profile runs along the boundary of the TT*. This results in an infinite number of stages being required as the profile must pass through a saddle point (see Figure 4.22). No feed distribution policy can prevent this occurrence; therefore *feed distribution for sharp-product specifications is pointless*. Reduction of the number of required stages under these circumstances is impossible (see Figure 4.23).

At sharp-split conditions, the attainable/feasible composition region shrinks to a single path between the distillate and bottoms compositions.
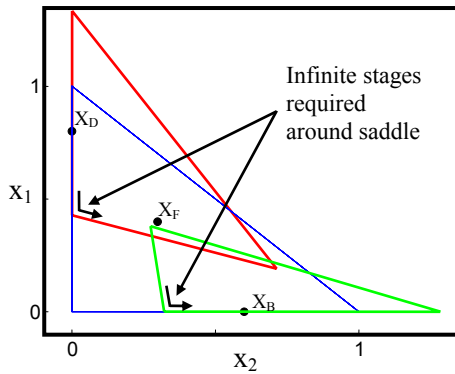
Figure 4.22: Sharp-split TTs require infinite stages
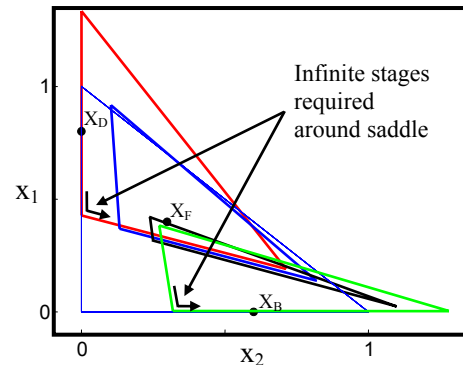
Figure 4.23: Distributed feed does not reduce the number of required stages for sharp split.

The second condition is associated with lowering the minimum reflux ratio or making infeasible separations feasible. If the column reflux ratio is such that the boundaries of the rectifying and stripping TTs border each other, a situation is reached where reduction of the reflux ratio will prevent any feasible separation (see Figure 4.24).

This condition is, in fact, the true two-product column minimum reflux ratio. It represents the smallest reflux ratio at which infeasible separations can be made feasible (see Figure 4.25). The only reason that distributed feed could produce a feasible separation from "infeasible" conditions was that there was an overlap of the rectifying and stripping TTs (see Figure 4.20).

It is the TT and not the profile itself that dictates minimum reflux for two-product distillation columns. The infeasible separation in Figure 4.20 has a non-sharp product specification. The composition profiles and boundaries of the TTs therefore do not coincide. Distributing the feed, in this case, produces a path between the rectifying and stripping profiles because the additional TTs, introduced, can overlap them both. This cannot occur when the reflux ratio is below true minimum and the rectifying and stripping TTs do not overlap as Figure 4.26 and Figure 4.27 illustrate. *Infeasible sharp split separations can never be made feasible without increasing the reflux ratio.*
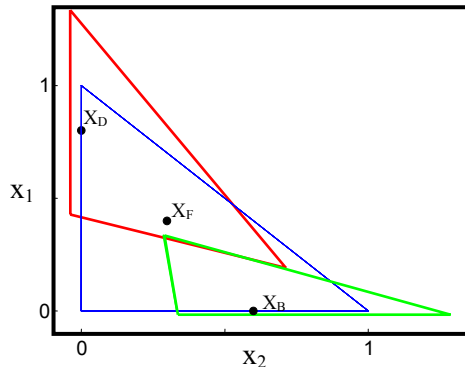
Figure 4.24: Non-sharp-split TTs at true minimum reflux
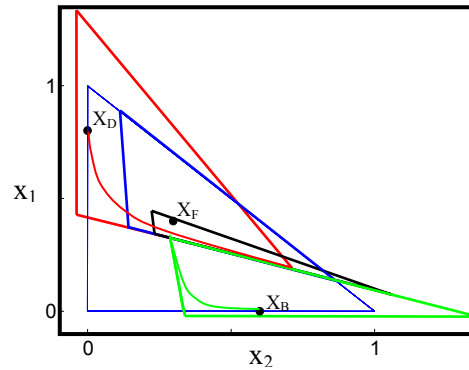
Figure 4.25: Distributed feed non-sharp-split TTs at true minimum reflux
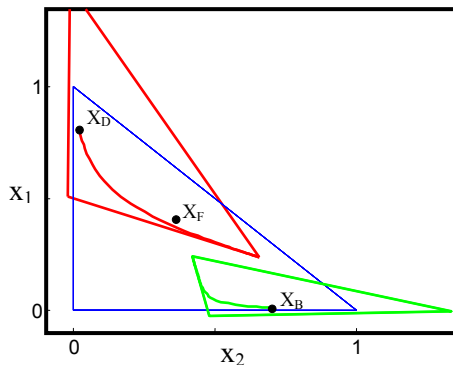
Figure 4.26: Rectifying and stripping TTs and profiles below true minimum reflux
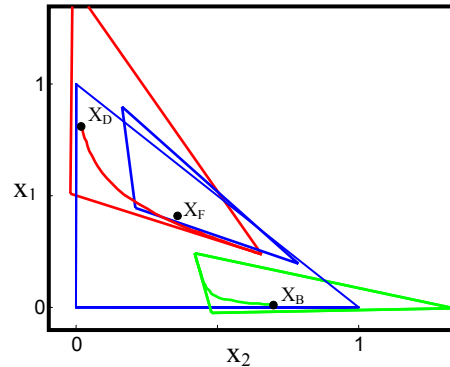
Figure 4.27: Rectifying and stripping TTs and profiles with additional distributed feed TT below true minimum reflux

4.10 Discussion

The decision of whether or not to make use of feed distribution is largely dependent on the "sharpness" of the required separation. Because all potential benefits are nullified when the split is sharp, feed distribution is pointless at these conditions. If, however, a non-sharp split is satisfactory, then using many feed points has the potential to lower the operating reflux ratio as well as reduce the required number of stages. Understanding the effects of feed addition quantities at each point as well as positioning of the feed points is of utmost importance. Ill placement of feed points can actually increase the number of required stages instead of reducing them. Consider figure 3.9 for example. If the first feed point (F_1) was placed on the stage where the composition on the tray was equal to that at the intersection of the red rectifying profile and the boundary of the pink TT

and the quantity of feed added to the column produced the pink TT, an infinite number of stages would be required in the CS below that feed point. Feed point placement dictates the position in composition space where the column composition profile leaves one CPM for another. Tracking the required stages along a trajectory is obviously very important. Although the number of stages is a hidden variable within a CPM, tracking it is fairly simple. Once operating profiles have been chosen for the separation we simply track variable n in the difference point equation when producing the profiles. Integration is started using the upper/top liquid composition of each CS as an initial condition. These are determined from the intersection of desired operating profiles in the CPMs. In the same way, the optimal feed stage for a single feed tray column can be determined.

When designing a distributed feed column, the designer must take cognisance of the effects of feed addition quantities at each feed point. Feed quantities dictate the form of the resulting CPMs. The designer must therefore add the correct quantity of feed to produce a desired set of composition trajectories. This can only be done with a comprehensive understanding of the topological effects of feed addition. It is hoped that this work will arm the designer with this required understanding.

Chapter 5:

Novel Separation System Design Using "Moving Triangles"

This work was published in Computers and Chemical Engineering in 2004 (see Holland et al, 2004 b). The original paper contained an error regarding the feasibility of one half of the "bow-tie" region (defined later). This is corrected here. Michaela Tapp offered valuable insight in the development of this work, but it is almost exclusively my own.

Abstract

Shortcut design techniques have been employed in the initial design of traditional distillation systems. Current techniques are not useful in the design of novel or complex configurations however. We will show that by using column profile mapping "moving triangles" to model the behaviour of column sections (CS), any distillation configuration, no matter how complex, can be modelled and its behaviour more thoroughly understood. As an example, a thermally coupled column will be modelled using column profile maps. It is suggested that by gaining an understanding of the behaviour of the configuration quickly and easily, using column profile maps, time and money can be saved by avoiding poor initial decisions and designs.

5.1 Introduction

The synthesis of feasible distillation columns for multi-component mixtures is a primary objective in the field of distillation and shortcut design techniques have been employed in the design of traditional distillation systems for a number of years. Some of these techniques use the differential equations (DE's) introduced by Doherty (Doherty & Perkins, 1978). These DE's are based on the Underwood (Underwood, 1948) equations and are used to determine the composition profiles along the length of the rectifying and stripping sections in a distillation column. A separation was considered to be feasible if these liquid profiles intersected. Operation leaves have been defined by Wahnschafft (Wahnschafft et al, 1992) and Castillo (Castillo et al, 1998). They represent the total attainable composition region in a distillation column section for defined product compositions. The limitation of the operation leaf method is that it is essentially limited to simple one feed two product distillation columns and a maximum of 4 component mixtures. In addition, as these techniques are all based on the afore mentioned DE's they are no longer valid near the feed stage as the DE's do not describe the transition from the rectifying to the stripping section. Until now there has been no simple technique to determine the optimal placement of the feed. When we consider the literature for multi-component systems, most of the current design rules for the placement of the feed tray are based on heuristics (i.e. Akashah (1979), Hengstebeck (1961), Kirkbridge (1944)). The effect of the composition of the feed or even modelling multiple feed trays is almost always performed by rigorous design simulations, (i.e. Yeomanns, 1998b) which provide no overall insight into the operation of the columns. In fact the general failing of most existing shortcut techniques is that they fail to adequately describe any separation system more complex than the two column section configuration and also do not offer insights into problems such as feed placement. No currently available shortcut design technique can properly model configurations such as multiple feed columns, side-draw columns, coupled columns etc. To address this problem a more creative design approach needs to be employed.

Franklin (1986,1988) examined the Underwood equations more extensively and discovered that these equations could be used to generate a family of liquid profiles with a common compositional offset from their respective vapour profiles in ternary and quaternary systems. He suggested that these "maps" of profiles could be used to model counter-current vapour-liquid equilibrium systems including not only distillation, but also absorption or stripping columns. Tapp et al (2004) showed that similar three component maps (tracking liquid profiles) termed Column Profile Maps (CPM's) could be produced using the difference point equation (Hoffman, 1964; Hauan, 1998) (see equation (1) below) to model individual column sections.

Tapp et al (2004) defined a column section (CS) as a length of column between points of addition or removal of material and/or energy.

The Difference Point Equation:

$$\frac{dX}{dn} = \left(\frac{1}{R_\Delta} + 1\right)[X - Y(X)] + \frac{1}{R_\Delta}[X_\Delta - X] \qquad \text{(5.1)}$$

To produce a CPM for a CS an R_Δ (reflux) and an X_Δ (difference point) are defined. This constraint is equivalent to setting a scaled net-molar-flow for the column section. Choosing arbitrary initial conditions, integration is performed both as $n \rightarrow \infty$ and $n \rightarrow -\infty$. Using this technique the entire ternary space (x_1 vs. x_2) can be populated with column profile trajectories with common net-molar-flow. Tapp et al (2004) showed that the CPM's at finite reflux are simply transforms of the residue curve maps. The transform shifts the fixed points of the system in the space, maintaining (in constant relative volatility systems) the shape of the boundaries initially defined by the mass balance triangle ([*]MBT) i.e. the profiles connecting the fixed points are straight. This has resulted in the phenomenon being referred to as "Moving Triangles" (See Figure 5.1 and Figure 5.2).

---

[*] The MBT is defined by: $0 < x_1 < 1$; $0 < x_2 < 1$; $0 < x_3 < 1$

It will be shown that by making use of the CS breakdown approach for columns as well as CPM's, introduced by Tapp et al (2004), any configuration of column, no matter how complex can be effectively designed and a general understanding of the interaction of parameters achieved. As an illustration, a thermally coupled (Petlyuk) column will be broken down into column sections and designed (for a ternary constant relative volatility system) using CPM's. Due to the complexity of this problem, two simplifying scenarios where the system is at overall infinite reflux will be analysed. In the first, all vapour flow rates will be set equal to their respective liquid flow rates in a column section. In the second case these flow rates will have different values in the feed and side-draw column sections. While Tapp et al (2004) introduced CPMs and discussed their topological properties, the emphasis of this paper will be to introduce CPMs as a design and analysis tool for distillation. It is not the authors' objective to completely solve the Petlyuk problem but simply show how CPMs may be used to begin to understand and design these and other complex columns. A full design and analysis of the Petlyuk column, using CPMs, will be presented in future work.
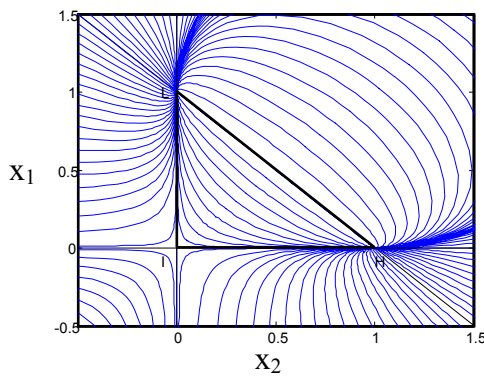
Figure 5.1: Residue Curve Map
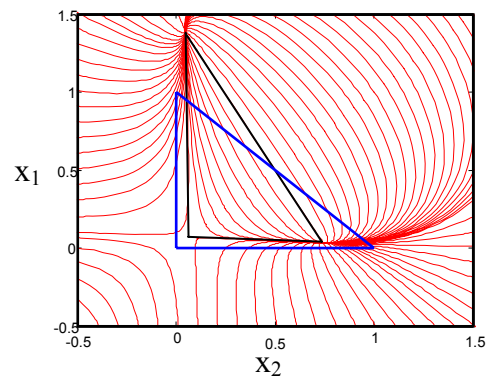
Figure 5.2: Transformed Profile Map for $X_\Delta = [0.3, -0.2]$ and $R_\Delta = 9$

* It should be noted that all vectors are of the form $[x_1, x_2, x_3]$
  Subscript 1, 2 and 3 represent the light, heavy and intermediate components respectively.

5.2 Complex Column Configuration Design

One of the most difficult to design and least understood distillation columns is the Petlyuk column. Its complexity arises due to the thermal coupling of a large main column and a smaller pre-fractionator. Without the constraints of condensers and reboilers on the pre-fractionator, the multiple degrees of freedom in design lead to many solutions, which are difficult to determine without the CPM technique. It is now convenient to outline this design procedure.

The general design methodology using CPM's is as follows:

- *Break column configuration into CS's* - All columns can be broken down into a number of column sections by simply identifying lengths of column between areas of addition or removal of material and/or energy (Tapp et al, 2004). The Petlyuk, although more complicated than most arrangements, is no different. It can be broken down into six column sections. This breakdown is illustrated in Figure 5.3 below.
- *Set X_Δ for the CS which will meet the primary product's specification*. The most important products are quite often the distillate or bottoms. In this case, the value of X_Δ will be equal to the product composition for these sections. The choice of difference point will be discussed in greater detail later.
- *Choose an operating R_Δ for this section.*
- *Determine by mass balance, the X_Δ and/or R_Δ of the remaining section(s).* X_Δ (or R_Δ) may need to be set for other sections in the configuration, depending on the total degrees of freedom.
- *Produce the CPM's for all CS's and superimpose these to determine feasible operating profiles.* If no feasible solutions are found or the other products do not meet required specifications, the entire process must be repeated with different choices of X_Δ and or R_Δ.
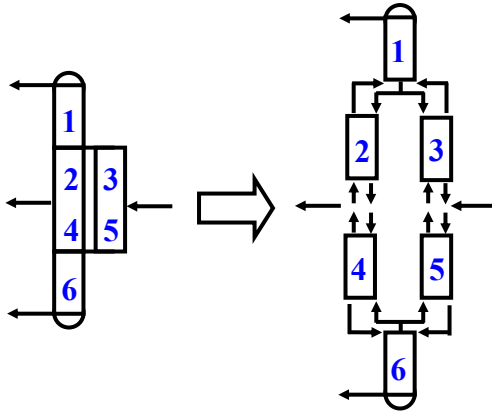
Figure 5.3: Column section breakdown for a Petlyuk column
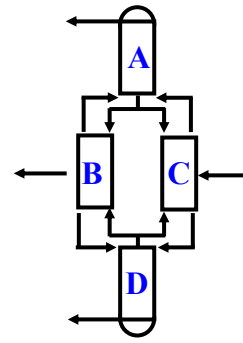
Figure 5.4: Infinite reflux Petlyuk column breakdown

5.2.1 Difference Points and Feasibility Criteria for Petlyuk Column Sections

To design any separation configuration it is necessary to understand which difference points as well as profiles of the resulting CPM are feasible for steady state operation. The former problem is not a trivial matter and is the subject of ongoing research. We can, however, make some preliminary statements about X_Δ.

– In general, the difference point for a CS need not be a composition in the column (Tapp et al, 2004). The only case where the difference point composition has to exist within the column is for sections with total condensers and total reboilers (sections 1 and 6 in the Petlyuk column). These sections behave in the same way as standard rectifying and standard stripping sections respectively, no matter what CS or operation they are attached to. The difference point equations for these examples simply reduce to the DE's defined by Doherty (1978). For these column sections only one composition profile is valid and the rest of the column profile map is superfluous.

– An arbitrary CS not terminated by a condenser or reboiler can operate anywhere in composition space (Tapp et al, 2004). Negative $X_{\Delta i}$'s are perfectly valid. Absorption columns or sections between feed points in a distributed feed column quite often operate under these conditions. This means that the remaining four CS's of the Petlyuk column (sections 2-5)

can operate at any difference points (even those outside the MBT) subject only to mass balance constraints.

Not all choices of Δ, R_Δ and X_Δ that satisfy the overall mass balance of the Petlyuk column are feasible design parameters. The choice of X_Δ and R_Δ for each of the column sections and the interaction between them is not trivial. In fact there are a number of criteria regarding the profiles of each CPM that need to be satisfied for a feasible design. These include:

- Intersection of feasible liquid profiles in the CPM's for sections 1,2 and 3 at a point

- Intersection of feasible liquid profiles in the CPM's for sections 2 and 4.

- Intersection of feasible vapour profiles corresponding to the CPM's for sections 4, 5 and 6 at a point.

Due to the complexities mentioned above, we will simplify the problem by looking at two special cases of Petlyuk column operation. In the first of these cases, all sections will operate at infinite reflux, while in the second case the reflux for sections 2-5 will be finite.

5.2.2   Simplified Problem: All sections at infinite reflux

5.2.2.1   **The infinite reflux Difference Point Equation**

The intuitive initial response when considering the infinite reflux Petlyuk column is to assume that all sections operate on a residue curve as Δ is 0. If we expand the difference point equation (Equation 5.1) we find that this is not necessarily the case.

$$\frac{dX}{dn} = \left(\frac{V}{L}\right)[X - Y(X)] + \left(\frac{\Delta}{L}\right)\left[\left(\frac{VY^T - LX^T}{\Delta}\right) - X\right] \qquad \textbf{(5.2)}$$

If $X^T \neq Y^T$ when $L = V$, the difference point equation becomes:

$$\frac{dX}{dn} = \left[X - Y(X)\right] + \left[Y^T - X^T\right]$$

$$\frac{dX}{dn} = \left[X - Y(X)\right] + \delta \qquad\qquad (5.3)$$

where $\delta = Y^T - X^T$

δ is the difference in composition between the vapour and liquid streams and is called the *difference vector* for the CS. The difference vector is constant all along the length of a CS.

For CS 1 and 6 $X^T = Y^T$ and $L = V$. These sections operate on a residue curve as $\delta = 0$. Sections 2-5 need not have $X^T = Y^T$ and can be described by Equation 5.3.

At these conditions the column section breakdown of Figure 5.3 can be simplified. Because no or infinitesimal amounts of material are removed at the side-draw or added at the feed, the operation of CS 2 is identical to CS 4 and operation of CS 3 is identical to CS 5. For these sections $\delta_2 = \delta_4$ and $\delta_3 = \delta_5$. The new CS breakdown is seen in Figure 5.4.

Because any material entering section A must leave at the same point, this CS is identical in performance to a total condenser mixing material from sections B and C liquefying and then returning it to these sections at a different composition. Analogously, section D behaves like a reboiler. Sections B and C in the already simplified Figure 5.4 and this even more simplified representation will be shown to be helpful in understanding the interaction of the two columns sections. Since we already know that A and D operate on residue curves running from their respective mixing points to the product compositions, the determination of the behaviour of the so-called "coupled column" system (B and C) *is* our only interest.
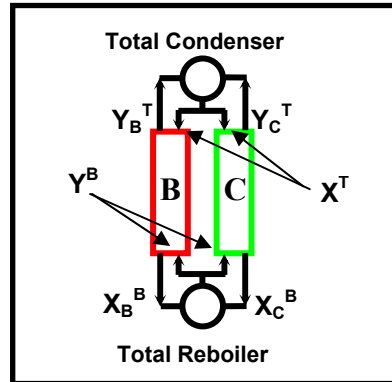
Figure 5.5: Coupled column sections

5.2.2.2 **Properties of the Difference Vector (δ)**

- If $\delta_i > 0$ There is a net flow of component i *up* the column. Component i is said to be in *rectifying* mode.

- If $\delta_i < 0$ There is a net flow of component i *down* the column. Component i is said to be in *stripping* mode.

- $\sum \delta_i = \sum (Y^T_i - X^T_i) = \sum Y^T_i - \sum X^T_i = 0$.

  This suggests that not all components can move in the same direction in a CS. (Unlike normal columns at finite reflux). Some components move up while others move down.

5.2.2.3 **Mass Balance for the coupled column system**

Material balance over the condenser yields:

$$V_B Y_B + V_C Y_C = L_B X_B + L_C X_C$$

$$\delta_B = -\delta_C$$

The CS difference vectors have equal magnitude but opposite sign. Components moving up the CS B have to move down CS C and vice versa. Once the value of δ is chosen for one half of the coupled column system, the value for the other half is set.

5.2.2.4 **Qualitative effects of δ direction**

Because δ is a vector, behaviour of the resulting CPM's can be characterised by its direction and magnitude. We can identify three different directions that result in qualitatively different behaviour of the CPM (see Figure 5.6). These directions correspond to changes of sign of the components of the system i.e. to the axes. A summary of δ_i in these directions can be seen in Table 5.1. Each region is split into two sub-regions. Sub-region **b** has opposite sign to sub-region **a**. If δ lies in sub-region **a** for CS C then δ for CS B is in sub-region b of the same region (I, II, III).
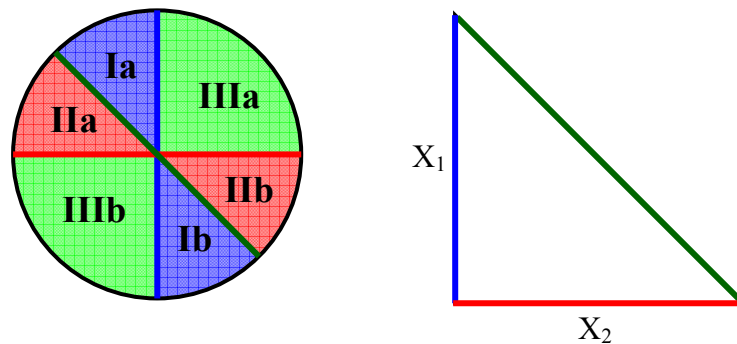
Figure 5.6: Schematic representation of regions of δ characterising CPM behaviour and corresponding component axes.

Direction	Ia	Ib
Component 1	+ve	-ve
Component 2	-ve	+ve
Component 3	-ve	+ve
	IIa	IIb
Component 1	+ve	-ve
Component 2	-ve	+ve
Component 3	+ve	-ve
	IIIa	IIIb
Component 1	+ve	-ve
Component 2	+ve	-ve
Component 3	-ve	+ve

Table 5.1: Summary of δ_i behaviour in each of the 3 defining regions

The overall difference of qualitative behaviour can be summarised using pinch point curves. Figure 5.7 to Figure 5.9 illustrate how the pinch point curves and therefore general form of the CPM's differ along each direction of δ. These loci of

points were constructed by solving for the stationary solutions of the infinite reflux difference point (Equation 5.3) at constant arbitrary δ vector orientations within each region while varying the vector magnitude.
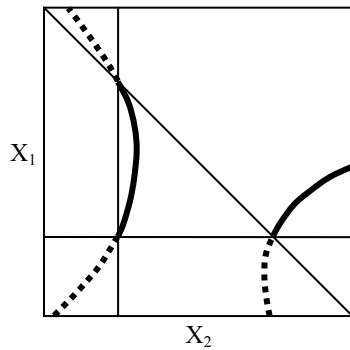
| **Figure 5.7: Pinch curve Region δ in I** | **Figure 5.8: Pinch curve Region δ in II** | **Figure 5.9: Pinch curve Region δ in III** |
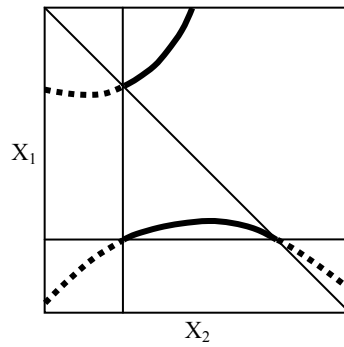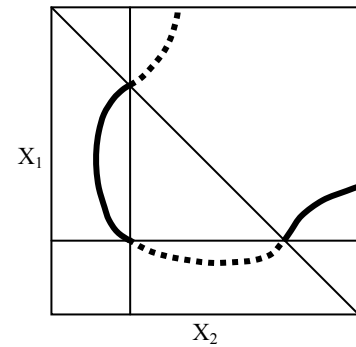
——————— a
·············· b

5.2.2.5 Design of the coupled system using CPM's

The methodology for design of the coupled column system is virtually the same as that described for the full Petlyuk configuration. Firstly a difference vector is chosen for either of the CS's. The CPM's for both are then generated by populating the composition space with trajectories produced by integrating the infinite reflux difference point equation (Equation 5.3). The CPM's are then superimposed and the feasible operating profiles determined. It is useful to reinforce what these feasibility criteria for the system are.

- Liquid profiles must intersect at the top of the CS's as both are fed the same composition by the condenser.
- Vapour profiles must intersect at the bottom of the CS's as both are fed the same composition by the reboiler.

The second criterion highlights an important point. For a full representation, of the composition profiles of the coupled system, both liquid and vapour profiles should be produced. CPM's typically track liquid profiles as they are generated using the

difference point equation (Equation 5.1). If vapour and liquid maps of both CS's are generated and superimposed, the effectiveness of the technique is diminished because the "density" of profiles makes them impossible to interpret. We can, however, ensure that the second criterion is satisfied by simply using the liquid trajectories. Mass balance dictates that the curvature, of vapour profiles, be very similar to that of the liquid profiles. This is due to the constant compositional offset represented by δ. It can be concluded that if two liquid profiles (of different column sections) intersect, the corresponding vapour profiles will also intersect (see Figure 5.10). The overall system will be satisfied wherever the superimposed profiles intersect twice (once for the first criterion and a second time for the second criterion).

The general form of any solution can be seen in Figure 5.10below.
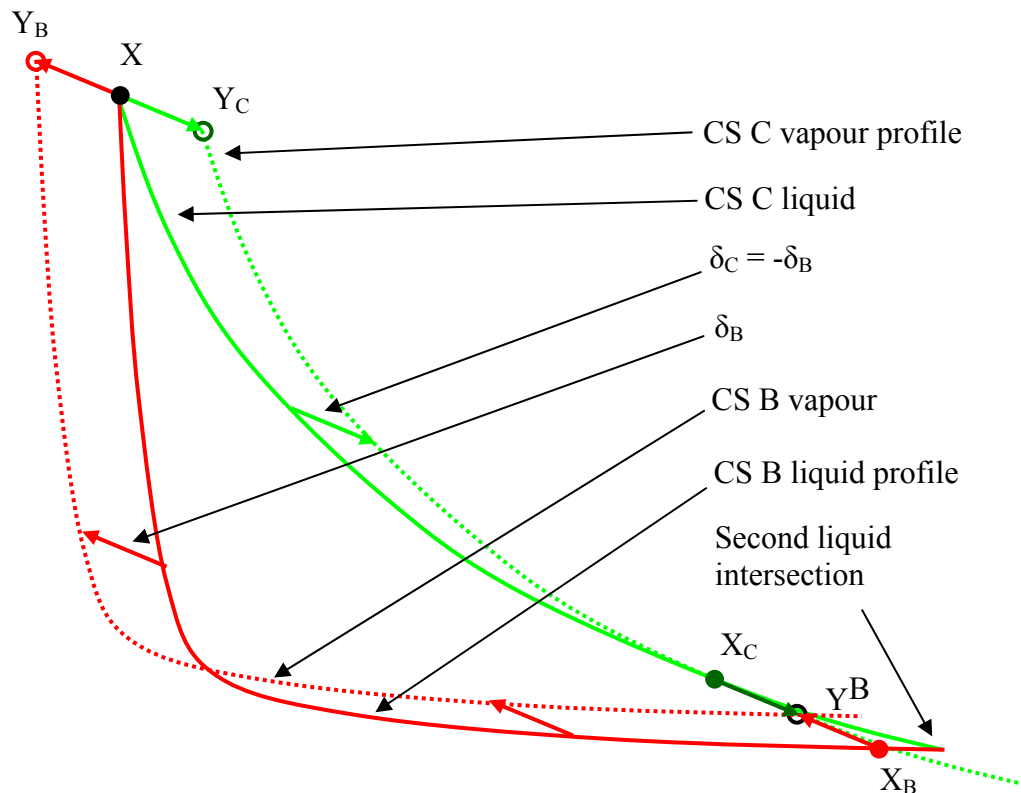
Figure 5.10: General form of solutions for coupled system

Now that the general form of the solutions is known, we can choose an arbitrary δ for one of the CS's and generate the CPM's. Below are CPMs produced with $\delta_B =$ [0.02;-0.06] and $\delta_C =$ [-0.02; 0.06] (region II); Figure 5.11 and Figure 5.12 respectively.
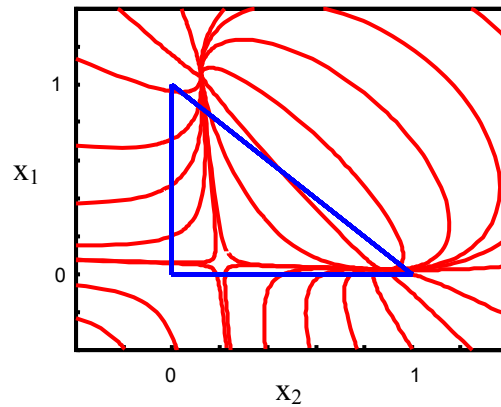
Figure 5.11: CPM for $\delta_B =$ [0.02;-0.06]
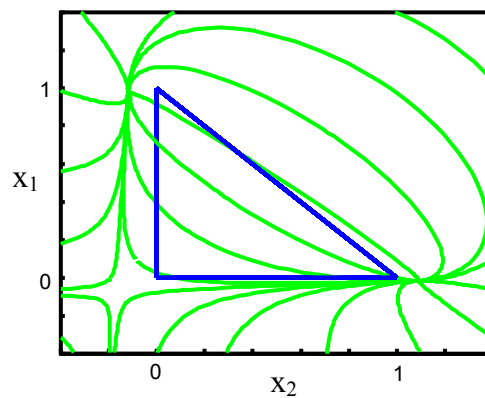
Figure 5.12: CPM for $\delta_C =$ [-0.02;0.06] (-δ_B)
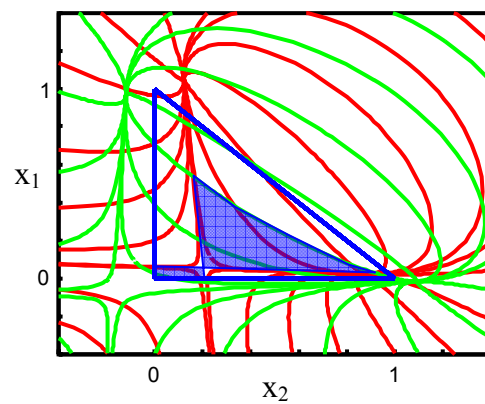
Figure 5.13: Superimposed CPM's

After superimposing the CPM's for each CS, it is simple to find the regions of double intersection of liquid profiles. This region is bound on two sides by the borders of the transformed triangle of the CS B (δ_B = [0.02;-0.06]). There is another boundary defined by the CS C profile running through the stable pinch point of the CS B CPM. The shaded region of Figure 5.13 covers all double intersections of liquid profiles for this choice of δ_B and δ_C. In general this region has a "bow-tie" shape. The smaller of the two shaded regions of the "bow-tie" (shown in the corner of the MBT in Figure 5.13 above) is, in fact, infeasible. If we consider the topology sampled here, we see that the direction of increasing stage number along the two sets of profiles is opposite between any two double intersecting points. That is to say the first intersection represents the top of one column section and the bottom of the other and vice versa for the second intersection. Therefore, this area of double intersections cannot produce feasible operating profiles

It is worth noting that even for the extremely simplified case of overall infinite reflux, the Petlyuk column exhibits multiplicity of steady state solutions. Although the number of stages may vary from one solution to another it is clear that the potential for multiplicity exists.

In general only values of δ chosen in regions I and II result in double intersections and therefore feasible solutions of the coupled column system. δ's chosen in region III never produce double intersection and consequently no feasible solutions.

5.2.3   Simplified Problem: Overall infinite reflux

The second simplifying case of the Petlyuk column we will look at is one of overall infinite reflux with finite operation of the coupled columns, i.e. a column that draws infinitesimal product flows, but does not necessarily operate with L=V in sections 2, 3, 4 and 5. For this scenario, we can once again refer to the simplified column section representations of Figure 5.4 and Figure 5.5.

The section breakdown in this case is the same as in the previous example, because the product draw and feed do not affect the difference point of the sections, as they are infinitesimal.

In this case, as in the previous one, sections A and D operate on residue curves, because all the vapour fed to a condenser must return as liquid (and vice versa for the reboiler) hence L must equal V and the difference point equation becomes:

$$\frac{dX}{dn} = [X - Y(X)] \qquad\qquad \textbf{(5.4)}$$

(This is equivalent to the residue curve differential equation.)

The split of liquid and vapour flows from sections A and D, respectively, does not have to be equal and therefore L_B is not necessarily equal to V_B and hence sections B and C need not operate on residue curves or the infinite reflux difference point equation curves defined by Equation 5.3. There are however, analogous mass balance constraints on the operating values of Δ_B, Δ_C, $r_{\Delta B}$, $r_{\Delta C}$, $X_{\Delta B}$ and $X_{\Delta C}$.

5.2.3.1 *Mass Balance and Reflux Ratios for Column Sections B and C*

Mass balance over mixing points:
$$L_A X_A + V_B Y_B + V_C Y_C = V_A Y_A + L_B X_B + L_C X_C$$

However $L_A = V_A$ and $X_A = Y_A$

Therefore $\Delta_B X_{\Delta B} = -(\Delta_C X_{\Delta C})$ and $\Delta_B = -\Delta_C$

From the mass balance it can be concluded that both sections must operate with the same difference point with equal magnitude but opposite directional net fluxes. This suggests, as in the previous example that components in rectifying mode in CS B will be in stripping mode in CS C.

The variables governing the operation of the coupled sections (B and C) include $r_{\Delta B}$, $r_{\Delta C}$, β_L (the ratio of liquid flow rates) and β_V (the ratio of vapour flow rates).

There are two degrees of freedom i.e. two of these variables can be set. It is convenient as well as useful to set the reflux ratios of each of the coupled sections. This is due to the fact that the topology of the column profile map is dependent on the reflux ratio chosen for a section. From mass balance it can be shown that the relative liquid flow rates i.e. the split ratio is:

$$\beta_L = L_B/L_C = - r_{\Delta B} / r_{\Delta C} \tag{5.5}$$

5.2.3.2   Design using CPM's

To design the coupled column system (sections B and C) we must determine which design criterion is most important. Using this criterion a basis for the choice of R_Δ and X_Δ for sections B and C can be found. For this example, we will set an intermediate product specification of 90%. Achieving this specification will be the primary concern when designing for X_Δ. Because this design specification can be achieved by any residue curve passing through the product spec region, the problem is purely academic but does allow insights into the more complicated finite reflux six-section design.

For constant relative volatility ternary systems, Tapp et al (2004) showed that CPM's have three fixed points corresponding to solutions of the difference point equation when the derivative is zero. These fixed or pinch points can be found by solving the resulting algebraic equations for X_P (as seen below) if the values of R_Δ and X_Δ are specified.

$$\frac{dX}{dn} = 0 \;\Rightarrow\; \left(\frac{1}{r_\Delta}+1\right)[X_P - Y(X_P)] + \frac{1}{r_\Delta}[X_\Delta - X_P] = 0 \tag{5.6}$$

This implies that the "transformed triangle" and hence the CPM can be produced without integrating the difference point equation because the CPM is known to be a simple transform of the residue curve map (except in the case of bifurcation of the solutions). See Figure 5.14 below.
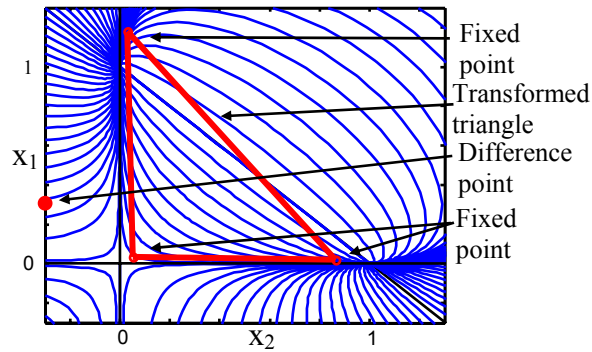
Figure 5.14: Transformed triangle for $X_\Delta = [0.3, -0.3]$ $r_\Delta = 19$
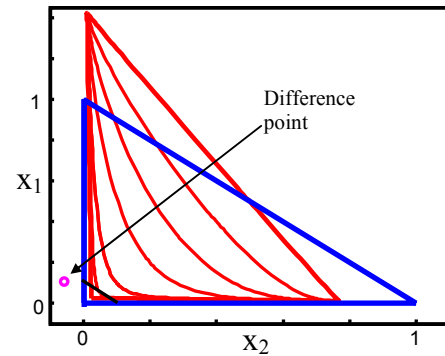
Figure 5.15: Transformed triangle satisfying spec with $X_\Delta = [0.1083, -0.0583]$

If the transformed triangle can be found algebraically by simply specifying the R_Δ and X_Δ, then the reverse must also be true. By knowing the fixed points of a CPM we must be able to determine R_Δ and X_Δ. In fact, if we take the liberty of specifying R_Δ, only the value of one fixed point is required to determine the difference point, X_Δ.

$$X_\Delta = X_P - (R_\Delta + 1)[X_P - Y(X_P)] \tag{5.7}$$

This result is very powerful, as it indicates that the designer can actually position the transformed triangle as required. Column section B of the infinite reflux Petlyuk column can be designed to meet the 90% intermediate product specification by positioning the saddle point of the transformed triangle within the product spec region. The fixed point should not be positioned on the product line, as the profile running around the corner of the transformed triangle requires infinite stages to do so. In effect, the design must be capable of doing "better" than what is theoretically required to satisfy the specification (See Figure 5.15). All profiles running through this product region will be feasible composition profiles for column section B. The column profile that is tangential to the product specification line at a point is the last trajectory that will satisfy the intermediate product requirements.

Now that the design parameters for section B can be determined, we can design column section C. By mass balance, both sections operate at the same X_Δ. The

values of Δ, however, must have opposite sign but equal magnitude. To design the CPM, all that needs to be specified, is the reflux ratio for section C and it can then be determined if the overall separation is feasible. The criteria for feasible column profiles in the coupled sections are the same as in the previous example:

- Intersection of liquid profiles at the top of column sections B and C (both are fed by the liquid from section A).
- Intersection of vapour profiles at the bottom of column section B and C (both are fed by the vapour from section D).

Again we can make use of the superimposition of the CPM's to find intersecting profiles. We also need only utilise the liquid trajectories as similar conclusions can be drawn, about the shape of the vapour trajectories, to those from the previous example. i.e. we once again need to find liquid profiles in the two CPM's that intersect twice.

Below is an illustration of superimposed CPM's satisfying the intermediate product specification with all areas of double intersecting profiles highlighted (Figure 5.16). The corner side of the "bow-tie" region has been omitted.
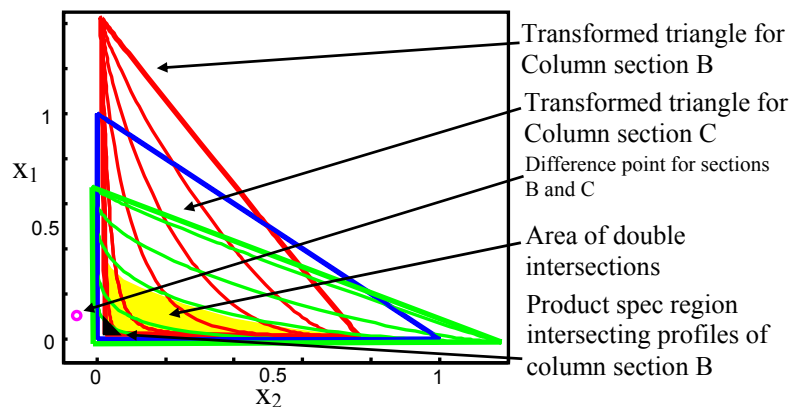
Figure 5.16: Superimposed transformed triangles for coupled column system

5.2.3.3   *Finalising the design*

We now have all sets of solutions for the coupled column sections of the infinite reflux Petlyuk column. All that is required now is the determination of the operating profiles. The full column profiles will be of the form seen in Figure 5.17 below.
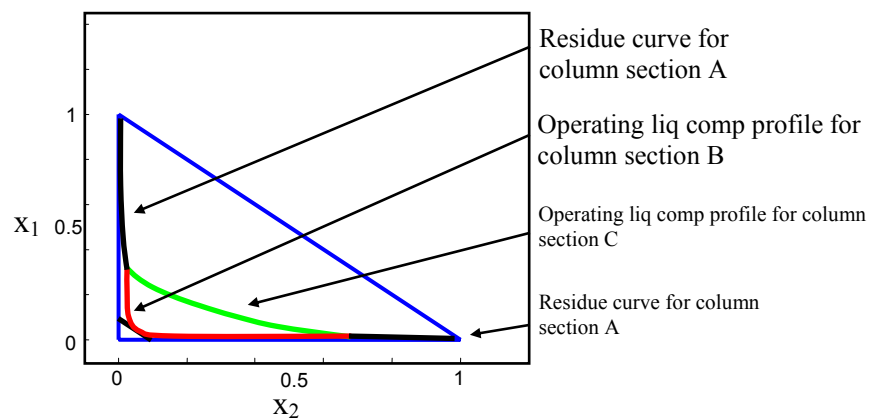
Figure 5.17: Finalised operating liquid column profiles

5.3 Discussion

The true power of the column profile map technique for distillation column design is the graphical insight it gives into the behaviour of proposed column configurations. Many other techniques involved trial and error and are based on rules of thumb which do not improve the designers understanding of the interaction of design parameters. All feasible CPM designs can be used very effectively as initialisation tools for rigorous design packages such as ASPEN Plus or Pro2. In fact the results from rigorous simulations vary only slightly from those achieved through the CPM design despite the fact that an assumption of equimolar overflow is made when using the difference point equation. The CPM's also allow insight into the control and operability of various configurations.

Designs such as those illustrated here have many solutions as can be seen in Figure 5.13 and Figure 5.16. All profiles within the shaded areas (excluding the smaller half of the "bow-tie" region of Figure 5.13) are potential steady state liquid composition profiles. Because there are so many steady state solutions there

is potential for control problems for this particular configuration. Not all solutions that are possible, meet the intermediated product requirement, so there may potentially be trouble maintaining this specification.

Although the finite reflux problem has not been solved here, the results of this design allow insights into the finite problem. The curvature of profiles on either side of the coupled sections will not vary greatly, so the form of the solution will be similar. The same operability challenges will be evident in the finite column as there are also regions of profiles that satisfy the mass balance and result in feasible columns. Although the choice of difference point for each coupled column section is more difficult at finite reflux, it can be done systematically by a choice of the general form of profiles required, acceptable refluxes and placement of fixed points. Any vapour-liquid equilibrium separation configuration can be addressed in this way and modelled successfully. A full finite reflux Petlyuk column design procedure using CPMs will be detailed in future work.

5.4 Conclusions

The CPM / "moving triangle" technique is a very powerful shortcut design tool. Any vapour-liquid equilibrium separation configuration, no matter how complex, can be modelled by simple addition of the column sections and hence CPM's comprising the configuration. The CPM's allow an understanding of the behaviour of parameters involved in the design. The design does not need to be performed "blind" in a trial and error approach as often results when the designer resorts to rules of thumb or rigorous design packages. The final CPM design, however, can be used to initialise rigorous simulation packages when more accurate results are required. Ultimately, because a greater understanding of the design process is achieved and because the technique is quick and simple, the designer can make good decisions early on in the design process thereby saving time and money which could otherwise have been wasted on a poor initial design.

Chapter 6:

Petlyuk Column Design

Sharp Split

Abstract

Currently employed short-cut design techniques tend to be configuration specific. Few can be employed on complex distillation configurations. In this work we will demonstrate, in detail, the use of column profile maps (CPMs) for the comprehensive analysis and design of complex distillation systems by applying the CPM technique to the design of the fully thermally coupled (Petlyuk) distillation column at sharp-split conditions. It is shown that for set product composition specifications and set reflux ratio, only a small region of key parameters (vapour and liquid split ratios) result in feasible separations. These results and hence the CPM design procedure are validated by the work of Halvorsen and Skogestad (2001). It is also shown that the minimum reflux solution can be found using the methodology. The results are valid for all zeotropic separation synthesis

6.1 Introduction

Distillation is one of the most utilised large scale industrial method of mixture separation. It is a very energy intensive process and accounts for a significant percentage of plant utility costs. A survey (Ognisty, 1995) conducted in the mid 1990's estimates that energy inputs to distillation columns in the United States accounts for approximately 3% of the countries entire energy consumption. It is clear that the efficiency of the separation can have a substantial influence on the profitability of a process and methods of improving the energy efficiency of distillation systems are, therefore, constantly sought.

One alternative, to the energy intensive, traditional distillation configurations, which has offered promise, are the thermally coupled distillation columns. These include side-strippers, side-rectifiers and fully thermally coupled configurations also known as Petlyuk columns. The energy demand of these and traditional columns has been well studied over the years: Petlyuk et al (1965); Stupin and Lockhart (1972); Hendry et al (1973); Doukas and Luyben (1978); Tedder and Rudd (1978); Westerberg (1985); Fidkowski and Krolikowski (1987); Glinos and Malone (1988); Carlberg and Westerberg (1989); Rudd (1992); Triantafyllou and Smith (1992); Wolff and Skogestad (1995); Westerberg and Wahnschafft (1996); Finn (1996). It has been shown analytically (Fidkowski and Krolikowski, 1987) that for three component zeotropic separations, the Petlyuk column has the lowest overall energy demand. The other thermally coupled configurations also require less energy than the traditional direct and indirect splits.

Thermally coupled configurations offer, not only, the potential for utility savings but for capital savings as well. Traditional direct and indirect configurations require two shells, two condensers and two reboilers for three component zeotropic separations. Side-rectifiers and side-strippers eliminate the requirement of one reboiler and one condenser respectively, while the Petlyuk column eliminates the requirement of one of each. Furthermore the two shell Petlyuk arrangement can be replaced with a single shell containing an internal divider or

wall. This is known as the dividing wall (Wright, 1949) or partitioned column and is thermodynamically equivalent to the Petlyuk column if there is no heat transfer through the dividing wall.

Clearly the Petlyuk column has many qualities which make it an attractive alternative to traditional configurations and yet relatively few have actually been employed industrially. Until fairly recently BASF was the sole industrial proponent of the dividing wall column (Kaibel, 1988, 1995). In the last few years, Sumito Heavy Industries Co. together with Kyowa Yuka (Parkinson, 1998) and MW Kellogg Limited together with BP Amoco (Lestak et al, 1999) have employed dividing wall columns. Other recent examples include German (Kolbe and Wenzel, 2002), American (Schultz, 2002) and South African companies. The major concern over the use of Petlyuk or dividing wall columns appears to be related to the efficient design and control of these arrangements.

The standard Petlyuk arrangement, of prefractionator and main column, suffers from the drawback that the pressure in the prefractionator is neither uniformly higher nor uniformly lower than the pressure in the main column. The vapour draw in the main column is required to be at a higher pressure than that at the bottom of the prefractionator while the vapour feed from the top of the prefractionator is required to be at a higher pressure than at the corresponding feed point in the main column (see Figure 6.4). New arrangements have been suggested (Agrawal and Fidkowski, 1998) that remove this issue by having unidirectional vapour flow either from the first to the second shell or vice versa. In these arrangements either the bottoms or the distillate is taken from the feed column. The dividing wall column can also suffer controllability problems due to the pressure differential across the dividing wall. This issue can be resolved by simply making use of equal stages on either side of the partition and hence enforcing an equal pressure drop on either side of the divide. A number of studies (Wolff and Skogestad 1995; Halvorsen and Skogestad, 1997, 1999; Abdul Mutalib and Smith, 1998a, 1998b) have been performed on the control and operation of the dividing wall column. Theoretical studies (Halvorsen and

Skogestad, 1997, 1999) suggest that maintaining column product specifications while operating close to the minimum column energy requirement is difficult without good control strategies. A pilot plant study (Abdul Mutalib and Smith, 1998b) of the control issue reported stable column responses, to feed disturbances, using temperature control. A product purity offset was reported, however.

The industrial reservations regarding the efficient design of the Petlyuk and dividing wall columns are likely related to the difficulty involved in rigorous simulation. Due to the thermal coupling of the prefractionator and main column a number of internal variables such as flows and compositions are required to be estimated when using iterative simulation packages. This requires advance knowledge of the solution output in order to achieve the solution. The less accurate the estimate of the unknown parameters, the less likely the iterative routine will converge to a solution. This issue, as well as general design issues, have been addressed in literature (Fonyo et al, 1974; Tedder and Rudd, 1978; Spadoni and Stramigioli, 1983; Triantafyllou and Smith, 1992; Amminudin et al, 2001), with varying success, but without a comprehensive understanding of the form of the Petlyuk solution and operating parameters.

One of the fundamental breakthroughs regarding the understanding of the dynamics and steady state operation of the Petlyuk column was the development of the analytical solution for minimum vapour requirement for sharp-splits (Fidkowski and Krolikowski, 1987). The solution makes use of the Underwood equations (Underwood, 1948) and the "carry-over" of the Underwood roots from one column section to another. This methodology, used to derive the minimum vapour flow equations, was then used to derive the Petlyuk "optimality region" for infinite stages and sharp splits (Halvorsen and Skogestad, 1997). The "optimality region" is a section of parameter space defined by the Petlyuk's vapour and liquid split ratios containing all feasible split ratios for set sharp/pure product specifications and set reflux ratio. The form of the "optimality region" was studied at various reflux ratios, feed compositions, feed qualities and relative volatilities. In terms of a general understanding of the column dynamics and

steady state, the study of the "optimality region" has been very successful. In terms of its use for design purposes, however, the methodology does suffer a number of drawbacks when put to practical use. It is only directly applicable to constant relative volatility systems as the Underwood equations are only valid for this set of thermodynamics. The generation of individual Petlyuk solutions from values within the "optimality region" still requires iterative solving methods. The non-sharp "optimality region" cannot be generated without extensive direct simulation.

It is our intention in this work to detail the use of Column Profile Maps (CPMs) (Tapp et al, 2004) as a design and optimisation tool for the Petlyuk column and to generate the "optimality region" for all zeotropic thermodynamics and product specifications. We will, however, refer to the "optimality region" as the "feasible region" as it is the set of split ratios resulting in feasible Petlyuk separations. The generation of the feasible region will be performed from a topological perspective and the net flow of components within the Petlyuk column will be analysed in detail. Although we will also make use of constant relative volatility assumptions, the graphical nature of the procedure will allow for the methodology's applicability to all zeotropic thermodynamics. The sharp-split solution and topological phenomena will be used to generate non-sharp split solutions where infinite stages are not necessarily required. The non-sharp minimum reflux solution will be detailed with reference to the sharp-split minimum reflux solution. This chapter will deal, solely, with the sharp-split solution and will lay down fundamental concepts and definitions which will be employed in the following chapter which addresses the non-sharp Petlyuk problem. By employing the CPM technique it will be shown that all required design parameters, even total required stages, feed stage and side-draw stage come "naturally" from the solution.

Assumptions:

- We will address the three component problem in this work.

- Constant molar overflow is assumed for all distillation modelling.

- An assumption of constant relative volatility is also made although the results are applicable to all three component zeotropic thermodynamics.

- Feed material is assumed to be at saturated liquid or saturated vapour conditions.

- Perfect mixing is assumed over all mixing points.

6.2 Column Profile Maps

CPMs, which were introduced by Tapp et al (2004), are maps of composition trajectories generated for a column section with constant net-molar-flow using the difference point equation (see Equation 6.1 below). The difference point equation (DPE) for column section (CS) k is defined as follows:

$$\frac{dX}{dn} = \left(\frac{1}{R_{\Delta k}} + 1\right)\left[X - Y^*(X)\right] + \frac{1}{R_{\Delta k}}\left[X_{\Delta k} - X\right] \tag{6.1}$$

Where: $X_{\Delta k} = (1 + R_{\Delta k})Y^T - R_{\Delta k}X^T$ and $R_{\Delta k} = \dfrac{L_k}{\Delta_k}$

- X is a liquid phase composition vector
- $Y^*(X)$ is the equilibrium vapour composition vector
- $R_{\Delta k}$ is the reflux ratio of CS k
- V_k is the vapour flow rate of CS k
- L_k is the liquid flow rate of CS k
- Δ_k is the net flow of CS k defined as $\Delta_k = V_k - L_k$
- n is a stage number equivalent
- X^T is the liquid composition vector at the top of the CS
- Y^T is the vapour composition vector at the top of the CS
- $X_{\Delta k}$ is the difference point of CS k

To produce a CPM, the DPE is solved at various initial conditions, throughout composition space (for n→∞ and n→-∞), after the selection of constants $X_{\Delta k}$ and $R_{\Delta k}$. A CPM can be seen in Figure 6.1 below. The solutions or composition profiles/trajectories tend to infinity or terminate at stationary points. For three-component, constant relative volatility, systems there are three stationary point solutions present in a CPM. These are characterised as unstable, saddle point or stable nodes (see Figure 6.1). The stationary points of a system are equivalent to pinch point compositions in a CS. We can draw straight lines through the stationary points of the system. The boundaries thus formed separate regions of qualitatively different topology.

The position of these stationary points (and boundaries) and subsequently the qualitative form of the CPM, for a particular system, is dependent on $X_{\Delta k}$ and $R_{\Delta k}$. For a set reflux ratio ($R_{\Delta k}$), the stationary points can be "shifted" around composition space by varying $X_{\Delta k}$. Similarly, for a constant $X_{\Delta k}$ value the stationary points can be "shifted" around composition space (along pinch point curves) by varying $R_{\Delta k}$. As $R_{\Delta k} \rightarrow \infty$, the stationary points tend to the pure component values of the mass balance triangle (*MBT) and the DPE collapses to the residue curve equation (see Equation 6.2). At these conditions, the boundaries of the CPM lie on the axes and the CPM becomes topologically equivalent to the residue curve map (RCM).

$$\frac{dX}{dn} = \left[X - Y^*(X) \right]$$
(6.2)

The CPM is in fact a simple transform of the RCM. The topology present in each region of the RCM (defined between the axes) is "transformed" at finite reflux and shifted around composition space (see Figure 6.2 and Figure 6.3).

By analysing the position of the stationary points, Tapp et al (2004) identified seven regions of $X_{\Delta k}$ placement that resulted in qualitatively different CPMs. These seven regions correspond to regions of the RCM with differing topology

---

* The MBT is defined by: $0 < x_1 < 1$; $0 < x_2 < 1$; $0 < x_3 < 1$

(seen Figure 6.2). Because the different topology of the residue curve map corresponds to the regions of X_Δ placement and the form of this topology is retained in the CPM, we can identify the shifted topology by referring to "*transformed regions*". A transformed region (TR) simply represents topology that is qualitatively similar to topology present in the residue curve map within a particular difference point region. Figure 6.3 shows the seven transformed regions of a CPM.

The fact that the form of the RCM topology is retained at finite reflux implies that we do not need to solve the DPE to determine the qualitative form of the CPM. We need only solve for the stationary points. This is computationally simple and can in fact be done analytically for three component constant relative volatility systems. By extending straight lines between the points we can produce a "*transformed triangle*" (TT). The TT retains all the qualitative topological information of the CPM (see Figure 6.1).
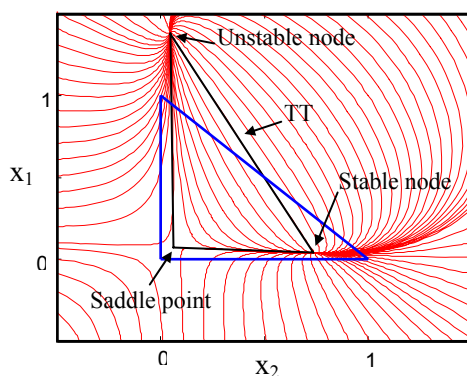
Figure 6.1: Column Profile Map for $X_\Delta = [0.3, -0.2]$ and $R_\Delta = 9$

Note: x_1 – Light Component, x_2 – Heavy Component, x_3 – Intermediate Component
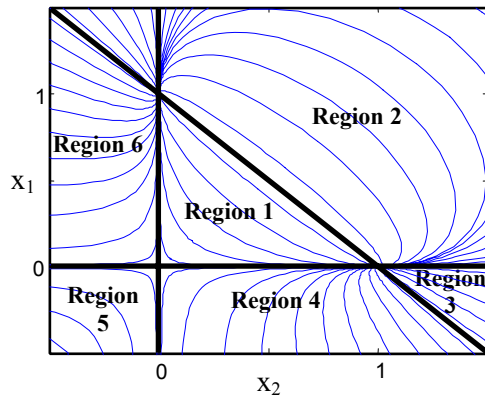
Figure 6.2: Difference point regions of Residue Curve Map
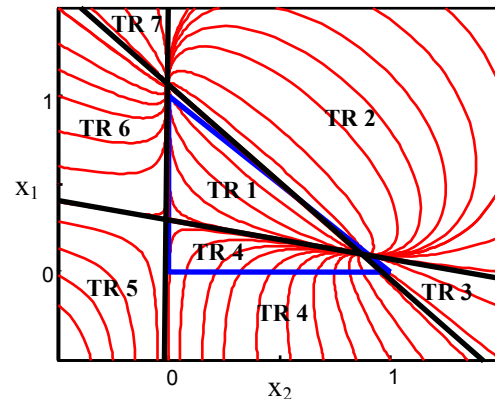
Figure 6.3: Transformed regions of Column Profile Map

6.3 Properties of Δ_k, $X_{\Delta k}$ and $R_{\Delta k}$

Δ_k which is defined as the difference between the vapour and liquid flows in CS k is a net flow of material within the column section. This net flow can be thought of as a pseudo stream flowing up or down the CS. If $V_k > L_k$, then $\Delta_k > 0$ and we have a net flow or pseudo stream flowing up the CS. But if $V_k < L_k$, then $\Delta_k < 0$ and we have a net flow or pseudo stream flowing down the CS. The value of Δ_k is the same at any point along the length of the CS.

The difference point ($X_{\Delta k}$) can be thought of as the pseudo composition vector of Δ_k, and is physically valid anywhere in composition space – both inside and outside the MBT. Because $X_{\Delta k}$ is a pseudo composition, the elements sum to 1 i.e. $\sum_{i=1}^{3} X_{\Delta k-i} = 1$. $X_{\Delta k-i}$, is the composition of element i in the pseudo stream Δ_k and $\Delta_k X_{\Delta k-i}$ is the net flow of component i within CS k. A positive value is a net flow of component i up and a negative value is a net flow of component i down the column section. If $X_{\Delta k-i}$ is negative, the direction of the net flow of component i is opposite to that of the Δ_k and the sum of the remaining components is greater than 1.

The reflux ratio is defined as the ratio of liquid flowing down the CS to the net flow in the CS. Because of its dependence on Δ_k, $R_{\Delta k}$ can be either positive (when $\Delta_k > 0$) or negative (when $\Delta_k < 0$). CPMs generated for a fixed difference point and positive reflux ratios are qualitatively different from those generated with the same difference point and negative reflux ratio.

6.4 CPM Design Methodology

Holland et al (2004 b) first introduced the methodology for distillation system design using CPMs. They illustrated the design of the Petlyuk column at overall infinite reflux. The outline for the methodology they introduced is as follows:

- *Break column configuration into column sections.*
- *Choose difference points(X_Δ) and reflux ratio (R_Δ) for the most important column sections*
- *By material balance determine the difference points and reflux ratios of the remaining sections.*
- *Produce column profile maps (CPMs) for each of the sections and superimpose them to determine feasible operating profiles (if they exist).*

We will address the finite reflux problem in a similar way. The above procedure cannot be employed directly due to the difficulty involved with choosing operating parameters (such as reflux ratios) for the prefractionator. It is very difficult to intuitively choose reflux ratios for the prefractionator column sections that will result in feasible designs. The general idea, nevertheless, is fundamental to our methodology. The column will be broken into column sections in the same way. Difference points will be chosen for the most important column sections – when the degrees of freedom are available. Feasibility of designs will always be determined by the superimposition of CPMs for each section.

To simplify the task a sharp-split specification on all products will be made i.e. the distillate product is assumed to contain effectively no heavy component

material, the bottoms product is assumed to contain effectively no light component material and the side-draw product is assumed to be effectively pure intermediate component material. The non-sharp split problem will be addressed in future work.

It will be shown that, by employing this design methodology, it is possible to find all solutions (if they exist) for a particular overall column reflux ratio (rectifying reflux ratio) and product choice. An understanding of column parameter dynamics can also be gleaned. When feasible solutions do not exist, the method allows the designer to determine when or why they do not exist. Furthermore, analysis of the column using the method allows a minimum overall column reflux ratio to be determined.

6.5 Column Section Breakdown and Net Flow

We shall begin the design process by breaking the Petlyuk column down into column sections. A schematic representation of the column can be seen in Figure 6.4 below. We can apply the column section breakdown approach used by Tapp et al (2004) to identify individual column sections within the configuration. Tapp et al (2004) defined column sections as lengths of column between points of addition or removal of material and/or energy. Using this definition, we can identify six column sections in the configuration. The column section breakdown is seen in Figure 6.5 below.

Column section 1 (CS 1) is a standard rectifying section terminated by a total or partial condenser. Column section 6 (CS 6) is a standard stripping section terminated by a total or partial reboiler. Column sections 2-5 will be referred to as the "*coupled column sections*".
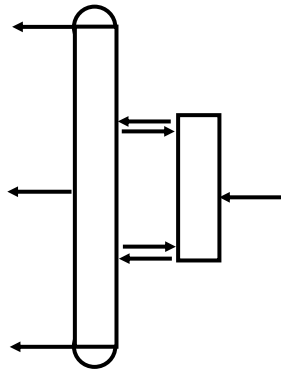
Figure 6.4: Petlyuk column (main column with prefractionator)
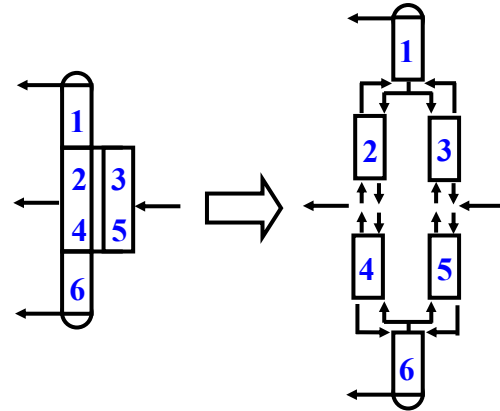
Figure 6.5: Column section breakdown for the Petlyuk column

6.5.1   Net Flow and Difference Point Material Balances in the Petlyuk Column

Δ_k is a pseudo stream within a column section. Because of this Δ_k has to obey the material balance in the same way that real streams do. This can be seen by performing a material balance at the point where feed material is added between to column sections (CS 3 and CS 5). See Figure 6.6 below.
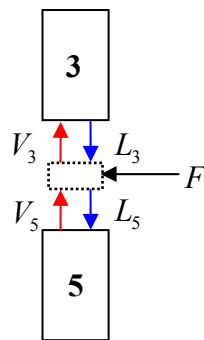
$$L_3 + V_5 + F = L_5 + V_3$$

Rearranging we obtain :

$$V_5 - L_5 + F = V_3 - L_3$$

But, $\Delta_k = V_k - L_k$

Therefore :

$$\Delta_5 + F = \Delta_3$$

$$\Delta_3 - \Delta_5 = F$$

(6.3)

Figure 6.6

As mentioned above, Δ_k can be positive or negative depending on the magnitude of the vapour and liquid flow rates. Equation 6.3 can be satisfied by various combinations of, positive and negative, Δ_3 and Δ_5 values. For example certain positive values of both Δ_3 and Δ_5 would satisfy Equation 6.3, as would certain negative values. Δ_3 could also be positive and Δ_5 negative. Negative Δ_3 and positive Δ_5 values, however, would violate the material balance. These net flow scenarios are illustrated in Figure 6.7a-d below.

CS 3 and 5:

| Figure 6.7a: Feasible net flow pattern ($\Delta 3 > 0$, $\Delta_5 > 0$) | Figure 6.7b: Feasible net flow pattern ($\Delta_3 < 0$, $\Delta_5 < 0$) | Figure 6.7c: Feasible net flow pattern ($\Delta_3 > 0$, $\Delta_5 < 0$) | Figure 6.7d: Infeasible net flow pattern ($\Delta_3 < 0$, $\Delta_5 > 0$) |

This may seem like a trivial result, unless we recall that the reflux ratio for a column section is a function of Δ_k and can be positive or negative. This result suggests that there are multiple reflux ratio combinations possible in the Petlyuk configuration. These combinations result in multiple, qualitatively different, CPMs that may be employed for the design. Some of the available combinations may provide more efficient separations. This implies that the net flow within the configuration may be advantageous or disadvantageous to the separation.

Let us now analyse the net flow combinations of the remaining mixing points in the configuration.

CS 1, 2 and 3:

Column section 1 (CS 1) is a standard rectifying section. It produces a product - the distillate. The distillate flow is equal to the net flow in CS 1 because these streams are defined in the same way. To produce a product V_1 is always greater than L_1; hence the net flow can only be positive in CS 1. The net flows in CS 2 and 3 can be either positive or negative. The various combinations are seen in Figure 6.8a-d below.

| Figure 6.8a: Feasible net flow pattern ($\Delta_2 > 0$, $\Delta_3 > 0$) | Figure 6.8b: Feasible net flow pattern ($\Delta_2 > 0$, $\Delta_3 < 0$) | Figure 6.8c: Feasible net flow pattern ($\Delta_2 < 0$, $\Delta_3 > 0$) | Figure 6.8d: Infeasible net flow pattern ($\Delta_2 < 0$, $\Delta_3 < 0$) |

CS 4, 5 and 6:

Column section 6 (CS 6) is a standard stripping section. It produces a product - the bottoms. The bottoms flow has equal magnitude but opposite sign to the net flow in CS 6 because the bottoms is defined as L_6-V_6. Since L_6 must be greater than V_6 to produce a product, the net flow can only be negative in CS 6. The net flows in CS 4 and 6 can be either positive or negative. The various combinations are seen in Figure 6.9a-d below.

Figure 6.9 a: Feasible net flow pattern ($\Delta_4<0, \Delta_5<0$)	Figure 6.9b: Feasible net flow pattern ($\Delta_4<0, \Delta_5>0$)	Figure 6.9c: Feasible net flow pattern ($\Delta_4>0, \Delta_5<0$)	Figure 6.9d: Infeasible net flow pattern ($\Delta_4>0, \Delta_5>0$)

CS 2 and 4:

The net flows in CS 2 and 4 can be either positive or negative. The various combinations are seen in Figure 6.10a-d below.

Figure 6.10 a: Feasible net flow pattern ($\Delta_2>0, \Delta_4>0$)	Figure 6.10b: Feasible net flow pattern ($\Delta_2<0, \Delta_4>0$)	Figure 6.10c: Feasible net flow pattern ($\Delta_2<0, \Delta_4<0$)	Figure 6.10d: Infeasible net flow pattern ($\Delta_2>0, \Delta_4<0$)

By combining the feasible net flow scenarios in each column section and disregarding those that are infeasible we see that there are, in fact, *five possible net flow patterns in the Petlyuk column*. This result is quite surprising in light of the single flow pattern possible in a two product column (up in the rectifying section and down in the stripping section). These five flow patterns will, undoubtedly, allow profiles from a much wider range of qualitatively different CPMs to be sampled. The five scenarios are named net flow pattern 1 through 5 and are illustrated in Figure 6.11a-e.
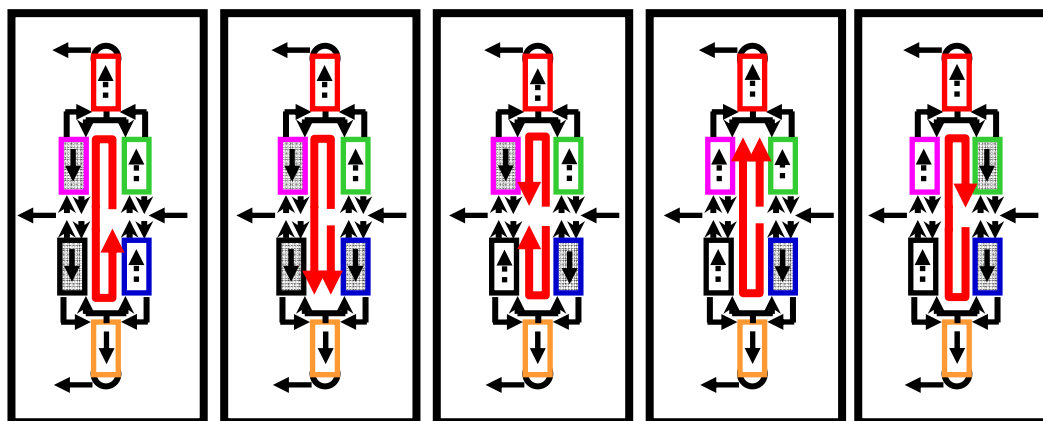
Figure 6.11a: Net flow pattern 1   **Figure 6.11b: Net flow pattern 2**   **Figure 6.11c: Net flow pattern 3**   **Figure 6.11d: Net flow pattern 4**   **Figure 6.11e: Net flow pattern 5**

Physically these flow patterns are induced by control on the vapour and liquid split ratios into the coupled column sections (CS 2-5) from the stripping and rectifying sections, respectively. The net flow of material within the column can also be thought of in terms of the distributions of feed material.

The feed material in Figure 6.11c is distributed between the top and bottom halves of the column, so that there is net flow of material in both directions. If the net amount of material directed to the bottom half of the column is increased, the case in Figure 6.11d is achieved. In this case, in order to maintain material balance, the material must be directed upwards, on the product side, in both CS 2 and 4. This is due to the fact that the side-draw flow rate is not large enough to change the direction of the net flow from CS 4 to CS 2. If the net amount of material directed to the top half of the column is increased, however, the case in Figure 6.11b is achieved. This case is the exact opposite of that in Figure 6.11d. The net flow of material on the product side is downwards for the same reasons given above. By increasing the material directed to the top half even further, the material eventually circulates (anti-clockwise in Figure 6.11a) within the coupled sections, flowing upwards in CS 5 instead of downwards. Conversely, if the material directed downwards on the feed side is increased further, the case in Figure 6.11e is achieved where material is circulated in the opposite direction (clockwise in Figure 6.11e).

The largest drawback to the configuration being operated with the net flow patterns 1, 2, 4 and 5 (Figure 6.11a, b, d and e) is that the net flow in the column sections at the side-draw (CS 2 and CS 4) is in the same direction. This results in the reflux ratios of the sections having the same sign. The side-draw has the effect of lowering the reflux from one column section to the other. If both refluxes are negative, the reflux of CS 4 will have a larger magnitude than that of CS 2. If the magnitude of the reflux of CS 2 is to be large enough to have the column operating on specification, the CS 4 reflux must be very high. *This ultimately means that CS 1 and CS 6 must operate at a fairly high reflux and the column will be energy intensive*. This is also true if both refluxes are positive. The net flow pattern 3 (Figure 6.11c) does not have this drawback and is therefore likely to be the most energy efficient operating mode.

6.5.2   Difference Points and the Material Balance

Because difference points are like pseudo compositions, they obey linear mixing rules. This can be shown by performing a component material balance at the feed point between CSs 3 and 5. See Figure 6.12.
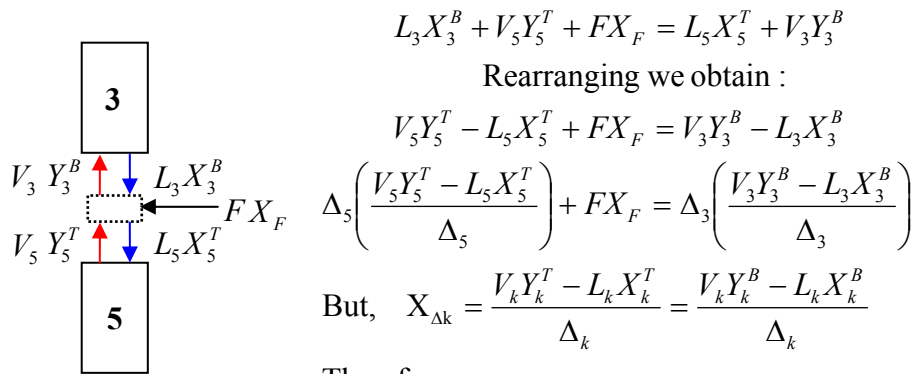
$$L_3 X_3^B + V_5 Y_5^T + F X_F = L_5 X_5^T + V_3 Y_3^B$$

<div align="center">Rearranging we obtain :</div>

$$V_5 Y_5^T - L_5 X_5^T + F X_F = V_3 Y_3^B - L_3 X_3^B$$

$$\Delta_5 \left(\frac{V_5 Y_5^T - L_5 X_5^T}{\Delta_5} \right) + F X_F = \Delta_3 \left(\frac{V_3 Y_3^B - L_3 X_3^B}{\Delta_3} \right)$$

But, $X_{\Delta k} = \dfrac{V_k Y_k^T - L_k X_k^T}{\Delta_k} = \dfrac{V_k Y_k^B - L_k X_k^B}{\Delta_k}$

Therefore :

$$\Delta_5 X_{\Delta 5} + F X_F = \Delta_3 X_{\Delta 3} \tag{6.4}$$

Figure 6.12:

Geometrically this is equivalent to difference points $X_{\Delta 3}$ and $X_{\Delta 5}$ lying on a straight line through X_F, in composition space. Their relative positions will depend

on the sign and magnitude of Δ_3 and Δ_5. Table 6.1 summarises the various possibilities for CS 3 and 5.

The dependence of the difference point positions on the net flow implies that there will be as many relative difference point placement scenarios as there are net flow patterns. This is, indeed, the case and these will be explored in more detail later.

Net Flow Pattern	Δ_3	Δ_5	Relative Positions of Difference Points
1	+	+	$X_{\Delta5}$ $X_{\Delta3}$ X_F
2, 3, 4	+	-	$X_{\Delta5}$ X_F $X_{\Delta3}$
5	-	-	$X_{\Delta3}$ $X_{\Delta5}$ X_F
	-	+	Infeasible

Table 6.1: Geometric Interpretation of Material Balance over CS 3 and 5

6.6 Composition Matching Criteria

The approach of treating the Petlyuk column as a number of column sections and piecing the solutions to these (the CPMs) together, as apposed to finding the solution to the entire column through iteration, results in the designer having to be mindful of certain composition matching criteria which need to be satisfied. Composition matching is required at all points where column sections meet. We will now discuss the required criteria at each of these four mixing points.

Composition Matching Criterion 1:
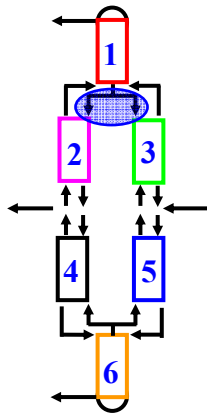
Figure 6.13a:

The liquid profiles from CS 1, CS 2 and CS 3 must all intersect if they are to be considered as possible operating profiles. This is simply due to the fact that the liquid leaving the bottom of CS 1 is divided between CS 2 and CS 3; hence this composition must exist on all three profiles. If CS 1 was not a standard rectifying section and the CPMs of all three column sections were superimposed, any three intersecting profiles from these maps could be thought of as possible solutions to the three-column

section system. The situation is somewhat simplified by the fact that CS 1 is a rectifying section as only one profile on this CPM is valid. Rectifying sections have to operate on profiles that pass through the distillate composition or the composition in equilibrium with this stream, hence only one profile is valid. Any profiles from the CPMs of CS 2 and CS 3 intersecting on this solution are valid however.

Composition Matching Criterion 2:
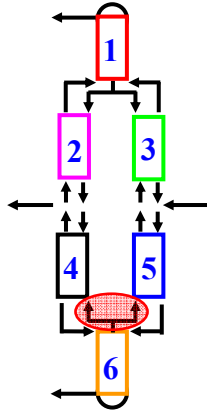
Figure 6.13b:

The vapour profiles of the CS 4, CS 5 and CS 6 must all intersect because CS 4 and CS 5 are both fed vapour by CS 6, which is a standard stripping section. Only one profile of the CS 6 vapour CPM is valid as the vapour stripping profile must pass through either the bottoms composition or composition in equilibrium with this stream. Any profiles from the vapour CPMs of CS 4 and CS 5 intersecting on this solution are valid.

Composition Matching Criterion 3:
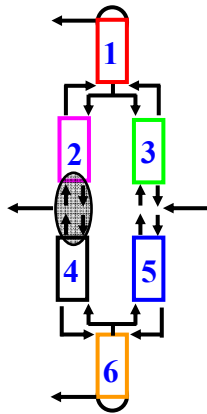
Figure 6.13c:

Both the liquid and vapour profiles of CS 2 and CS 4 must intersect. There is no composition change in either the vapour or liquid material from the bottom of CS 2 to the top of CS 4. This is because material is removed from, not added to, the liquid or vapour streams. Valid profiles must intersect at the side-draw composition.

Composition Matching Criterion 4:
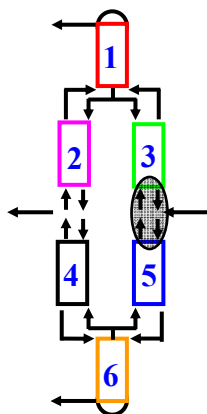
Figure 6.13d:

The liquid or vapour profiles of CS 3 and CS 5 must intersect. If the feed material is vapour then we assume that it mixes perfectly and instantly with the vapour stream from CS 5 to produce the bottom vapour stream of CS 3. It is assumed that there is no mass transfer to the liquid stream leaving CS 3 and that this composition is the same as the top liquid composition in CS 5. Similarly if the feed is liquid, it is assumed that the vapour composition at the top of CS 5 is the same as that at the bottom of CS 3.

It is important to note that if the composition at which the matching criterion, of one phase is satisfied, is identified on CPM k and CPM k+1 and the difference points used to generate the two CPMs satisfy the material balance, the compositions of associated passing streams will satisfy the material balance required of that phase. This means that if we superimpose CPMs to determine where the matching criteria are satisfied, we need not worry about satisfying the material balance and finding associated compositions of the other phase. These will automatically be satisfied and can easily be calculated, if required, using the definitions of the difference point and net flow of the particular CS.

6.7 Feasible Topology

It would be very useful during the design process to be able to determine ranges of feasible column parameters (such as reflux ratio etc) without generating every possible solution in doing so. Unfortunately, however, there is no analytical way of tracking arbitrary solutions within each CPM and determining whether or not they produce feasible Petlyuk column solutions, unless an explicit function exists for these profiles.

In this chapter, to bypass this problem, we will look at the case where there is a sharp-split on all the products. Restricting ourselves to this class of solution enables us to determine the exact position of all viable column section profiles for any set of parameters. We will now investigate why this is possible by analysing the effects of each sharp product specification.

Firstly, however, we must clarify the definition of individual sharp product specifications.

- A *sharp distillate product specification* is one in which the light and intermediate components appear in finite quantities, but the heavy component appears in infinitesimal quantities.

- A *sharp bottoms product specification* is one in which the heavy and intermediate components appear in finite quantities, but the light component appears in infinitesimal quantities.

- The side-draw product can be sharp in terms of the light component (infinitesimal light component material but finite intermediate and heavy component material), sharp in terms of the heavy component (infinitesimal heavy component material but finite intermediate and light component material) or sharp in terms of the light and heavy components (effectively pure intermediate component material). For this work, a *sharp side-draw product specification* will be taken as one which is sharp in terms of both the light and heavy components.

With clarified definitions we are now in a position to analyse the topological effects of the sharp product specifications.

6.7.1   Implications of Sharp Distillate Product Specifications

A sharp distillate product specification means that the distillate product (X_D) is effectively confined to the light-intermediate axis (x_1 axis).

But $X_D = \dfrac{V_1 Y_1^T - L_1 X_1^T}{D} = X_{\Delta 1}$ i.e. the difference point of CS 1 ($X_{\Delta 1}$) is equal to the distillate composition. *This means that $X_{\Delta 1}$ is a real composition in the column and is confined to the light-intermediate axis.*

If we analyse the rectifying profile as well as the movement of the CS 1 transformed triangle (TT) - which is equivalent to analysing the movement of the stationary points – while varying $X_{\Delta 1}$ (at constant $R_{\Delta 1}$), we notice that as the difference point is moved closer to the light-intermediate axis, the profile and one of the TT boundaries approach the axis as well. The TT boundary, defined between the unstable node and the saddle point, approaches the axis from negative heavy component space, while the rectifying composition profile approaches from positive heavy component space. When the difference point is effectively on the

axis, the afore-mentioned TT boundary lies here too and *the rectifying profile runs along the boundaries of this triangle*. Figure 6.14a-c illustrate this phenomenon.
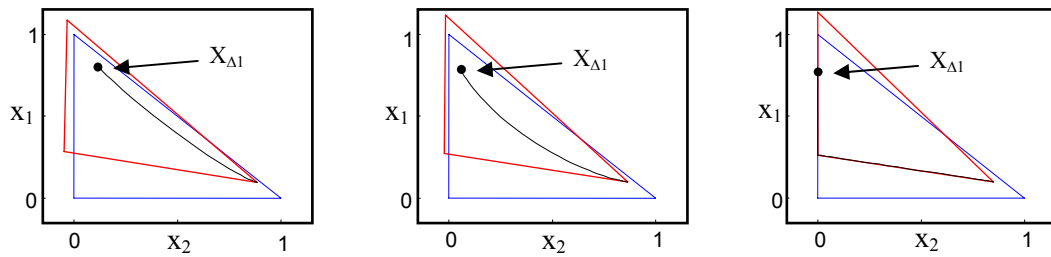
Figure 6.14 a-c: Rectifying profiles for difference points at varying distances from the light-intermediate axis.Implications of Sharp Bottoms Product Specifications

A sharp bottoms product specification means that the bottoms product (X_B) is effectively confined to the heavy-intermediate axis (x_2 axis).

But $X_B = \dfrac{V_6 Y_6^B - L_6 X_6^B}{-B} = \dfrac{V_6 Y_6^B - L_6 X_6^B}{\Delta_6} = X_{\Delta 6}$ i.e. the difference point of CS 6

($X_{\Delta 6}$) is equal to the bottoms composition. *This means that $X_{\Delta 6}$ is a real composition in the column and is confined to the intermediate-heavy axis.*

If we analyse the stripping profile and CS 6 TT, in the same way as we did for the sharp distillate specification, we notice that as we move $X_{\Delta 6}$ towards the intermediate-heavy axis the stripping profile and one of the TT boundaries move towards each other and the axis as well. When $X_{\Delta 6}$ lies effectively on the axis, the TT boundary defined between the saddle-point and stable node lies here too and *the stripping profile runs along the boundaries of this triangle*. Figure 6.15a-c illustrate this phenomenon.
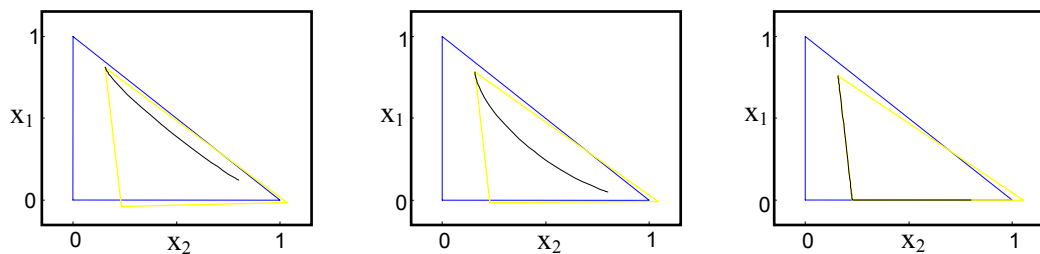
Figure 6.15: Stripping profiles for difference points at varying distances from the intermediate-heavy axis.

6.7.2   Implications of Sharp Side-Draw Product Specifications

Analysis of the CS 2 and 4 TTs is not possible until we have discussed the feasible placements of $X_{\Delta 2}$ and $X_{\Delta 4}$. For now, however, it will suffice to state that because the CS 2 profile has to satisfy matching criteria 1 and 3 it will *run effectively on the light-intermediate axis and also along the boundaries of the CS 2 TT*. Similarly, the CS 4 profile has to satisfy composition matching criteria 2 and 3 and will *run effectively on the intermediate-heavy axis and the CS 4 TT boundaries*.

6.7.3   Implications of Sharp Product Specifications for CS 3 and CS 5

Because the product placement forces composition matching criteria 1 and 2 to be satisfied close to the axes, the CS 3 and CS 5 profiles, respectively, will be forced to satisfy these compositions too. We will see later that the difference points of these sections must also lie on the axes and these profiles therefore run along the boundaries of their respective TTs.

6.7.4   Summary of the Topological Effects of Sharp-Split Specifications

The topological effect of a sharp product specification is, clearly, to force the composition profile of the CS, from which the product is drawn, to operate on the boundary of its associated TT. By specifying all products as sharp we force, not only the composition profiles of these product CSs but *all the configuration composition profiles to operate on their associated TTs*.

This means we need only produce the TTs, instead of the entire CPM, for any set of parameters, to immediately determine whether or not all the column section solutions will satisfy the Petlyuk matching criteria and therefore produce a feasible column design. Instead of focusing on the intersection of many individual solutions, we can simply focus on the overlap of the TTs concerned. We need, in fact, only analyse the liquid TT. It is a product of the vapour-liquid equilibrium that if a TT for one phase overlaps, the other will overlap also (see Appendix D for details).

6.8 General form of the Petlyuk Composition Profiles

If the development of a design tool is to be successful, we need a qualitative understanding of the form Petlyuk composition profiles would take for ideal systems. We can look at each of the six column sections separately and postulate what an efficient well designed profile would look like.

 CS 1 is a rectifying section. Profiles for this section will run from the distillate composition, along the light-intermediate axis, getting rapidly richer in the intermediate component and slowly richer in the heavy component. We know that these profiles run along the boundaries of their TTs (for sharp-splits) and should therefore run through the saddle point composition. At the saddle point, they will "tear" away from the light-intermediate axis (x_1 axis) and quickly gain in the heavy component until the composition profile pinches within the MBT. We know that the profiles must pinch within the MBT by analysing the, positive reflux, pinch point curves for qualitatively different $X_{\Delta k}$ placement produced by Tapp et al. (2004). The stable nodes of CPMs, produced for difference points within difference point region 1, always lie within the MBT (for ideal systems). The probable form of the liquid and vapour solutions can be seen in Figure 6.16a below. Using the profiles as a basis, the probable form of the TTs will be similar to that seen in Figure 6.16b.

Solutions for the stripping section (CS 6) will behave in the same way with respect to the intermediate composition moving away from the product (in this case the bottoms composition) and will "tear" away from the intermediate-heavy axis (x_2 axis) at a saddle point but now becoming rapidly richer in the light component. The stripping profiles will pinch at unstable nodes within the MBT. This is ascertained, again, by consulting the pinch point curves (for negative reflux ratios) produced by Tapp et al (2004). The stripping profiles can be seen in Figure 6.17a. Again using the profiles as a basis the probable form of the TTs will be similar to that of Figure 6.17b.

The main purpose of CS 2 is to transport the intermediate component from the top half of the column to the side-draw. The amount of heavy component transported here should be minimal. The composition trajectories for CS 2 must, therefore, run (along the light-intermediate axis) from the side-draw composition (high purity intermediate composition) gaining in the light component until they reach the rectifying trajectories and satisfy composition matching criterion 1. It is possible for these profiles to pinch at the top of the CS. If this were to happen, the pinch point would be an unstable node. The probable form of the trajectories would be similar to those seen in Figure 6.18a. The TTs are likely of the form seen in 6.18b.

CS 4 transports the intermediate from the bottom half of the column to the side-draw. Very little light component material should be transported in this section. The profiles for CS 4 should run from the side-draw, along the intermediate-heavy axis, to meet up with the stripping section profiles and satisfy composition matching criterion 2. It is feasible for these profiles to pinch at the bottom of the CS. In this case the pinch point would be a stable node. The resulting profiles would look like those in Figure 6.19a and the corresponding TTs would likely be of the form seen in Figure 6.19b.

CS 3 is required to transport both light-component material to CS 1 and intermediate material to CS 2. As these sections must process as little heavy-component material as possible (for product purity purposes) this material must be minimised in CS 3 as well. Potential profiles for CS 3 will run from the point where CS 2's profile meets the rectifying profile, along the light-intermediate axis, towards a saddle point and then tear away from the boundary towards the feed composition, where either the liquid or vapour profile will intersect the CS 5 profile as shown in Figure 6.20a and Figure 6.20b.

CS 5 must transport heavy component material to CS 6 and intermediate component material to CS 4 with minimal light material. Potential profiles will run from the point where CS 4's profile meets the stripping profile, along the

intermediate-heavy axis, towards a saddle point and then tear away from the boundary towards the feed composition, where they meet up with the CS 3 profiles as shown in Figure 6.21a and Figure 6.21b.

The complete set of composition profiles and corresponding TTs for the Petlyuk column can be seen in Figure 6.22a and Figure 6.22b, respectively. Figure 6.22b, clearly shows how all composition matching criteria (required for a feasible design) are satisfied by the overlap of the liquid TTs concerned.

With an understanding of the probable form of Petlyuk solutions we are now in a position to test column parameters for potential feasibility. Values for these parameters which result in dramatically different topological phenomena, for each CS, from that discussed above and do not result in the satisfaction of the composition matching criteria required can be discarded.

Note: Unless otherwise stated, within composition diagrams a solid line will denote the liquid phase while a dotted line will denote vapour phase (except lines CLL1 and CLL2 – defined later). Red lines (within composition diagrams) are associated with CS 1, pink with CS 2, green with CS 3, black with CS 4, blue with CS 5 and yellow with CS 6. The light component composition (x_1) will always be represented on the y-axis while the heavy component composition (x_2) will be represented on the x-axis. The MBT will always be represented by a blue triangle.

Legend: Composition Diagrams

————	Liquid composition CS 1	....	Vapour composition CS 1
————	Liquid composition CS 2	....	Vapour composition CS 2
————	Liquid composition CS 3	....	Vapour composition CS 3
————	Liquid composition CS 4	....	Vapour composition CS 4
————	Liquid composition CS 5	....	Vapour composition CS 5
————	Liquid composition CS 6	....	Vapour composition CS 6
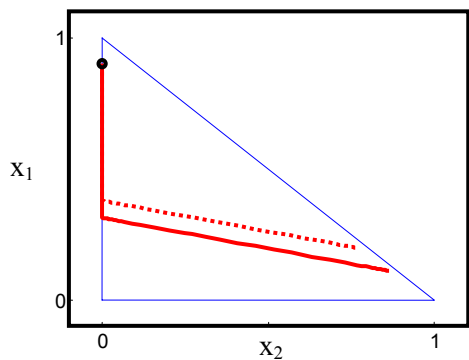
Figure 6.16a: Rectifying composition profiles
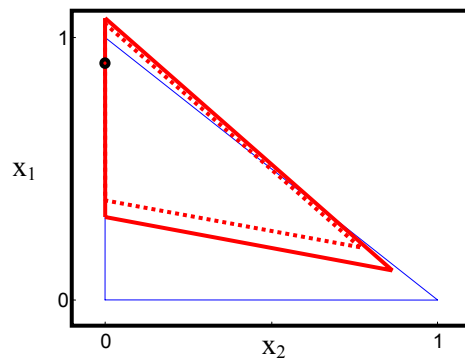
Figure 6.16b: Rectifying section TTs
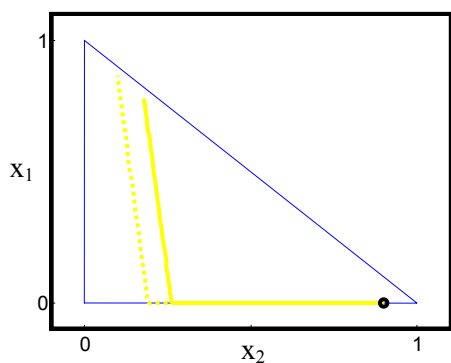
Figure 6.17a: Stripping composition profiles
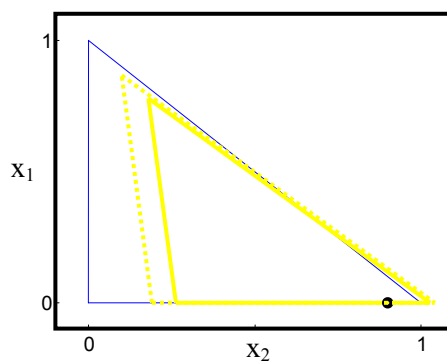
Figure 6.17b: Stripping section TTs
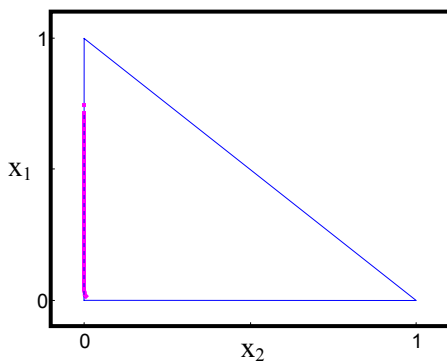
Figure 6.18a: CS 2 composition profiles
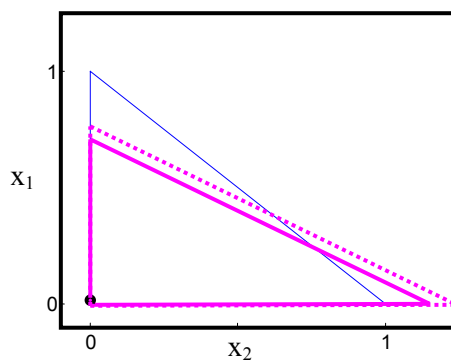
Figure 6.18b: CS 2 TTs
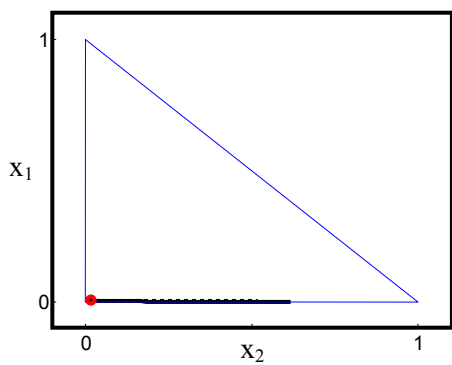
Figure 6.19a: CS 4 composition profiles
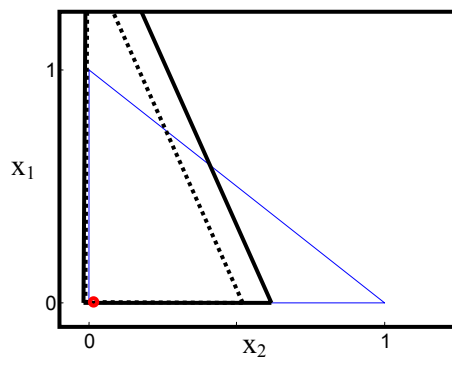
Figure 6.19b: CS 4 TTs
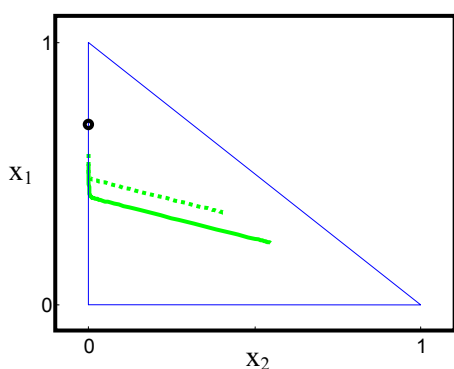
Figure 6.20a: CS 3 composition profiles
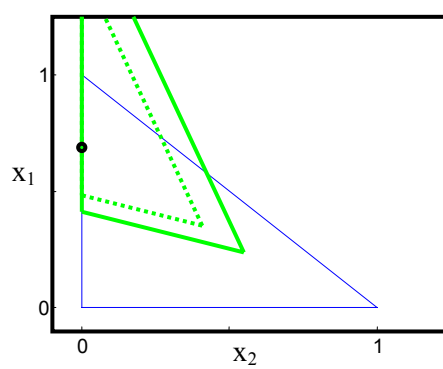
Figure 6.20b: CS 3 TTs
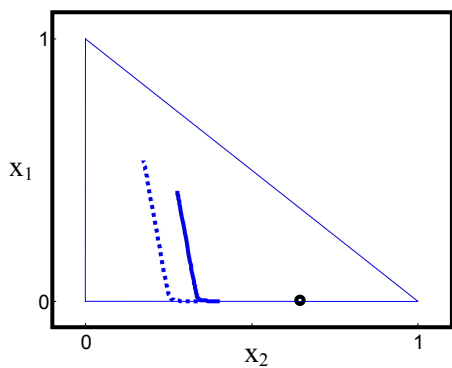
Figure 6.21a: CS 5 composition profiles
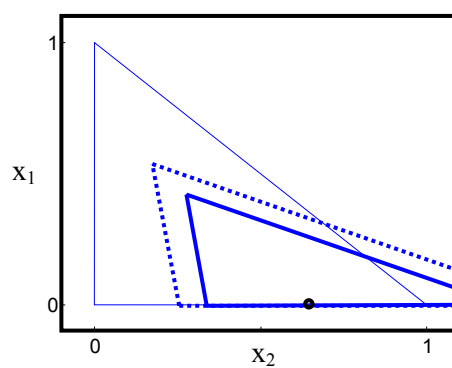
Figure 6.21b: CS 5 TTs
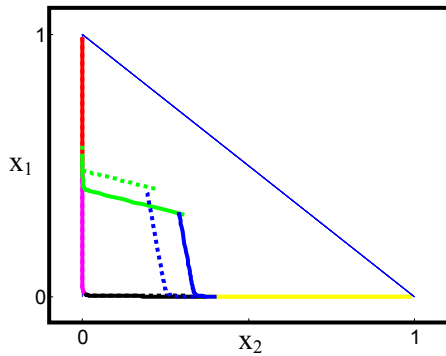
Figure 6.22a: Petlyuk composition profiles
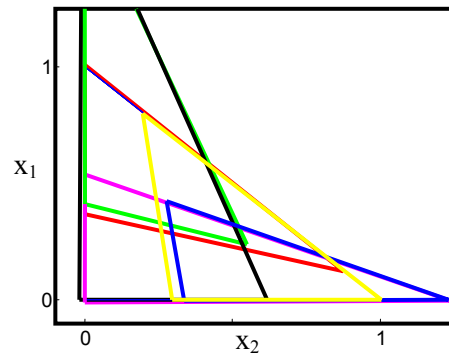
Figure 6.22b: All six column section TTs

6.9 Degrees of Freedom and Variable Selection

6.9.1 Degrees of Freedom

The Petlyuk column, due to the thermal coupling of the main column with a prefractionator, is a fairly complicated column to design. This complication arises as a result of the multiple degrees of freedom (DOF) introduced to the design by the coupling. In distillation systems, for simplicity, we can divide these DOF into composition variables, overall material balance variables and internal material balance variables. With simple distillation columns, for a given feed, there are only three degrees of freedom - one of the product composition variables may be specified (i.e. X_D or X_B), one overall material balance variable may be specified (i.e. distillate or bottoms rate) and one of the internal material balance variables may be specified (i.e. reflux ratio or boil-up ratio).

For the Petlyuk column, however, for a given feed there are two product compositional DOF, two overall material balance DOF, one internal compositional DOF and three internal material balance DOF (two in the coupled sections and one in either the rectifying or stripping sections). In total eight DOF. This, clearly, adds many levels of complexity to the design process.

It is important to note that the total required stages, feed stage and side-draw stage are not considered as degrees of freedom when designing using the CPM technique. These variables result as a solution from the process once all other DOF have been specified. They can be determined by tracking variable n in the difference point equation (Equation 6.1) for any particular Petlyuk solution.

Some of the possible design variables include:

$R_{\Delta k}$ CS k reflux ratio

$X_{\Delta k}$ CS k difference point

D   Distillate flow rate

B   Bottoms flow rate

S   Side-draw flow rate

L_k CS k internal liquid flow rate

V_k CS k internal vapour flow rate

Φ_V Vapour split ratio (V_2/V_1)

Φ_L Liquid split ratio (L_2/L_1)

$\Phi_V{}'$ Vapour split ratio (V_4/V_6)

$\Phi_L{}'$ Liquid split ratio (L_4/L_6)

Of the multiple possible design variables only eight may be specified. We will now discuss the selection of these variables and their effects on the design.

6.9.2   Variable Selection

It is important in this geometric based design process to work with, where possible, variables whose effects on the entire configuration are understood. Variables such as the reflux ratio, for instance, are useful when analysing a single column section, as we can intuitively comprehend its effects on the composition profile. However, the influence of changes of reflux ratio in one column section on the composition profile of another column section may be more difficult to understand. Generally, the interaction of variables becomes more and more complex as they are coupled by the connection of column sections. For this reason

the design approach we will take, although fairly intuitive, will be used in an attempt to "uncouple" the rectifying and stripping sections from the remainder of the column by specifying either of these sets of variables independently.

As mentioned previously we shall be dealing with sharp splits on all products. The distillate will be chosen to contain almost no heavy material, the bottoms product will be chosen to contain effectively no light material and the flow rates of these product streams will be chosen such that the side-draw will, effectively, be pure intermediate product. Specifying these variables (Δ_1, $X_{\Delta 1}$, Δ_6, $X_{\Delta 6}$) satisfies four DOF; two compositional and two overall material balance DOF. If we now specify an internal variable (e.g. reflux) of either the rectifying (CS 1) or stripping sections (CS 6), both sections will be completely satisfied and no freedom will exist for the selection of other variables in either. We will specify the reflux of CS 1 ($R_{\Delta 1}$), as apposed to that of CS 6, although this is completely arbitrary. Once $R_{\Delta 1}$ is specified the reflux of CS 6 can be determined by material balance. Five DOF have now been specified. The conditions within the coupled sections (CS 2-5) are dependant on the conditions of the rectifying and stripping sections and the remaining three DOF.

Of the three remaining DOF, one is a compositional DOF and two are internal material balance DOF. As CS 1 and CS 6 are completely specified, these remaining variables must be specified in CS 2 to CS 5. The choice of compositional variable will be discussed in greater detail later, but for now it will suffice to state that we will specify the difference point of CS 2 ($X_{\Delta 2}$). The remaining variables, both internal material balance variables, are the most difficult to choose. As mentioned above working with reflux, although convenient for single column sections, becomes less useful when multiple sections are connected. If we decided to work with the reflux ratio of one of the coupled column sections it would not be obvious what effect changes to this variable would have on the other sections. Another issue would be the choice of column section to work with. Although this may be more obvious for other variables, it does present an issue here.

The variables we will choose to work with are Φ_V and Φ_L, which are defined, respectively, as the ratio of vapour and liquid in CS 2 to that in CS 1. We will refer to these variables as split ratios although Φ_V is, in fact, a mixing ratio. Similar variables can be defined in terms of vapour and liquid flow rates in CS 6. The decision to work with the CS 1 definition is simply a matter of convenience. The use of Φ_V and Φ_L will lead to a very useful representation of coupled column section variables as well as feasible column solutions.

6.10 Difference Point Placement for the Petlyuk Column

With all the external DOF specified we must now turn our attention to the remaining internal DOF. We are required to specify one internal composition variable. The available composition variables are the difference points ($X_{\Delta k}$) of the coupled column sections, the placement of which are critical to the feasibility of the design. The behaviour of the TT is dependent on two variables, namely the difference point (X_{Δ}) and the reflux ratio (R_{Δ}). The form of the CPM changes as the placement of the difference point changes. It is crucial that the difference point for a column section is placed correctly so that the resulting CPM satisfies all required feasible column criteria. It is, however, impossible to have all difference points in the Petlyuk configuration placed optimally as only one DOF remains but we can place one point such that it facilitates the composition matching of the others.

In making the choice of difference point, it is necessary to identify sections for which the required design specifications are more difficult to achieve with arbitrary parameter sets. If we consider that CS 2 and CS 4 are required to achieve a product specification, it is logical that the difference point of either of these two sections is chosen such that the intermediate product composition can be achieved. We will arbitrarily choose to place the difference point of CS 2 (although placing $X_{\Delta 4}$ would be just as effective).

To determine the optimal placement of $X_{\Delta 2}$ the requirements of this column section must be understood. Firstly, CS 2 is required to achieve a particular composition, specifically the side-draw composition; therefore the CPM for CS 2 must provide trajectories which intersect this composition point. Secondly, the profile is required to intersect the rectifying profile; therefore it should run from the side-draw composition, close to the light-intermediate axis and cross the rectifying profile.

From a material transport perspective the main purpose of CS 2 is the transport of the intermediate component to the side-draw. If the side-draw composition is required to be very "pure", CS 2 should not transport large quantities of light or heavy component material i.e. the pseudo composition of the net flow ($X_{\Delta 2}$) should have a high intermediate component percentage. This does not exclude difference points with non-zero light and heavy components, however. High purities are possible in a column section even if the net flow does involve large "impurity" flows because a single phase can be sampled. This can be explained if we consider that at a difference point the vapour and liquid compositions are equal (this is shown in Equation 6.6), but as compositions away from the difference point are sampled a "gap" opens up between the vapour and liquid compositions (as shown in Equation 6.7). Difference points associated with large impurities can, therefore, generate trajectories of one phase achieving high purities while the other does not. An illustration of this is seen in Figure 6.23 below.

The difference point is defined as:

$$X_{\Delta k} = \left(1 + R_{\Delta k}\right)Y_k^T - R_{\Delta k}X_k^T$$

Rearranging

$$Y_k^T = \frac{X_{\Delta k} + R_{\Delta k}X_k^T}{\left(1 + R_{\Delta k}\right)} \tag{6.5}$$

If $X_k^T = X_{\Delta k} \Rightarrow Y_k^T = \dfrac{X_{\Delta k} + R_{\Delta k}X_{\Delta k}}{\left(1 + R_{\Delta k}\right)} = X_{\Delta k}$ \hfill (6.6)

If $X_{k-3}^T \approx 1$ but $X_{\Delta k-3} < 1 \Rightarrow Y_{k-3}^T = \dfrac{X_{\Delta k} + R_{\Delta k}X_{k-3}^T}{\left(1 + R_{\Delta k}\right)} \neq X_{k-3}^T \neq X_{\Delta k-3}$ \hfill (6.7)

Minimising difference point impurities should improve overall performance though, by the simple logic that if there is a smaller net flow of "impurity" material through the section, there is less to be separated from the intermediate component. If we consider this argument only, the difference point for CS 2 should be placed near the intersection of the x_1 and x_2 axes (pure intermediate).
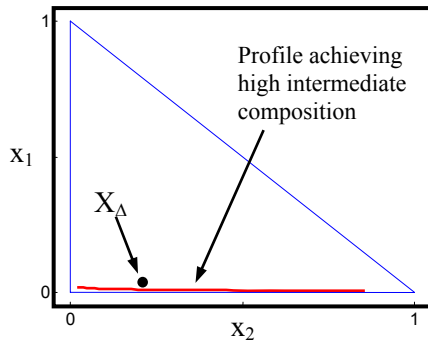
Figure 6.23: Low intermediate purity difference point with liquid profile sampling high intermediate purity
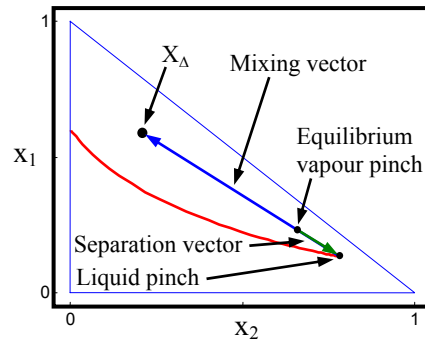
Figure 6.24: **Mixing and separation vector co-linearity**

It is possible to use geometrical ideas to confirm our intuitive net flow arguments above. Tapp et al (2004) illustrated that a qualitative understanding of the CPM could be achieved by studying the pinch point curves resulting from difference points placed arbitrarily in each of the 7 qualitatively different regions of the composition space that were identified (see Figure 6.2). By noting where the nodes of the system move, we can identify which (difference point) regions of the space would result in favourable trajectories at the side-draw. As mentioned above the required profile in CS 2 needs to intersect the rectifying profile. The rectifying profile will run close to the light-intermediate axis (see Figure 6.16a), so any profile running from a high purity side-draw composition to the rectifying profile will do likewise (see Figure 6.18a and b). If the column section operates at negative reflux the profile will reach an unstable node stationary point close to the light-intermediate axis of the MBT (see Figure 6.18b). If it is operated at positive reflux, the profile will terminate outside the MBT but also close to the axis (see Figure 6.25a and b). $X_{\Delta2}$ must produce a pinch point curve that runs close to this

boundary. We can determine areas of possible $X_{\Delta 2}$ placement geometrically by using the co-linearity condition of the mixing and separation vectors at the pinch point. Pinch points only occur in composition space when the mixing vector (X_{Δ} - X) is collinear with the separation vector ($X - Y^{*}(X)$) (see Figure 6.24).
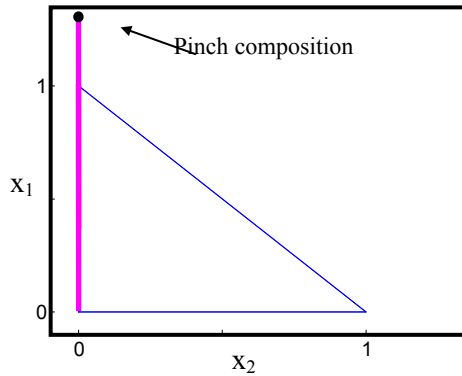
Figure 6.25a: CS 2 profile pinching outside MBT for $R_{\Delta 2}$>0
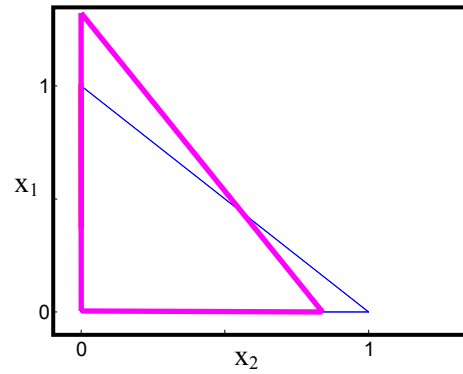
Figure 6.25b: TT for CS 2 for $R_{\Delta 2}$>0

All that is required is to choose (desirable) potential pinch points on the residue curve map and extend lines along the direction of the tangent of individual residue curves at these points (separation vectors are tangential to the residue curve at their liquid composition). If we extend straight lines, from points close to the light-intermediate axis, along the residue curve tangents we can find lines of possible $X_{\Delta 2}$ values. Figure 6.26 illustrates lines of $X_{\Delta 2}$ values that satisfy three arbitrarily chosen pinch points. Pinch points chosen close to the axis produce lines of X_{Δ} close to the axis, therefore if the $X_{\Delta 2}$ is placed close to the light-intermediate axis the pinch point curve will run very close to this boundary and consequently so will potential profiles. This will satisfy the side-draw composition requirement as well as the rectifying profile intersection.

As was illustrated previously, difference points obey linear mixing rules. The CS 2 and CS 4 difference points must lie on a straight line running through the side-draw composition. If the placement of $X_{\Delta 2}$ is to be finalised we must determine the implications of this placement on $X_{\Delta 4}$. If $X_{\Delta 2}$ is placed at an arbitrary position along the light-intermediate axis and X_S is placed very close to the pure

intermediate composition, linear mixing rules will force $X_{\Delta 4}$ to lie along the light-intermediate axis as well. However, if $X_{\Delta 4}$ was chosen independently we would, by the same logic applied to the placement of $X_{\Delta 2}$, position $X_{\Delta 4}$ along the intermediate-heavy axis (CS 4 profiles must run from the side-draw composition along this axis to the stripping profile). The only possible way to satisfy the requirements for both difference points, for sharp-splits on the side-draw, is if $X_{\Delta 2}$ and $X_{\Delta 4}$ are placed very close to both axes i.e. close to the pure intermediate component. Because the side-draw is placed very close to the pure intermediate component all three points must in fact exist at the same composition. This result agrees with the intuitive net flow arguments made above. Suitable difference point placements for each of the column sections, for each net flow pattern, are seen in Figure 6.27a-e. The relative positioning of the difference points is dependent on the net flow in each column section and subsequently the final positioning of $X_{\Delta 3}$ and $X_{\Delta 5}$ is a function of the remaining internal material balance variables which will be discussed next. Because difference points obey linear mixing rules, $X_{\Delta 3}$ is, however, constrained to the material balance line though the distillate composition $(X_{\Delta 1})$ and $X_{\Delta 2}$, while $X_{\Delta 5}$ is constrained to the material balance line through the bottoms composition $(X_{\Delta 6})$ and $X_{\Delta 4}$.

It fascinating to note, that for net flow patterns 1, 2, 4 and 5 *$X_{\Delta 3}$ or $X_{\Delta 5}$ must operate outside of the MBT*. This forces the net flow of some of the components within CS 3 and CS 5 to flow in opposite directions. The fact that these difference points operate outside the MBT also introduces the potential for interesting topology to be shifted into the MBT for these column sections.
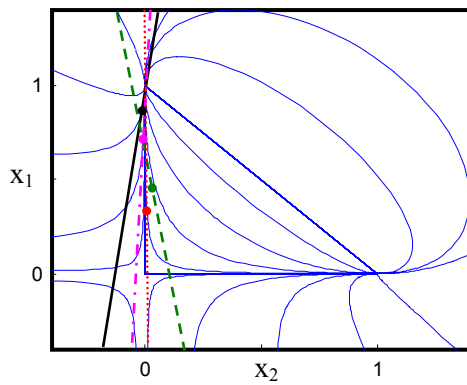
Figure 6.26: Residue curve tangent lines at potential pinch points
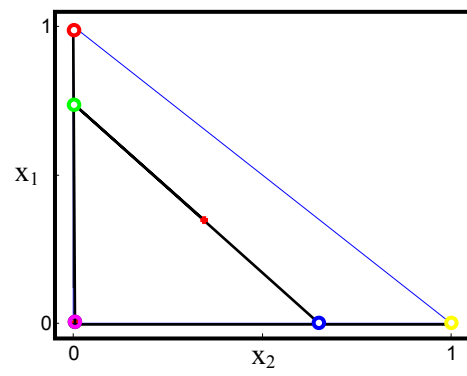
Figure 6.27a: Material balance – net flow pattern 3
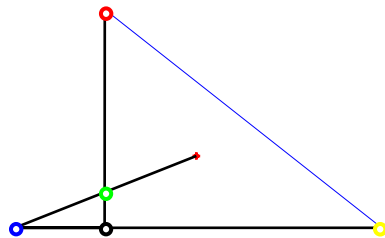
Figure 6.27b: Material balance – net flow pattern 1
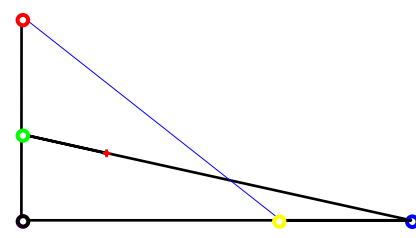
Figure 6.27c: Material balance – net flow pattern 2
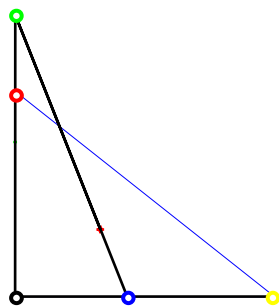
Figure 6.27d: Material balance – net flow pattern 4
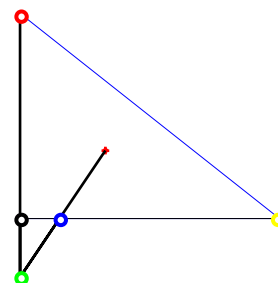
Figure 6.27e: Material balance – net flow pattern 5

Legend Figure 6.27a-e:

○	$X_{\Delta 1}$
○	$X_{\Delta 2}$
○	$X_{\Delta 3}$
○	$X_{\Delta 4}$
○	$X_{\Delta 5}$
○	$X_{\Delta 6}$

6.11 Variable Representation in Φ_V vs. Φ_L Space

The split ratios were introduced in our discussion of variable selection above and are the internal material balance variables chosen for the design process. Our choice of other variables was largely based on our intuitive understanding of their effects. Because we do not have this advantage with our choice of Φ_V and Φ_L we shall represent coupled-column-section variables we do understand in split ratio space. We shall also define boundaries in this space that represent physical limits on the column section internal flows. These representations will help effect an intelligent selection of the liquid and vapour splits.

6.11.1 Net Flow Regimes in Φ_V vs. Φ_L Space

The various net flow patterns can be controlled or achieved by manipulating the split ratios. The regimes can readily be visualised, in Φ_V vs. Φ_L space, by producing lines of zero net flow for the coupled column sections (see Figure 6.28). The dependence of the net flow, for each of the coupled column sections, on the vapour and liquid split ratios from CS 1 can be seen in the Equation 6.8-6.11 below. The split ratios for both the liquid and vapour are defined, as mentioned previously, in terms of the respective flows from CS 1. As a consequence, all the equations below are functions of the reflux ratio in CS 1. The CS 4 and CS 5 zero net flow lines are both functions of the distillate flow rate as well as the side-draw flow rate and feed flow rate respectively.

$$\Delta_2 = \Phi_V \Delta_1 (R_{\Delta 1} + 1) - \Phi_L \Delta_1 R_{\Delta 1} = 0 \quad \Rightarrow \quad \Phi_L = \frac{(R_{\Delta 1} + 1)}{R_{\Delta 1}} \Phi_V$$

(6.8)

$$\Delta_3 = (1 - \Phi_V)\Delta_1(R_{\Delta 1} + 1) - (1 - \Phi_L)\Delta_1 R_{\Delta 1} = 0 \quad \Rightarrow \quad \Phi_L = \frac{(R_{\Delta 1} + 1)}{R_{\Delta 1}} \Phi_V - \frac{1}{R_{\Delta 1}}$$

(6.9)

$$\Delta_4 = \Phi_V(\Delta_1 R_{\Delta 1} + \Delta_1) - \Phi_L \Delta_1 R_{\Delta 1} + S = 0 \quad \Rightarrow \quad \Phi_L = \frac{(R_{\Delta 1} + 1)}{R_{\Delta 1}} \Phi_V + \frac{S/\Delta_1}{R_{\Delta 1}}$$

(6.10)

$$\Delta_5 = \left(1 - \Phi_V\right)\left(\Delta_1 R_{\Delta 1} + \Delta_1\right) - \left(1 - \Phi_L\right)\Delta_1 R_{\Delta 1} - F = 0 \quad \Rightarrow \quad \Phi_L = \left(\frac{R_{\Delta 1} + 1}{R_{\Delta 1}}\right)\Phi_V + \left(\frac{F/\Delta_1 - 1}{R_{\Delta 1}}\right)$$

(6.11)

By dividing up the Φ_V vs. Φ_L space with lines of zero net flow for each of the coupled sections, we can identify regions within the space of different overall net flow pattern. These are labelled 1 to 5 in Figure 6.28. Above the $\Delta_5 = 0$ line (blue) values of Φ_V and Φ_L produce values of $\Delta_5 > 0$, while below the line values of $\Delta_5 < 0$ are produced. Similarly for the $\Delta_3 = 0$ line (green), above the line are values of $\Delta_3 > 0$, while below are values of $\Delta_3 < 0$. The inverse is true for lines $\Delta_2 = 0$ (pink) and $\Delta_4 = 0$ (black). Above these lines negative values are produced, while below positive values are produced.

Each of the regions between these lines and between the lines and the boundaries of the space produce a different net flow pattern in the coupled sections. These are the flow patters illustrated in Figure 6.11a-e. This behaviour, described above, is summarised in Table 6.2 below.
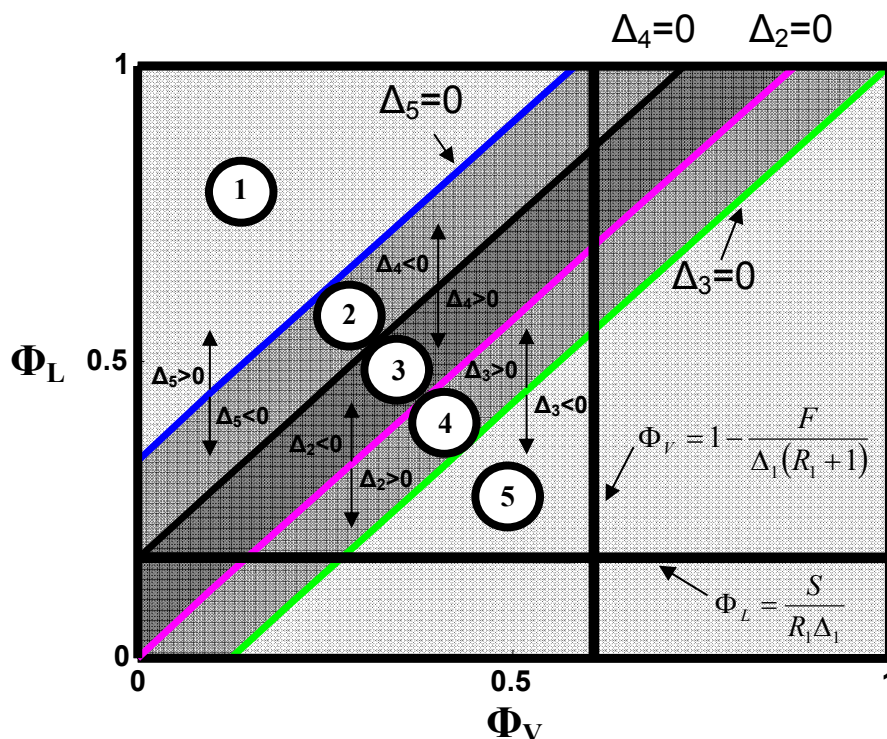
Figure 6.28: Net Flow Regimes in Φ_V vs. Φ_L

Region From Figure 6.28	Δ Direction CS2	Δ Direction CS3	Δ Direction CS4	Δ Direction CS5	Illustrated By
1	- ve	+ ve	- ve	+ ve	**Figure 6.11a**
2	- ve	+ ve	- ve	- ve	**Figure 6.11b**
3	- ve	+ ve	+ ve	- ve	**Figure 6.11c**
4	+ ve	+ ve	+ ve	- ve	**Figure 6.11d**
5	+ ve	- ve	+ ve	- ve	**Figure 6.11e**

Table 6.2: Summary of net flow regions illustrated in Figure 6.28

6.11.2 Physical Limits on Φ_V and Φ_L

Because of the definition of the split ratios, there are values of both Φ_V and Φ_L, which cannot be produced. The vapour split ratio, at which the vapour flow in CS 3 is equal to the feed rate, represents an upper physical limit on the value of Φ_V for a column with vapour feed. The exact value of this limit can be calculated using Equation 6.12.

$$\Phi_V = 1 - \frac{F}{\Delta_1 (R_{\Delta 1} + 1)} \tag{6.12}$$

Material balances calculated with values of Φ_V greater than this upper limit will produce negative vapour flow values in CS 5. Similarly, for a column with liquid side-draw, if the liquid split ratio is specified such that the value for the liquid flow in CS 2 is smaller than the side-draw rate, negative liquid flows in CS 4 will result in any material balance. The split ratio value at which the liquid flow in CS 2 is equal to the side-draw rate, therefore, represents a lower limit on the value of Φ_L. This limiting value can be calculated with Equation 6.13.

$$\Phi_L = \frac{S}{R_{\Delta 1} \Delta_1} \tag{6.13}$$

Both these limits are illustrated in Figure 6.28.

6.11.3 Reflux Ratio in Φ_V vs. Φ_L Space

The reflux ratio of the coupled sections can also be conveniently represented in the Φ_V vs. Φ_L space. Because of the definitions of the split ratios, lines of constant reflux are straight. The equations for the constant reflux lines for each of the coupled column sections are seen below (Equations 6.14-6.19). These equations are also all functions of $R_{\Delta 1}$. The form of the $R_{\Delta 4}$ and $R_{\Delta 5}$ equations are dependant on the phase of the side-draw and feed material respectively.

$$R_{\Delta 2} = \frac{\Phi_L R_{\Delta 1}}{\Phi_V(R_{\Delta 1}+1) - \Phi_L R_{\Delta 1}} \quad \Rightarrow \quad \Phi_L = \Phi_V \frac{R_{\Delta 2}(R_{\Delta 1}+1)}{R_{\Delta 1}(R_{\Delta 2}+1)} \tag{6.14}$$

$$R_{\Delta 3} = \frac{(1-\Phi_L)R_{\Delta 1}}{(1-\Phi_V)(R_{\Delta 1}+1) - (1-\Phi_L)R_{\Delta 1}} \quad \Rightarrow \quad \Phi_L = (\Phi_V - 1)\frac{R_{\Delta 3}(R_{\Delta 1}+1)}{R_{\Delta 1}(R_{\Delta 3}+1)} + 1 \tag{6.15}$$

$R_{\Delta 4}$ - Liquid side-draw $\tag{6.16}$

$$R_{\Delta 4} = \frac{\Phi_L R_{\Delta 1} - S/\Delta_1}{\Phi_V(R_{\Delta 1}+1) - \Phi_L R_{\Delta 1} + S/\Delta_1} \quad \Rightarrow \quad \Phi_L = \Phi_V \frac{R_{\Delta 4}(R_{\Delta 1}+1)}{R_{\Delta 1}(R_{\Delta 4}+1)} + \frac{S}{\Delta_1 R_{\Delta 1}}$$

$R_{\Delta 4}$ - Vapour side-draw $\tag{6.17}$

$$R_{\Delta 4} = \frac{\Phi_L R_{\Delta 1}}{\Phi_V(R_{\Delta 1}+1) - \Phi_L R_{\Delta 1} + S/\Delta_1} \quad \Rightarrow \quad \Phi_L = \Phi_V \frac{R_{\Delta 4}(R_{\Delta 1}+1)}{R_{\Delta 1}(R_{\Delta 4}+1)} + \frac{SR_{\Delta 4}}{\Delta_1 R_{\Delta 1}(R_{\Delta 4}+1)}$$

$R_{\Delta 5}$ - Liquid Feed: $\tag{6.18}$

$$R_{\Delta 5} = \frac{(1-\Phi_L)R_{\Delta 1} + F/\Delta_1}{(1-\Phi_V)(R_{\Delta 1}+1) - (1-\Phi_L)R_{\Delta 1} - F/\Delta_1} \quad \Rightarrow \quad \Phi_L = (\Phi_V - 1)\frac{R_{\Delta 5}(R_{\Delta 1}+1)}{R_{\Delta 1}(R_{\Delta 5}+1)} + 1 + \frac{F}{\Delta_1 R_{\Delta 1}}$$

$R_{\Delta 5}$ - Vapour Feed: $\tag{6.19}$

$$R_{\Delta 5} = \frac{(1-\Phi_L)R_{\Delta 1}}{(1-\Phi_V)(R_{\Delta 1}+1) - (1-\Phi_L)R_{\Delta 1} - F/\Delta_1}$$

$$\Rightarrow \quad \Phi_L = (\Phi_V - 1)\frac{R_{\Delta 5}(R_{\Delta 1}+1)}{R_{\Delta 1}(R_{\Delta 5}+1)} + 1 + \frac{FR_{\Delta 5}}{\Delta_1 R_{\Delta 1}(R_{\Delta 5}+1)}$$
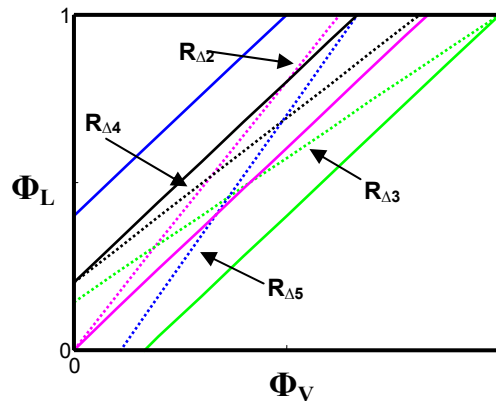
Figure 6.29: Constant reflux lines in Φ_V vs. Φ_L

The sign of the reflux is dependent on the sign of the net flow, therefore the regions of the space corresponding to positive and negative net flow, for each of the sections, correspond to positive and negative reflux for those sections as well. Infinite reflux lines originate from the zero net flow lines (both positive and negative infinite reflux). The lines fan out, away from their respective zero net flow lines, as the absolute value of the reflux is reduced (see Figure 6.29). These representations enable us to intuitively determine the effects of a particular choice of Φ_V and Φ_L on the reflux of coupled sections.

6.11.4   Constant X_Δ in Φ_V vs. Φ_L Space

It is possible to find split ratio lines that result in constant $X_{\Delta k\text{-}i}$ for the coupled-column-sections i.e. varying the split ratios along these lines does not shift the difference points. This can be useful if we wish to design a column that directs individual components within the coupled column sections in a specific way. We are confined to values for the variable difference points ($X_{\Delta 3}$, $X_{\Delta 5}$) along straight lines between the distillate and bottoms product compositions and $X_{\Delta 2}$ (see Figure 6.27a-e above), but we can control exactly where along these lines a particular difference point lies. Below is an expression for one of these constant X_Δ lines (Equation 6.20) – this equation has been generated for CS 3, but similar expressions can be derived for CS 5.

$$\Phi_L = \frac{(R_{\Delta 1}+1)}{R_{\Delta 1}}\Phi_V + \frac{1}{R_{\Delta 1}}\left(\frac{X_{\Delta 3-i} - X_{\Delta 1-i}}{X_{\Delta 2-i} - X_{\Delta 3-i}}\right) \tag{6.20}$$

where $X_{\Delta 3-i}$ is a control on component i for the difference point of CS 3.

Again we notice that this line is straight. Its slope is of equal gradient to the zero net flow expressions generated above. Figure 6.30 below illustrates an example of a constant X_Δ line at an $X_{\Delta 3\text{-}1}$ value of 0.6 (light component). We can see that in this particular case this value is only satisfied in region 3 of split ratio space.
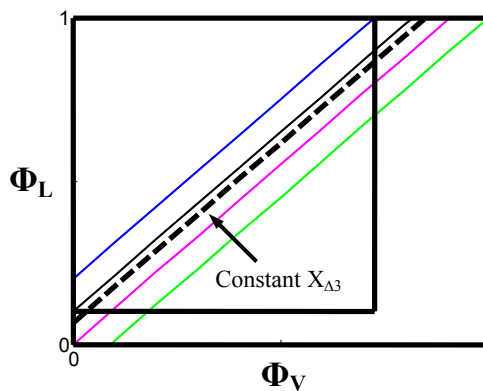
Figure 6.30: Constant X_Δ lines in Φ_V vs. Φ_L space.

6.12 Constructing Split Ratio Regions of Feasibility

The design procedure thus far has involved the allocation of product composition and flow, the reflux ratio of CS 1 as well as the difference point of CS 2. Let us assume for now that our arbitrary choice of $R_{\Delta 1}$ will result in a potentially feasible Petlyuk solution i.e. solutions exist for this reflux ratio. Following the discussion of the representation of net flow pattern regions and reflux ratios in Φ_V vs. Φ_L space we are now in a position to choose values for the vapour and liquid split ratios. We have a number of tools at our disposal. We can generate the net flow regions for our choice of $R_{\Delta 1}$ and products. This immediately allows us to narrow down our range of choice of values for Φ_V and Φ_L by deciding on our region of operation. Furthermore we now have an understanding of the effects of our choice on the reflux ratios of the coupled column sections.

<u>Note:</u> Transformed Triangle Boundary Definitions

For the following sections it will be convenient to label the boundaries of the TTs. A boundary defined between an unstable node and a saddle point of TT "k" will be referred to as boundary "A_k". A boundary defined between a stable node and a saddle point of TT "k" will be referred to as boundary "B_k". The final boundary defined between an unstable node and a stable node will be referred to as boundary "C_k" of the TT. Figure 6.31 below illustrates these boundary definitions. Unless otherwise stated this will always refer to liquid TT boundaries. Vapour TT boundaries will be referred to as "vapour boundary A_k", etc.
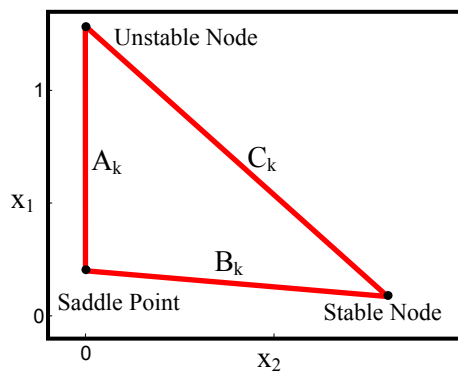
**Figure 6.31: Transformed triangle boundary
definitions**

6.12.1 Coupled Column Section Minimum Reflux

Let us assume that we have allocated all variables including Φ_V and Φ_L and that the resulting solutions are the superimposed TTs of Figure 6.22b. For this solution we can see that all the required matching criteria are satisfied.

- TTs of CS 1, CS 2 and CS 3 overlap.
- TTs of CS 2 and CS 4 overlap.
- TTs of CS 3 and CS 5 overlap.
- TTs of CS 4, CS 5 and CS 6 overlap.

The reflux ratios of CS 1 and CS 6 are specified parameters and as such their TTs are fixed. The TTs of CS 2 and CS 4 produce a substantial overlap with these, so

it is clear that their reflux ratios are higher than is required for feasibility. These refluxes are set by our choice of Φ_V vs. Φ_L. If we allowed these values to be changed we could vary other parameters. If we were to reduce $R_{\Delta2}$, until boundary C_2 just touched boundary B_1 (see Figure 6.32) a minimum reflux ratio for CS 2 could be found. This is possible because $X_{\Delta2}$ is fixed and the corresponding TT is only a function of $R_{\Delta2}$. The same is true for CS 4. $X_{\Delta4}$ is fixed because $X_{\Delta2}$ was placed at the side draw composition – hence $X_{\Delta4}$ is constrained to this value for all choices of $R_{\Delta4}$ and Φ_V and Φ_L. We can reduce $R_{\Delta4}$ until the boundary C_4 just touches boundary A_6 (see Figure 6.33) and find a minimum $R_{\Delta4}$. These minima can both be represented in Φ_V vs. Φ_L space as illustrated before (see Figure 6.36). The $R_{\Delta2MIN}$ defined above is always < 0 and $R_{\Delta4MIN}$ is always > 0.

Any value of Φ_V and Φ_L between the minimum $R_{\Delta2}$ line (dashed pink) and the CS 2 zero net flow line (solid pink) will produce an overlap of TT 2 and TT 1 with a value of $R_{\Delta2}<0$. No Φ_V and Φ_L values above the minimum $R_{\Delta2}$ line will ever produce an overlap and hence a feasible Petlyuk design for our chosen $R_{\Delta1}$ and products, so we can discard this entire region when choosing our split ratios. Similarly, the region between the minimum $R_{\Delta4}$ line (dashed black) and the CS 4 zero net flow line (solid black) will produce an overlap of TT 4 and TT 6. The value of $R_{\Delta4}$ here is >0. Values of Φ_V and Φ_L below the minimum $R_{\Delta4}$ line can be discarded.

It should be noted that we cannot immediately discard the regions below the CS 2 or above CS 4 zero net flow lines. These regions produce reflux ratios with opposite sign ($R_{\Delta2} > 0$, $R_{\Delta4} < 0$) to the minima discussed above as they are in different net flow regions. Because of this both sets of matching criteria are satisfied. The overlap of TT 2 and TT 1 is automatically satisfied because the unstable node of CPM 2 lies outside the MBT above the unstable node of CPM 1 (see Figure 6.34). This topological phenomenon is always true for CPMs produced from positive differences points with positive reflux ratios. The overlap of TT 4 and TT 6 is also satisfied because the stable node of CPM 4 lies outside the MBT beyond the stable node of CPM 6 (see Figure 6.35). This topological

phenomenon is always true for CPMs produced from positive differences points with negative reflux ratios. Although these guaranteed overlaps might seem like an advantage, they cannot be achieved simultaneously - the resulting net flow pattern is infeasible (up in CS 2 and down in CS 4). One of the CSs must operate with a reflux ratio of the same sign as its minimum reflux ratio. This means that the only region of Φ_V vs. Φ_L space that will satisfy both matching criteria and produce feasible net flow patterns in sections 2 and 4 is between the minimum reflux ratio lines of both CSs (above $R_{\Delta4MIN}$ and below $R_{\Delta2MIN}$). No value picked outside this range will ever produce a feasible Petlyuk solution, whether the split is sharp or not.
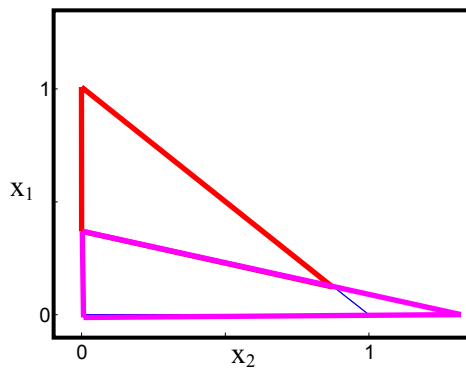
Figure 6.32: TT for CS 1 and CS 2 at minimum $R_{\Delta2}$
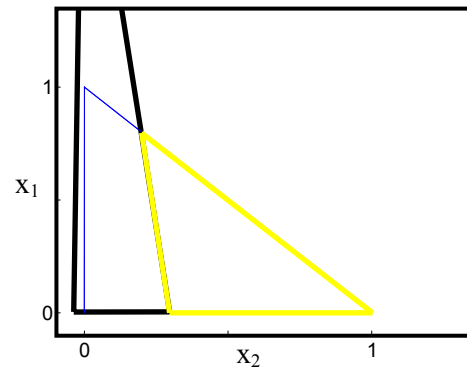
Figure 6.33: TT for CS 4 and CS 6 at minimum $R_{\Delta4}$
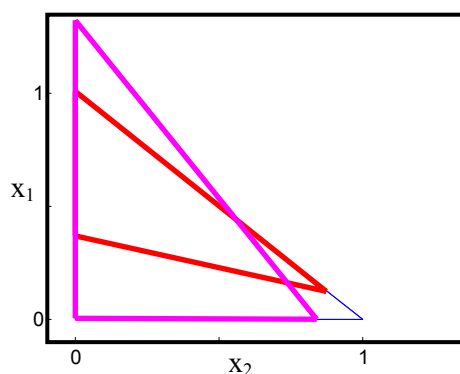
Figure 6.34: TT for CS 1 and CS 2 for positive $R_{\Delta2}$
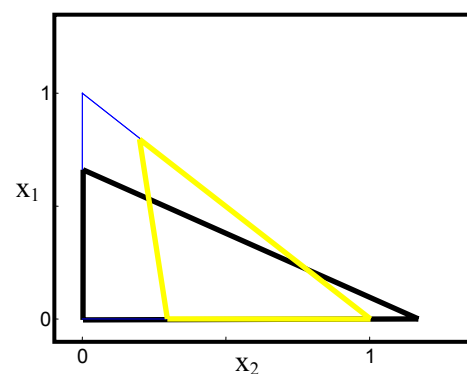
Figure 6.35: TT for CS 4 and CS 6 for negative $R_{\Delta4}$
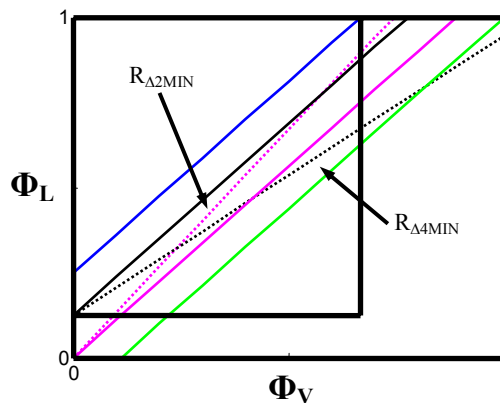
Figure 6.36: Minimum $R_{\Delta 2}$ and $R_{\Delta 4}$ in Φ_V vs. Φ_L space

6.12.2 Limiting Conditions for Overlap of TT 3 and TT 5

We have substantially reduced the range of possible split ratio choices by identifying regions (in Φ_V vs. Φ_L space) resulting in negative vapour or liquid flows, categorising regions of differing net flow patterns and producing lines of minimum reflux ratio for CS 2 and CS 4 based on two of the required matching criteria. We will now turn our attention to another of the matching criteria – the overlap of TT 3 and TT 5. The split ratios chosen for the example in Figure 6.22b produced a large overlap of these TTs. If we start at these split ratios and increase the vapour split incrementally at constant liquid split, the TTs of CS 3 and CS 5 will shift as seen in Figure 6.37a-b below. At a certain value, boundaries B_3 and C_5 of TT 3 and TT 5 respectively will actually be collinear. This represents the final Φ_V value at the constant Φ_L value, previously chosen, that will produce an overlap of these TTs. Conversely, if we incrementally increase Φ_L at constant Φ_V the TT will shift as seen in Figure 6.38a-b. Eventually a value of Φ_L will be reached at which boundary C_3 and boundary A_5 just touch and are also collinear. Another remarkable property of the material balance is that these collinear boundaries will, in fact, always pass through the feed composition for constant-relative-volatility systems (vapour TT boundaries for vapour feed and liquid TT boundaries for liquid feed). Consequently, we immediately have an idea of their placement for all values of Φ_L and Φ_V.

Holland et al (2004 b) discussed the eigenvector fields underlying systems whose vapour-liquid-equilibrium can be modelled using the separation vector:

$$S = (X-Y*(X))$$ **(6.21)**

The eigenvectors of the difference point equation and the residue curve equation are only a function of the separation vector and completely independent of the difference point and reflux ratio. The eigenvector field, therefore, is the same for all CPMs of a particular system. Any liquid composition profile terminating at a stationary point approaches (the node) along the direction of the eigenvector at the point. Holland et al (2004 b) demonstrated that the eigenvectors at the singularities, of constant-relative-volatility systems, always point along the direction of the TT boundaries. Because the boundaries are straight in these systems, the eigenvectors at each singularity point directly at the other singularities. Any point chosen along one of these boundaries will have eigenvectors that point directly at the singularities, which define it. If we calculate the direction of the two eigenvectors at the feed composition we can immediately determine the two lines of co-linearity of the boundaries of TT 3 and TT 5. We will name the co-linearity line of smaller (absolute) gradient, Co-Linearity Line 1 (CLL1) (see Figure 6.39) and the line of larger (absolute) gradient, Co-Linearity Line 2 (CLL2) (see Figure 6.40). Once we know these two lines we can solve for all values of Φ_L and Φ_V that result in TT 3 and TT 5 bordering each other. This is done by simply choosing points along the co-linearity lines and, realising that these points must be satisfied by nodes of either of the TTs, determining the associated values of Φ_L and Φ_V. These values can be plotted in Φ_L vs. Φ_V space. Figure 6.41 illustrates an example of these lines of Φ_L and Φ_V solutions, which divide values resulting in TT 3 and TT 5 overlap from those resulting in no overlap. There are of course two lines of solutions corresponding to the two co-linearity lines through the feed point. These lines are straight due to the linearity of CLL1, CLL2 and the material balance. The red line represents all points resulting in the lining-up of boundaries B_3 and C_5 of TT 3 and TT 5 respectively (i.e. generated from CLL1). We will refer to this line generated from CLL1 as Phi-Eigenvector-Boundary-1 (PEB1). To the left of PEB1 the boundary B_3 will be below CLL1 and boundary C_5 will be above it – a potential overlap. This is only a

potential overlap because the stable node of TT 3 might lie further "left" than the unstable node of TT 5 – i.e. closer to the light-intermediate axis. To the right of PEB1 the relative positions of boundary B_3 and boundary C_5 will be inverted - hence no potential overlap. The blue line represents all points resulting in the lining-up of boundaries C_3 and A_5 (i.e. generated from CLL2). We will refer to this line generated from CLL2 as Phi-Eigenvector-Boundary-2 (PEB2). Below PEB2 boundary C_3 will lie to the right of CLL2 and boundary A_5 will lie to the left – potential overlap. Again this is only a potential overlap because the unstable node of TT 5 might lie "below" the stable node of TT 3 (closer to the intermediate-heavy axis). Above PEB2 boundary C_3 will lie to the left of CLL2 and boundary A_5 will lie to the right – hence no potential overlap. If we focus our attention on the area between PEB1 and PEB2, on the side of potential overlaps for both, we find that the uncertainty in this region for one line is removed by the other. An overlap of TT 3 and TT 5 is guaranteed for values of Φ_L and Φ_V chosen here.

Note: CLL1 and CLL2 (and consequently PEB1 and PEB2) are phase dependent. If vapour feed is added to the column, vapour boundaries B_3 and C_5 will line up along CLL1 while vapour boundaries C_3 and A_5 will line up along CLL2. The eigenvector directions in this case are not the eigenvectors of the standard separation vector as vapour profiles do not approach their pinch points along these directions. Vapour profiles approach pinch points along, and vapour TT boundaries line up along, eigenvectors of the differential equations which have separation vectors expressed in terms of the vapour composition.
i.e. $S = (X^*(Y) - Y)$

6.12.3 Satisfying the Remaining Matching Criteria

In our development of the minimum reflux line for CS 2 we neglected the third column section involved in the required composition matching. TT 3 must overlap not only TT 5 but also TT 2 and TT 1. An intersection with TT 1 is always guaranteed in region 1, 2 and 3, however, as $X_{\Delta 3}$ is within the MBT and operates with a positive reflux ratio. The same reasoning, as discussed previously for

positive reflux in CS 2, prevails (see Figure 6.34). TT1/TT3 overlaps, as we will see later, only occur in regions 4 and 5 under specific circumstances. The overlap of TT 3 with TT 2 is more difficult to guarantee. What we can show, though, is that when a node of TT 2 (unstable) lies on top of a node from TT 1 (saddle), a TT 3 node (saddle) must lie at this same point and the respective boundary lines must then be collinear (Appendix E). It can also be shown that when these nodes lie on top of each other and the split ratios are adjusted along lines of constant X_Δ (i.e. making the changes of the TT's only a function of the changes to R_Δ), $R_{\Delta3}$ decreases, shifting boundary B_3 away from the intermediate boiler and towards the light boiler. The rate at which $R_{\Delta3}$ decreases is smaller than the rate at which $R_{\Delta2}$ increases, however, and we can therefore infer that TT 1, 2 and 3 will overlap for all split ratio values in regions 1, 2 and 3 below the minimum $R_{\Delta2}$ line (see Appendix F for details). If we assume that this movement of TTs is true not only for situations in which nodes are directly on top of each other, but also for situations when boundaries touch we can be certain that if TT 2 and TT 1 overlap, all three TTs will overlap.

Similar logic to that used above for the matching criteria of CS 1, 2 and 3 can be used for that of CS 4, 5 and 6. TT 5 is always guaranteed of overlapping TT 6, in region 3, 4 and 5, by the same reasoning used for the overlap of TT 4 with TT 6 at negative $R_{\Delta4}$ (see Figure 6.35). $X_{\Delta5}$ lies within the MBT and $R_{\Delta5}$ is negative in region 3, 4 and 5. Also using reflux arguments, as above, it can be shown that TT 4 overlaps TT 5 for all values of split ratio space in regions 3, 4 and 5 above the minimum $R_{\Delta4}$ line.

The final matching criterion is the requisite overlap of the TTs of CS 2 and CS 4. This criterion is automatically satisfied because the difference points of CS 2 and CS 4 have the same value. For ideal systems, positive difference points always lie within their respective transformed triangles. As these points are the same for both sections, the TTs have to overlap by default.

6.12.4 Overall Column Feasibility in Φ_V vs. Φ_L Space

We have considered all the required composition matching criteria and found regions of split ratio space that satisfy them. We are now in a position to determine if there are regions that satisfy all requirements simultaneously and hence yield feasible Petlyuk designs. Figure 6.42 below illustrates examples of the PEB1 and PEB2 lines. Superimposed on these lines are the minimum reflux lines for CS 2 and CS 4. If we consider all these lines together and the individual regions of feasibility for each matching criterion, we can see that there is a region that satisfies all matching criteria for our selection of $R_{\Delta 1}$ and products. Any choice of Φ_L and Φ_V within this region will result in a feasible Petlyuk column design. This is extremely powerful because we no longer have to guess values for the split ratios. We have a method to actually calculate feasible split ratio combinations and understand their implications, for the design. From a very large range of potential split ratio values (0 to 1 for both), we have reduced the possible choices to a very small region. It is clear that, for this choice of reflux ratio, it is very difficult to arbitrarily choose split ratios that would result in a feasible design. We will discuss the effects of $R_{\Delta 1}$ in depth later, but for now it will suffice to say that this region grows in size if $R_{\Delta 1}$ is increased and shrinks if $R_{\Delta 1}$ is decreased. This result holds with our intuitive understanding of distillation, which is that separations are more difficult at low reflux than at high reflux.

The feasible region of split ratios is bound on each side by one of the lines generated from the matching criteria. Because these boundaries represent limiting conditions for certain column sections it is useful to explore the conditions along these boundaries further.

Along the $R_{\Delta 2MIN}$ line, TT 2 borders TT 1. If we disregard the default infinite stage requirement of sharp-split separations, we can immediately conclude that, in this special case, it will take an infinite number of stages for the CS 2 composition profile to reach the rectifying profile because the unstable node pinch point lies on the boundary of TT 1. All split ratios chosen along the section $R_{\Delta 2MIN}$ line

between point "A" and "B", in Figure 6.42, will result in an infinite number of required stages for CS 2 and hence an unstable pinch point at the top of CS 2. Similarly, all split ratios chosen between points "A" and "D" along the $R_{\Delta 4MIN}$ line will result in an infinite number of required stages for CS 4. This condition results in a stable pinch at the bottom of the CS.

The intersection of the $R_{\Delta 2MIN}$ line and the $R_{\Delta 4MIN}$ line is more interesting. This specific choice of split ratios is denoted the "balanced main column". This operating point is characterised by minimum feasible vapour flow through CS 2 and CS 4. At these conditions TT 2 borders TT1 and TT 4 borders TT 6. There are two pinching column sections – an unstable node at the top of CS 2 and a stable node at the bottom of CS 4.

Between points "B" and "C" along PEB2, boundary C_3 borders boundary A_5. CS 3 is at minimum reflux conditions along this line. The line does not result in a single minimum reflux value as in $R_{\Delta 2MIN}$ and $R_{\Delta 4MIN}$, but a series of minimum $R_{\Delta 3}$ values corresponding to different values of $X_{\Delta 3}$. This minimum reflux is characterised by a stable node pinch point at the bottom of CS 3 (in the middle of the prefractionator).

At the intersection of PEB2 and the $R_{\Delta 2MIN}$ line (point "B") both CS 2 and CS 3 will pinch (an unstable node at the top of CS 2 and a stable node at the bottom of CS 3).

Between points "C" and "D" along PEB1, boundary C_5 borders boundary B_3. CS 5 is at minimum reflux along this line. The line, also, does not result in a single minimum reflux value but a series of minimum $R_{\Delta 5}$ values corresponding to different values of $X_{\Delta 5}$. The top of CS 5 will terminate at an unstable pinch point.

At the intersection of PEB2 and the $R_{\Delta 4MIN}$ line (point "D"), CS 4 will pinch in a stable node at the bottom and CS 5 will terminate in an unstable pinch point at the top.

At point "C", PEB1 and PEB2 intersect. This point is denoted the "preferred split" and is characterised by minimum feasible vapour flow through the prefractionator. This particular set of split ratio values will result not only in a stable pinch point for CS 3 and an unstable pinch point for CS 5, but in these points coinciding, at the feed composition, in a "double-feed-pinch" point. Figure 6.43 illustrates the TTs of a "double-feed-pinch" Petlyuk column. The "double-feed-pinch" point is of course phase dependent. Vapour feed columns will exhibit a vapour profile "double-feed-pinch" point - although it should be noted that both phases in both cases will pinch.
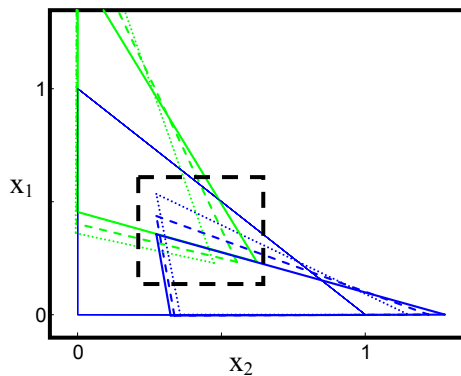
Figure 6.37a: Liquid TT 3 and TT 5 shift at constant ΦL varying ΦV
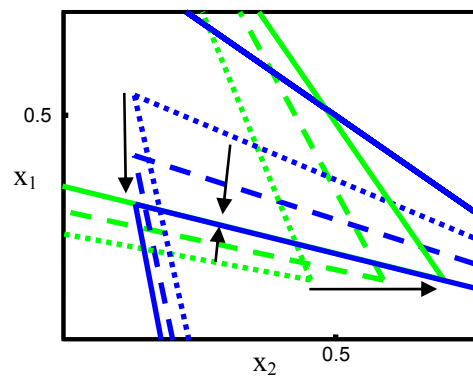
Figure 6.37b:: Zoom of highlighted area from figure 6.37a
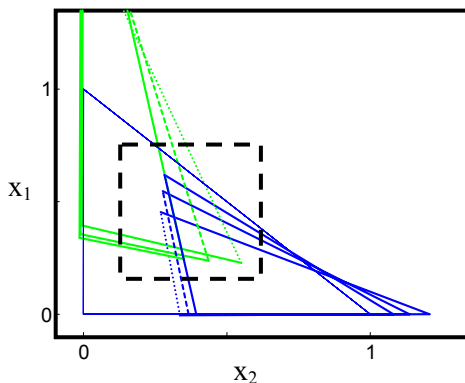
Figure 6.38a: Liquid TT 3 and TT 5 shift at constant ΦV varying ΦL
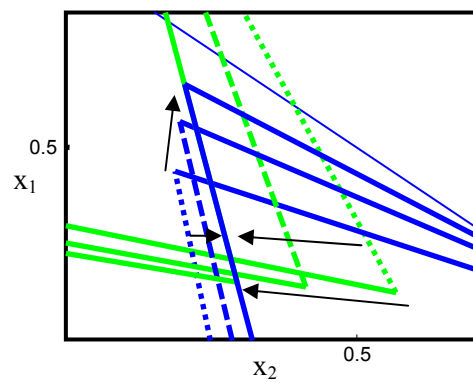
Figure 6.38b: Zoom of highlighted area from figure 6.38a
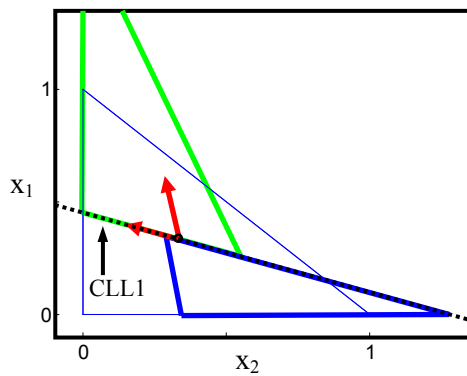
Figure 6.39: Triangles bordering along CLL1
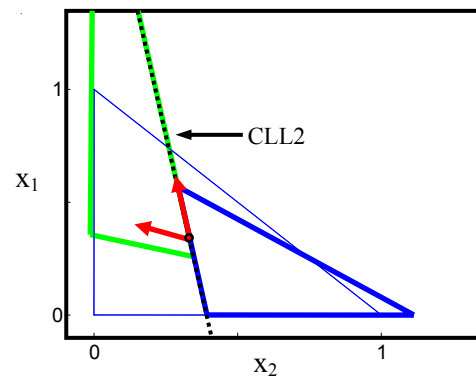
Figure 6.40: Triangles bordering along CLL2
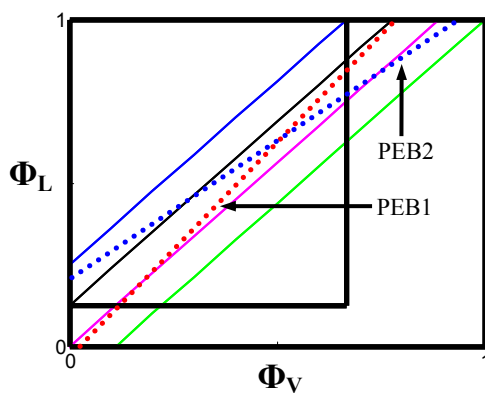
Figure 6.41: PEB1 and PEB2
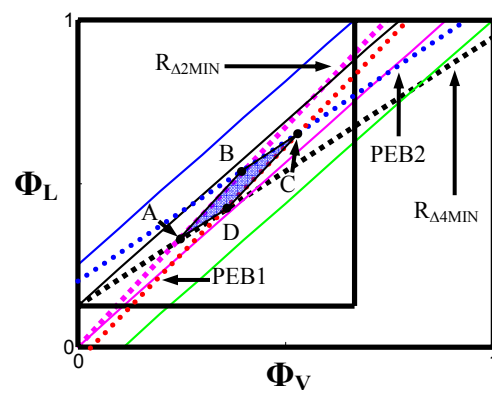
Figure 6.42: Region of ΦL and ΦV space resulting in feasible Petlyuk solutions.

6.13 Overall Minimum Reflux

Throughout this work so far we have assumed that the overall column reflux ratio, $R_{\Delta 1}$, is large enough to produce a feasible solution. The design procedure described above is a waste of time if the column reflux ratio is not high enough. A trial and error approach of choosing a reflux ratio and testing for feasible solutions is definitely not desirable. Fidkowski and Krolikowski (1987) derived analytical expressions for the sharp-split Petlyuk column minimum reflux ratio with saturated liquid feed. Halvorsen and Skogestad (2001) modified these expressions to include feed material of any quality. It was shown that the overall column minimum reflux for sharp splits is equal to the maximum of two sharp simple column splits namely: light component to the intermediate-heavy axis and heavy

component to light-intermediate axis. These expressions are applicable to constant relative volatility systems only. It would be useful to gain an understanding the topological implications of the minimum reflux solution so that any zeotropic system may be handled. We will now revisit two of the composition matching criteria and try and understand their implications for minimum column reflux ratio.

Earlier we showed that if TT 2 and TT 1 touch, boundary B_3 must be collinear with C_2 and B_1 (see Appendix E) – the matching criteria of these column sections is then satisfied. We also showed that the last overlap of TT 3 and TT 5 occurs when boundaries of these triangles are collinear and run through the feed point (at CLL1 and CLL2). It is clear that we cannot satisfy both these situations with any arbitrary choice of column reflux ratio ($R_{\Delta 1}$). If $R_{\Delta 1}$ is too small TT 3 will not be able to simultaneously overlap TT 1 and 2 as well as TT 5 (see Figure 6.44, Figure 6.45 and Figure 6.46). The same problem is evident in the required composition matching at the bottom half of the column i.e. the matching of compositions in CS 4, 5 and 6 (see Figure 6.47, Figure 6.48 and Figure 6.49). The main problem is that the two sets of collinear lines – the first set being the CS 2 and 4 minimum reflux collinear boundaries and the second being CLL1 and CLL2 - will occur in the wrong position relative to each other in composition space. The CS 2 minimum reflux line will lie "above" CLL1, closer to the light component. This means that any adjustment of split ratios in favour of satisfying the TT 3 and TT 5 overlap will reduce the reflux of CS 2 at a higher rate than the reflux of CS 3 and hence make satisfying the TT 1, 2, 3 matching criterion impossible (the inverse argument to that made in Appendix F). In this case the minimum $R_{\Delta 2}$ line will lie below PEB1 in split ratio space, so overall column feasibility is impossible (see Figure 6.50). The key to resolving the minimum $R_{\Delta 1}$ issue lies with boundary B_1 (or boundary A_6) and the feed composition point.

Let us attempt to resolve the issue of satisfying matching criteria at the top half of the column. Boundary B_1 acts as a "watershed", with intersection of the TTs on one side and no intersection on the other. When $R_{\Delta 2}$ is reduced from the

minimum, TT 1 and 2 will not overlap and neither will TT 2 and 3. TT 3, however, shifts "down" and must shift in this direction to overlap TT 5. The "watershed" needs therefore to be shifted down far enough that when TT 3 is shifted to overlap TT 5 for the "first time", in the co-linearities CLL1 and CLL2 at the feed point, it has not yet reached the point when its boundary is collinear with boundary B_1. This indicates that boundary B_1 must be closer to the intermediate-heavy boundary than the feed composition – the feed point must be contained within the boundaries of the TT 1. The minimum column reflux ratio will then be the value resulting in boundary B_1 running through the feed point. Obviously, because the matching criteria of CS 3 and 5 is feed phase dependent, the relevant CS 1 TT defining the column overall minimum reflux is also phase dependent – if the feed is vapour, the vapour boundary B_1 will run through the feed composition. We can conclude, by similar logic that the feed point must lie within the TT 6 (of relevant phase). The true minimum column reflux ratio will be the smallest value that allows the feed to be contained within both TT 1 and 6 – i.e. contained within one and situated on the border of the other. The TTs for a column at minimum reflux is shown in Figure 6.51. This topological observation explains, from a composition profile perspective, why the sharp-split Petlyuk minimum reflux ratio is equal to the maximum of the two simple column splits.
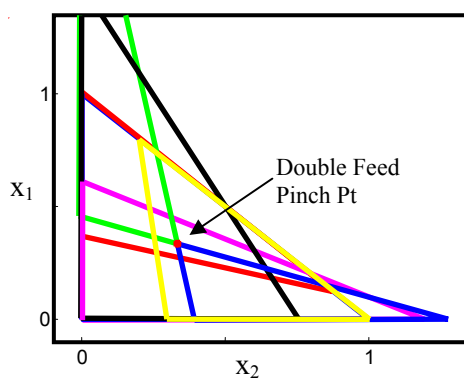
Figure 6.43: Double feed pinch column TTs – saturated liquid feed
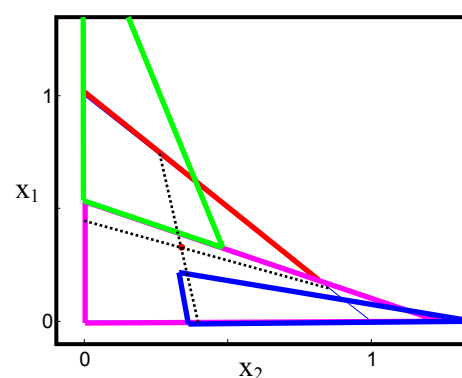
Figure 6.44: **Matching criterion 1 satisfied but criterion 4 is not**
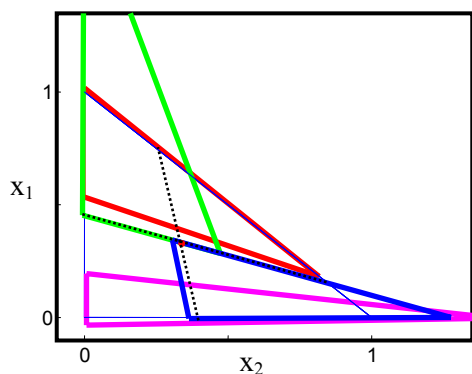
Figure 6.45: Matching criterion 4 satisfied along CLL1 but criterion 1 is not.
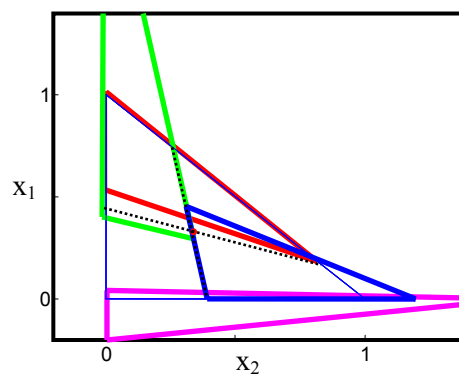
Figure 6.46: Matching criterion 4 satisfied along CLL2 but criterion 1 is not.
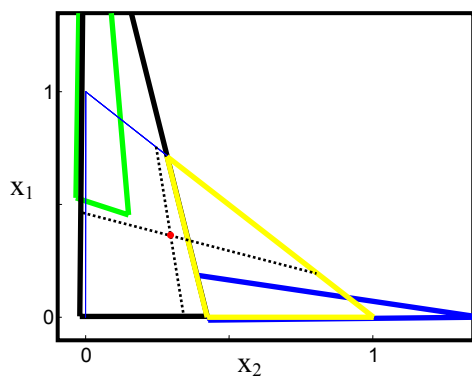
Figure 6.47: Matching criterion 2 satisfied but criterion 4 is not
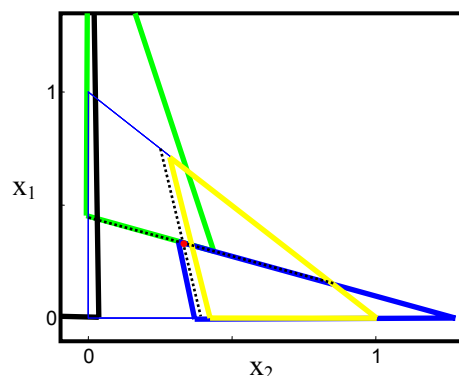
Figure 6.48: Matching criterion 4 satisfied along CLL1 but criterion 2 is not.
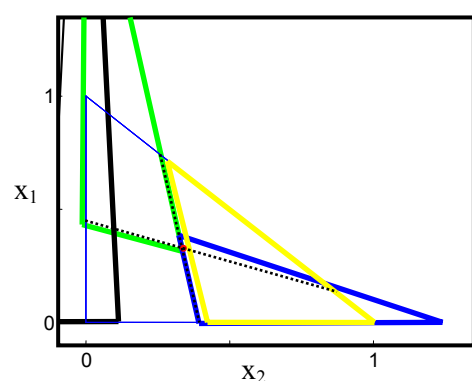
Figure 6.49: Matching criterion 4 satisfied along CLL2 but criterion 2 is not.
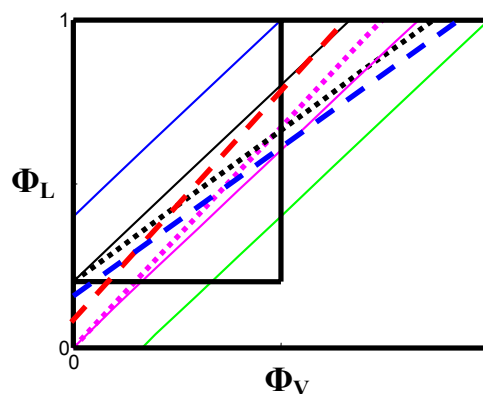
Figure 6.50: No overlap of feasible regions in split ratio space below min column reflux.
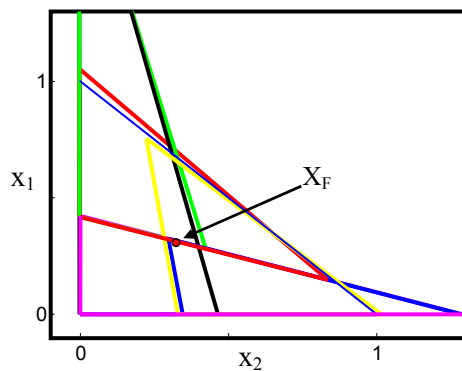
Figure 6.51: TT for column at minimum reflux
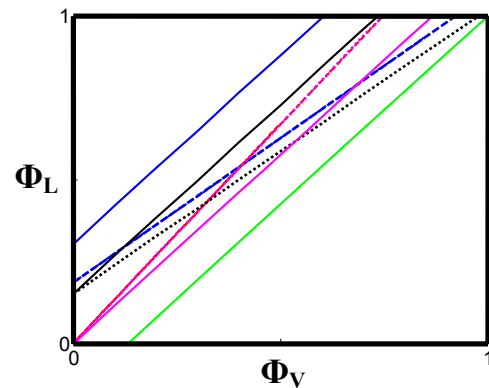
Figure 6.52: Region of feasibility shrinks to line at minimum reflux

6.14 The Effect of Varying $R_{\Delta 1}$

Halvorsen and Skogestad (2001) performed an extensive analysis of the feasible/optimality region at various reflux ratios, feed qualities and relative volatilities. We will now outline the more common feasible region effects for saturated liquid feed as well as changes to the zero net flow lines and negative flow boundaries upon variation of reflux ratio.

6.14.1 CS 2 and CS 4 minimum reflux

When the value of $R_{\Delta 1}$ is increased the area of TT 1 inside the MBT increases, as boundary B_1 moves away from the light component. The value of $R_{\Delta 2MIN}$ required for TT 2 to border TT 1 is, therefore, reduced as boundary C_2 is much closer to $X_{\Delta 2}$. We find that $R_{\Delta 4MIN}$ is similarly reduced because $R_{\Delta 6}$ is increased the moment $R_{\Delta 1}$ is increased - to maintain material balance. The net result of the reduction in the values of $R_{\Delta 2MIN}$ and $R_{\Delta 4MIN}$ is that these lines, in split ratio space, now fan out further from their respective zero net flow lines (infinite reflux lines). See Figure 6.53 below. For of our choice of relative volatilities and product points, the $R_{\Delta 2MIN}$ line shifts much slower than the $R_{\Delta 4MIN}$ line.

6.14.2 Negative Flow Boundaries

The negative flow boundaries are described by Equation 6.6 and Equation 6.7. It is clear that the value of Φ_V, in Equation 6.6, must increase as $R_{\Delta 1}$ increases, because the second term in this equation is negative and its magnitude decreases. The negative flow boundary in split ratio space must therefore shift to the right - closer to $\Phi_V = 1$. The value of Φ_L, in Equation 6.7, on the other hand, must decrease as the denominator increases. The negative flow boundary, described by Equation 6.7, will shift downwards towards $\Phi_L = 0$ as $R_{\Delta 1}$ increases. (See Figure 6.54)

6.14.3 Zero Net Flow Boundaries

Each of the zero net flow lines shifts towards the $\Phi_L = \Phi_V$ line as $r_{\Delta 1}$ is increased. This occurs because the gradients of these straight lines, described by Equation 6.2 to Equation 6.5, tend to 1 and the Φ_L-intercepts tend to 0 as $R_{\Delta 1} \rightarrow \infty$. As a consequence the area of net flow regions 2,3 and 4 decrease. (See Figure 6.56 and Figure 6.57)

6.14.4 PEB1 and PEB2

With increasing $R_{\Delta 1}$ the slope of PEB1 decreases slightly and its Φ_L-intercept shifts downwards. The slope of PEB2 also decreases, but its Φ_L-intercept increases, moving upwards along the Φ_L axis. For our choice of products and constant relative volatilities, we again see a marked difference in the rate of change of two boundaries of the same type, in split ratio space. PEB1 shifts far more rapidly than PEB2. (See Figure 6.55)

6.14.5 Feasible Φ_L and Φ_V regions

The shifting of the various boundaries in split ratio space combine to increase the overall area of the feasible Φ_L and Φ_V region as $R_{\Delta 1}$ is increased (see Figure 6.58). This effectively makes the separation easier as a larger range of split ratios result in feasible designs than before. At minimum overall column reflux the feasible region has zero area (see Figure 6.52). The region effectively "grows" from this zero area at minimum reflux as $R_{\Delta 1}$ is increased - as would be expected. The most

interesting effect of the increase of the feasible region area is that at high enough $R_{\Delta 1}$ values, the region crosses into the four remaining net flow regions (see Figure 6.59 and Figure 6.62). The associated net flow patterns can therefore be produced in feasible designs if $R_{\Delta 1}$ is sufficiently large. We have now confirmed the intuitive arguments about the required magnitude of the column reflux ratio for net flow patterns 1, 2, 4 and 5 discussed previously. These flow patterns are indeed only possible at high reflux ratio. Figure 6.60, Figure 6.61, Figure 6.63 and Figure 6.64 each show the six liquid TTs of a feasible Petlyuk design for net flow patterns 1, 2, 4 and 5.
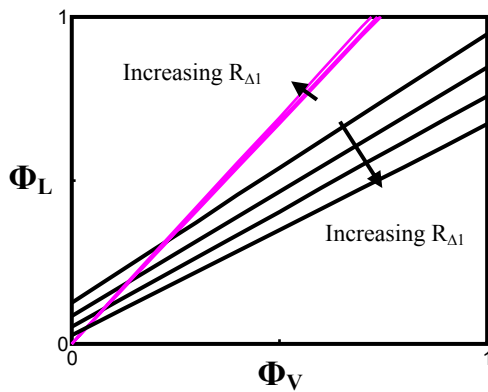
Figure 6.53: $R_{\Delta 2MIN}$ and $R_{\Delta 4MIN}$ at varying reflux
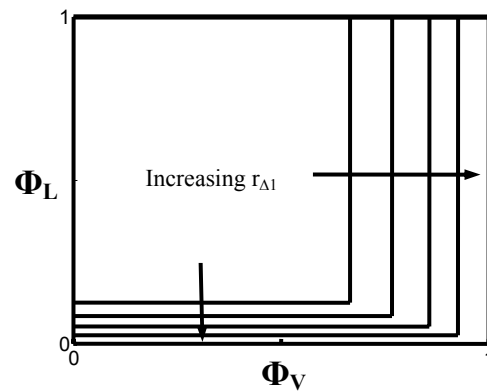
Figure 6.54: Negative flow boundaries varying reflux
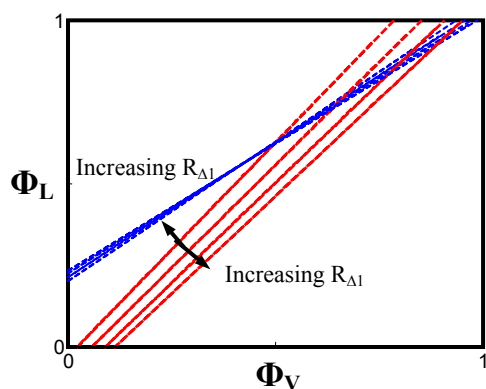
Figure 6.55: **PEB1 and PEB2 varying reflux**
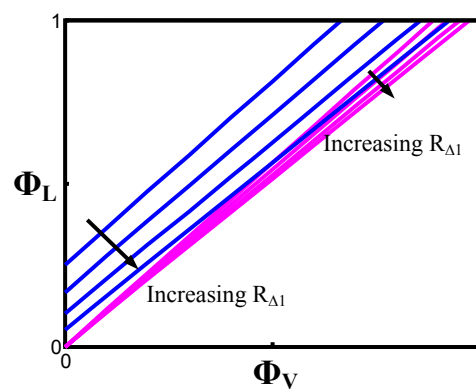
Figure 6.56: Δ_5 **and** Δ_2 **zero net flow lines varying reflux**
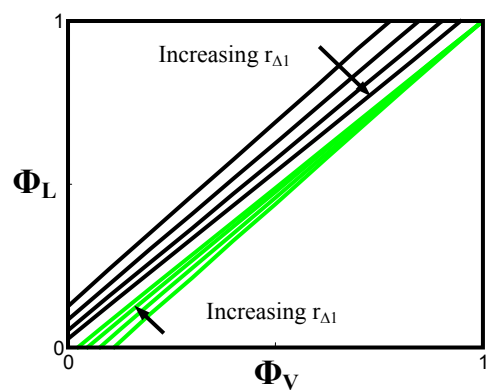
Figure 6.57: Δ_3 **and** Δ_4 **zero net flow lines varying reflux**
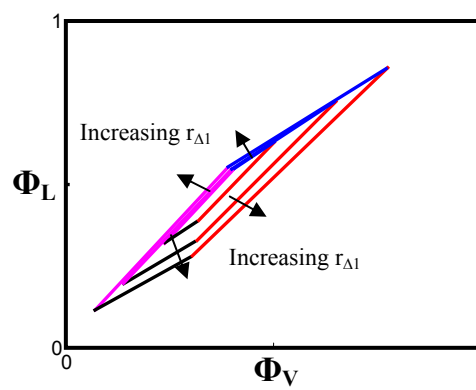
Figure 6.58: Feasible region varying reflux
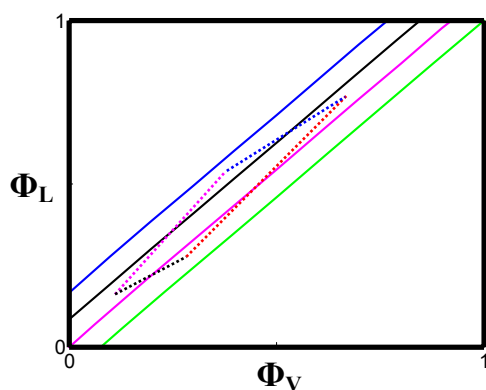
Figure 6.59: Feasible solutions in region 2, 3 and 4
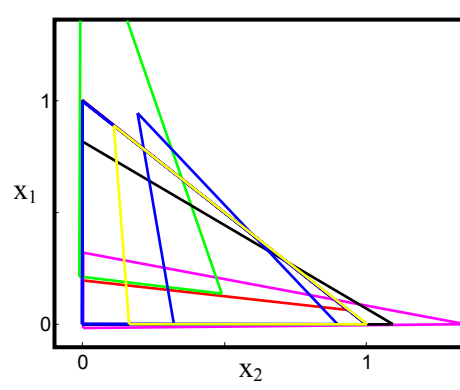
Figure 6.60: **Feasible TTs for net flow pattern 2**
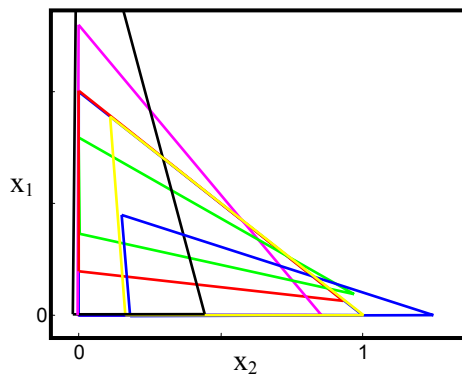
Figure 6.61: Feasible TTs for net flow pattern 4
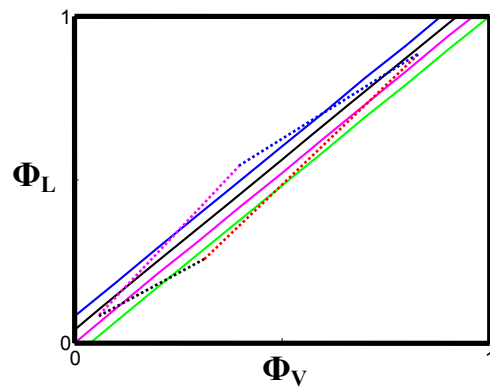
Figure 6.62: Feasible solutions in region 1, 2, 3, 4 and 5
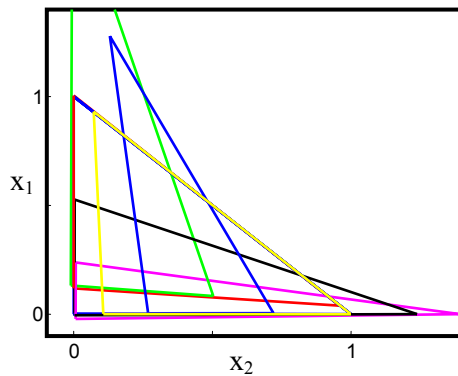
Figure 6.63: Feasible TTs for net flow pattern 1
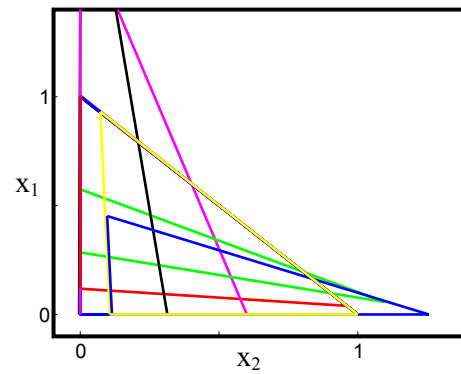
Figure 6.64: Feasible TTs for net flow pattern 5

6.15 Discussion

In this work we have successfully modelled the Petlyuk column. The column is broken down into column sections and a CPM is produced for each of these sections using the difference point equation. These CPMs can then be superimposed and feasible operating profiles found.

This design procedure is graphical but can be performed quickly and with little computational effort. Instead of producing entire CPMs, the procedure can be performed by simply tracking the stationary solutions of the difference point

equation. Using these stationary solutions a transformed triangle can be produced that enables us to track all regions of CPM topology without solving the difference point equation.

The importance of the reflux ratio to the qualitative form of the CPM/TT has led to a comprehensive analysis of the feasible net flow patterns in the Petlyuk configuration. We have shown that there are *five* possible net flow patterns. These are flow patterns 1 to 5. The net flow pattern within the column is determined by the choice of vapour and liquid split ratios. Regions, of split ratio space, resulting in each of these flow patterns can be found by producing zero net flow lines for the coupled column sections.

Net flow pattern 3 is the most efficient mode of operation. Feasible column solutions can be produced at lower reflux ratio for this flow pattern than for the other four patterns. This fact leads to a very useful analytical test of Petlyuk operation. *If the operating split ratios result in flow patterns other than net flow pattern 3 we can immediately conclude that the column is operating inefficiently.*

Variables other than net flow can be represented in split ratio space. In fact, the representation of variables in split ratio space is a very powerful tool for analysing and understanding Petlyuk column parameters. We can very simply produce lines of split ratios corresponding to coupled-column section reflux ratios, lines of constant difference point values and also generate regions corresponding to negative internal flow rates. However, the most powerful result is that by producing PEB 1 and 2 as well as minimum reflux ratio lines for CS 2 and 4 we can construct a region of split ratios that result in feasible Petlyuk column designs. *These regions contain all feasible split ratios values that allow the design specifications to be met.*

The feasible region, of split ratio solutions, is exactly equivalent to the optimality region defined by Halvorsen and Skogestad (2001). The CPM methodology is broader in scope, however, as it can be applied to all zeotropic systems. Although

the topological boundaries, between stationary points, of non-ideal systems have a degree of curvature, straight lines offer very good approximations to these boundaries. As such feasible regions can be generated for these systems with a fair degree of accuracy. The methodology also allows the generation of individual solutions containing all the required design parameters as well as composition profiles.

Feasible regions illustrate that the choice of vapour and liquid split ratios, in the Petlyuk column, cannot be made arbitrarily. For reflux ratios above the minimum, only a very small region of split ratio space results in feasible designs. The designer would be very fortunate to arbitrarily choose a feasible split ratio pair. The choice of split ratios within this feasible region can also not be made arbitrarily. Values, chosen along the boundaries of the region, result in an infinite number of required stages. Although we have analysed sharp-split separations in this work, which, by their nature, require infinite stages, the feasible region boundaries can be generated for non-sharp-splits as well. This will be performed in the next chapter. These non-sharp-split boundaries also coincide with an infinite number of required stages.

From a stage number and split ratio perspective it is clear why producing Petlyuk designs, for desired separations, is difficult using iterative solving methods. Convergence problems aside, without an understanding of the effects of parameters such as reflux ratio and the split ratios it is exceedingly difficult to determine the required number of stages for a separation. For a set number of stages the designer would typically choose arbitrary split ratios and reflux ratios. These are very unlikely to produce the desired separation and the designer must resort to trial and error. If we now couple this trial and error approach with iterative convergence problems it is evident that current design methods are not particularly efficient. The CPM approach on the other hand has allowed us to not only generate individual solutions, but find *all possible solutions* for a set of column parameters (reflux ratio and product flow rates). For non-sharp splits, parameters like the total number of required stages, feed stage and side-draw stage

are a natural product of the process. These can be determined by tracking variable n along each composition profile of a column section.

Determining column minimum reflux ratio, for any zeotropic thermodynamics, is one of the most powerful results of the methodology. We can determine this value directly by analysing the position of the feed point relative to the boundaries of TT 1 and TT6 as described previously. We can, however, also determine if a design is infeasible by analysing the boundaries in split ratio space. If the boundaries of the split ratio feasible region occur in the wrong position relative to each other, the designer can immediately infer that the design at the chosen parameters is infeasible. In this case, either the column reflux ratio or product flow rates must be altered in order to make the separation feasible.

At minimum reflux the feasible region has zero area. It is simply a line at these conditions. As the reflux is increased, the area of the feasible region increases i.e. more split ratios become feasible for operation. This holds with the intuitive understanding that separation by distillation becomes easier as the reflux ratio is increased. If the designer wishes to operate the column with net flow patterns 1, 2, 4 or 5, it is simple to determine the minimum column reflux ratio required. When the feasible region crosses into the relevant net flow region (of split ratio space), after increasing $R_{\Delta 1}$, this flow pattern becomes feasible. Although these flow patterns hold no obvious advantages for zeotropic systems, they do, in fact, hold very exciting advantages for azeotropic systems. *These flow patterns allow for the sampling of very "unusual" difference points which quite often allow distillation boundaries to be crossed.*

In summary the CPM methodology for Petlyuk design is very powerful and efficient. The procedure for generating the feasible/optimality region and minimum reflux is not quite as elegant as the analytical methods employed by Halvorsen and Skogestad (2001), but does allow the determination of all feasible solutions and minimum reflux ratio, for all zeotropic systems. On selecting a reflux ratio and split ratio pair, individual column solutions can be generated

without requiring iteration. Parameters such as feed stage placement, side-draw stage placement, total required stages, column section stage requirements as well as internal vapour and liquid traffic are a natural outcome of the procedure. The solutions generated from the procedure can be used for the effective initialisation of rigorous iterative simulation packages such as ASPEN Plus and do not vary drastically from the solutions generated using these packages.

In the following chapter we will detail the determination of the feasible region for non-sharp separations. This will include difference point selection as well as minimum reflux determination. Minimum reflux cannot be determined the same way as detailed here, or via the use of the Underwood equations, for sharp separations. Rather an understanding of the system topology and topological shifts is required.

Chapter 7:

Petlyuk Column

Design for Non-Sharp Product Specifications

This work has been prepared in the form of a paper for future publication and follows on from that presented in Chapter 6. In the previous chapter an analysis of sharp-product Petlyuk separations was performed. The results of this work are now extended to include non-sharp product specifications

---

Abstract

Halvorsen and Skogestad (2001) comprehensively studied the Petlyuk column at sharp-split conditions In this work we apply the column profile map (CPM) technique to the design and analysis of the Petlyuk column at non-sharp product specifications. It is shown that very interesting and counter-intuitive net-molar-flows are feasible in the Petlyuk column. At these conditions the net-molar-flow of the intermediate boiling component in a column section can be opposite to that of the light and heavy boiling components. We also analyse the "feasible region" of column parameters for the non-sharp separation in relation to that of the sharp-split Furthermore a minimum reflux condition is found for all product specifications.

7.1 Introduction

The analysis of sharp split separations in the Petlyuk column, performed in the previous chapter, gives very useful insight into its operation and a general understanding of the interaction of design parameters. The generation of a feasible region of split ratios for these separations is very powerful when beginning the design process. The sharp split is, however, a special mode of operation and does not allow a complete understanding of the column. From a practical design perspective it is hampered by the infinite stage assumption. Another drawback is that these design methods are essentially based on the composition of stationary points which give rise to the infinite stage assumption. The composition of saddle points, unstable and stable nodes play equally important roles in these methods. However, for many systems, the thermodynamics prevent composition profiles from running close to their saddle points even if the product selection is essentially pure. This results in significant solution, prediction errors. The method therefore encounters serious problems with these systems. A more comprehensive understanding of the column behaviour and possible design strategies is required.

In this chapter we will investigate the operation of the Petlyuk column at non-sharp split conditions. We will see that the difference point placement for non-sharp separations can be drastically different from the sharp split case. Very interesting and counterintuitive component net-molar-flows result as a consequence of this. We will also produce a non-sharp feasible region and show how this can be very different from that of the sharp-split. Finally, we will determine an optimum split ratio pair for any particular reflux ratio choice. This solution results in the smallest stage requirement and hence lowest capital investment for the separation. The ultimate aim of this work is to produce a comprehensive Petlyuk design tool for zeotropic systems and all operating conditions.

7.1.1   Assumptions

We will address the three component problem in this work. Constant molar overflow is assumed for all distillation modelling. An assumption of constant relative volatility is also made although the results are applicable to all three component zeotropic thermodynamics. Feed material is assumed to be at saturated liquid or saturated vapour conditions. Perfect mixing is assumed over all mixing points.

7.1.2   Composition Diagram Legend

Composition Diagram Legend: Unless otherwise stated, within composition diagrams a solid line will denote the liquid phase while a dotted line will denote the vapour phase (except lines CLL1 and CLL2). Red lines (within composition diagrams) are associated with CS 1, pink with CS 2, green with CS 3, black with CS 4, blue with CS 5 and yellow with CS 6. The light component composition (x_1) will always be represented on the y-axis while the heavy component composition (x_2) will be represented on the x-axis. The MBT will always be represented by a blue triangle. Arrows on composition profiles indicate the direction of increasing n i.e. the direction down the length of a column section.

Transformed Triangle Boundary Definitions: We will label the TT boundaries in the same way as the previous chapter. A boundary defined between an unstable node and a saddle point of TT "k" will be referred to as boundary "A_k". A boundary defined between a stable node and a saddle point of TT "k" will be referred to as boundary "B_k". The final boundary defined between an unstable node and a stable node will be referred to as boundary "C_k" of the TT. Figure 7.1 below illustrates these boundary definitions. Unless otherwise stated this will always refer to liquid TT boundaries. Vapour TT boundaries will be referred to as "vapour boundary A_k", etc.
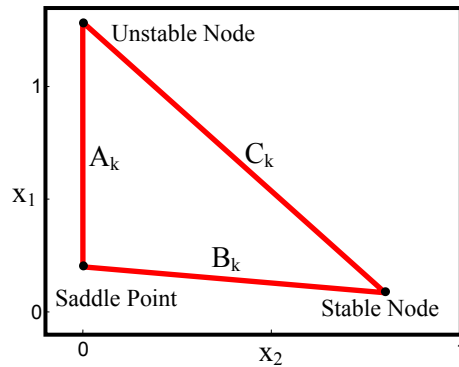
Figure 7.1: Transformed triangle boundary definitions

7.1.3   Relaxing Sharp Split Constraints

There are a number of important results from the previous chapter which will be useful to emphasise. These include the following:

- For sharp-splits $X_{\Delta 2} = X_{\Delta 4} = X_S$. This is true for all operating reflux ratios and all net flow patterns.

- X_S lies essentially on the origin for sharp-splits. Because $X_{\Delta 2}$ and $X_{\Delta 4}$ must operate at this composition too, all the Petlyuk column section difference points lie effectively on an axis in composition space.

- Because all difference points lie on an axis and because of the effect of difference point placement on the form of the column profile map (CPM), each of the column section transformed triangles (TTs) is positioned with at least on boundary on an axis too.

- Operating composition profiles run effectively on the boundaries of their associated TTs. Therefore the "movement" of TTs when varying column parameters matches the "movement" of operating composition profiles.

These results emphasise the convenience of the sharp-split specification. Instead of tracking individual composition profiles, when varying column parameters, only the TT and hence stationary points needed to be tracked. When the sharp-split constraint is lifted it becomes very difficult to determine feasible operating profiles and hence construct feasible parameter regions.

In order to simplify this task, when constructing feasible split ratio regions, we will relax the constraints on each product composition separately. The results of the product specification change will be compared to the sharp-split results.

We will adjust the side-draw product first followed by the distillate and bottoms products. It is important to note that the side-draw product must remain non-sharp if either the distillate or bottoms product is non-sharp, in order for the separation to be feasible; profiles from the side-draw product have to intersect the rectifying and stripping profiles. This will be explored in greater detail later.

Before feasible split ratio regions can be constructed the effect of non-sharp product specifications on the columns difference points must be analysed. Relaxing the sharp-split assumption on the side-draw product introduces design complications that were not encountered previously. When "impurities" are introduced in the side-draw, $X_{\Delta 2}$ and $X_{\Delta 4}$ need not operate at this composition. In fact, for non-sharp splits, having both these values at the side-draw composition, in general, only produces feasible designs for net flow pattern 3. Each net flow pattern requires specific (and different) placements of the difference points.

We will investigate the required region of operation of each column section difference point. Once these have been found we will determine which combinations of $X_{\Delta 2}$ and $X_{\Delta 4}$ placement result in feasible placement for the remaining coupled column sections.

7.2 Difference Point Selection

7.2.1   Feasible Difference Point Regions

Using the design approach and variable selection discussed in the previous chapter, we have the freedom to assign one difference point value. Previously we selected $X_{\Delta2}$ to fulfil this degree of freedom. However, it was shown that for sharp-splits $X_{\Delta2}$ can only operate at the side-draw composition. This confines boundaries of each of the coupled column section TTs to the axes. This is not the case for non-sharp splits. We now have considerable freedom in the placement of difference points and consequently considerable freedom of movement of the associate TTs. It would be very useful if we could narrow down our choice of difference point placement to particular regions in composition space.

All coupled column section difference points are linked through material balance. Placement of one difference point affects the placement of all others. It does not confine them to specific values until the split ratios have been selected but does confine them to certain ranges of values or regions of operation. The difference point region of operation has a fundamental effect on the qualitative topology a column section can sample.

Selection of a difference point value should fulfil a number of requirements. Firstly, it should satisfy the requirements of the associated column section. For example, if placing $X_{\Delta2}$, we must ensure that the difference point is positioned such that it allows CS 2 to achieve/sample the side-draw composition and satisfy matching criterion 1. Secondly, the difference point placement should allow a range of values for the remaining difference points that, in turn, allow the other coupled sections to satisfy the matching criteria.

Before any difference point value can be selected we must determine which ranges of values for each difference point allow the satisfaction of the matching criteria. This is equivalent to determining which difference point regions result in "useful" topology for each of the coupled column sections.

The term "useful" topology is qualitative but is based on column section matching criteria requirements and the general form of Petlyuk solutions that was discussed in our analysis of sharp-splits. The non-sharp solution form will not vary dramatically from that of the sharp-split but because of the additional topological freedom (introduced by the freedom of difference point selection) will require additional constraints. By determining the form of and constraints on each section's composition profile, we can determine the qualitative placement of each TT and hence determine the required placement of each difference point.

We will now summarise the qualitative requirements of any candidate TT for each coupled column section.

7.2.1.1   Topological Requirements of Coupled Column Sections

- <u>CS 2</u>: The CS 2 solutions must satisfy matching criteria 1 and 3 i.e. run from the side-draw composition to the rectifying profile. "Useful" topology in this case will include trajectories that originate from the unstable node and gain rapidly in the intermediate component and gradually in the heavy component, down the length of the column section. This refers exclusively to TR 1. However, because the boundaries of TT 2 are no longer confined to the axes – as in the sharp-split case – ill chosen $X_{\Delta 2}$ values can result in TTs with trajectories that leave physically relevant composition space and that, therefore, do not satisfy matching criterion 1 (see Figure 7.3). We will therefore impose the following condition: *Boundary A₂ must lie in positive heavy component space – to the right of the light-intermediate axis.* See Figure 7.2. This ensures that if the reflux magnitude is large enough, composition matching will be guaranteed.

- <u>CS 3</u>: The CS 3 solutions must satisfy matching criteria 1 and 4 i.e. run from the intersection of the rectifying and CS 2 profiles to the CS 5 composition profile. "Useful" topology for TT 3 is defined here as topology that gains in the heavy component down the length of the column section. This refers,

specifically, to TR 1 and TR 4. However, because the boundaries of TT 3 are no longer confined to the axes – as in the sharp-split case – ill chosen X_{A3} values can result in CS 2 trajectories potentially running to the left of the TT 3 saddle point and not intersecting useful topology (see Figure 7.5). We therefore impose the following condition: *Boundary A_3 must lie in negative heavy component space - to the left of the light-intermediate axis.* See Figure 7.4. This ensures that if the reflux magnitude is large enough, composition matching will be guaranteed.

- <u>CS 4</u>: The CS 4 solutions must satisfy matching criteria 2 and 3 i.e. run from the side-draw composition to the stripping profiles. "Useful" topology in this case will include trajectories that originate from the stable node and gain rapidly in the intermediate component and gradually in the light component, up the length of the column section. This refers exclusively to TR 1. However, because the boundaries of TT 4 are no longer confined to the axes – as in the sharp-split case – ill chosen X_{A4} values can result in TTs with trajectories that leave physically relevant composition space and that, therefore, do not satisfy matching criterion 2 (see Figure 7.7). We will therefore impose the following condition: *Boundary B_4 must lie in positive light component space - above the intermediate-heavy axis.* See Figure 7.6. This ensures that if the reflux magnitude is large enough, composition matching will be guaranteed.

- <u>CS 5</u>: The CS 5 solutions must satisfy matching criteria 2 and 4 i.e. run from the intersection of the stripping and CS 4 profiles to the CS 3 composition profile. "Useful" topology for TT 5 is defined here as topology that gains in the light component up the length of the column section. This refers, specifically, to TR 1 and TR 6. However, because the boundaries of TT 5 are no longer confined to the axes – as in the sharp-split case – ill chosen X_{A5} values can result in CS 4 trajectories potentially running below the TT 5 saddle point and not intersecting useful topology (see Figure 7.9). We therefore impose the following condition: *Boundary B_5 must lie in negative light component space –*

below the intermediate-heavy axis. See Figure 7.8. This ensures that if the reflux magnitude is large enough, composition matching will be guaranteed.
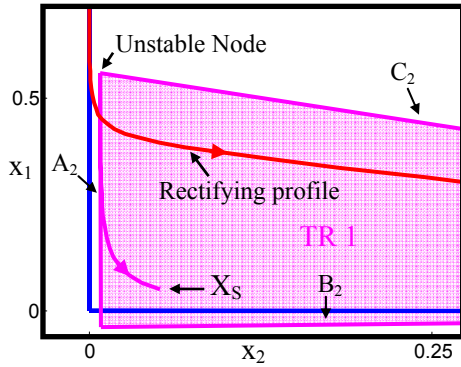
Figure 7.2: CS 2 profile satisfying matching criterion 1
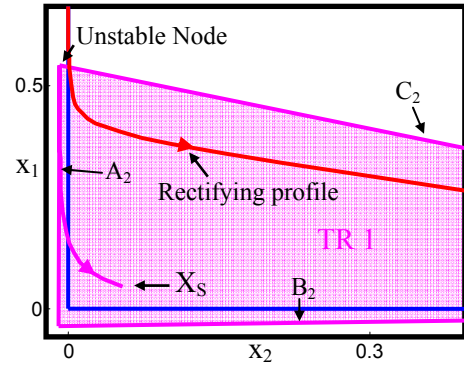
Figure 7.3: CS 2 profile not satisfying matching criterion 1
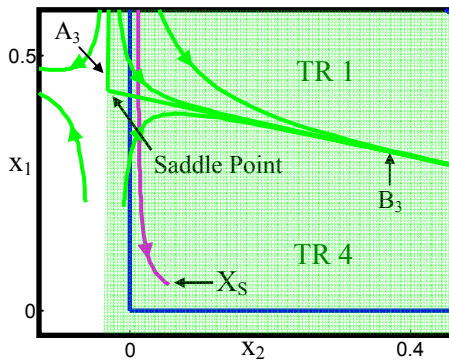
Figure 7.4: CS 2 profile sampling "useful" TT 3 topology
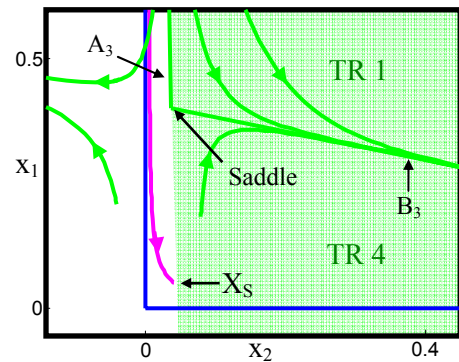
Figure 7.5: CS 2 profile does not sample "useful" TT 3 topology
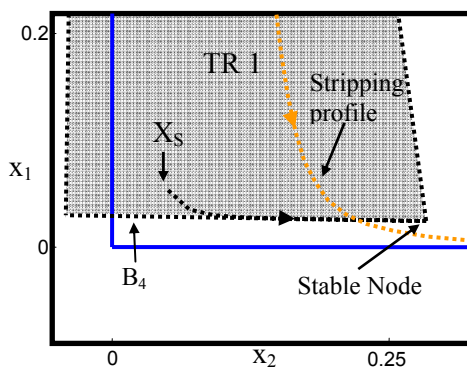
Figure 7.6: CS 4 vapour profile satisfying matching criterion
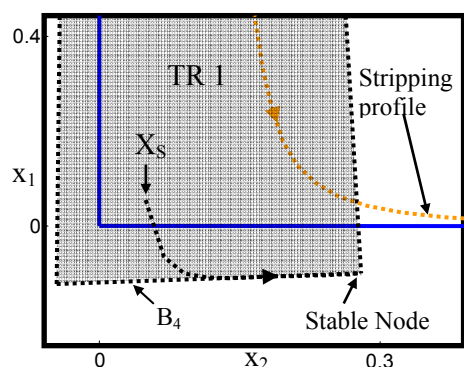
Figure 7.7: CS 4 vapour profile not satisfying matching criterion
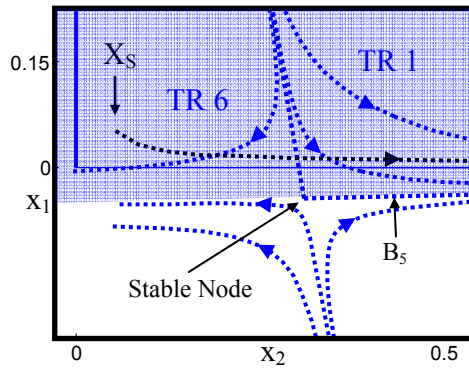
Figure 7.8: CS 4 profile sampling "useful" TT 5 topology
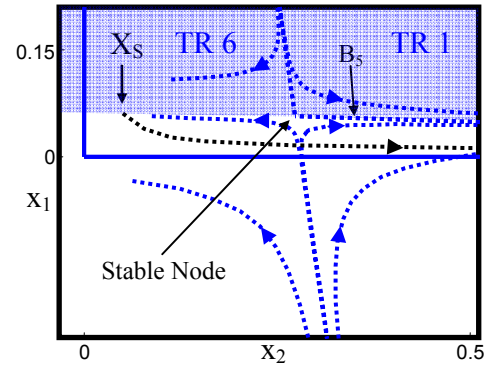
Figure 7.9: CS 4 profile does not sample "useful" TT 5 topology

7.2.1.2   Net Flow Pattern and the Difference Point Placement

It is not only the region of difference point placement that determines the qualitative form of a TT. The reflux ratio and hence net flow in a column section also has a significant influence. TTs produced from positive and negative reflux are qualitatively dissimilar. Therefore the selection of a particular difference point region of operation - to produce a desire qualitative form of TT - is only valid for a particular reflux sign or net flow direction. This implies that difference point placement is dependent on the net flow pattern of operation i.e. each net flow pattern requires different placement of the difference points for the coupled column sections.

This is clearly illustrated by a simple example. Consider a column to be operated at net flow pattern 1. If $X_{\Delta 2}$ was placed at the side-draw composition, material balance would result in $X_{\Delta 4}$ also being positioned at this point (see Equation 7.1 below).

$$\Delta_4 X_4 = \Delta_2 X_2 + S X_S$$
$$\Delta_4 X_4 = X_S (\Delta_2 + S)$$
$$X_4 = X_S \frac{(\Delta_2 + S)}{\Delta_4}$$

(7.1)

For net flow pattern 1, the refluxes of both CS 2 and 4 are negative. A pinch point curve for negative reflux with X_Δ placed in difference point region 1 can be seen in Figure 7.10 below.

As discussed in *section 7.2.1.1* above, the topological feasibility requirement of TT 2 is that boundary A_2 lie in positive heavy component space. We can see, from the positions of the unstable and saddle branches of the pinch point curve of Figure 7.10, that A_2 would, indeed, lie in positive heavy component space if $X_{\Delta 2}$ was placed in difference point region 1 and the column section was operated at negative reflux. The placement of $X_{\Delta 2}$, in this region, is acceptable for net flow pattern 1.
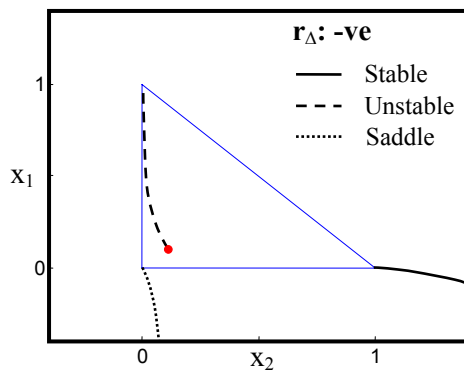
Figure 7.10: Pinch point curve for difference point region 1 at negative reflux
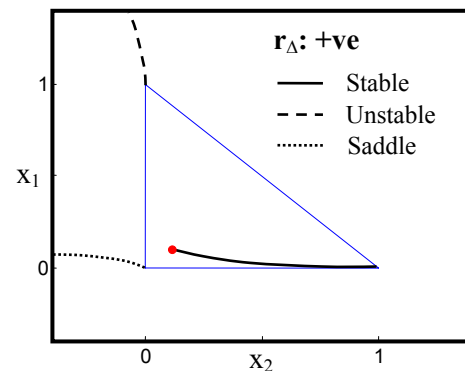
Figure 7.11: Pinch point curve for difference point region 1 at positive reflux

The topological feasibility requirement of TT 4 is that boundary B_4 lie in positive light component space. However, the saddle and unstable branches of the pinch point curve in Figure 7.10 lie below the intermediate-heavy axis. Therefore B_4 would lie in negative light component space. Difference point region 1 is clearly an unacceptable region of operation for $X_{\Delta 4}$, if CS 4 is operated at negative reflux. Hence, a column can not be operated at net flow pattern 1 with $X_{\Delta 2} = X_{\Delta 4} = X_S$.

If we maintain the desired difference point selection of $X_{\Delta 2} = X_{\Delta 4} = X_S$ but operate the column at net flow pattern 3, instead of net flow pattern 1, the reflux of CS 2 would still be negative but the reflux of CS 4 would now be positive. The results for CS 2 described above are still valid for net flow pattern 3. $X_{\Delta 2}$ can operate in

difference point region 1 for net flow pattern 3. We must now consult a pinch point curve for difference point region 1 at positive reflux to determine if the placement of $X_{\Delta 4}$ is acceptable. Figure 7.11 shows such a pinch point curve. The stable and saddle branches of this pinch point curve are above the intermediate-heavy axis i.e. in positive light component space. Therefore, boundary B_4 will lie in light component space. Hence, difference point region 1 is an acceptable region of placement for $X_{\Delta 4}$ when the column is operated at net flow pattern 3.

This example illustrates that, in general, each net flow pattern requires different placement of the difference points. By considering each difference point separately, we can determine which regions of placement are acceptable, for that point, for each net flow pattern. By combining the results for each of the coupled column sections we can find combinations of difference point placement that produce feasible topology and potential Petlyuk solutions.

7.2.1.3   Regions of Feasible $X_{\Delta 2}$ and $X_{\Delta 4}$ Placement

As $X_{\Delta 2}$ and $X_{\Delta 4}$ selection is critical for achieving the side-draw composition, we will now analyse which difference point regions of placement produce feasible topology for CS 2 and 4. By combining the results for both column section difference points we can narrow down the options of possible placement. We will consider these difference points completely independently of the remaining coupled section difference points.

Figures G.1-14 (in Appendix G) below show pinch point curves at positive and negative reflux, for difference points placed in each of the seven difference point regions. By considering the topological requirements for CS 2 and CS 4 in conjunction with these figures we can analyse the feasibility of each qualitatively different X_{Δ} placement, in the same manner as in the above example (*section 7.2.1.2*).

Specifically the methodology is as follows:

- Determine the operating reflux of the CS (i.e. +ve or -ve).

- Select a candidate difference point region.

- Consult the pinch point curve for the candidate difference point region and operating reflux.

- Determine if the topological requirements of the CS are met by the selected pinch point curve. If the topological requirements are met the difference point region is deemed feasible.

- Construct combinations of $X_{\Delta 2}$ and $X_{\Delta 4}$ placement. These will be net flow dependent.

- If both placement scenarios in the combination are feasible, the combination is deemed feasible. If either is infeasible the combination is deemed infeasible.

Tables 7.1, 7.2 and 7.3 summarise the results for potential combinations of placement of $X_{\Delta 2}$ and $X_{\Delta 4}$ for all net flow patterns. Each combination is illustrated graphically on a material balance line. The overall material balance is given by Equation 7.2.

$$\Delta_4 X_{\Delta 4} = \Delta_2 X_{\Delta 2} + S X_S \qquad\qquad \textbf{(7.2)}$$

Graphically, Equation 7.2 dictates that for net flow patterns 1 and 2, $X_{\Delta 2}$ must lie between $X_{\Delta 4}$ and X_S, for net flow pattern 3, X_S must lie between $X_{\Delta 4}$ and $X_{\Delta 2}$ and for net flow patterns 4 and 5, $X_{\Delta 4}$ must lie between $X_{\Delta 2}$ and X_S. The feasibility of each point is reported separately in Table 7.1, 7.2 and 7.3. These feasibilities are then used to report an overall feasibility of the combination.

Note: CS 2 and CS 4 require significant flows of the intermediate component, to satisfy the side-draw demand, so we have only considered difference point regions 1, 4, 5, and 6 here.

Legend (Tables 7.1, 7.2 and 7.3):

•	X_S	**❘**	Light Component Net Flow Direction
•	$X_{\Delta 2}$	**❘**	Intermediate Component Net Flow Direction
•	$X_{\Delta 4}$	**❘**	Heavy Component Net Flow Direction

Table 7.1: Summary of $X_{\Delta 2}$ and $X_{\Delta 4}$ placement for Net Flow Patterns 1 & 2

Net Flow Pattern 1&2	$X_{\Delta 2}$ Position	CS 2 Net Flow Direction	$X_{\Delta 4}$ Position	CS 4 Net Flow Direction	Overall Feasibility
	Acceptable	↓ ↓ ↓	Unacceptable	↓ ↓ ↓	Infeasible
	Acceptable	↓ ↓ ↓	Acceptable	↑ ↓ ↓	Feasible
	Acceptable	↓ ↓ ↓	Acceptable	↑ ↓ ↑	Feasible
	Acceptable	↓ ↓ ↓	Unacceptable	↑ ↓ ↑	Infeasible
	Acceptable	↑ ↓ ↓	Acceptable	↑ ↓ ↓	Feasible
	Acceptable	↑ ↓ ↓	Acceptable	↑ ↓ ↑	Feasible
	Unacceptable	↑ ↓ ↑	Acceptable	↑ ↓ ↑	Infeasible
	Unacceptable	↓ ↓ ↑	Acceptable	↑ ↓ ↑	Infeasible
	Unacceptable	↓ ↓ ↑	Unacceptable	↓ ↓ ↑	Infeasible

Table 7.2: Summary of $X_{\Delta 2}$ and $X_{\Delta 4}$ placement for Net Flow Pattern 3					
Net-Molar-Flow Pattern 3	$X_{\Delta 2}$ Position	CS 2 Net Flow Direction	$X_{\Delta 4}$ Position	CS 4 Net Flow Direction	Overall Feasibility
	Acceptable	↓ ↓ ↓	Acceptable	↑ ↑ ↑	Feasible
	Acceptable	↓ ↓ ↓	Unacceptable	↓ ↑ ↑	Infeasible
	Acceptable	↓ ↓ ↓	Unacceptable	↓ ↑ ↓	Infeasible
	Acceptable	↓ ↓ ↓	Acceptable	↑ ↑ ↓	Feasible
	Acceptable	↑ ↓ ↓	Acceptable	↑ ↑ ↑	Feasible
	Unacceptable	↑ ↓ ↑	Acceptable	↑ ↑ ↑	Infeasible
	Unacceptable	↓ ↓ ↑	Acceptable	↑ ↑ ↑	Infeasible

Table 7.3: Summary of $X_{\Delta 2}$ and $X_{\Delta 4}$ placement for Net Flow Patterns 4 & 5

Net-Molar-Flow Pattern 4&5	$X_{\Delta 2}$ Position	CS 2 Net Flow Direction	$X_{\Delta 4}$ Position	CS 4 Net Flow Direction	Overall Feasibility
(plot)	Unacceptable	↑ ↑ ↑	Acceptable	↑ ↑ ↑	Infeasible
(plot)	Unacceptable	↓ ↑ ↑	Acceptable	↑ ↑ ↑	Infeasible
(plot)	Acceptable	↓ ↑ ↓	Acceptable	↑ ↑ ↑	Feasible
(plot)	Acceptable	↑ ↑ ↓	Acceptable	↑ ↑ ↑	Feasible
(plot)	Unacceptable	↓ ↑ ↑	Unacceptable	↓ ↑ ↑	Infeasible
(plot)	Acceptable	↓ ↑ ↓	Unacceptable	↓ ↑ ↑	Infeasible
(plot)	Acceptable	↓ ↑ ↓	Unacceptable	↓ ↑ ↓	Infeasible
(plot)	Acceptable	↓ ↑ ↓	Acceptable	↑ ↑ ↓	Feasible
(plot)	Acceptable	↑ ↑ ↓	Acceptable	↑ ↑ ↓	Feasible

7.2.2 Overall Material Balance for Feasible Difference Points – Determining $X_{\Delta 3}$ and $X_{\Delta 5}$ Placement Feasibility

Now that we have determined the feasible placement of difference points, for CS 2 and CS 4, for all of the possible net flow patterns, we must determine the effect of these possible placements on the remaining coupled column section difference points. We can then determine which difference point placement combinations produce feasible topology for all the coupled column sections.

Let us make use of the first feasible combination from Table 7.1 as an example. In this combination, $X_{\Delta 2}$ is situated in difference point region 1 and $X_{\Delta 4}$ is situated in difference point region 4. Table 7.1 presents all the results for net flow pattern 1 and 2. Let us consider only net flow pattern 1 for now.

We need to determine the regions of operation, of $X_{\Delta 3}$ and $X_{\Delta 5}$, dictated by material balance. The material balance at the bottom of the rectifying section is given by Equation 7.3.

$$\Delta_1 X_{\Delta 1} = \Delta_2 X_{\Delta 2} + \Delta_3 X_{\Delta 3} \tag{7.3}$$

For net flow pattern 1 $\Delta_1 > 0$, $\Delta_2 < 0$ and $\Delta_3 > 0$. Therefore, $X_{\Delta 3}$ must lie between $X_{\Delta 2}$ and $X_{\Delta 1}$ in composition space.

The material balance at the top of the stripping section is given by Equation 7.4.

$$\Delta_6 X_{\Delta 6} = \Delta_4 X_{\Delta 4} + \Delta_5 X_{\Delta 5} \tag{7.4}$$

For net flow pattern 1 $\Delta_6 < 0$, $\Delta_4 < 0$ and $\Delta_5 > 0$. Therefore, $X_{\Delta 4}$ must lie between $X_{\Delta 5}$ and $X_{\Delta 6}$ in composition space.

Finally, the material balance over the feed stage is given by Equation 7.5.

$$\Delta_3 X_{\Delta 3} = \Delta_5 X_{\Delta 5} + FX_F \tag{7.5}$$

As stated above, for net flow pattern 1 $\Delta_3 > 0$ and $\Delta_5 > 0$. Therefore, $X_{\Delta 3}$ must lie between $X_{\Delta 5}$ and X_F in composition space.

If we now produce a material balance construction for each of the above material balances with $X_{\Delta 2}$ in difference point region 1 and $X_{\Delta 4}$ in difference point region 4

(with suitable choices for the distillate, bottoms and side-draw composition) we can determine the possible regions of $X_{\Delta3}$ and $X_{\Delta5}$ placement.

Figure 7.12 illustrates the results of such a material balance construction. The relative position of the difference points is a function of the column split ratio choices. The difference points can be shifted by changing the operating choice for the split ratios. For this construction, regardless of split ratio changes, $X_{\Delta5}$ is constrained to difference point region 5 if $X_{\Delta2}$ is considered fixed. The point cannot move into positive light component space because it is constrained by the material balance with $X_{\Delta4}$ (which for the example has been placed in difference point region 4). $X_{\Delta5}$ is constrained to this region for all but the most extreme choices $X_{\Delta2}$ (high heavy component value). At extreme conditions $X_{\Delta5}$ could shift into difference point region 4. $X_{\Delta3}$ is constrained to difference point region 1 for all split ratio choices in this example.

We must now determine the feasibility of $X_{\Delta3}$ and $X_{\Delta5}$ placement. By consulting the relevant pinch point curves (Figures AI.1 and AI.5), we can see that both difference points produce feasible topology for CS 3 and CS 5. All the regions of difference point placement for the coupled column section are therefore acceptable. A feasible Petlyuk design is possible for these difference point choices.

Legend: Figure 7.12 to Figure 7.16	
●	$X_{\Delta2}$
●	$X_{\Delta3}$
●	$X_{\Delta4}$
●	$X_{\Delta5}$
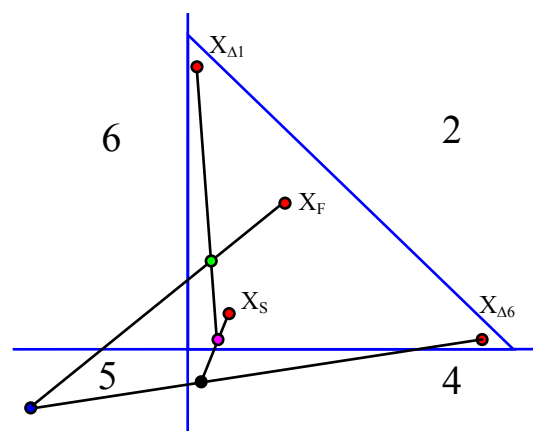
Figure 7.12: Material balance construction for net flow pattern 1

Figure 7.13 to Figure 7.14 illustrate examples of material balance constructions for net flow patterns 1, 2, 4 and 5 with two, qualitatively different, feasible placements of $X_{\Delta 2}$ and $X_{\Delta 4}$. Excluding extreme conditions, we can see that for each net flow pattern $X_{\Delta 3}$ and $X_{\Delta 5}$ can only exist in one difference point region. This is true for all $X_{\Delta 2}$ and $X_{\Delta 4}$ placement scenarios.

By consulting Figures AI.1-14, as above, we can see that all the positions of the differences points in Figure 7.14 to Figure 7.16 are acceptable. *Hence we have found feasible difference point placement combinations for all the net flow patterns.* Table 7.4 lists regions of feasible placement for all the coupled column sections while Figure 7.17 to Figure 7.21 illustrate the actual net component flow direction possibilities.
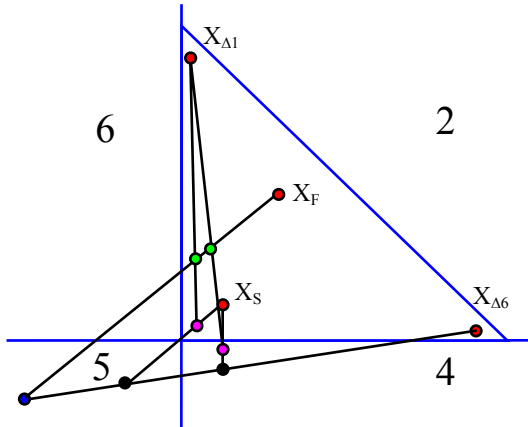
Figure 7.13: Two different, feasible difference point placement scenarios – Net flow pattern 1
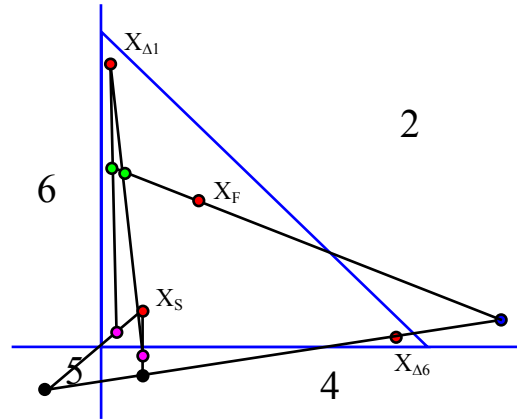
Figure 7.14: Two different, feasible difference point placement scenarios – Net flow pattern 2
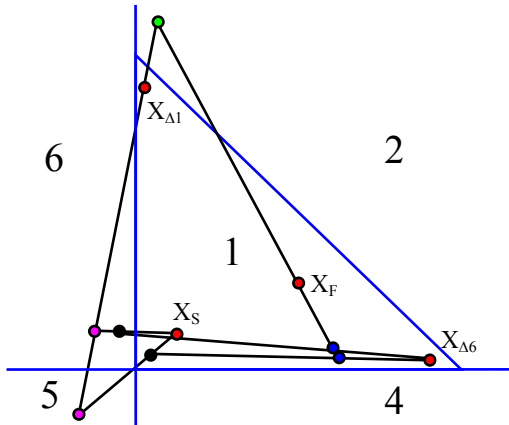
Figure 7.15: Two different, feasible difference point placement scenarios – Net flow pattern 4
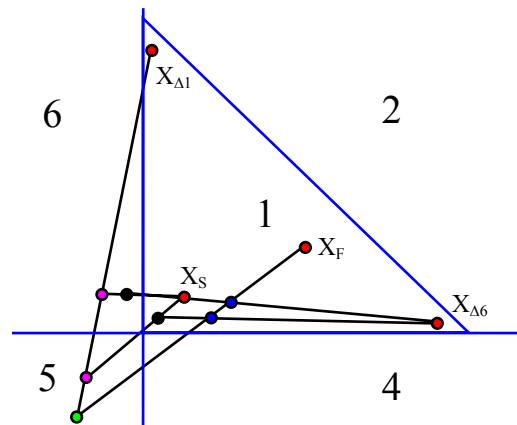
Figure 7.16: Two different, feasible difference point placement scenarios – Net flow pattern 5

Net Flow Pattern	$X_{\Delta2}$ (Region)	$X_{\Delta3}$ (Region)	$X_{\Delta4}$ (Region)	$X_{\Delta5}$ (Region)
1	1,4	1	4,5	5
2	1,4	1	4,5	2
3	1,4	1	1,6	1
4	5,6	2	1,6	1
5	5,6	5	1,6	1

Table 7.4: Summary of Regions Feasible Difference Point Placement for all Net flow Patterns
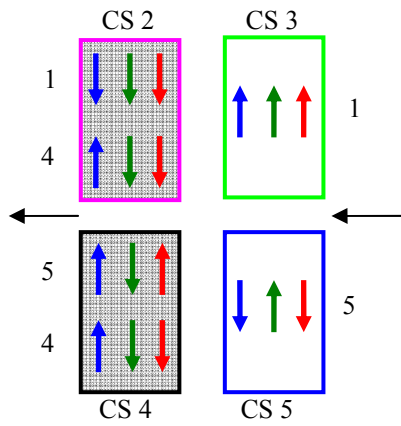
Figure 7.17: Feasible component net-molar-flow scenarios – Net Flow Pattern 1
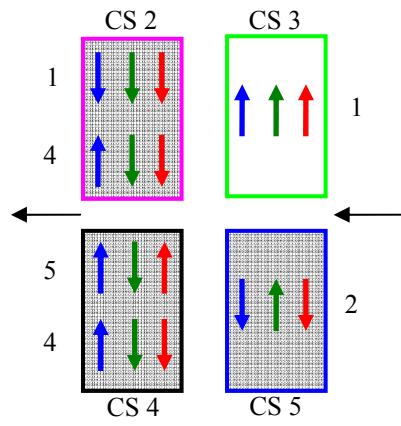
Figure 7.18: Feasible component net-molar-flow scenarios – Net Flow Pattern 2
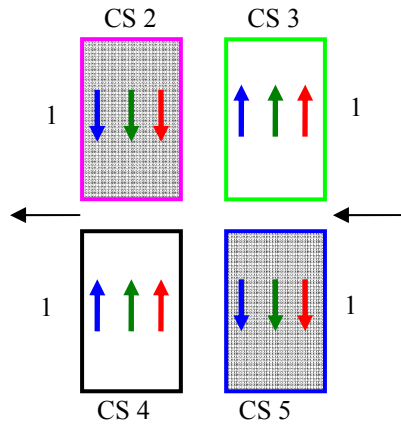
Figure 7.19: Feasible component net-molar-flow scenarios – Net Flow Pattern 3
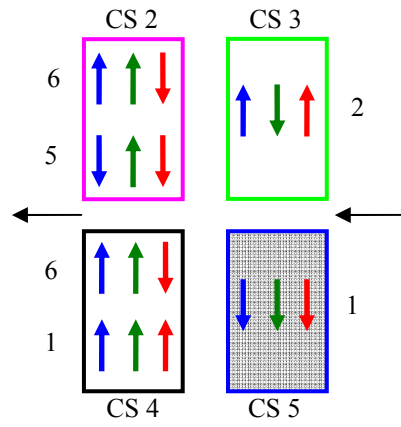
Figure 7.20: Feasible component net-molar-flow scenarios – Net Flow Pattern 4
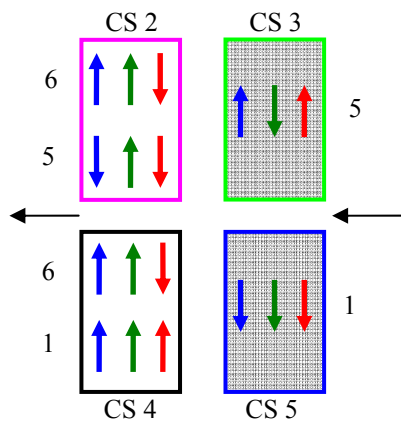
Figure 7.21: Feasible component net-molar-flow scenarios – Net Flow Pattern 5

7.2.3   Implications of Feasible Difference Point Placement for Net Flow

From the required feasible topology, we have determined regions of possible placement of $X_{\Delta 2}$ and $X_{\Delta 4}$, but we have not yet discussed the implications of this placement on the column net-molar-flow.

Net flow pattern 1&2:
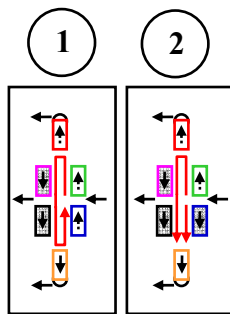
These flow patterns require $X_{\Delta 2}$ to be placed in regions 1 or 4 and $X_{\Delta 4}$ to be placed in regions 4 or 5. This makes intuitive sense from a component net-molar flow perspective. Δ is negative in CS 2 and CS 4 for these flow patterns (i.e. net flow down the CS). If $X_{\Delta 2}$ is in either region 1 or 4, the heavy component value of $X_{\Delta 2}$ is positive, hence $\Delta_2 X_{\Delta 2\text{-}2}$ is negative and the heavy component moves down the column section.

Hence heavy component material directed to the top-half of the column by CS3 is recovered in CS 2 and directed to the bottom-half of the column. If $X_{\Delta 4}$ is in either region 4 or 5, the light component value of $X_{\Delta 4}$ is negative, hence $\Delta_4 X_{\Delta 4\text{-}1}$ is positive and the light component moves up the column section. Light component material directed to the bottom-half of the column by CS 5 is, therefore, recovered in CS 4 and directed to the top-half of the column. Note that, despite this, movement of the light component in CS 2 down and heavy component in CS 4 up are still feasible, but the heavy component flow can only move down in CS 2 and the light component can only move up in CS 4. From a component recovery perspective it would seem logical that the best region of operation of both difference points for these flow patterns would be region 4. This would result in a positive net-molar flow of the light component and negative net-molar flow of the heavy component in both sections. These component net flow alternatives for net flow patterns 1 and 2 are illustrated in Figure 7.17 and Figure 7.18, respectively.

Net flow pattern 3:
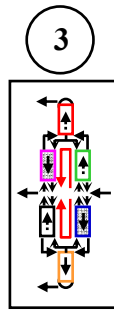
Net flow pattern 3 requires $X_{\Delta 2}$ to be placed in regions 1 or 4 and $X_{\Delta 4}$ to be placed in regions 1 or 6. Placement of the difference points in these regions maintains a negative net flow (down the column section) of the heavy component in CS 2 ($\Delta_2 X_{\Delta 2\text{-}2}$ is negative) and a positive net flow (up the column section) of the light component in CS 4 ($\Delta_4 X_{\Delta 4\text{-}1}$ is positive). This holds with our understanding of these sections.

CS 2 transports intermediate component material to the side-draw and recovers heavy component material from the top half of the column while CS 4 also transports intermediate component material to the side-draw but recovers light component material from the bottom half of the column. The component net flow for net flow pattern 3 is illustrated in Figure 7.19.

Net flow pattern 4&5:
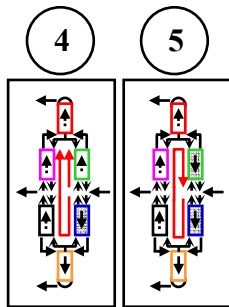
These flow patterns require $X_{\Delta 2}$ to be placed in regions 5 or 6 and $X_{\Delta 4}$ to be placed in regions 1 or 6. This also makes intuitive sense from a component net-molar flow perspective. Δ is positive in CS 2 and CS 4 for these flow patterns (i.e. net flow up the CS). If $X_{\Delta 2}$ is in either region 5 or 6, the heavy component value of $X_{\Delta 2}$ is negative, hence $\Delta_2 X_{\Delta 2\text{-}2}$ is negative and the heavy component moves down the column section.

Once again heavy component material directed to the top-half of the column by CS3 is recovered in CS 2 and directed to the bottom-half of the column. If $X_{\Delta 4}$ is in either region 1 or 6, the light component value of $X_{\Delta 4}$ is positive, hence $\Delta_4 X_{\Delta 4\text{-}1}$ is positive and the light component moves up the column section. Hence light component material directed to the bottom-half of the column by CS 5 is recovered in CS 4 and directed to the top-half of the column. Again, despite these net-molar-flow requirements, movement of the light component in CS 2 down and heavy component in CS 4 up are still feasible. From a component recovery

perspective it would seem logical that the best region of operation of both difference points for these flow patterns would be region 6. This would result in a positive net-molar flow of the light component and negative net-molar flow of the heavy component in both sections. These component net flow alternatives for net flow patterns 4 and 5 are illustrated in Figure 7.20 and Figure 7.21, respectively.

General Net Flow Observations:

- For all net flow patterns the heavy component net flow direction in CS 2 is downwards. This leads to the conclusion that one of the fundamental functions of CS 2 is the recovery of heavy component material directed to the top half of the column. This material is directed either to the side-draw or bottoms product. Analogously, the role of CS 4 is the recovery of light component material directed to the bottom half of the column. Indeed the light component net-molar-flow direction is always up in CS 4. This material is directed either to the side-draw or distillate product.

- Despite the differing bulk material flow direction, flow patterns 1 and 2 exhibit exactly the same component net-molar-flow possibilities, as do flow patterns 4 and 5.

- For all flow patterns the intermediate component is the only species to change direction in CS 3 and 5.

- The potential for the coupled column section difference points to operate in either regions 2 or 5 for net flow patterns 1, 2, 4 and 5 and still result in feasible columns (at the very least from a material balance and topological perspective) is quite startling. The net-molar flow of the intermediate component in regions 2 and 5 is opposite to both the light and heavy components (See Figure 7.17, Figure 7.18, Figure 7.20 and Figure 7.21). This operation is counter-intuitive. One usually expects the net-molar flow to be influenced by the volatilities of the components, that is, one would not expect a column to operate with the light component moving down a CS and the heavy component moving up. These basic preconceived ideas are not contradicted in any of the other feasible difference point regions for net flow patterns 1, 2, 4 & 5. We will investigate this phenomenon in

greater detail later and determine whether or not a full column can, in fact, be designed to operate at these conditions.

7.2.4 Refining Difference Point Selection to Guarantee Feasibility

It should be noted that not all placements of the difference points, for the net flow patterns in the associated regions, result in feasible solutions. CS 2 and 4 profiles can still fail to satisfy matching criterion 1 and 2 respectively - even if they remain within the MBT - if the difference points are not placed appropriately. The liquid CS2 profile can pass between the liquid rectifying profile and the light-intermediate axis (see Figure 7.22), while the CS 4 vapour profile can pass between the vapour stripping profile and the intermediate-heavy axis (see Figure 7.23).

To ensure the intersection of profiles, we need to choose difference points with pinch point curves that cross the rectifying and stripping profiles (see Figure 7.24 and Figure 7.25). This guarantees that if the reflux of the associated column section is high enough, the profiles will intersect.

The bound of feasible $X_{\Delta 2}$ placements can be found by studying the case where the unstable node of the CS 2 trajectory lies on the distillate composition. This is the "last" trajectory satisfying the intersection. If we extend a separation vector from this pinch point, as we did in the previous chapter, we can find the line of all difference points producing this node (see Figure 7.26). This construction can be used to determine the line of difference points because the separation and mixing vectors are collinear at the node.

A similar construction can be performed to determine the bound of $X_{\Delta 4}$ placements (see Figure 7.27). This construction is only really necessary when the specified products are not at all sharp i.e. the distillate contains large quantities of heavy component material and the bottoms contains large quantities of light component material. In this case the separation vector boundary will lie far from

the axes. However, for relatively sharp splits the $X_{\Delta 2}$ and $X_{\Delta 4}$ bounds lie very close to the light-intermediate and intermediate-heavy axes respectively. For design we need only track the movement of the difference points across these axes.

7.3 Feasible Product Composition Selection

The discussion of difference point placement highlights an obvious issue that we have not yet addressed. That is the placement of X_S. As sharp split constraints are lifted from the product specifications complexities are added to the design process that include not only difference point selection but product composition selection as well. We are not free to specify these independently, even if we determine the feed composition from the product compositions. If the distillate or bottoms products are not sharp, there are restrictions on the selection of the side-draw composition. These restrictions occur because of the potential for profiles originating from X_S to bypass the rectifying or stripping profiles in the same way discussed above (*section 7.2.4*). This is illustrated in Figure 7.22 and Figure 7.23.

The issue is easily resolved if we apply the same reasoning applied for difference point selection above (*section 7.2.4*) i.e. the last CS 2 trajectory that guarantees intersection with the rectifying profile will terminate at an unstable node situated on the distillate composition and the last CS 4 trajectory that guarantees intersection with the rectifying profile will terminate at a stable node situated on the bottoms composition.

If we set $X_S=X_{\Delta 2}=X_{\Delta 4}$, then X_S is a difference point and exactly the same logic in generating boundaries of possible side-draw composition can be applied – that is extend separation vectors from the nodes to find lines of possible placement.

However, if $X_S{\neq}X_{\Delta 2}{\neq}X_{\Delta 4}$, then X_S is not a difference point. In this case the separation vector boundaries do not apply. The separation vector boundaries only apply for difference point placement. To ensure feasibility, for this scenario, X_S

must lie within both TT 2 and TT 4. This allows X_S to sample feasible topology and allows for the satisfaction of matching criterion 3.

To guarantee this we must find TT boundaries A_2 and B_4 that run through the distillate and bottoms compositions, respectively. For constant relative volatility systems this entails evaluating the eigenvectors, of the difference point equation (Equation 6.1), at the two nodes and extending lines along the eigenvector directions associated with these TT boundaries (eigenvector point along the boundaries of TTs for constant relative volatility systems). See Figure 7.28. Because we require vapour composition matching at the node on $X_{\Delta 6}$, we make use of the eigenvectors of the differential equations which have separation vectors expressed in terms of the vapour composition i.e. $S = (X^*(Y) - Y)$. See Figure 7.29.
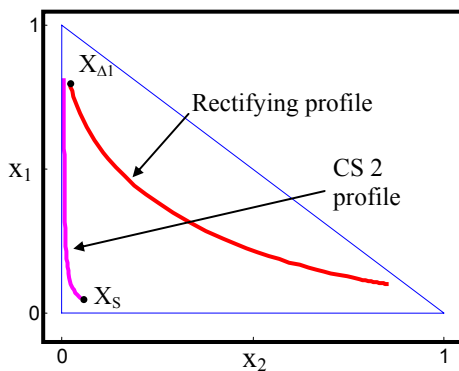
Figure 7.22: CS 2 trajectory bypassing rectifying profile – matching criterion 1 not satisfied
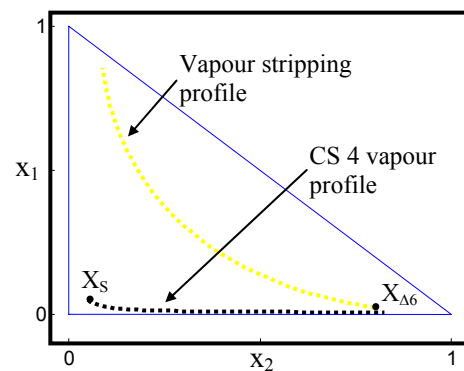
Figure 7.23: CS 4 trajectory bypassing stripping profile – matching criterion 2 not satisfied
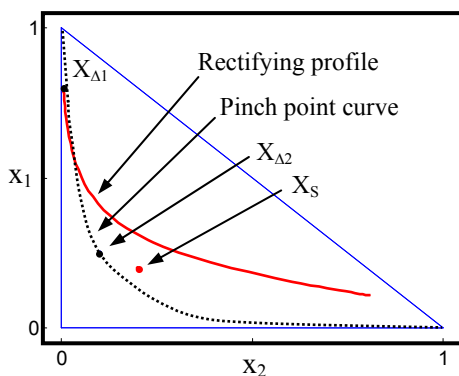
Figure 7.24: $X_{\Delta 2}$ (region 1) pinch point curve intersecting rectifying profile
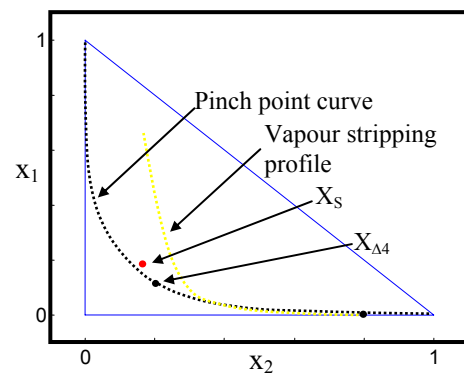
Figure 7.25: $X_{\Delta 4}$ (region 1) pinch point curve intersecting vapour stripping profile
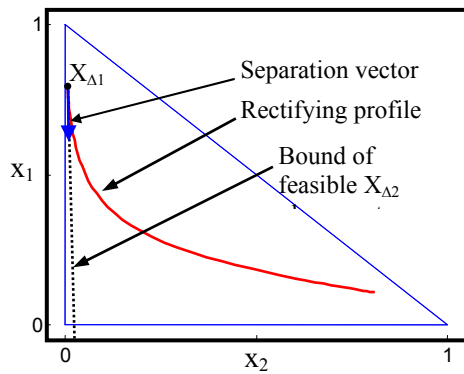
Figure 7.26: Separation vector at distillate composition defining X$_{\Delta 2}$ placement bound
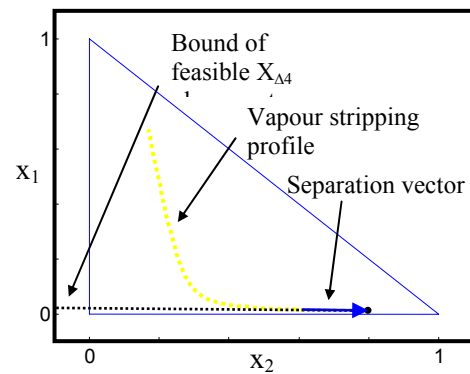
Figure 7.27: Separation vector at bottoms composition defining X$_{\Delta 4}$ placement
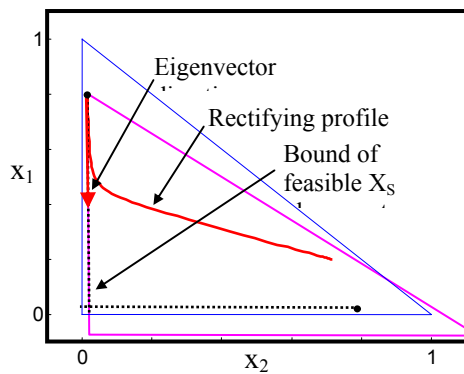
Figure 7.28: Eigenvector at distillate composition defining X$_S$ placement bound
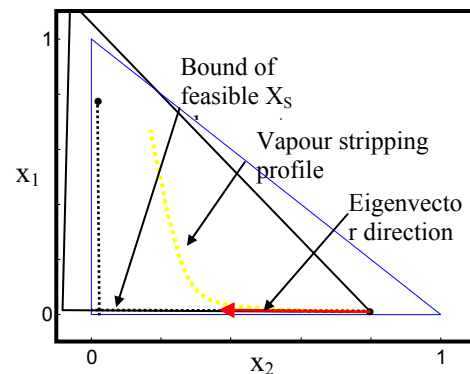
Figure 7.29: Eigenvector at bottoms composition defining X$_S$ placement bound

7.4 Constructing Feasible Split Ratio Regions

7.4.1 Feasible Regions for Different Net Flow Patterns

In general, each net flow pattern requires different placement of the difference points. We use the term "in general" here because feasible columns can sometimes be produced for net flow patterns operating with qualitatively sub-optimal difference points. This arises from the potential of operating profiles, which pinch outside the MBT, to satisfy the matching criteria before leaving physically relevant composition space. The possibility of this phenomenon occurring becomes less and less likely as the distillate and bottoms product specifications are made "less" sharp. *As a result, feasible regions generated for a*

particular difference point set will only be considered valid for the corresponding net flow pattern. Hence we will assume that the zero net flow lines (which separate split ratio regions resulting in different net flow patterns) represent potential boundaries of the feasible region in split ratio space.

7.4.2 Sharp Distillate and Bottoms Specifications, Non-Sharp Side-Draw Specification

To construct feasible regions we must assign actual values to one of the coupled column section difference points. We will continue our policy of placing $X_{\Delta 2}$ ahead of $X_{\Delta 4}$. This is a completely arbitrary policy. $X_{\Delta 4}$ values can be calculated after the selection of an operating split ratio pair.

Once a value for $X_{\Delta 2}$ has been specified, we can proceed to constructing the feasible split ratio region. To simplify our task we will relax the sharp-split specification on each product composition in turn. Let us begin by considering the case where we have a sharp-split on the distillate and bottoms specifications, but a non-sharp side-draw specification. This greatly simplifies our task because in this case, as in the sharp-split case, the CS 1 and CS 6 composition profiles run along the boundaries of their respective TTs.

7.4.2.1 Net flow Pattern 1, 2, 4 and 5: $X_{\Delta 2} = X_{\Delta 4} = X_S$

From Table 7.1 and Table 7.3 we can see that placing $X_{\Delta 2}$ and $X_{\Delta 4}$ in difference point region 1, for exists for net flow patterns 1, 2, 4 and 5, does not result in feasible separations. Hence no feasible split ratio region exists for net flow patterns 1, 2, 4 and 5 for this difference point specification.

7.4.2.2 Net flow Pattern 3: $X_{\Delta 2} = X_{\Delta 4} = X_S$

If $X_{\Delta 2}$ and $X_{\Delta 4}$ are placed at the side-draw composition we can construct the minimum CS 2 and CS 4 reflux boundaries as before (for sharp-splits). When TT boundary C_2 borders boundary B_1, CS 2 is at its minimum reflux. Similarly, when vapour TT boundary C_4 borders vapour boundary A_6 CS 4 is at its minimum reflux. The $R_{\Delta 2MIN}$ and $R_{\Delta 4MIN}$ boundaries are unaffected by the non-sharp side-draw specification. That is to say, they are qualitatively the same as their sharp-split equivalents.

The eigenvector boundaries are slightly affected by non-sharp side-draw specifications, however. When the specification was sharp, the CS 3 and CS 5 profiles ran along the boundaries of their respective TTs. This resulted from the fact that the CS 1 and CS 2 trajectories intersected, effectively, on the light-intermediate axis (see Figure 6.16a and Figure 6.18a) and the CS 4 and CS 6 trajectories intersected, effectively, on the intermediate-heavy axis (see Figure 6.17a and Figure 6.19a)– one boundary of each of the TTs lies effectively on an axis for sharp product specifications. With the non-sharp side-draw specification this is no longer the case. Both sets of trajectories intersect "away" from the axes and only TT 1 and TT 6 will have a boundary effectively on an axis. See Figure 7.31.

It can be shown that only transformed region 4, of CPM 3, and transformed region 6, of CPM 5, will ever be sampled in satisfying matching criteria 1 and 2, respectively, for these product specifications (See Figure 7.37, Figure 7.38 and Appendix H for details). Consequently, CS 3 and CS 5 trajectories originating from the respective intersections will always intersect if the TTs overlap (see Figure 7.31 and Figure 7.32). However, they can also lie "away" from their respective TTs and still intersect. Because of this we can reach a situation where the operating profiles intersect even when the TTs do not overlap. Figure 7.33 and Figure 7.34 illustrate feasible operting profiles when TT 3 and TT 5 do not overlap across collinearity line 1 (CLL1). Figure 7.35 and Figure 7.36 illustrate feasible operting profiles when TT 3 and TT 5 do not overlap across collinearity

line 2 (CLL2). *Hence the eigenvector boundaries no longer represent the limit of possible operation in split ratio space.*

The feasible region will always "grow" but never "shrink" over the eigenvector boundaries when the side-draw specification is not sharp. This is due to the potential feasibility of the non-overlapping TT3 and TT5. This "growth" has zero size where the eigenvector boundaries (PEB1 and PEB2) intersect. At this point both CS 3 and CS 5 must pinch i.e. the profile and the TT have to coincide; hence there will be zero growth here. The "growth" increases in size along the length of both eigenvector boundaries until they reach the $R_{\Delta 2MIN}$ and $R_{\Delta 4MIN}$ reflux boundaries. See Figure 7.30.
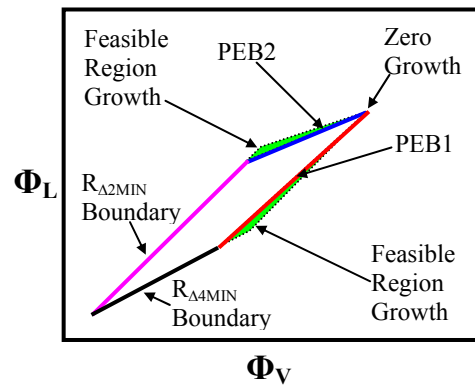
Figure 7.30: Feasible region growth adjacent to PEB1 and PEB2 for non-sharp side-draw specifications

The overall growth of the feasible region is negligible in comparison to the size of the region incorporated by the original four (sharp-split) boundaries and, for design purposes, can generally be neglected. Also all split ratios chosen within the original boundaries are still feasible. Below, in Figure 7.39 and Figure 7.40, are the complete feasible regions and original boundaries for two systems with differing relative volatilities. It is clear from these examples that the region "growth" is very small and irrespective of the relative volatility can, generally, be neglected. Notice also that the sharp-split boundaries have crossed the $\Delta_2=0$ and $\Delta_4=0$ net flow lines, which now represent new boundaries of the feasible region.

Note: Feasible region growth was determined by simulation. Split ratios were chosen and solutions for each column section were generated. CS 1 and CS 6

solutions were generated from the distillate and bottoms products, respectively. CS 2 and CS 4 solutions were generated from the side-draw composition. If these solutions satisfied matching criteria 1 and 2, respectively, these intersection points were used as starting points (initial conditions) to generate solutions for CS 3 and CS 5. If these profiles intersected (satisfied composition matching criterion 4) the overall solution was deemed feasible and hence the split ratios chosen were deemed feasible.
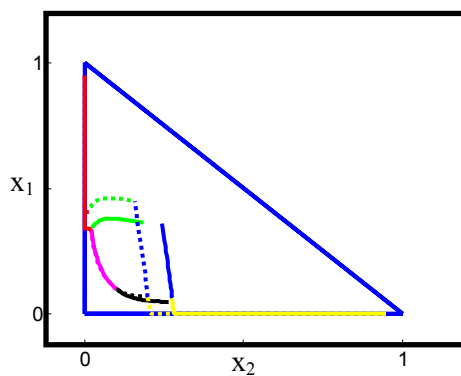
Figure 7.31: Feasible composition profiles for non-sharp side-draw specifications when TT 3 and TT 5 overlap
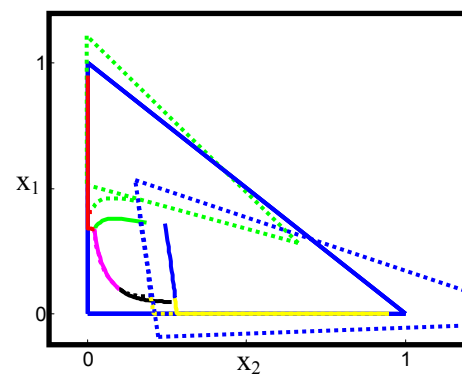
Figure 7.32: Feasible TTs for non-sharp side-draw specifications when TT 3 and TT 5 overlap – with TT 3 and TT 5
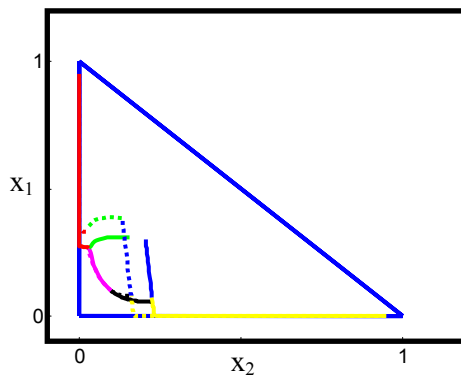
Figure 7.33: Feasible composition profiles for non-sharp side-draw specifications when TT 3 and TT 5 do not overlap across CLL1
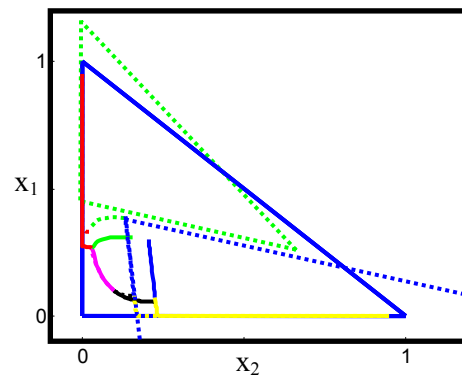
Figure 7.34: Feasible TTs for non-sharp side-draw specifications when TT 3 and TT 5 do not overlap across CLL1
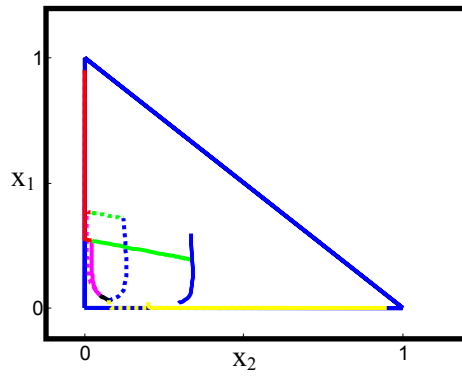
Figure 7.35: Feasible composition profiles for non-sharp side-draw specifications when TT 3 and TT 5 do not overlap across CLL2
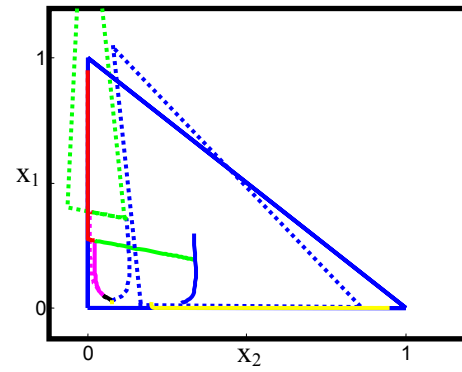
Figure 7.36: Feasible TTs for non-sharp side-draw specifications when TT 3 and TT 5 do not overlap across CLL2
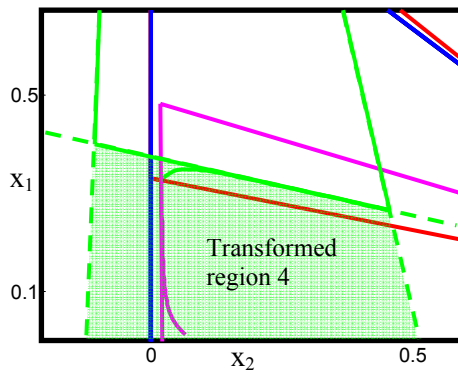
Figure 7.37: Matching criterion 1 satisfied in transformed region 4 of CPM 3
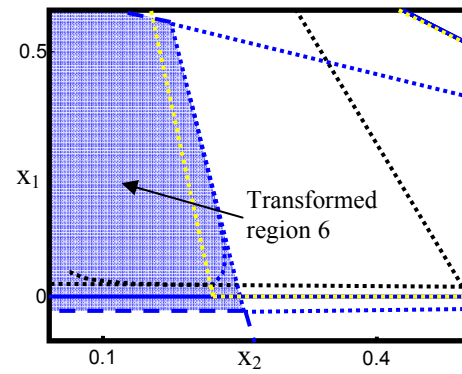
Figure 7.38: Matching criterion 2 satisfied in transformed region 6 of CPM 5
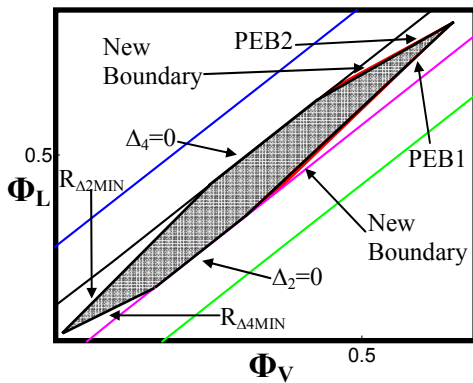
Alpha	[2, 1, 1.5]
Reflux Ratio	10
Feed	[1/3, 1/3, 1/3]
Side-Draw	[0.05, 0.05, 0.90]
Distillate	[0.95, 0, 0.05]
Bottoms	[0, 0.95, 0.05]

Figure 7.39: Feasible region for $X_{\Delta 2} = X_{\Delta 4} = X_S$ with growth adjacent to PEB 1 and 2 and new boundaries $\Delta_2 = 0$ and $\Delta_4 = 0$
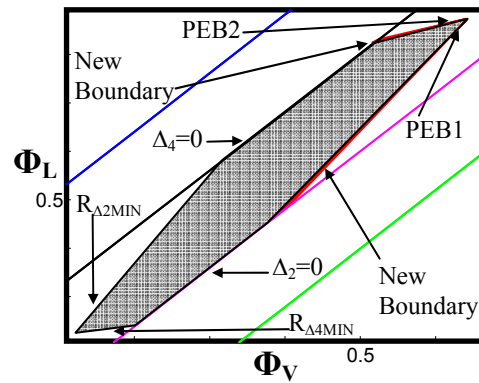
Alpha	[5, 1, 3]
Reflux Ratio	5
Feed	[1/3, 1/3, 1/3]
Side-Draw	[0.05, 0.05, 0.90]
Distillate	[0.95, 0, 0.05]
Bottoms	[0, 0.95, 0.05]

Figure 7.40: Feasible region for $X_{\Delta 2} = X_{\Delta 4} = X_S$ with growth adjacent to PEB 1 and 2 and new boundaries $\Delta_2 = 0$ and $\Delta_4 = 0$

7.4.2.3   Net flow Pattern 3: $X_{\Delta 2} \neq X_{\Delta 4} \neq X_S$

To generate the feasible region for net flow pattern 3, when $X_{\Delta 2} \neq X_{\Delta 4} \neq X_S$, the results from Table 7.2 indicate that we are required to place $X_{\Delta 2}$ in region 1 or 4 and $X_{\Delta 4}$ in region 1 or 6. The feasible region itself is, however, defined after the specification of one of these variables. Again we will arbitrarily choose to specify $X_{\Delta 2}$. $X_{\Delta 4}$ will therefore be a function of the values of $X_{\Delta 2}$, X_S and the two split ratios. This means that the value of $X_{\Delta 4}$ will not be optimal for all values of the split ratios but will vary along a material balance line through $X_{\Delta 2}$ and X_S. Depending on the orientation of this material balance line, $X_{\Delta 4}$ can, potentially, enter a difference point region other than 1 or 6, most obviously, by crossing the intermediate-heavy axis into either region 4 or 5.

$\underline{X_{\Delta 4\text{-}i} = 0 \text{ Boundaries:}}$

To prevent this from happening we can generate an $X_{\Delta 4}$ boundary in split ratio space that simply represents the line across which the light component net flow changes sign. These boundaries are the constant $X_{\Delta\text{-}i}$ lines discussed in the previous chapter (see Equation 6.20). Two forms of the constant $X_{\Delta 4\text{-}i}$ lines are

seen below (Equation 7.6 and Equation 7.7). Equation 7.6 is independent of the overall net flow in the CS. Equation 7.7, however, allows us to better understand the influence of the net-molar flow of individual components. When $X_{\Delta 4\text{-}i}=0$ both equations are exactly equivalent.

$$\Phi_L = \frac{(R_1+1)}{R_1}\left(\frac{X_{\Delta 2i} - X_{\Delta 4i}}{X_{\Delta 2i} - X_{\Delta 4i}}\right)\Phi_V + \frac{S}{\Delta_1 R_1}\left(\frac{X_{Si} - X_{\Delta 4i}}{X_{\Delta 2i} - X_{\Delta 4i}}\right) \tag{7.6}$$

or equivalently

$$\Phi_L = \frac{(R_{\Delta 1}+1)}{R_{\Delta 1}}\Phi_V + \frac{S}{\Delta_1 R_{\Delta 1}}\left(\frac{X_{Si}}{X_{\Delta 2i}}\right) - \frac{(\Delta_4 X_{\Delta 4i})}{\Delta_1 R_{\Delta 1} X_{\Delta 2i}} \tag{7.7}$$

If $X_{\Delta 2}$ is in difference point region 1 and we wish to prevent $X_{\Delta 4}$ from entering difference point region 4, we can generate an $X_{\Delta 4\text{-}1}=0$ boundary. One such boundary is seen in Figure 7.41. By analysing Equation 7.7 we can determine whether the area above or below this line corresponds to positive $X_{\Delta 4\text{-}1}$ values. For net flow pattern 3, Δ_4 is positive and $X_{\Delta 4\text{-}1}$ is required to be positive. All other variables of the final term in Equation 7.7 are also positive. These values result in the Φ_L-intercept of Equation 7.7 being smaller than the intercept for the case where $X_{\Delta 4\text{-}1}=0$, hence all values below this boundary represent values of $X_{\Delta 4\text{-}1}>0$.
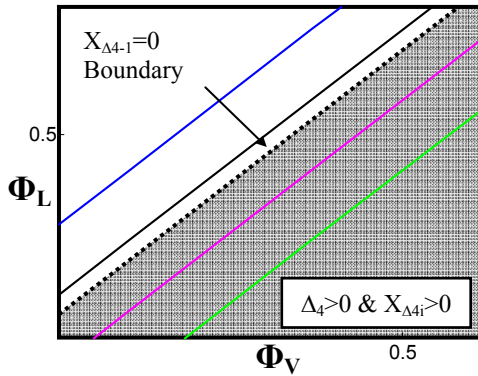
Figure 7.41: $X_{\Delta 4\text{-}1} = 0$ split ratio boundary
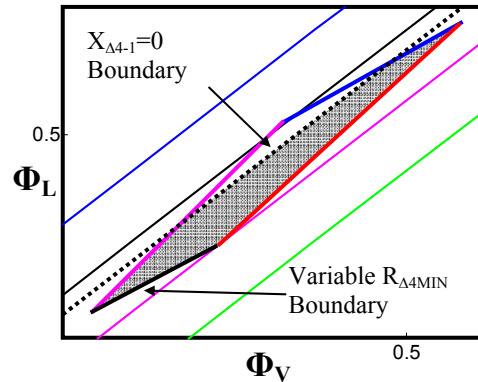
Figure 7.42: $X_{\Delta 4\text{-}1} = 0$ and variable $R_{\Delta 4MIN}$ split ratio boundaries for net flow pattern 3 and $X_{\Delta 2} \neq X_{\Delta 4} \neq X_S$

Split ratios chosen above this line yield negative light component net flows for CS 4. Conversely those chosen below the line yield positive CS 4 light component net flows. As we require (for feasibility) that light component flows are positive in this CS all split ratios, chosen above the $X_{\Delta 4\text{-}1}=0$ boundary, are infeasible. This

specification reduces the size of the region defined by the original four boundaries (R2Min, R4Min, PEB1, PEB2).

This is not always the case. For lower reflux ratios than the one used to generate the above example, the $X_{\Delta4-1}=0$ boundary can lie outside the original feasible region. Also if $X_{\Delta2-1} < X_{S-1}$, $X_{\Delta4}$ cannot cross the light-intermediate axis and the boundary therefore does not exist.

Variable $R_{\Delta4MIN}$ Boundary:

For this case where the $X_{\Delta4}$ value is variable, the constant reflux $R_{\Delta4MIN}$ boundary is not defined. Instead a minimum reflux value is defined for each value of $X_{\Delta4}$. The procedure for determining these minimum reflux values is the same as for the constant reflux case. The calculated minimum reflux values can then be mapped to split ratio space. The new boundary, thus formed, is not necessarily straight and depends on the shape of the CS 6 trajectories – i.e. each point on the trajectory corresponds to a minimum CS 4 reflux and $X_{\Delta4}$ value (see Figure 7.42).

7.4.2.4   Net Flow Pattern 1 & 2: $X_{\Delta2} \neq X_{\Delta4} \neq X_S$

For net flow pattern 1 & 2 feasibility we are required to place $X_{\Delta2}$ in difference point regions 1 or 4 and $X_{\Delta4}$ in difference point regions 4 or 5. The value of $X_{\Delta4}$ is again variable and lies on a straight line through X_S and $X_{\Delta2}$. If $X_{\Delta2}$ is placed in difference point region 4 there is no possibility that $X_{\Delta4}$ can shift into regions 1 or 6 and the $X_{\Delta4-1}=0$ boundary is not required (see Figure 7.43). If, however, $X_{\Delta2}$ is placed in region 1, $X_{\Delta4}$ is able to cross the intermediate-heavy axis for certain choices of Φ_V and Φ_L. In this case we are required to generate the $X_{\Delta4-1}=0$ boundary to remove infeasible choices of Φ_V and Φ_L. The light component net-molar-flow requirement is positive in CS 4 for all net flow patterns. Consulting Equation 7.7 we notice that this again only results in feasible $\Delta_4X_{\Delta4-1}$ values below the $X_{\Delta4-1}=0$ boundary (see Figure 7.44). The lower bound of feasibility, for these flow patterns is the $\Delta_4=0$.
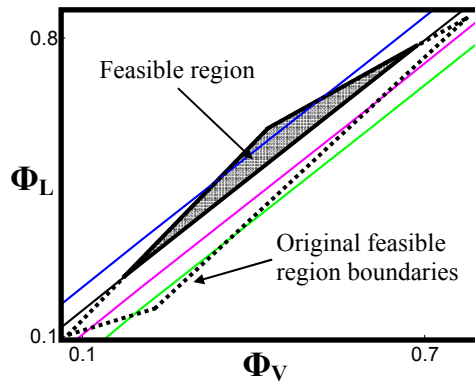
Figure 7.43: Feasible region for net flow patterns 1 and 2 with $X_{\Delta2\text{-}1} < 0$
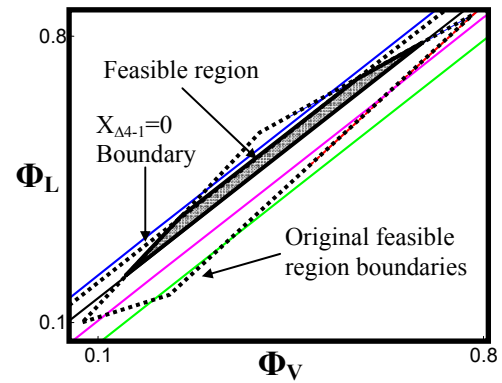
Figure 7.44: Feasible region for net flow patterns 1 and 2 with $X_{\Delta2\text{-}1} > 0$

We notice that, in the case of Figure 7.44, a large portion of the feasible region is removed by the presence of the $X_{\Delta4\text{-}1}=0$ boundary. For control purposes we would obviously like the feasible region to be as large as possible. The boundary presence is therefore undesirable. From this perspective, placing $X_{\Delta2}$ in region 4 ahead of region 1 seems preferable. The $R_{\Delta2MIN}$ required increases as $X_{\Delta2}$ is shifted away from the rectifying profile, however. This also has the effect of reducing the feasible region area. A trade-off between these two effects is required. $X_{\Delta2}$ should be placed as close to the rectifying profile as possible without introducing the $X_{\Delta4i}=0$ boundary into the feasible region. Consideration should also be made for the $R_{\Delta4MIN}$ values required to satisfy matching criterion 2.

7.4.2.5   Net Flow Pattern 4 & 5: $X_{\Delta2} \neq X_{\Delta4} \neq X_S$

For net flow pattern 4 & 5 feasibility we are required to place $X_{\Delta2}$ in difference point regions 5 or 6 and $X_{\Delta4}$ in difference point regions 1 or 6. We must again be aware of the potential movement of $X_{\Delta4}$ across the intermediate-heavy axis. For these flow patterns $X_{\Delta4}$ must lie between $X_{\Delta2}$ and X_S, therefore $X_{\Delta4}$ can only cross the intermediate-heavy axis if $X_{\Delta2}$ is in region 5. In this case $X_{\Delta2\text{-}1}<0$ but $\Delta_4>0$ and we require $X_{\Delta4\text{-}1}>0$, therefore the final term of Equation 7.7 is positive and all feasible values lie above the $X_{\Delta4i}=0$ boundary in split ratio space (see Figure 7.45).
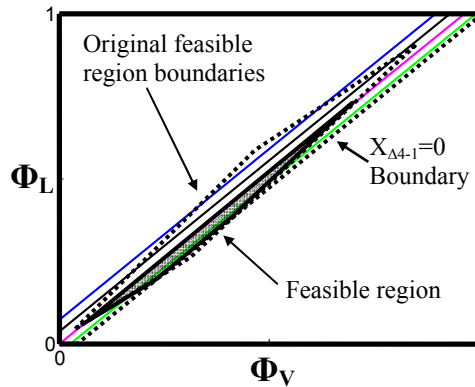
**Figure 7.45: Feasible region for net flow patterns 4
and 5 with $X_{\Delta 2\text{-}1} < 0$**

7.4.2.6   Parameter Effects on the Feasible Region "Growth"

<u>Side-Draw Composition:</u>

The size of the additional area of the feasible region is a strong function of the side-draw composition. As the side-draw composition tends to pure intermediate, the additional area tends to zero. As the impurities in the side-draw are increased the additional area increases. The additional feasible region adjacent to each of the eigenvector boundaries can be influenced independently by manipulating these impurities in the side-draw composition. If the heavy component composition, in this stream, is close to zero but the light component composition is not, the feasible region will only exhibit "growth" adjacent to PEB2 (see 6.42). This occurs because at these conditions composition matching criterion 1 occurs effectively on the light-intermediate axis and therefore the CS 3 trajectory runs along the boundary of TT 3 – hence only CS 5 can sample topology "far" from its TT (see Figure 7.46). Similarly, if the (side-draw) light component composition is close to zero but the heavy component is not, the feasible region will only exhibit "growth" adjacent to PEB1 (see Figure 7.48 and Figure 7.49).

Reflux Ratio:

The size of the additional area of the feasible region is also a function of the reflux ratio. As the reflux ratio is increased the size of the region increases. This is due to the fact that intersection, of CS 3 and CS 5 trajectories "away" from their respective TTs, becomes easier at higher reflux.
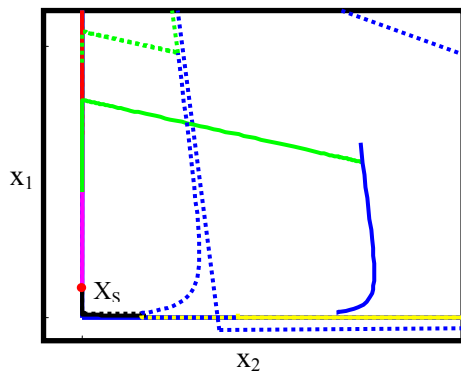
Figure 7.46: Feasible CS 3 and CS 5 Trajectories for non-Overlapping TT 3 and TT 5 in the CLL2 direction for Xs = [0.05;1e-10]
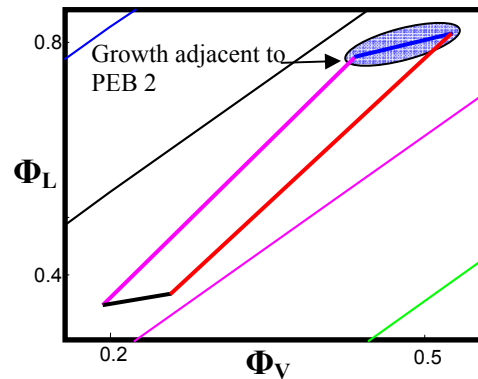
Figure 7.47: Growth occurs adjacent to PEB2 for significant light but infinitesimal heavy component impurities in the side-draw
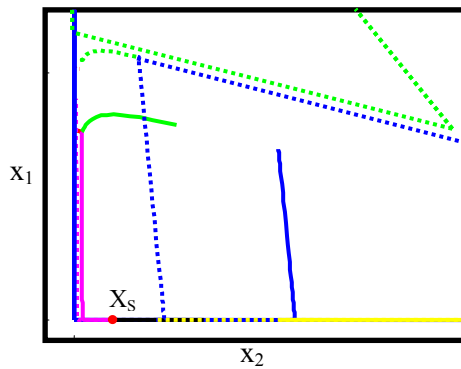
Figure 7.48: Feasible CS 3 and CS 5 Trajectories for non-Overlapping TT 3 and TT 5 in the CLL1 direction for Xs = [1e-10 ;0.05]
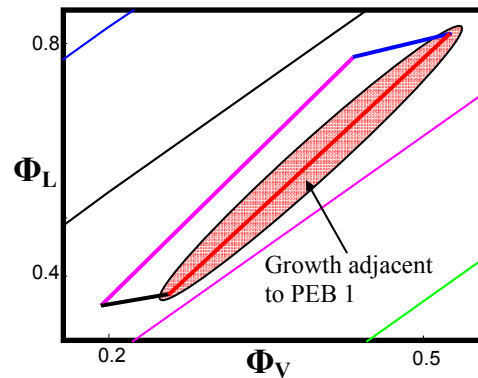
Figure 7.49: Growth occurs adjacent to PEB1 for significant heavy but infinitesimal light component impurities in the side-draw

7.4.3   Sharp Bottoms Specification, Non-Sharp Distillate and Side-Draw Specifications

Let us now consider the case where we have a sharp-split bottoms specification, but non-sharp distillate and side-draw specifications. The effects due to these product specifications are common to all net flow patterns and feasible difference point placements. Note that in light of the discussion on side-draw composition selection above (*section 7.3*), a small heavy component impurity flow is required in the side-draw stream in order to satisfy matching criterion 1. As a result the boundaries and other features present, in the non-sharp side-draw feasible region, discussed above (*section 7.4.2*), will be present at these conditions too when applicable.

At these specifications the CS 6 composition profiles run along the boundaries of their respective TTs. The $R_{\Delta 4MIN}$ feasible region boundary can therefore be constructed in exactly the same way as for sharp-splits and non-sharp side-draw specifications. The $R_{\Delta 2MIN}$ feasible region boundary, however, is affected by the introduction of heavy component material in the distillate product. This occurs because the rectifying profile no longer runs along the boundary of TT 1, but lies within it. CS 2 now requires a higher reflux ratio in order to satisfy composition matching criterion 1 (see Figure 7.50). This increase in R_{2Min}, compared to the sharp-split case, results in the associated split ratio boundary shifting "inside" the sharp-split $R_{\Delta 2MIN}$ boundary and consequently removing an area of split ratios which were previously feasible. This is clearly evident in Figure 7.57 and Figure 7.59. Both show a marked decrease in the size of the feasible region. This effect is very significant if the light and intermediate component relative volatilities are close and large, but becomes smaller when the relative volatilities are evenly spaced. Similar intermediate and heavy component relative volatilities which are dissimilar, or "far", from the light component relative volatility result in a negligible decrease in the feasible region area (see Figure 7.61).

The fact that matching criterion 1 is satisfied within TT 1 creates the potential for CS 3 trajectories to originate within TR 1 of CPM 3 (see Figure 7.53). As a result,

matching criterion 4 need not be satisfied when boundaries B_3 and C_5 are collinear (see Figure 7.52) – i.e. PEB 1 no longer represents a boundary of feasible split ratios. The feasible region actually "shrinks" and the new boundary lies within the sharp-split boundaries close to PEB 1 (see Figure 7.57, Figure 7.59 and Figure 7.61). The degree of "shrinkage" increases from zero, at the intersection of PEB 1 and PEB 2, along PEB 1 until it reaches the $R_{\Delta4MIN}$ boundary. The intersection of PEB 1 and PEB 2 always represents a feasible solution because the TT 3 stable node and TT 5 unstable node coincide at this split ratio – i.e. the CS 3 composition profile is exactly on TT 3.

The degree of "shrinkage" of the feasible region along PEB 1 follows the same pattern as that discussed for $R_{\Delta2MIN}$ with respect to various relative volatilities. This is evident in Figure 7.57 and Figure 7.59 where larger decreases in feasible region area due to changes in $R_{\Delta2MIN}$ correspond to larger decreases due to "shrinkage" across PEB 1. The phenomenon is, obviously, also affected by the heavy component composition of the distillate. The sharper the product specification, the smaller the effect and conversely the less sharp the distillate specification the greater the effect.

It should be noted that this effect is in competition with the "growth" of the feasible region (due to impurities in the side-draw) discussed above (*section 7.4.2*). In some instances, despite the non-sharp distillate specification there is no "shrinkage" at all but an extension to the region across PEB 1 as the side-draw effects take precedence. It should also be noted that PEB 2 is unaffected at these conditions except by the non-sharp side-draw specification.

7.4.4   Sharp Distillate Specification, Non-Sharp Bottoms and Side-Draw Specifications

The effects due to these product specifications are also common to all net flow patterns and feasible difference point placements. In this case a small light component impurity flow is required in the side-draw stream in order to satisfy

matching criterion 2. The boundaries and other features present, in the non-sharp side-draw feasible region, discussed above (*section 7.4.2*), will, therefore, be present at these conditions too when applicable.

If we have a sharp distillate specification, but non-sharp bottoms and side-draw specifications the CS 1 composition profiles run along the boundaries of their respective TTs but the stripping profiles do not. The $R_{\Delta2MIN}$ feasible region boundary, in this case, can be constructed in the same way as for sharp-splits and non-sharp side-draw specifications. The $R_{\Delta4MIN}$ feasible region boundary, however, is affected by the introduction of light component material in the bottoms product. The reason for this is that the vapour stripping profile no longer runs along the boundary of vapour TT 6, but lies within it. CS 4 now requires a higher reflux ratio in order to satisfy composition matching criterion 2 (see Figure 7.51). The larger R_{4Min}, for these specifications, compared to that required in the sharp-split case, results in a shift of the $R_{\Delta4MIN}$ split ratio boundary into the feasible area defined for sharp-splits consequently removing a portion of previously feasible split ratios. This is clearly evident in Figure 7.58 and Figure 7.60. All show a decrease in the area of the feasible region on the same scale seen for the non-sharp distillate $R_{\Delta2MIN}$ boundary. The trend followed in this case is opposite to that shown for R_{2Min}. The effect is significant if the heavy and intermediate component relative volatilities are close and small, but becomes less so when the relative volatilities are evenly spaced. Similar intermediate and light component relative volatilities which are dissimilar, or "far", from the heavy component relative volatility result in a small decrease in the feasible region area (see Figure 7.56). This logic and the effects on $R_{\Delta4MIN}$ hold if $X_{\Delta4}$ is variable or constant, so feasible regions constructed for $X_{\Delta2} \neq X_{\Delta4} \neq X_S$ will all exhibit a decrease in area compared to the sharp-split case.

For non-sharp bottoms specifications, the fact that matching criterion 2 is satisfied within vapour TT 6 creates the potential for CS 5 trajectories to originate within TR 1 of vapour CPM 5 (see Figure 7.55). As a result, matching criterion 4 need not be satisfied when boundaries B_3 and C_5 are collinear (see Figure 7.54) – i.e. as

in the case of PEB 1, for non-sharp distillate specifications, PEB 2 now no longer represents a boundary of feasible split ratios. In this case the feasible region also "shrinks" and the new boundary, again, lies within the sharp-split boundaries but now close to PEB 2 (see Figure 7.56, Figure 7.58 and Figure 7.60). The removed region of feasibility also has zero area at the intersection of PEB 1 and PEB 2 and increases along PEB 2 until it reaches the $R_{\Delta 2MIN}$ boundary.

In this case, there is also a common trend followed by the infeasible region adjacent to PEB 2 and the removed area of feasibility adjacent to the $R_{\Delta 4MIN}$ boundary with respect to the relative volatilities. Figure 7.58 and Figure 7.60 illustrate this, where larger decreases in feasible region area due to changes in $R_{\Delta 4MIN}$ correspond to larger decreases due to "shrinkage" across PEB 2. As in the case of heavy component impurities in the distillate, this phenomenon is, obviously, also affected by impurities (light component) in the bottoms. The sharper the product specification, the smaller the effect and conversely the less sharp the specification the greater the effect.

This phenomenon also mirrors the pervious case with respect to its competition with the effect, on the feasible region, due to side-draw impurities. Here in some instances, despite the non-sharp bottoms specification there is no "shrinkage" but an extension to the region across PEB 2 as the side-draw effects take precedence. Also, it should be noted that PEB 1 is unaffected at these conditions except by the non-sharp side-draw specification as PEB 2 was unaffected by the non-sharp distillate specification.
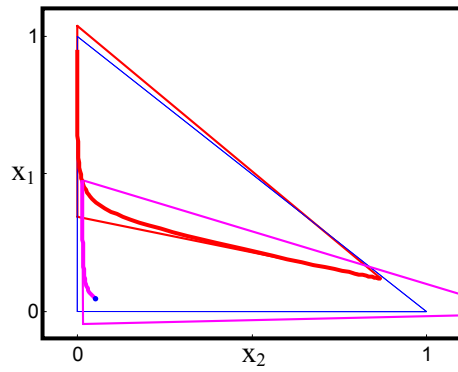
Figure 7.50: CS 2 at minimum reflux for non-sharp distillate specification
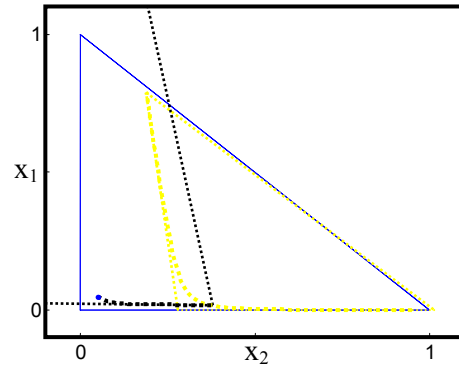
Figure 7.51: CS 4 at minimum reflux for non-sharp bottoms specification
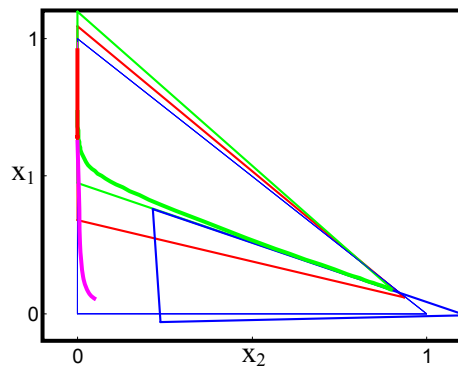
Figure 7.52: Matching criterion 4 not met despite bordering of TT 3 and TT 5. (vapour feed)
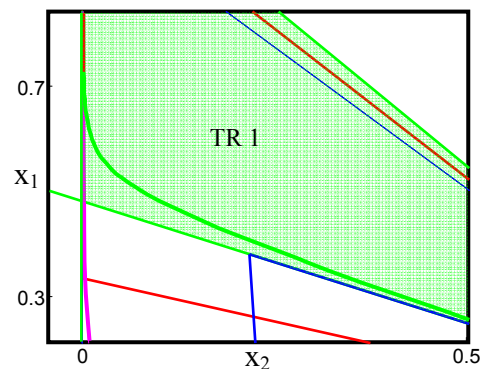
Figure 7.53: CS 3 trajectory originating within TR 1 of CPM 3
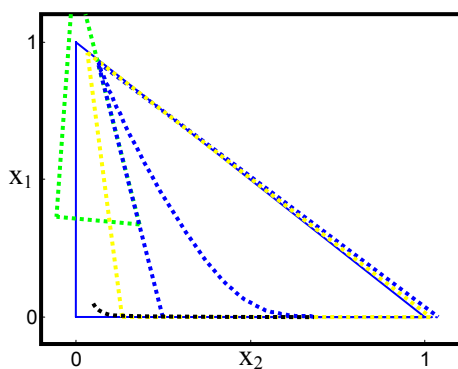
Figure 7.54: Matching criterion 4 not met despite bordering of TT 3 and TT 5.
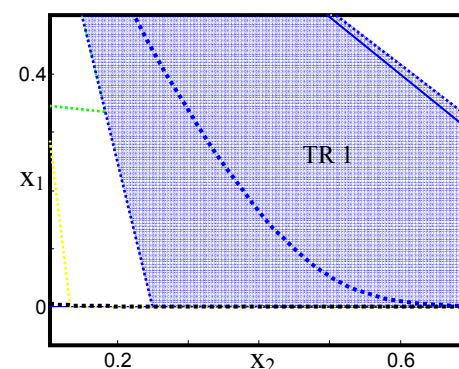
Figure 7.55: CS 5 trajectory originating within TR 1 of CPM 5
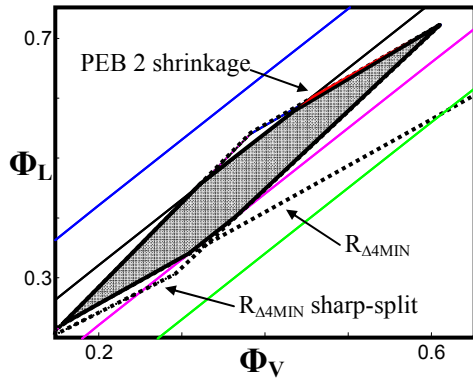
Alpha	[2, 1, 1.5]
Reflux Ratio	10
Feed	[1/3, 1/3, 1/3]
Side-Draw	[0.05, 0.05, 0.90]
Distillate	[0.95, 0, 0.05]
Bottoms	[1e-5, 0.95, 4.999e-2]

Figure 7.56: Feasible region for non-sharp bottoms specifications with shrinkage adjacent to PEB 2
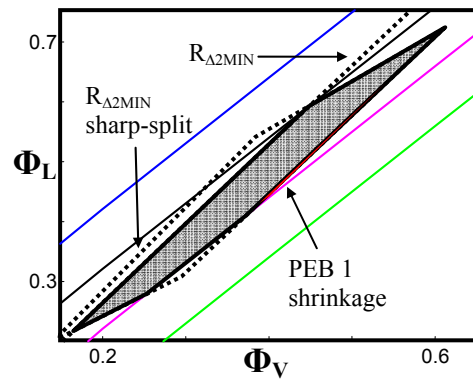
Alpha	[2, 1, 1.5]
Reflux Ratio	10
Feed	[1/3, 1/3, 1/3]
Side-Draw	[0.05, 0.05, 0.90]
Distillate	[0.95, 1e-5, 4.999e-2]
Bottoms	[0, 0.95, 0.05]

Figure 7.57: Feasible region for non-sharp distillate specifications with shrinkage adjacent to PEB 1
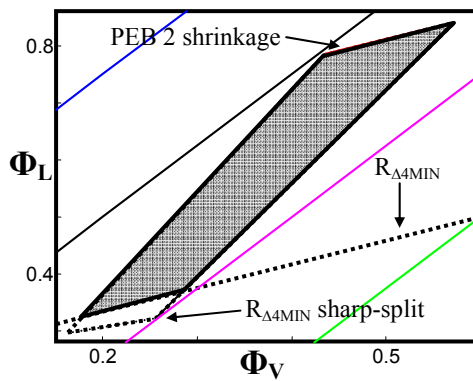
Alpha	[5, 1, 3]
Reflux Ratio	4
Feed	[1/3, 1/3, 1/3]
Side-Draw	[0.05, 0.05, 0.90]
Distillate	[0.95, 0, 0.05]
Bottoms	[1e-5, 0.95, 4.999e-2]

Figure 7.58: Feasible region for non-sharp bottoms specifications with shrinkage adjacent to PEB 2
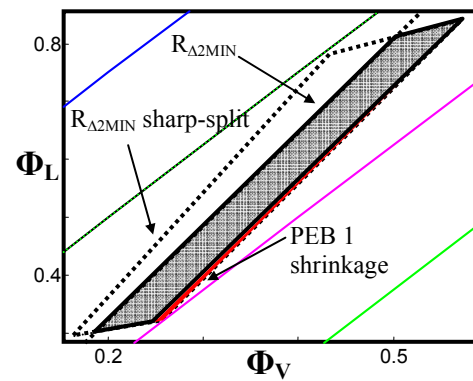
Alpha	[5, 1, 3]
Reflux Ratio	4
Feed	[1/3, 1/3, 1/3]
Side-Draw	[0.05, 0.05, 0.90]
Distillate	[0.95, 1e-5, 4.999e-2]
Bottoms	[0, 0.95, 0.05]

Figure 7.59: Feasible region for non-sharp distillate specifications with shrinkage adjacent to PEB 1
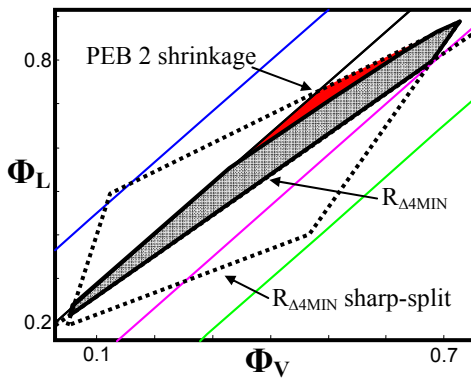
Alpha	[5, 1, 2]
Reflux Ratio	6
Feed	[1/3, 1/3, 1/3]
Side-Draw	[0.05, 0.05, 0.90]
Distillate	[0.95, 0, 0.05]
Bottoms	[1e-6, 0.95, 4.999e-2]

Figure 7.60: Feasible region for non-sharp bottoms specifications with shrinkage adjacent to PEB 2
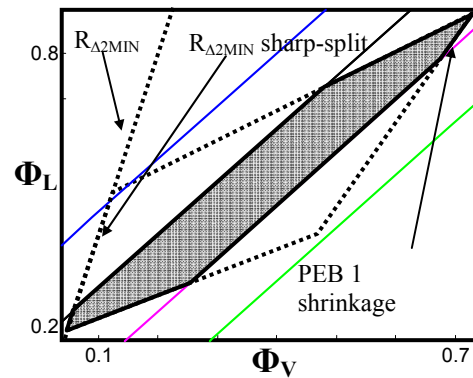
Alpha	[5, 1, 2]
Reflux Ratio	6
Feed	[1/3, 1/3, 1/3]
Side-Draw	[0.05, 0.05, 0.90]
Distillate	[0.95, 1e-5, 4.999e-2]
Bottoms	[0, 0.95, 0.05]

Figure 7.61: Feasible region for non-sharp distillate specifications with shrinkage adjacent to PEB 1

7.5 Optimisation

7.5.1 Optimising Difference Point Placement

We have discussed the regions of placement of the difference points for each column section as well as "separation vector" bounds within these regions, but we have not discussed the selection of actual values. The net-component flow arguments made in the previous chapter are still valid for non-sharp separations, but we need not place $X_{\Delta 2}$ and $X_{\Delta 4}$ at the side-draw composition. Indeed this specification, as we have discussed in the section on difference point placement above (*section 7.2*), is invalid for net flow patterns 1, 2, 4 and 5. What we can say is that the "impurities" in the net flow of CS 2 and 4 should not be large compared to the side-draw composition. This essentially means that $X_{\Delta 2}$ and $X_{\Delta 4}$ should be placed close to X_S in composition space. Despite these arguments and those above (*section 7.2*), a large area of difference point placements result in feasible solutions and we, therefore, still have considerable freedom in our choice. How do we decide which placement is optimal or at least better than others?

One factor on which to base our choice is controllability. Halvorsen and Skogestad (1999) discussed the effects of disturbances on the operating conditions of the column. Disturbances can shift the operating values of the split ratios out of the feasible/ optimality region. This will cause the column to operate off specification. Maximising the area of the feasible region will minimise the effects of disturbances by ensuring that a larger disturbance is required in order to force the operating split ratios out of the region. *We could, therefore, select $X_{\Delta 2}$ and $X_{\Delta 4}$ such that they maximise this area*.

Below, in Figure 7.62 to Figure 7.67, are contour maps of minimum required CS 2 and 4 reflux ratios for a grid of difference point values for net flow pattern 3. $X_{\Delta 2}$ and $X_{\Delta 4}$ were placed at each point in the grid and the minimum CS reflux ratio required for (composition matching) feasibility was determined. The contour maps are produced for set distillate and bottoms compositions at a constant column reflux ratio. The curvature of the contours depends on the sharpness of the product specifications. Sharp product specifications, on average, require lower CS 2 and 4 reflux ratios. These values increase dramatically as "impurities" are increased in the product streams. This is simply due to the fact that non-sharp operating profiles are far from their TTs and hence the CS 2 and 4 profiles have "further" to go in order to satisfy composition matching, hence higher refluxes are required. The dark blue colours represent low refluxes while the dark reds represent high refluxes.

The optimal placement for both $X_{\Delta 2}$ and $X_{\Delta 4}$ appears to be near the upper right hand corner of each contour map (point C in Figure 7.62 to Figure 7.67) for these grids. X_S, however, operates at [0.05;0.05] for these examples, so placement of both difference points at their optimal value is not possible. This is true in general. For sharp product specifications (distillate and bottoms), the placement of $X_{\Delta 2}$ near the light-intermediate axis with as high a light component value as possible (point A in Figure 7.62) and $X_{\Delta 4}$ close to the intermediate-heavy axis with as high a heavy component value as possible (point B in Figure 7.63) allows both CS 2

and 4 to operate at relatively low reflux ratios. This scenario would produce a larger feasible region than if both difference points were set equal to the side-draw composition. Difference points at the side-draw composition sample green contours corresponding to medium value refluxes.

As the sharpness of the product specification is reduced, the previous scenario loses its advantages over specifying the difference points at the side-draw composition. At the conditions of Figure 7.64 and Figure 7.65, both specifications would result in feasible regions of approximately equal size – the CS 2 and 4 reflux ratios sampled are roughly equal in both cases. In this case for simplicity placing the difference points at the side-draw composition would be preferable.

In Figure 7.66 and Figure 7.67, however, the situation has totally changed. Specifying $X_{\Delta 2}$ close to the light-intermediate axis (point A in Figure 7.66) and $X_{\Delta 4}$ close to the intermediate-heavy axis (point B in Figure 7.67) results in very high, required, CS 2 and 4 refluxes. Placement of both variables at the side-draw composition results in reasonable values, but the best placement of the two relative to each other is, in fact, to have $X_{\Delta 2}$ close to the intermediate-heavy axis (point B in Figure 7.66) and $X_{\Delta 4}$ close to the light-intermediate axis (point A in Figure 7.67). The optimal placement of the two difference points has actually switched over from that required for sharp distillate and bottoms splits.

There is clearly much room for optimisation of a design by manipulating these difference points. Their optimal values are ultimately dependent on the shape of the rectifying and stripping profiles and therefore the quantity of impurity material in the distillate and bottoms product streams. The relative importance of the placement of the two points should also be taken into consideration. If the reflux ratio of either CS 2 or 4 has a minimal effect on the area of the feasible region then emphasis should be placed on the placement of the difference point for the other. Also the direction of potential disturbances to the operating conditions should be taken into consideration. Halvorsen and Skogestad (1999) identified the "bad" direction of split ratio change in response to a disturbance. This direction is

normal to the column minimum reflux split ratio line (see Figure 7.68). Disturbances in this direction can rapidly increase the required operating reflux, whereas disturbances parallel to the column minimum reflux split ratio line, termed the "good" direction, require more gradual changes to the operating reflux ratio, in order to remain on specification. To minimise "bad" direction disturbance effects, the difference points should be chosen such that the width of the feasible region in the "bad" direction is maximised. This typically means that the choice of one of the two difference points will take precedence over the other – only one of the corresponding minimum reflux boundaries ($R_{\Delta 2MIN}$ or R_{4MIN}) is approximately normal to the bad direction. In Figure 7.68, $R_{\Delta 2MIN}$ is normal to the "bad" direction and therefore the optimal placement of $X_{\Delta 2}$ would take precedence over $X_{\Delta 4}$ during optimisation.

Note: in Figure 7.62 to Figure 7.67 red lines represent contours of high reflux ratio while blue curves represent lines of lower reflux ratio
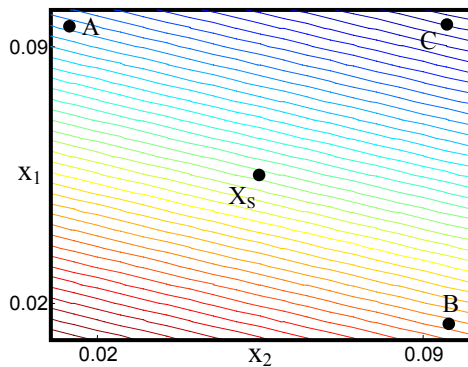
Alpha	[2, 1, 1.5]
Reflux Ratio	7
Feed	[1/3, 1/3, 1/3]
Side-Draw	[0.05, 0.05, 0.90]
Distillate	[0.95, 1e-10, 0.05]

Figure 7.62: Minimum CS 2 reflux contours at sharp-split conditions varying $X_{\Delta 2}$
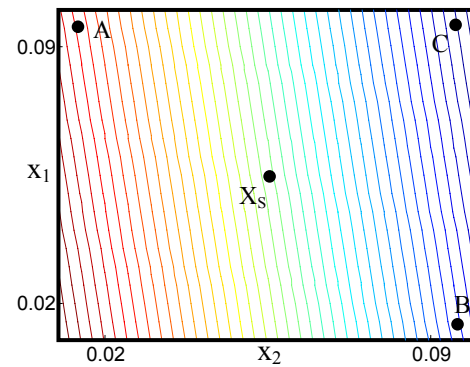
Alpha	[2, 1, 1.5]
Reflux Ratio	7
Feed	[1/3, 1/3, 1/3]
Side-Draw	[0.05, 0.05, 0.90]
Bottoms	[1e-10, 0.95, 0.05]

Figure 7.63: Minimum CS 4 reflux contours at sharp-split conditions varying $X_{\Delta 4}$
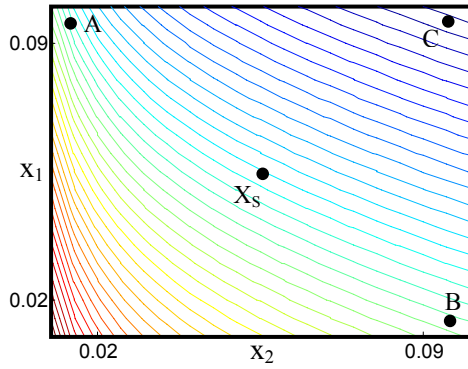
Alpha	[2, 1, 1.5]
Reflux Ratio	7
Feed	[1/3, 1/3, 1/3]
Side-Draw	[0.05, 0.05, 0.90]
Distillate	[0.95, 1e-6, 0.05]

Figure 7.64: Minimum CS 2 reflux contours at non-sharp split conditions varying $X_{\Delta 2}$
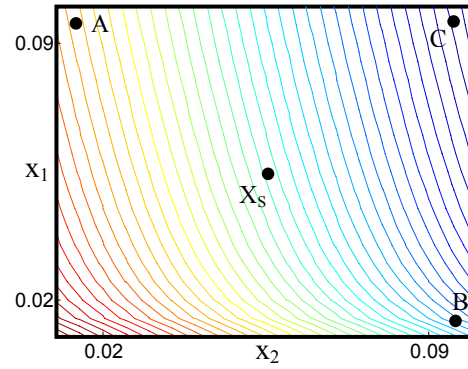
Alpha	[2, 1, 1.5]
Reflux Ratio	7
Feed	[1/3, 1/3, 1/3]
Side-Draw	[0.05, 0.05, 0.90]
Bottoms	[1e-6, 0.95, 0.05]

Figure 7.65: Minimum CS 4 reflux contours at non-sharp split conditions varying $X_{\Delta 4}$
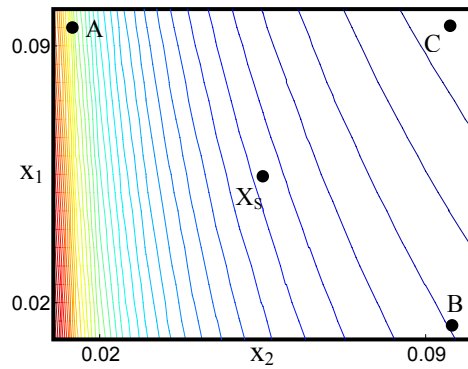
Alpha	[2, 1, 1.5]
Reflux Ratio	7
Feed	[1/3, 1/3, 1/3]
Side-Draw	[0.05, 0.05, 0.90]
Distillate	[0.95, 1e-4, 0.05]

Figure 7.66: Minimum CS 2 reflux contours at non-sharp split conditions varying $X_{\Delta 2}$
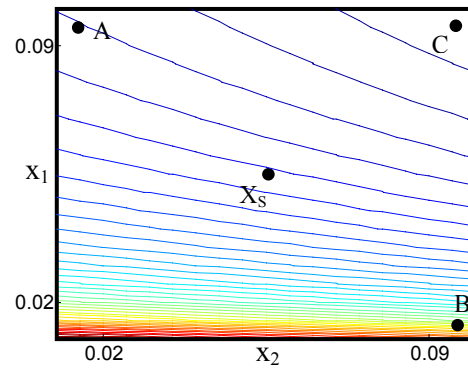
Alpha	[2, 1, 1.5]
Reflux Ratio	7
Feed	[1/3, 1/3, 1/3]
Side-Draw	[0.05, 0.05, 0.90]
Bottoms	[1e-4, 0.95, 0.05]

Figure 7.67: Minimum CS 4 reflux contours at non-sharp split conditions varying $X_{\Delta 4}$
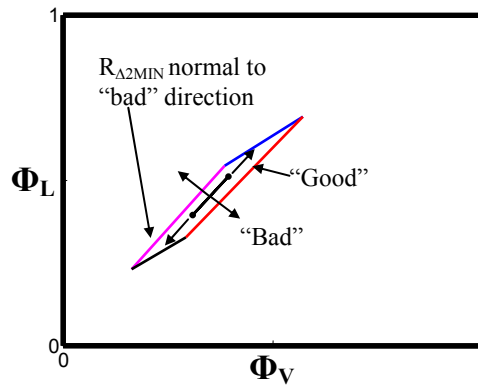
**Figure 7.68: "Good" and "Bad" directions of
split ratio change due to disturbances**

7.5.2   Optimal Split Ratio Choice - Stage Requirements

Unlike sharp-split separations which require an infinite number of stages, non-sharp separations have finite stage requirements. The infinite stage requirement for sharp splits arises from the necessity, of one or more of the CS operating profiles, to pass through the saddle point of the corresponding TT. This phenomenon does not occur in non-sharp Petlyuk separations. An infinite number of stages can still be required, but this is simply due to one or more or the column sections pinching. These pinch points are either stable or unstable nodes but never saddle points.

We track the formation of these pinch points, with variation of the split ratios, by producing the feasible region boundaries. These are the only split ratio values that result in an infinite number of required stages for non-sharp separations. All the values within the feasible region result in finite stages requirements. Using the CPM methodology for design it is computationally simple to determine the number of stages required for the column after the selection of a particular split ratio pair. Tracking variable n of the difference point equation and then summing the values in each column section, the total number of required stages can be determined. If this process is repeated at various points throughout the feasible region, a contour map of stage requirement can be produced for the specific parameter set (see Figure 7.73).

We can gain a better understanding of the distribution of stages within the column by analysing the various sections of the column independently. The stage requirement of the prefractionator (CS 3 and 5) will be infinite at or close to the eigenvector boundaries PEB 1 and PEB 2. It will decrease as split ratio values away from these boundaries are sampled and reach a minimum close to the intersection of $R_{\Delta2MIN}$ and $R_{\Delta4MIN}$ (see Figure 7.71 and Figure 7.72). The product side coupled column sections (CS 2 and 4) will exhibit the opposite behaviour. Infinite stages will be required on the $R_{\Delta2MIN}$ and $R_{\Delta4MIN}$ boundaries but this will decrease for split ratios chosen towards the interior and reach a minimum at or close to the intersection of PEB 1 and PEB 2 (see Figure 7.69 and Figure 7.70).

If we sum all the stages within the column, the effect of the feed side and product side coupled column sections balance each other. Infinite stages are required on or close to all the boundaries and this requirement decreases towards the interior, reaching a minimum somewhere within this interior (see Figure 7.73 and Figure 7.74).

Through this process it is possible to optimise the design for a specific reflux ratio. By minimising the stage requirement we minimise the capital investment for the separation. The true minimum stage requirement varies from system to system and also with variation of parameters. This is evident in Figure 7.73 and Figure 7.74. The minimum solution is close to the centre of the feasible region in Figure 7.73, but much closer to the $R_{\Delta2MIN}$ $R_{\Delta4MIN}$ intersection in Figure 7.74. If mass computation of the stage requirement is undesirable, a good approximation can be achieved at the point of intersection of two lines constructed from opposite corners of the feasible region.
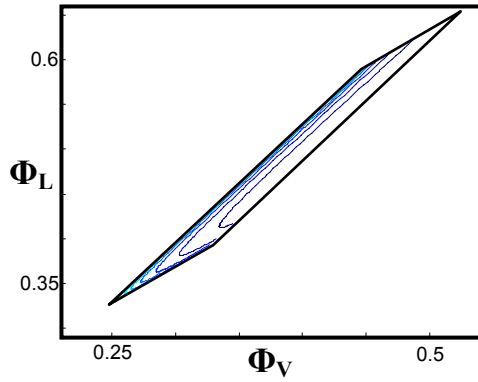
Figure 7.69: Stage requirement contours for CS 2 and 4
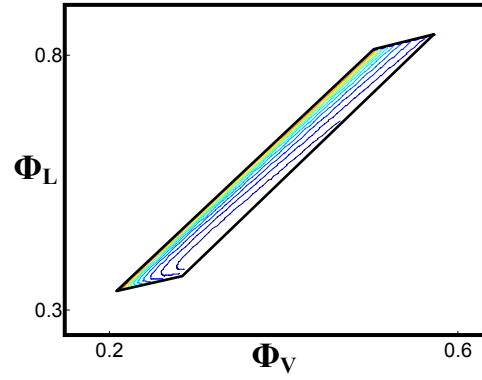
Figure 7.70: Stage requirement contours for CS 2 and 4
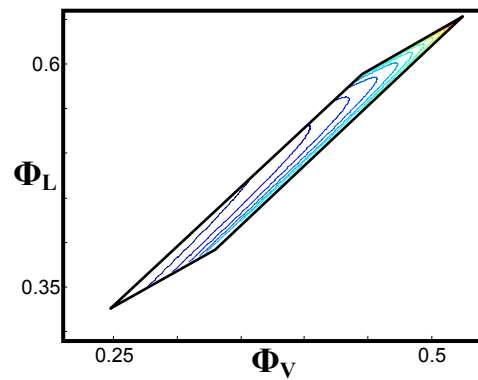
Figure 7.71: Stage requirement contours for CS 3 and 5
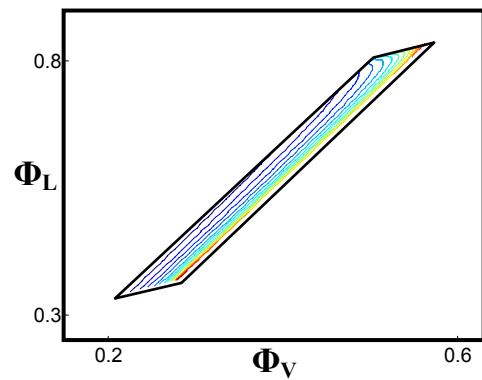
Figure 7.72: Stage requirement contours for CS 3 and 5
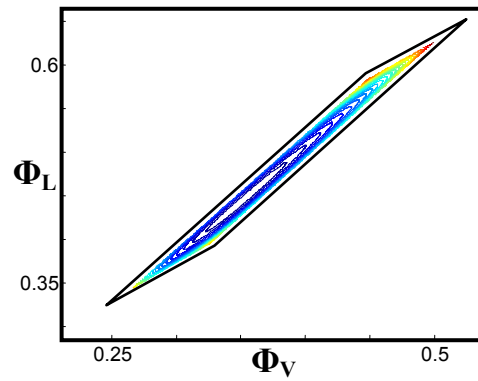
Figure 7.73: Total Petlyuk stage requirement contours

Alpha	[2, 1, 1.5]
Reflux Ratio	8
Feed	[1/3, 1/3, 1/3]
Side-Draw	[0.05, 0.05, 0.90]
Distillate	[0.95, 1e-5, 0.05]
Bottoms	[1e-5, 0.95, 0.05]
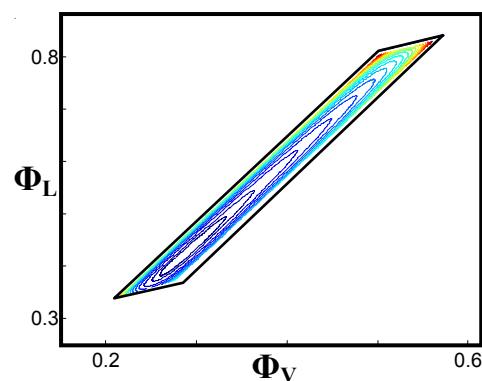
Figure 7.74: Total Petlyuk stage requirement contours

Alpha	[5, 1, 3]
Reflux Ratio	4
Feed	[1/3, 1/3, 1/3]
Side-Draw	[0.05, 0.05, 0.90]
Distillate	[0.95, 1e-5, 0.05]
Bottoms	[1e-5, 0.95, 0.05]

7.5.3 Overall Minimum Reflux

In the previous chapter we discussed the topological conditions for minimum reflux for sharp splits. It was shown that at minimum reflux, the boundary of TT 1 or TT 6 (of relevant phase) passes through the feed composition. The reflux ratio resulting from this topological condition is exactly equal to values calculated using the minimum reflux expressions derived by Fidkowski and Krolikowski (1987) and modified by Halvorsen and Skogestad (2001). When we relax the sharp product specification on the side-draw, we find that this same condition may be used to find minimum reflux. This is because the rectifying and stripping profiles run along the border of their TTs. Even though the CS 2 and 4 profiles do not, at minimum reflux we are only interested in their unstable and stable nodes respectively. These lie both on the profile and TT, hence exactly the same logic for finding minimum reflux topologically can be used. Minimum reflux ratios, determined using this rationale (for constant relative volatility systems), are exactly equal to those calculated using the non-sharp side-draw expression derived by Halvorsen (2001). Figure 7.75 shows the liquid TTs of all six column sections at minimum reflux for a sharp distillate and bottoms but non-sharp side-draw separation with saturated liquid feed. Notice that all matching criteria are satisfied and that this is topologically equivalent to the sharp-split case.
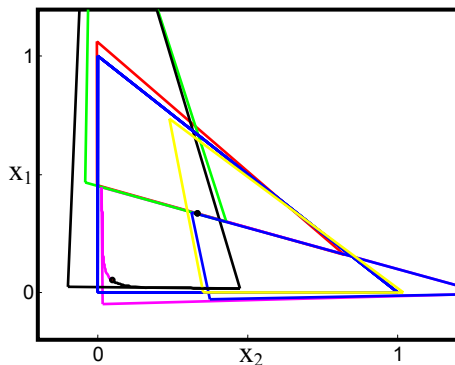
Figure 7.75: TTs for Petlyuk column with non-sharp side-draw spec at minimum reflux
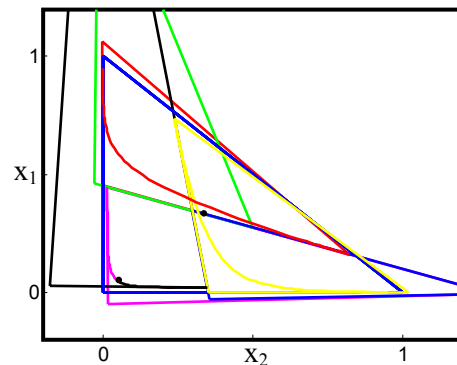
Figure 7.76: Infeasible non-sharp Petlyuk column with TTs at sharp-split minimum reflux condition

When we introduce impurities into the distillate and bottoms products we can no longer use the TTs of the column sections to find the minimum reflux condition.

None of the profiles run along the boundaries of their TTs, hence it is extremely difficult to track them when parameters are varied. The fact that the rectifying and stripping profiles no longer run along these boundaries suggests that when all six TTs meet the sharp-split minimum reflux conditions (i.e. border each other) the separation may in fact be infeasible (see Figure 7.76 – matching criterion 1 not met). Instead of analysing composition space to determine under what conditions the system is at minimum reflux, we will consider split ratio space.

At minimum reflux the feasible region shrinks to a line for sharp-splits. Two of the boundaries, either PEB 1 and $R_{\Delta 2MIN}$ or PEB 2 and $R_{\Delta 4MIN}$ collapse onto each other. At sharp-split conditions we have a hundred percent confidence in the validity and location of the boundaries. For non-sharp splits we have a hundred percent confidence in the validity of $R_{\Delta 2MIN}$ and $R_{\Delta 4MIN}$ and selection of split ratios between these lines will always result in the satisfaction of matching criteria 1 and 2. We do not, however, have confidence in the validity of PEB 1 and PEB 2. The feasible region can shrink or grow over these boundaries depending on the impurity content of the products. Therefore, there is some uncertainty surrounding the selection of split ratios between these two lines and their potential to result in the satisfaction of matching criterion 4. We do, however, have total confidence in the validity of the intersection of these lines. This set, of split ratios, results in a double pinch at the feed composition and is always a solution for composition matching criterion 4. We have confidence in this point because we can track the stationary points of CS 3 and 5 analytically.

Although the shrinkage of the feasible region is fairly small compared to the area contained within the four boundaries when the reflux is relatively high, at or close to minimum reflux it becomes very significant and our confidence in the validity of the region is low. We can, therefore, only consider split ratios that we are certain of at these low refluxes. Consider Figure 7.77. The red region has been produced for a relatively large reflux ratio. If we decrease the ratio, the $R_{\Delta 4MIN}$ boundary shifts upward and the overall area of the original region shrinks to that seen in the blue. We still have confidence that all the split ratios between $R_{\Delta 2MIN}$

and $R_{\Delta 4MIN}$ will satisfy matching criteria 1 and 2 and that a large portion between PEB 1 and PEB2 will satisfy criterion 4. If we decrease the reflux ratio even further until the $R_{\Delta 4MIN}$ boundary passes through the intersection of PEB 1 and PEB2, our confidence in satisfying criteria 1 and 2 is obviously intact but we have no confidence in the region, contained within the boundaries, to also satisfy criterion 4 and therefore produce a feasible column. The only point that will satisfy all matching criteria is the PEB 1 and PEB2 intersection. There may well be solutions within the region at this reflux or at a lower reflux, but we have no confidence in this. The minimum reflux at which we know for sure that we have a solution is, therefore, the reflux resulting in either $R_{\Delta 2MIN}$ or $R_{\Delta 4MIN}$ passing through the PEB 1 and PEB2 intersection. This is shown in Figure 7.78. We consider this to be the non-sharp split minimum reflux ratio.
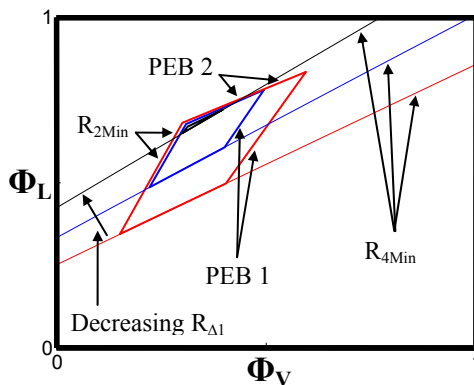
Figure 7.77: Changes to feasible region and $R_{\Delta 4MIN}$ with decreasing reflux ratio
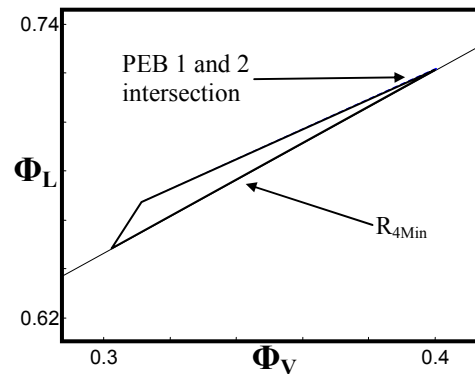
Figure 7.78: Minimum reflux condition for non-sharp splits – $R_{\Delta 4MIN}$ passing through the intersection of PEB 1 and 2

7.6 The Dividing Wall Column

The dividing wall column (DWC) is thermodynamically equivalent to the Petlyuk column if there is no heat transfer across the wall. DWCs are more popular than the original Petlyuk configuration because the practical difficulties, of transporting vapour from one shell to another, are removed. Also the DWC offers a significant capital saving by requiring only one shell. Like the Petlyuk column

there is a potential control issue associated with the pressure drop in the prefractionator in relation to that in the section adjacent to the side-draw. If the pressure drop, on either side of the dividing wall, is different, control problems will undoubtedly ensue. To avoid this problem, DWCs are often designed with a 50 % vapour split as well as an equal number of stages on either side of the dividing wall. This reduces the available degrees of freedom, but still facilitates some of the advantages of the Petlyuk column.

By performing the same stage count as before (to find the minimum stage requirement), we can determine the range of solutions that result in an equal number of stages on either side of the dividing wall. Thus we can find the entire feasible region for this class of problem and identify all potential DWCs operated with a 50/50 vapour split. Figure 7.79 and Figure 7.80 illustrate these feasible regions, superimposed over the general solution, for two systems. In both cases the range of operation is very small – only a very thin band of such solutions exist. It is interesting to note that the 50/50 vapour split solution does not always exist (see Figure 7.79).
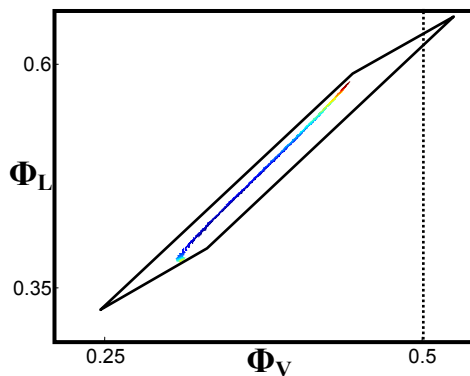
Figure 7.79: DWC solutions with stage contours – Alpha [2, 1, 1.5]
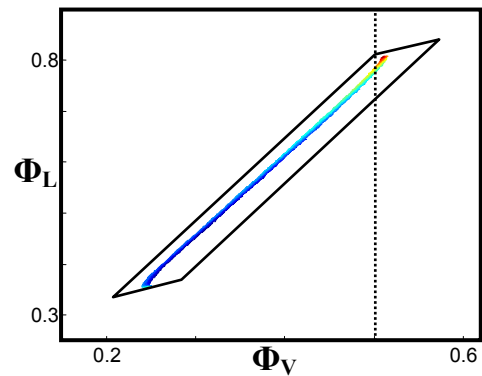
Figure 7.80: DWC solutions with stage contours – Alpha [5, 1, 3]

7.7 Discussion

7.7.1   Net-Molar Flow Anomalies

The net flow of individual components and the driving forces behind these net flows, in complex distillation configurations, are some of the most difficult concepts to reconcile with our conventional view of distillation. The simple column does not allow the generation of unusual net-molar-flows and it is easy to succumb to the idea that these are solely a product of component relative volatility. In a rectifying section the light component is the dominant species in the net flow and seems to draw the other components up the column with it. Similarly in a stripping section, the heavy component is in excess in the net flow and appears to draw the light and intermediate components down the column.

It is also not very difficult to intuitively comprehend the effects of distributed feed addition on component net-molar flows along the length of a two product column. As feed material is added, each component, in turn, achieves the role of dominant species. At the top the light component holds sway. As feed material is added the heavy component composition becomes high enough to ensure that it begins to descend instead of ascend. The intermediate component can still flow in either direction. When enough heavy material has been added (through feed addition) for this component to play the dominant role in the net flow, the intermediate net-molar-flow switches direction and begins to flow down the column. Finally, on further feed addition, the heavy component reaches a concentration high enough to draw all the components down.

All these phenomena fit really well with our intuitive understanding. How then do we explain the potential for bulk flow of the light and heavy components in the opposite direction to that of the intermediate component? Indeed, net flow patterns 1, 2, 4 and 5 seem to provide this potential, in the Petlyuk column. From a material balance perspective, if $X_{\Delta 2}$ and $X_{\Delta 4}$ are placed in difference point regions 1, 4, 5 or 6, the difference points of CS 3 and 5 can be forced to operate in

regions 2 and 5, where this anomalous net-molar-flow is made possible. The topological feasibility of CS 3 and 5, also does not preclude this potential. Neither does that of CS 2 or 4 if placed in difference point region 5. In fact, all feasible placements of the CS 2 and 4 difference points for net flow patterns 1, 2, 4 and 5 seem to dictate this region of operation for $X_{\Delta 3}$ and $X_{\Delta 5}$. Also, feasible split ratio regions can be generated for these modes of operation, as we have shown above (*section 7.4*) i.e. full theoretically feasible designs, where all composition matching criteria are satisfied, can be produced. There seems to be nothing preventing our acceptance of these possibilities except traditional distillation understanding.

In our investigation into the viable placement of difference points $X_{\Delta 2}$ and $X_{\Delta 4}$, however, we neglected certain placement scenarios that have a low probability of satisfying matching criteria 1 and 2. These placement scenarios can, theoretically, still produce feasible designs and if used would result in $X_{\Delta 3}$ and $X_{\Delta 5}$ operating in difference point regions such as 7 and 3, respectively. The net-molar-flows produced in these sections are far more consistent with our intuition. The intermediate component flows in the same direction as either the heavy or light components, which flow in opposite directions; the light component up and the heavy component down. Indeed it would be more comforting to assume this mode of operation as the more likely. However, not only is there a low probability of CS 2 and 4 profiles intersecting the rectifying and stripping profiles respectively, but if operated with the afore mentioned difference points, TT 3 and 5 would also be positioned such that the composition matching would be improbable. Boundary A_3 would lie in positive heavy component space (see Figure 7.5) and boundary B_5 would lie in positive light component space (see Figure 7.9).

If we return, for a moment, to the subject of sharp product splits we notice that in this scenario with very little or no freedom of difference point choice, a few net-molar-flow anomalies present themselves too. For net flow pattern 1, $X_{\Delta 5}$ lies on the intermediate-heavy axis between difference point regions 5 and 6; see Figure 6.27b. The net-molar-flow of the intermediate component, for this flow pattern

and difference point placement, is up the column, while the heavy component is down. This seems to hold with conventional logic. The light component, however, moves neither up nor down. There is no bulk flow of this component at all. That is not to say that there is minimal or no light component material in the liquid and vapour streams; there must be for the satisfaction of composition matching criterion 4 in the interior of the MBT. The bulk light component flow is simply not in the same direction as the bulk intermediate component flow. By conventional logic the lighter component should be drawing the intermediate component upwards, but it is not. The same phenomenon occurs for net flow pattern 2; see Figure 6.27c. Conversely, net flow patterns 4 and 5 produce a net flow of light component up, intermediate component down, but no net flow of heavy component; see Figures 6.27d-e. The heavy component does not draw the intermediate component down the column. These modes of operation cannot be avoided if feasible split ratios in net flow pattern regions 1, 2, 4 and 5 are sampled and the apparent anomaly in net-molar-flow is, clearly, a physical reality. Similarly the non-sharp, anomalous, net-molar-flows exhibited in CS 3 and 5 for these flow patterns are overwhelmingly more likely to occur than the "more intuitive" scenarios where $X_{\Delta 3}$ operates in difference point regions 4 or 7 and $X_{\Delta 5}$ operates in difference point regions 6 or 3.

It is the coupling of parallel column sections that provides the potential for these phenomena. For simple columns, where the sections are in series and products are drawn from the ends, unusual difference points cannot be produced. The sections have to produce actual product streams which are equivalent to their net flows. This coupled with the absence of "unusual" feeds confine simple columns to only two net-component flow possibilities. The possibilities increase considerably using feed distribution. The feed material does not instantly change the, product-equivalent, net flow of one section (rectifying) to that of another (stripping). Rather, the component net flow direction change is gradual, taking place over a number feed trays. The sections between the rectifying and stripping sections are non-product sections and the net-molar flows are, therefore, not confined to product flow equivalents. These sections are, however, in series and although they

feed each other "unusual" pseudo streams (net-molar flows) these are confined to only a limited range of pseudo compositions. Coupled sections, on the other hand, receive both real and pseudo feeds, as well as producing pseudo products. The fact that not only two, but in some cases three column sections meet at a mixing point provides dramatically more net-molar-flow possibilities and the potential for them to operate in counter-intuitive manners.

7.7.2   Non-Sharp Feasible Split Ratio Regions

Non-sharp separations exhibit complexities in the design process that are absent in sharp separation design. The most noticeable complication involves the freedom of difference point choice. Sharp splits specifications result in constrained difference points. $X_{\Delta 2}$ and $X_{\Delta 4}$ are constrained to the side-draw composition, while $X_{\Delta 3}$ and $X_{\Delta 5}$ are constrained to the light-intermediate and intermediate-heavy axes respectively. Because the difference point is so fundamental to the quantitative and qualitative composition profile topology and achievable compositions in a column section, the correct placement of this variable is critically important. Difference point selection must be made on the basis of net flow mode of operation. Each net flow pattern requires a qualitatively different choice for this variable. These choices are based on the direction of bulk flow within each column section.

The non-sharp product specifications and freedom of difference point choice result in feasible split ratio regions which are, often, quite dissimilar from the sharp-split versions. Understanding the influence of product impurities on the region of feasible split ratios is very important. For many thermodynamic systems producing composition profiles that run close to the system nodes, which is essentially the effect of true sharp split specifications, is extremely difficult and definitely not practical. In these situations even if a large number of stages is acceptable – as required for near sharp splits – the range of useful split ratios is unlikely to conform to the sharp-split feasible region. For effective design

purposes a thorough knowledge of this effect on the split ratio solutions is required.

We have categorised, in this work, the effects of non-sharp side-draw, distillate and bottoms specifications. Non-sharp side-draw products do not affect the qualitative method of minimum reflux calculation for CS 2 and 4. They do, however, generate extra solutions, outside the original sharp-split feasible region, adjacent to PEB 1 and PEB 2. If X_S contains light component impurities, growth will occur adjacent to PEB 2 and if it contains heavy component impurities, growth will occur adjacent to PEB 1. The fact that the region grows means that all split ratios within the original boundaries are still solutions and can be chosen here with total confidence in their validity.

A non-sharp distillate product, where the rectifying profile does not run close to its saddle point, results in a much higher minimum CS 2 reflux ratio compared to the sharp-split case. This effectively shifts the $R_{\Delta2MIN}$ boundary into the sharp-split region removing large areas of formerly feasible split ratios. The minimum reflux is easily and accurately determined by calculating the value at which the unstable node of the CS 2 trajectory lies on the rectifying section trajectory. This product specification also results in split ratio solutions, inside the PEB 2 feasible region boundary, becoming infeasible. This effect is slightly offset by region growth due to impurities in the side-draw product. For composition matching, non-sharp distillate products require heavy component impurities in the side-draw; hence the effects of solution growth and shrinkage around PEB 2 are set against each other.

Similarly, a non-sharp bottoms product, where the stripping profile does not run close to its saddle point, results in a much higher minimum CS 4 reflux ratio compared to the sharp-split case. This now shifts the $R_{\Delta4MIN}$ boundary into the sharp-split region, again, removing areas of formerly feasible split ratios. The minimum reflux, for CS 4, is easily and accurately determined by calculating the value at which the stable node of the CS 4 profile lies on the stripping profile.

This product specification also results in split ratio solutions inside the PEB 1 feasible region boundary becoming infeasible. Again the effects are somewhat counteracted by the growth of the region in this area. The growth in this case is due to light component impurities in the side-draw which are now required for the satisfaction of composition matching criterion 2.

The effective design, of non-sharp Petlyuk columns, is largely dictated by our confidence in the solution. The possibility of region "shrinkage" introduces an uncertainty in the validity of the solution. Our understanding of the cause of this phenomenon allows us to select split ratios, within the four boundaries, that we have more confidence in. All solutions between $R_{\Delta 2MIN}$ and $R_{\Delta 4MIN}$ satisfy matching criteria 1 and 2. Uncertainty surrounding split ratios close to these boundaries only occurs near their intersection with PEB 1 and PEB 2. The region shrinkage always decreases, along the length of PEB 1 and 2 from these intersections, to zero at the point where they, in turn, intersect. The split ratio set, at which these boundaries intersect, is always a solution, satisfying all matching criteria. Areas of potential infeasibility are often removed at higher reflux when the zero net-molar flow lines become new boundaries of the region. In general, the uncertainty in the solution validity is small and the boundaries, of the feasible region, discussed in this work represent an excellent approximation. Even if the uncertainty is significant, the CPM design methodology allows the verification of composition matching criteria, by hand, with very little computational effort and time wasting.

One of the most powerful results of this work is that by analysing the shifting of feasible region boundaries we can determine a column minimum reflux ratio for any product specifications - if these are feasible. Column minimum reflux occurs when either the $R_{\Delta 2MIN}$ or $R_{\Delta 4MIN}$ boundaries pass through the point of PEB 1 and PEB 2 intersection.

7.7.3   Non-Ideal Zeotropic Systems

The convenient property, of constant relative volatility system topology, is the fact that the boundaries, or profiles, between transformed topological regions, are straight. This makes the analysis of topological changes with parameter variation relatively simple. We simply have to track TTs, for sharp-splits, to determine if composition matching criteria are satisfied. Non-ideal zeotropic systems do not afford us this luxury. The boundaries between nodes always exhibit a degree of curvature. The only way to overcome this problem is to make straight boundary approximations when using these systems. To make matters worse, the eigenvectors at the stationary points need not point directly at the others of the system.   In the process of feasible region generation, however, the PEB boundaries are the only boundaries affected. $R_{\Delta 2MIN}$ and $R_{\Delta 4MIN}$ are unaffected because these can be calculated accurately in the same way detailed, in this work, for no sharp splits. We also have complete confidence in the intersection of PEB 1 and PEB 2 as this set of split ratios result in the double feed pinch and as mentioned before, must be a solution. In many ways, the design problems faced with non-ideal systems are exactly the same as those faced with non-sharp constant relative volatility systems. The ultimate pitfall is the inability to analytically track composition profiles. We have shown here, however, that by simply tracking the movement of the stationary points and generating appropriate split ratio boundaries, a fairly accurate approximation of the feasible region can be generated. At the very worst we know that the solutions lie between the $R_{\Delta 2MIN}$ and $R_{\Delta 4MIN}$ boundaries and the PEB 1 - PEB 2 intersection. This narrows the split ratio search dramatically. Generally, though, the feasible region approximations for all zeotropic systems is good and very importantly, minimum reflux solutions for both sharp and non-sharp splits can, quite certainly, be generated with a fair degree of accuracy.

7.8 Conclusions

The CPM technique has allowed a comprehensive analysis of the Petlyuk distillation column at both sharp and non-sharp conditions. Not only are we able to gain insight into the column behaviour, but can generate all possible, zeotropic system, solutions for sharp product conditions and very good approximations for non-sharp product specifications, with minimal computational effort. Individual solutions can easily be generated by selecting split ratios and then producing CPMs for each section. Column section stage requirement is a natural product of the technique and can be determined by tracking variable n of the difference point equation along the length of the chosen operating composition trajectories. No iteration is required to generate the solution which can be used for the successful initialisation of rigorous design packages. Minimum required reflux ratios can be found for any product specifications allowing utility costs to be minimised. Capital investment, also, can be minimised by finding optimal operating split ratios. This is particularly powerful as the technique allows not only design, but optimisation as well to ensure the best possible financial return.

Chapter 8:

Discussion

Thesis Results

In this work we have attempted to illustrate the use of column profile maps (CPMs) for the analysis and design of distillation systems. We believe that we have developed an extremely powerful and versatile tool that does not suffer some of the fundamental shortcomings of currently employed short-cut techniques.

Firstly, unlike many techniques, the CPM design and analysis methodology is not configuration specific. Many other short-cut design techniques are produced specifically for a particular configuration. This makes them very limited. New techniques must be developed each time a new configuration is analysed. The CPM technique allows the design of any separation configuration, no matter how complex.

We have presented illustrations of the effectiveness of the CPM methodology as an analysis tool by applying it to gain an understanding of the effects of feed distribution in a two product distillation column. A number of important results followed from this analysis. These are useful contributions to the field of distillation in their own right. They include the following:

- Feed distribution can be used to decrease the number of required stages for non-sharp separations.
- Non-sharp separations that are infeasible using a single feed tray can be made feasible by feed distribution if the associated rectifying and stripping section transformed triangles (TTs) overlap.
- True minimum reflux for a (two product) separation is represented graphically when the associated rectifying and stripping section TTs border each other.

- There are no advantages (from a topological perspective) in feed distribution for sharp separations.

- A feasible/attainable region of composition profiles exists for a distributed feed column for defined product specifications and reflux ratio.

A comprehensive analysis and design of the Petlyuk column has also been performed in this work. It has been shown that CPMs can be applied to both the sharp and non-sharp Petlyuk separation problems. Many of the results of the sharp-split Petlyuk analysis presented here are confirmed by the results obtained by Halverson and Skogestad (2001). These together with the non-sharp-split Petlyuk work also constitute very useful contributions to the field. Some of the most important results of this work are presented below.

- A feasible/attainable parameter (split ratio) region exists for the Petlyuk column for defined product compositions and column reflux ratio.

- At minimum reflux the feasible region is simply a line of solutions

- The boundaries of the non-sharp-split feasible region require an infinite number of stages.

- There are five material (net) flow patterns possible in the Petlyuk column. We have defined these as net flow patterns *1* through *5*.

- Net flow pattern *3* is the most efficient net flow pattern (for ideal systems). The minimum reflux solution always occurs at the net flow pattern 3 mode of operation.

- Net flow analysis can be used as a diagnostic tool. Zeotropic separations operating at net flow patterns other than *3* are clearly over refluxed.

- Counter-intuitive component net flows arise in the Petlyuk column due to column section coupling. The intermediate component net flow can be forced in the opposite direction (within a column section) to that of the light and heavy components.

- An optimal solution corresponding to the minimum stage solution exists in the non-sharp feasible region.

- The CPM technique can be used to generate individual Petlyuk solutions.

- The CPM technique can be used to optimise Petlyuk designs; Column control can be improved by selecting parameters that maximise the area of the feasible region.

The CPM technique can be used to generate full solutions for configurations. This is particularly useful because current rigorous simulation packages often encounter solution convergence problems with complex arrangements. The Petlyuk column is one such arrangement that has received attention in literature regarding this problem (Triantafyllou and Smith, 1992). Solutions generated using the CPM technique can be used successfully to initialise rigorous simulation routines.

Due to the graphical nature of the technique, it is difficult to describe specifics of the design elegantly and if there is a failing in this thesis it is that. Chapter 7 in particular suffers from this drawback as the relative, qualitative, positions of various topological features must be described. However, this does not detract from the effectiveness of the CPM design procedure which is, in fact, fairly simple. Once the general design methodology is understood, it can easily be applied to any configuration. An outline of this procedure is as follows:

- Break configuration into column sections.
- Determine all possible net flow patterns.
- Identify required composition matching criteria.
- Identify the form of advantageous topology for each column section based on product specifications and matching criteria.
- Based on desired topology for each column section determine regions of feasible difference point placement, for each net flow pattern.
- Determine minimum reflux conditions for each column section (if they exist).
- Select useful variables for representation of minimum reflux solution and determine regions of feasible parameter choice (if possible).

The Way Forward

Although the analysis and design of particular configurations has been discussed in this work, the CPM technique actually offers the potential for a design paradigm shift. Most separations are synthesised by assuming a separation configuration and trying to determine the potential capabilities of this configuration for the separation. This approach is severely limiting. By tackling the problem in this way the designer will almost always restrict themselves to standard equipment and miss significant opportunities that arise from novel arrangements. This is a standard approach by most design engineers. Instead of designing the standard equipment to achieve a separation, an approach of designing the separation to determine the required configuration should be taken. With this approach a designer could work backwards from a required composition profile and piece together a configuration to achieve it. This would be very advantageous if a separation path was known to be optimal or simply superior to that of standard equipment. The goal for efficient design would then be to determine the criteria defining an optimal composition profile.

Column profile maps have revealed many exciting future opportunities for distillation synthesis. One such opportunity is the efficient separation of azeotropic mixtures. Current azeotropic distillation methods require large scale recycling within separation networks. These are very costly as large heating and cooling duties are required. An azeotropic separation synthesis based on Column Profile Mapping offers the potential to reduce or remove recycle requirements and even reduce the number of columns required in a separation network. This is possible because columns that allow composition profiles to cross azeotropic distillation boundaries can be designed, using the CPM technique.

By simply shifting the topology adjacent to the simple distillation boundary, with appropriate difference points and reflux ratios, profiles straddling multiple distillation regions can be produced. These are not simply academic opportunities

which in practice would require impossible or hypothetical feeds. Existing configurations can be used to cross distillation boundaries.

Castillo et al (1998) showed that a single side-rectifier could be used to separate an acetone-chloroform-benzene mixture to fairly high purity products. This separation requires a composition profile crossing the simple distillation boundary defined between the acetone-chloroform binary azeotrope and the benzene pure component composition.

Other equipment can be used to perform this feat. A fully functional Petlyuk column can be designed to achieve relatively high product purities for this system. Below is a figure illustrating the composition profiles of such a Petlyuk column, designed using the CPM methodology (Figure 8.1). Notice that the composition profiles feeding the side-draw run directly over the distillation boundary.
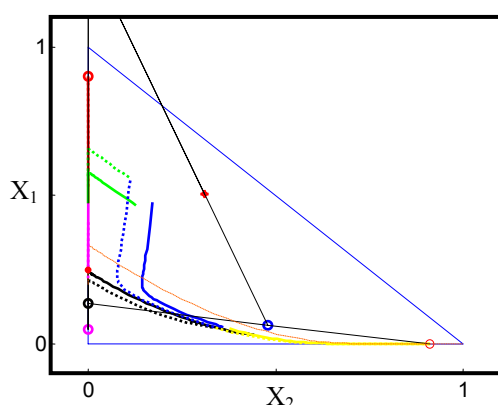
Figure 8.1: Petlyuk Column with operating profiles crossing distillation boundary
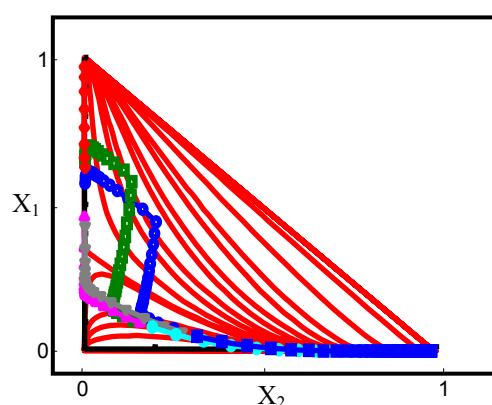
Figure 8.2: ASPEN Plus simulation results from simulation initialised with CPM design data

The column is not required to operate at particularly extreme conditions. The overall column reflux ratio is 7.70. Table 8.1 illustrates the operating parameters of each column section comprising the configuration. Figure 8.2 illustrates the results of an ASPEN Plus simulation initialised using the results of the CPM

design. The results are very similar, emphasising the effectiveness of the CPM methodology for initialisation purposes.

Column Section	Difference Point (X_Δ)		Reflux ratio (R_Δ)
	Acetone	Benzene	
1	0.9	0	7.70
2	0.05	-0.0001	6.26
3	1.3243	0.0001	8.42
4	0.1358	0.0004	3.14
5	0.0642	0.4799	-6.10
6	0	0.91	-14.4

Table 8.1: Operating parameters for Petlyuk column with composition profiles crossing the acetone-benzene-chloroform simple distillation boundary

It is interesting to note that this column is required to operate at net flow pattern 4. Without this mode of operation the column would not be able to achieve the distillation boundary crossing. For ideal systems these flow patterns are sub-optimal and offer no advantages over net flow pattern 3 but for azeotropic systems they are extremely useful for achieving novel separations.

There are exciting future prospects for developing the theory of azeotropic separation synthesis. This work should address topics such as the extent to which predefined configurations can "cross" distillation boundaries, the choice of configuration based on system topology, the synthesis of novel arrangements based on system topology, the minimum reflux requirement for azeotropic distillation etc. Column Profile Mapping applied to these problems could revolutionise the field of distillation which has for so long been thought of as understood.

Long term development of the CPM technique must address the issue of higher component mixtures. The technique does have the potential to address this issue

because large portions of the theory and approach are based on the placement of system nodes. Although these are more difficult to find and interpret for higher order systems, the method of their application to design and analysis of distillation arrangements is similar to that for three components. For instance, the true minimum reflux condition for a two product column, as discussed in Chapter 4, occurs when boundaries of the transformed triangles, for the two column sections, border each other. In four-component systems, the topological counterpart of the three-component transformed triangle is a three-dimensional pyramid. An equivalent four-component minimum reflux condition would, therefore, simply require the bordering of one of the surfaces of each of the two "transformed pyramids". Of course, determining when this condition is satisfied is not a trivial mathematical exercise, but is not impossible either.

The task is substantially simpler in other cases. Consider the determination of the minimum reflux of CS 2 of the Petlyuk column at sharp-splits conditions. The nodes of importance in this case (the unstable node of CS 2 and a saddle of CS 1) lie on an axis of the composition space (see Figure below). In this case we simply require that the nodes of the two transformed pyramids coincide. We know that the movement of these nodes is restricted to the axis and therefore need only vary the reflux ratio until the condition is met.
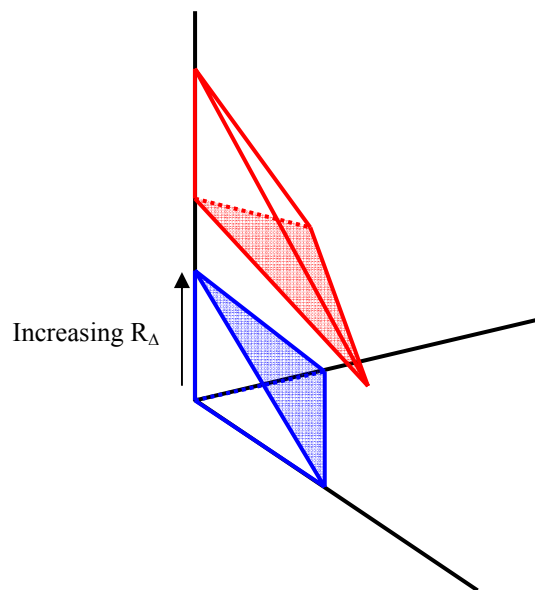
Figure 8.3: Increasing reflux ratio of Petlyuk column section 2 (for ideal 4 component sharp-split) to determine the section's minimum reflux

One of the most powerful attributes of the CPM technique is the potential for graphical visualisation and interpretation. This, unfortunately, is lost for systems of higher order than four components but many three-component graphical results can be generalised to include any number of components in a similar manner to that discussed above.

APPENDIX A: *Sequence of Column Sections to write "Reuel"*

$X_\Delta=[\ 0.1021\ 0.0691]$
$R_\Delta = 20$
$X_0 = [\ 0.005\ 0.5]$

$X_\Delta=[-0.45\ 1.5]$
$R_\Delta = 10.2$
$X_0 = [\ 0.13\ 0.3984]$

$X_\Delta= [0.6\ -0.2]$
$R_\Delta = -10$
$X_0 = [\ 0.02\ 0.2744]$

$X_\Delta= [0.15\ 0.1]$
$R_\Delta = -2$
$X_0 = [\ 0.1048\ 0.1718]$

$X_\Delta= [1.2\ -0.1]$
$R_\Delta = -13$
$X_0 = [\ 0.2013\ 0.3167]$

$X_\Delta= [-0.01\ 0.6]$
$R_\Delta = 2.2$
$X_0 = [\ 0.1406\ 0.1712]$

$X_\Delta= [0.4\ 0.1]$
$R_\Delta = 7$
$X_0 = [\ 0.1786\ 0.1439]$

$X_\Delta= [0.4\ 0.1]$
$R_\Delta = -3.2$
$X_0 = [\ 0.2263\ 0.2982]$

$X_\Delta= [0.4\ 0.3]$
$R_\Delta = -3.6$
$X_0 = [\ 0.2485\ 0.1479]$

$X_\Delta= [0.4\ 0.1]$
$R_\Delta = 7$
$X_0 = [\ 0.2819\ 0.1278]$

$X_\Delta= [0.4\ 0.3]$
$R_\Delta = -1.7$
$X_0 = [\ 0.3186\ 0.3057]$

$X_\Delta= [1.6\ -0.57]$
$R_\Delta = -13.89$
$X_0 = [\ 0.3868\ 0.1176]$

$X_\Delta=[1.6\ -0.4]$
$R_\Delta = -11$
$X_0 = [\ 0.4123\ 0.31]$

$X_\Delta=[-0.01\ 0.7]$
$R_\Delta = 2.312$
$X_0 = [\ 0.3937\ 0.1907]$

$X_\Delta=[0.5\ 0.05]$
$R_\Delta = -1.5$
$X_0 = [\ 0.4353\ 0.1008]$

$X_\Delta=[1.6\ -0.4]$
$R_\Delta = -10.8$
$X_0 = [\ 0.4709\ 0.110]$

$X_\Delta=[0.61\ 0.4]$
$R_\Delta = -1.2$
$X_0 = [0.5733\ 0.4267]$

$X_\Delta=[-0.2\ 1.2]$
$R_\Delta = 3.51$
$X_0 = [0.5618\ 0.0649]$

$X_\Delta=[0.61\ 0.049]$
$R_\Delta = 8$

Figure B.1: Sequence of column sections to write the word "Reuel" with the design

APPENDIX B

Mathematical Background

B.1. Eigenvalues and eigenvectors

Liapounov's first theorem states that the nature of a singular point X_S of equation (B.1) is topologically similar to the singular point of the linearized equations:

$$\frac{du}{dn} = J\left(X_S\right)u$$

$$u_i = x - X_S \qquad i = 1 \dots c - 1$$

$$J\left(X_S\right) = \begin{bmatrix} & & \vdots & & \\ \cdots & \left(\dfrac{\partial f_i}{\partial x_j}\right)_{p,x=const} & \cdots \\ & & \vdots & & \end{bmatrix}_{x=x_S} = \quad \textit{Jacobian matrix}$$

$$f_i = \frac{R_\Delta + 1}{R_\Delta}\left(x_i - y_i(x)\right) + \frac{1}{R_\Delta}\left(X_{\Delta_i} - x_i\right) \tag{B.1}$$

By assuming that the *n* x *n* matrix *J(X$_S$)* = [a$_{ij}$] is constant, that is, its entries do not depend on n, we are left with an eigenvalue problem, where the eigenvalue characterizes the kind of singularity that occurs and the pair of eigenvectors determine the asymptotic direction of the trajectories in the neighbourhood of the singularity. In order for a singular point to be investigated, it is necessary to set up the characteristic equation

$$\begin{vmatrix} a_{11} - \lambda & a_{12} \\ a_{21} & a_{22} - \lambda \end{vmatrix} = 0$$

and find its roots λ_1 and λ_2. (The characteristic equation shown is for a ternary system).

Each pair of eigenvectors represents the axis of a new coordinate system which separate different behaviour of the phase diagram around the singularity and the singularity being the origin. Linear independent eigenvectors separate the space into four regions, while collinear eigenvectors divide the space into two regions, as illustrated in figure B.1a and B.1b.
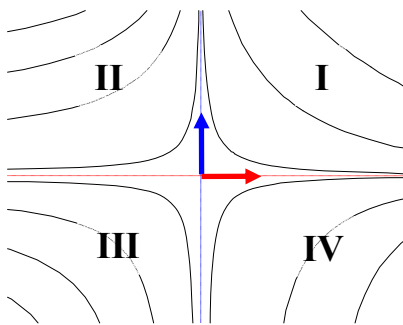
Figure B.1a: Example of a saddle node with two linear independent eigenvectors that divide the space into four regions.
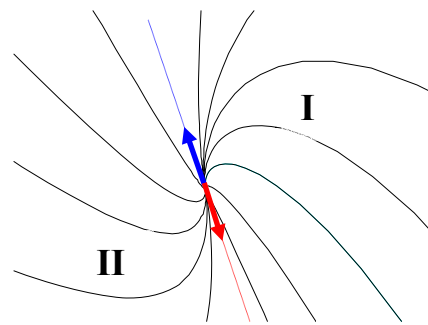
Figure B.1b: Example of a stable node with two collinear eigenvectors that divide the space in two regions.

Complex eigenvectors are a result of complex roots of the characteristic equation. The space consists of one region as there is no determinable asymptotic direction in the real space. I.e. a characteristic node for complex eigenvectors would be a stable focus, see Figure B.1c.
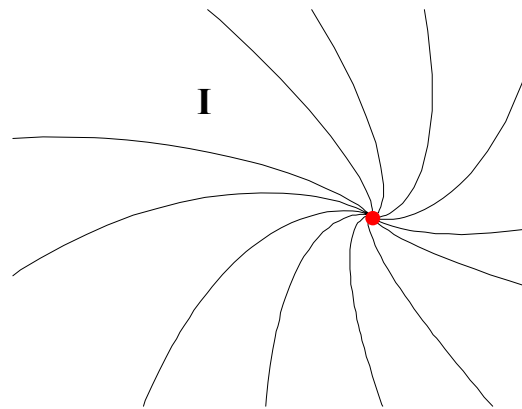
Figure B.1c: Example of a stable focus with complex eigenvectors that results in a space that consists of one region.

To characterize the kind of singularities in space it is necessary to look at the eigenvalues. The kind of singularity that can occur in a system is determined by the dimension of the characteristic equation. The eigenvalues for ternary systems are described by the sign of λ_1 and λ_2. (Quaternary systems are described by the signs of $\lambda_1\lambda_2$ and λ_3.) Hence for ternary systems there exists a limited combination of eigenvalues and therefore cases of singularities that can occur in the system.

B.2 Eigenvalue and eigenvector maps

As the eigenvectors are a function of the thermodynamics only ($v = f(y_i(x))$), there exists a unique eigenvector map for each system modelled by a particular set of thermodynamic data. The eigenvector map can be obtained by plotting the eigenvectors over a range of x.

In analogy to the eigenvector map there exists an eigenvalue map. As the eigenvalues are a function of $\lambda = f(y_i(x), R_\Delta.)$) eigenvalue maps can be plotted for every R_Δ for each system.

B.3 Cases of singularities occurring in a ternary system

Provided that $\det J(X_S) \neq 0$ the singularities are elementary and the following cases for a ternary system are possible:

1. The roots λ_1, λ_2 are distinct and real $\rightarrow$ two linear independent eigenvectors:

- $\lambda_1 < 0$, $\lambda_2 < 0$. The singular point is asymptotically stable (stable node);

- $\lambda_1 > 0$, $\lambda_2 > 0$. The singular point is asymptotically unstable (unstable node);

- $\lambda_1 < 0$, $\lambda_2 > 0$. The singular point is asymptotically unstable (saddle point);

2. The roots of the characteristic equation are complex: $\lambda_1 = p + i$q, $\lambda_2 = p - i$q $\rightarrow$ eigenvectors are complex:

- $p < 0$, q $\neq 0$. The singular point is asymptotically stable (stable focus);

- $p > 0$, q $\neq 0$. The singular point is asymptotically unstable (unstable focus);

- $p = 0$, q $\neq 0$. The singular point is asymptotically stable (midpoint);

3. The roots of the characteristic equation are not distinct $\rightarrow$ eigenvectors are collinear:

- $\lambda_1 = \lambda_2 < 0$. The singular point is an asymptotically stable node;

- $\lambda_1 = \lambda_2 > 0$. The singular point is an asymptotically unstable node;

The case $\det J(X_S) = 0$ results in non-elementary singularities of the following kind:

1. The roots of the characteristic equation has at most one zero eigenvalue $\rightarrow$ two linear independent eigenvectors:

- $\lambda_1 = 0$, $\lambda_2 < 0$. The singular point is an asymptotically stable half node-saddle (Doherty);

- $\lambda_1 = 0$, $\lambda_2 > 0$. The singular point is an asymptotically unstable half node-saddle (Doherty);

To be able to exploit the knowledge of the eigenvectors and eigenvalues we have to look at specific systems.

APPENDIX C

Sequence Of Column Sections To Write "Wits".

$X_\Delta = [\ 0.01\ 0.5]$
$R_\Delta = 20$

$X_\Delta = [-0.09575\ 0.4538]$
$R_\Delta = 5$

$X_\Delta = [-0.08848\ 0.45081]$
$R_\Delta = 5$

$X_0 = [0.1212\ 0.1589]$

$X_\Delta = [0.184\ 0.6867]$
$R_\Delta = 1.2$

$X_\Delta = [0.3\ 0.224234]$
$R_\Delta = -2.254$

$X_P = [0.168\ 0.6877]$

$X_\Delta = [-0.1\ 0.4465]$
$R_\Delta = 3.529$

$X_\Delta = [0.4\ 0.4678]$
$R_\Delta = -1.375$

$X_\Delta = [0.4\ 0.8733]$
$R_\Delta = -2.102$

$X_\Delta = [0.2508\ 0.4359]$
$R_\Delta \rightarrow \infty$

$X_\Delta = [0.3921\ 0.2897]$
$R_\Delta = 1$

$X_0 = [0.3112\ 0.3681]$

$X_\Delta = [0.6\ 0.16008]$
$R_\Delta = -2.347$

$X_\Delta = [0.4\ 0.8733]$
$R_\Delta = -2.102$

$X_\Delta = [0.6\ 0.103397]$
$R_\Delta = 0.70667$

$X_\Delta = [1.5\ -0.46903]$
$R_\Delta = -8.402$
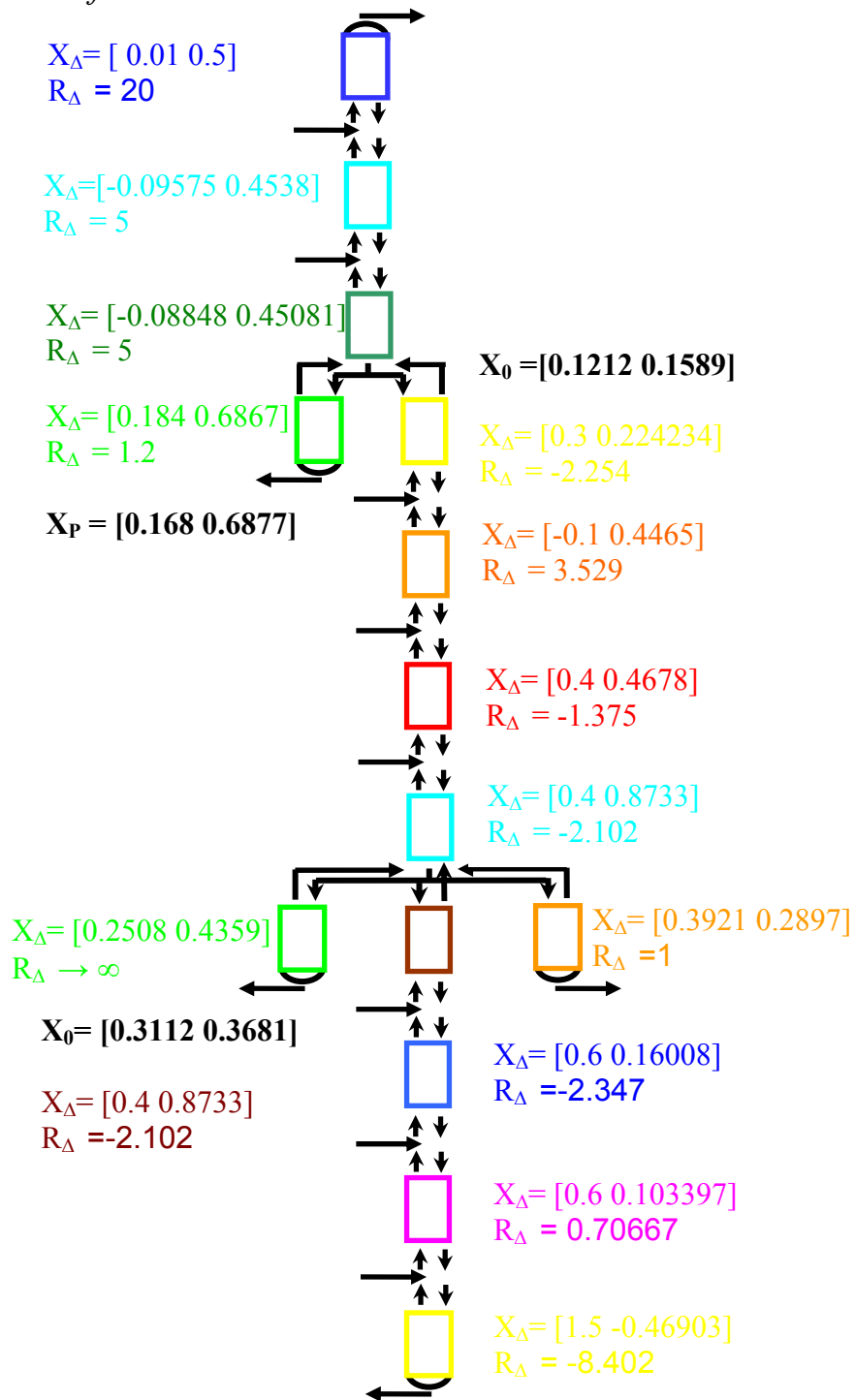
Figure C.1: Sequence of column sections to write the word "Wits" with the design parameters X_Δ and R_Δ.

APPENDIX D: *Proof of overlap of vapour TTs if liquid TTs*
   overlap.

Hypothesis: If two liquid TTs overlap, the corresponding vapour TTs will overlap also.

Consider two TTs (TT A and TT B) of a configuration with sharp product specifications that are required to achieve composition matching by overlapping close to an axis. The composition profiles of the corresponding sections run along the boundaries of these TTs. The extreme condition at which this composition matching can be satisfied is when stationary points of the two TTs coincide. i.e. $X_{PA} = X_{PB}$. The composition of vapour TT A in equilibrium with X_{PA} is Y_{PA}^*. This composition is a stationary point of vapour TT A. However, the equilibrium composition of X_{PB} is $Y_{PB}^* = Y_{PA}^*$ since $X_{PA} = X_{PB}$. This composition is also a stationary point of vapour TT B. Hence, we can conclude that if the liquid TTs touch at nodes the vapour TTs will also touch at nodes.

We can extend this argument to include, not only, situations where the liquid TTs touch but where they produce a small overlap. If $X_{PA} = X_{PB}$ and is then shifted, by changing parameters, such that light component value (for arguments sake) is increased and this shifting increases the liquid TT overlap, Y_{PA}^* must also shift in a direction that increases its light component value and will therefore increase the vapour TT overlap. Hence if liquid TTs (for sharp split) overlap, the corresponding vapour TTs will do likewise.

APPENDIX E: *Proof of Coinciding Pinch Points for CS 1, 2 and 3 at Sharp-Split Conditions.*

Hypothesis: If two stationary points of coupled CS system 1, 2 or 3 coincide at a point, a stationary point of the third section must also coincide at this point.
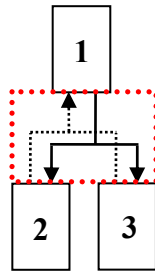
Figure E.1: Mixing point of CSs 1, 2 and 3

Material balance over streams from CSs 1, 2 and 3:

$$\Delta X_{\Delta 1} = \Delta X_{\Delta 2} + \Delta X_{\Delta 3}$$
$$V_1 Y_{P1} - L_1 X_{P1} = V_2 Y_{P2} - L_2 X_{P2} + \Delta X_{\Delta 3}$$

If liquid pinch points from sections 1 and 2 overlap i.e. $X_{P2} = X_{P1}$

Material Balance becomes :

$$V_1 Y_{P1} - L_1 X_{P1} = V_2 Y_{P2} - L_2 X_{P1} + \Delta X_{\Delta 3}$$

But at pinch point $Y_i = Y_i^*(X_i)$, (passing streams are in equilibrium), therefore :

$$Y_{P1} = Y_{P2} = Y_{P1}^*(X_{P1})$$
$$V_1 Y_{P1}^* - V_2 Y_{P1}^* - (L_1 X_{P1} - L_2 X_{P1}) = \Delta X_{\Delta 3}$$

But $L_3 = L_1 - L_2$ and $V_3 = V_1 - V_2$

$$V_3 Y_{P1}^* - L_3 X_{P1} = \Delta X_{\Delta 3}$$

Pinch X_{P1} and equilibrium Y_{P1}^* satisfy section 3 material balance. The only passing streams in the CPM 3 that satisfy both material balance and equilibrium are the pinch points, so $X_{P3} = X_{P1}$ and $Y_{P3}^* = Y_{P1}^*$.

APPENDIX F: *Proof of TT 1, 2 and 3 overlap for all Φ_V and Φ_L resulting in a negative value of $R_{\Delta2}$ where $|R_{\Delta2}| > |R_{\Delta2MIN}|$ at Sharp-Split Conditions.*

Hypothesis: At $R_{\Delta2MIN}$ boundaries B_1, C_2 and B_3 are collinear. Any values of Φ_V and Φ_L chosen such that $R_{\Delta2}<0$ and $|R_{\Delta2}| > |R_{\Delta2MIN}|$ will result in an overlap of TT 1, 2 and 3.

At $R_{\Delta2MIN}$, boundaries B_1, C_2 and B_3 are collinear. This is therefore a feasible solution of the CS 1-2-3 system. In order to determine whether or not TTs 1, 2 and 3 overlap for $|R_{\Delta2}| > |R_{\Delta2MIN}|$, we must determine the rate and direction of movement of the nodes of the respective TTs as Φ_V and Φ_L are varied. The positions of the nodes of a TT are dependent on X_Δ and R_Δ. Arbitrarily varying Φ_V and Φ_L results in dramatically different values of $R_{\Delta2}$, $R_{\Delta3}$ and $X_{\Delta3}$, and consequently, dramatically different positions of the stationary points. We need to negate the effect of variation of $X_{\Delta3}$ on the positions of the CS 3 stationary points so that we need only compare one variable type (i.e. reflux ratio of CS 2 and 3) and determine its effect on the rate of stationary point movement. If Φ_V and Φ_L are varied along lines of constant $X_{\Delta3-i}$, the rate of change of $R_{\Delta2}$ and $R_{\Delta3}$ can be compared. Once the rate of change of $R_{\Delta k}$ is known for each section, the rate of movement of the stationary points can be determined.

Below is the expression for Φ_V and Φ_L resulting in constant $X_{\Delta3-i}$ (Equation 6.20).

$$\Phi_L = \frac{(R_{\Delta1}+1)}{R_{\Delta1}}\Phi_V + \frac{1}{R_{\Delta1}}\left(\frac{X_{\Delta3-i} - X_{\Delta1-i}}{X_{\Delta2-i} - X_{\Delta3-i}}\right) \qquad \textbf{(6.20)}$$

We will vary Φ_V and Φ_L along these lines and determine the rate of change of $R_{\Delta2}$ and $R_{\Delta3}$. Examples of these lines are seen in the Figure F.1 below.

The reflux ratio for CS 3 is given by Equation 6.15 below:

$$R_{\Delta 3} = \frac{(1-\Phi_L)R_{\Delta 1}}{(1-\Phi_V)(R_{\Delta 1}+1)-(1-\Phi_L)R_{\Delta 1}} \tag{6.15}$$

Combining Equation 6.15 and Equation 6.20 to eliminate Φ_L and differentiating w.r.t. Φ_V we obtain:

$$\frac{dR_{\Delta 3}}{d\Phi_V} = \frac{-R_{\Delta 1}-1}{(1-\Phi_V)(R_{\Delta 1}+1)-\left(1-\dfrac{(R_{\Delta 1}+1)\Phi_V}{R_{\Delta 1}}-\dfrac{X_{\Delta 3-i}-X_{\Delta 1-i}}{R_{\Delta 1}(X_{\Delta 2-i}-X_{\Delta 3-i})}\right)R_{\Delta 1}}$$

$$= \frac{-(R_{\Delta 1}+1)}{\left(1+\dfrac{X_{\Delta 3-i}-X_{\Delta 1-i}}{X_{\Delta 2-i}-X_{\Delta 3-i}}\right)}$$

For sharp product splits the light component $X_{\Delta 1-i} \approx 1$ and $X_{\Delta 2-i} \approx 0$

$$\frac{dR_{\Delta 3}}{d\Phi_V} = \frac{-(R_{\Delta 1}+1)}{\left(\dfrac{1}{X_{\Delta 3-i}}\right)} = -X_{\Delta 3-i}(R_{\Delta 1}+1)$$

$$\tag{F.1}$$

The reflux ratio for CS 2 is given by equation below:

$$R_{\Delta 2} = \frac{\Phi_L R_{\Delta 1}}{\Phi_V(R_{\Delta 1}+1)-\Phi_L R_{\Delta 1}} \tag{6.14}$$

Combining equation Equation 6.14 and Equation 6.20 to eliminate Φ_L and differentiating w.r.t. Φ_V we obtain:

$$\frac{dR_{\Delta 2}}{d\Phi_V} = \frac{R_{\Delta 1}+1}{\Phi_V(R_{\Delta 1}+1)-\left(\dfrac{(R_{\Delta 1}+1)\Phi_V}{R_{\Delta 1}}+\dfrac{X_{\Delta 3-i}-X_{\Delta 1-i}}{R_{\Delta 1}(X_{\Delta 2-i}-X_{\Delta 3-i})}\right)R_{\Delta 1}}$$

$$= \frac{R_{\Delta 1}+1}{\left(\dfrac{X_{\Delta 1-i}-X_{\Delta 3-i}}{X_{\Delta 2-i}-X_{\Delta 3-i}}\right)}$$

For sharp product splits the light component $X_{\Delta 1-i} \approx 1$ and $X_{\Delta 2-i} \approx 0$

$$\frac{dR_{\Delta 2}}{d\Phi_V} = \frac{R_{\Delta 1}+1}{\left(1-\dfrac{1}{X_{\Delta 3-i}}\right)} = \frac{-X_{\Delta 3-i}(R_{\Delta 1}+1)}{(1-X_{\Delta 3-i})}$$

$$\tag{F.2}$$

From Equations F.1 and F.2, we see that both $R_{\Delta 2}$ and $R_{\Delta 3}$ decrease with increasing Φ_V along lines of constant $X_{\Delta 3-i}$. The rate of change of $R_{\Delta 2}$, with respect to Φ_V, is equal to the rate of change of $R_{\Delta 3}$ divided by $(1-X_{\Delta 3-i})$. In split ratio regions 1, 2 and 3: $0<(1-X_{\Delta 3-i})<1$ for all Φ_V and Φ_L (See Figure 6.27a, b and c). This means that the magnitude, of the rate of change of $R_{\Delta 2}$, is greater than that of $R_{\Delta 3}$ along lines of constant $X_{\Delta 3-i}$. $R_{\Delta 3}$, which is positive in region 3, becomes smaller as Φ_V is increased. Boundary B_3 consequently, shifts towards the light component. $R_{\Delta 2}$, which is negative, becomes more negative i.e. the magnitude of the negative $R_{\Delta 2}$ increases. Boundary C_2 also shifts towards the light component. However, due to the more rapid rate of change of $R_{\Delta 2}$ than $R_{\Delta 3}$, we can conclude that boundary C_2 will move towards the light component faster than boundary B_3 hence the two TTs will maintain overlap.

In split ratio region 4, the TTs overlap by default. Both TT2 and TT3 operate at positive reflux ratio. TT2 will look similar to Figure 6.34 and TT3 will look similar to TT2 in Figure 6.32 (except that the TT 3 saddle point and stable node will have higher light component values). Because the TT 2 unstable node is above $x_1 = 1$ and the TT 3 unstable node is below $x_1 = 1$, for all $R_\Delta > 0$, overlap is guaranteed. The same is true for split ratio region 5. Although in this region CS3 operates at negative reflux, the qualitative form of the TT3 always allows overlap with TT 2. We can say therefore that TT2 will overlap TT3 for all values of $R_{\Delta 2}>R_{\Delta 2MIN}$ as we can choose any constant $X_{\Delta 3-i}$ line along which to vary Φ_V.
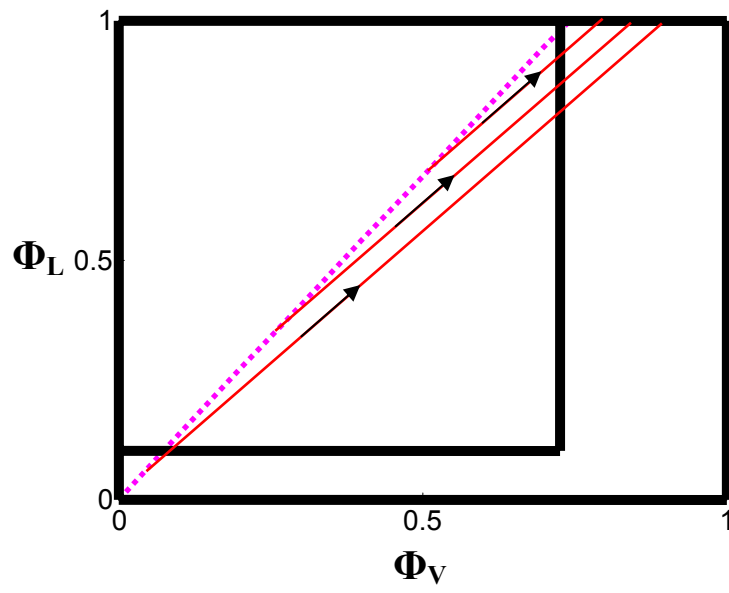
Figure F.1: Lines of Constant X_Δ derived for values of $X_{\Delta 3}$ between 0 and 1

Appendix G: *Pinch point curves for qualitatively different X_Δ placement.*

Figure G.1: Pinch point curve for difference point region 1 at positive reflux

Figure G.2: Pinch point curve for difference point region 1 at negative reflux

Figure G.3: Pinch point curve for difference point region 6 at positive reflux

Figure G.4: Pinch point curve for difference point region 6 at negative reflux

Figure G.5: Pinch point curve for difference point region 5 at positive reflux

Figure G.6: Pinch point curve for difference point region 5 at negative reflux
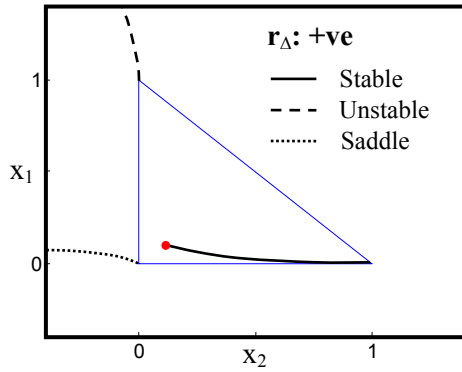
Figure G.7: Pinch point curve for difference point region 4 at positive reflux

Figure G.8: Pinch point curve for difference point region 4 at negative reflux

Figure G.9: Pinch point curve for difference point region 7 at positive reflux

Figure G.10: Pinch point curve for difference point region 7 at negative reflux
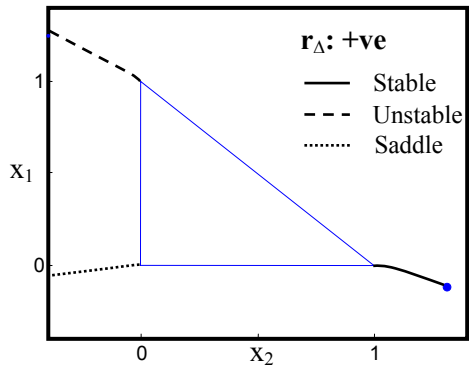
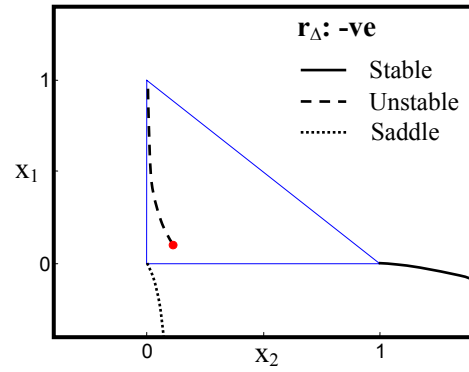**Figure G.11: Pinch point curve for difference point region 3 at positive reflux**
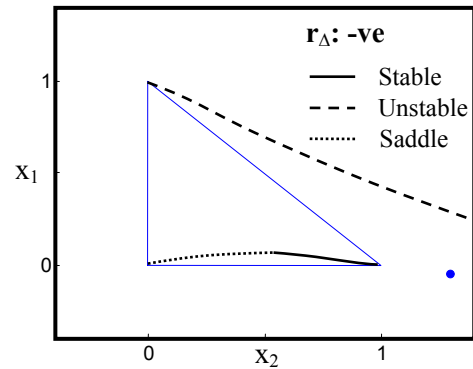
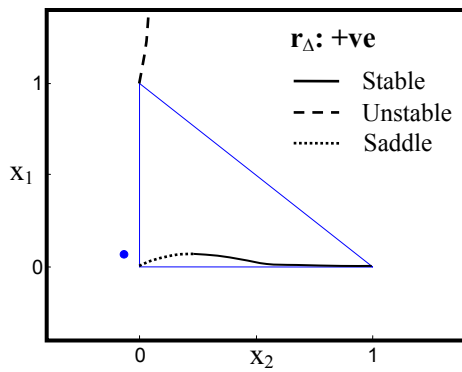**Figure G.12: Pinch point curve for difference point region 3 at negative reflux**
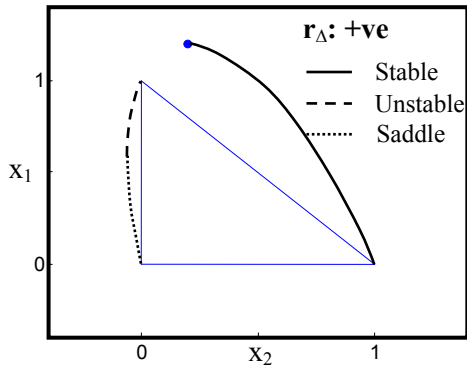
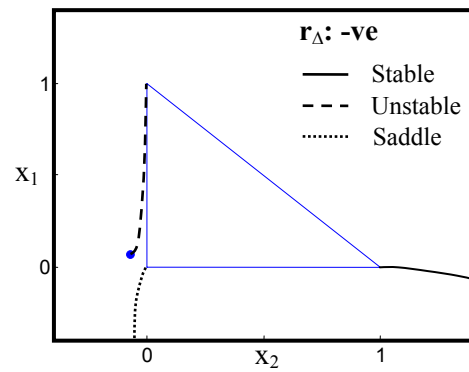**Figure G.13: Pinch point curve for difference point region 2 at positive reflux**

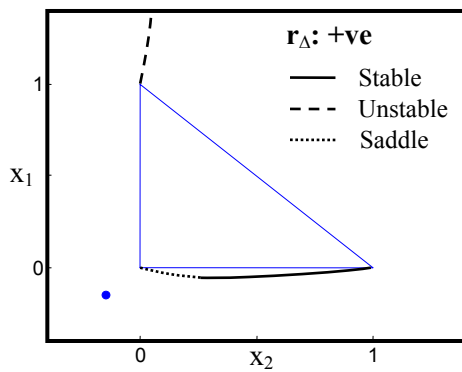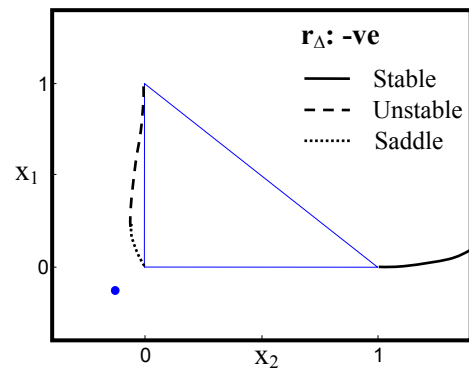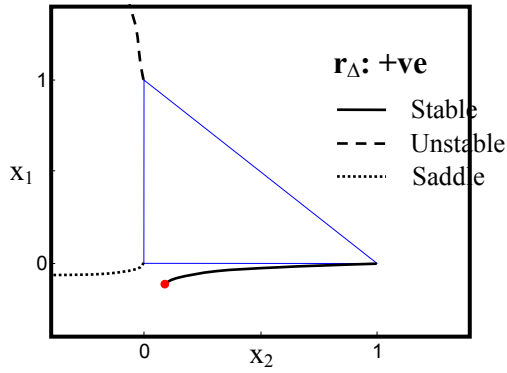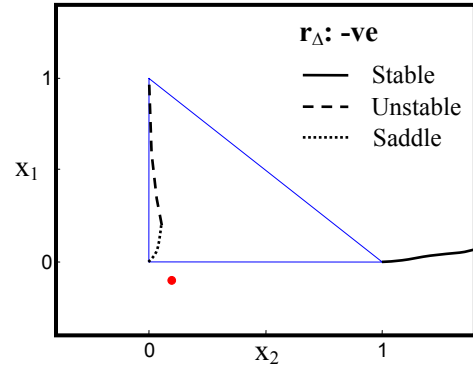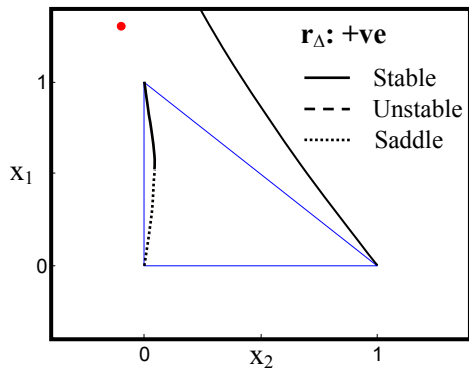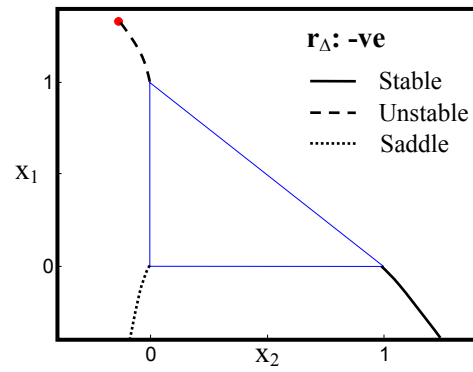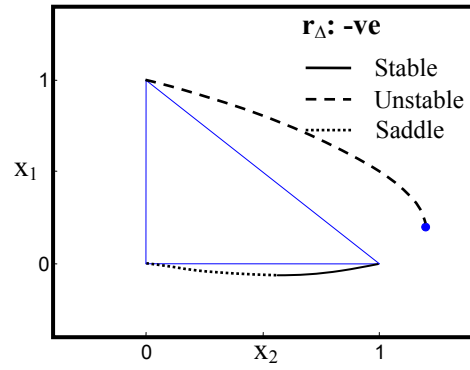**Figure G.14: Pinch point curve for difference point region 2 at negative reflux**

Appendix H: *Proof of region growth adjacent to PEB 1 and PEB 2 for sharp distillate and bottoms products but non sharp side-draw products.*

In the previous chapter we discussed the movement of the coupled column sections TTs with variation of the split ratios. We discussed how matching criterion 1 is always satisfied for split ratios resulting in $R_{\Delta 2}$ values greater than the minimum. (see Appendix F). This resulted from the fact that boundary B_3 always lies between the CPM 2 unstable node and boundary B_1. This implies that when the distillate specification is sharp but the side-draw specification is not so, matching criterion 1 will always be satisfied within transformed difference point region 4 of CPM 3 – i.e. only transformed region 4 of CPM 3 will ever be sampled in satisfying matching criterion 1. Similarly, if we consider matching criterion 4, for a sharp bottoms product specification we note that this intersection is always satisfied within transformed region 6 of CPM 5. This means that CS 3 profiles from TR 4 and CS 5 profiles from TR 6 which don't run along the TT boundaries can intersect – i.e. TT 3 and TT 5 do not always have to intersect to satisfy matching criterion 4 for these product specifications. This means that the true limits of feasible operation always lie outside the eigenvector boundaries.

Appendix I: *Derivation of the Difference Point Equation*

The generalised column section (CS) is defined as a length of column between points of addition or removal of mass or energy. The stages in a column section can be numbered from the bottom up (Figure I.1) or from the top down (Figure I.2).
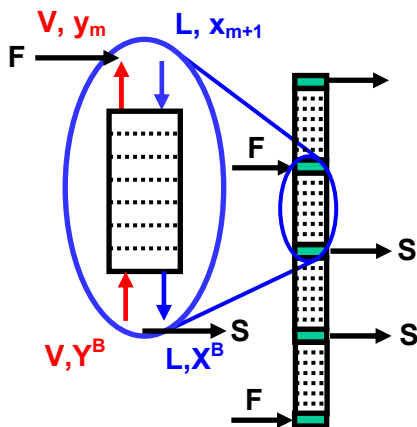
Figure I.1: Column section numbered from the bottom up
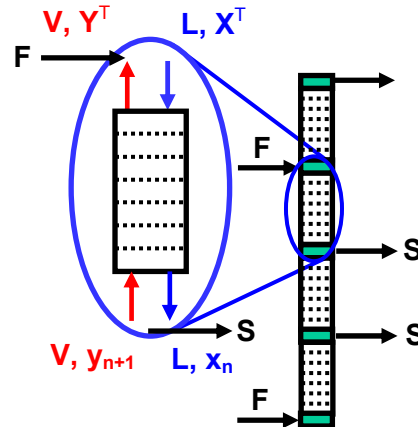
Figure I.2: Column section numbered from the top down

The compositional change from one stage to another can be determined by material balance. The difference equation describing this compositional change with stage number *m* (in Figure I.1) is seen in (I.1) below.

Van Dongen and Doherty (1985), approximated the rectifying and stripping difference equations with differential equations. This can be done for the generalised column section, as well, using an analogous derivation, as follows.

The material balance over the generalised column section in Figure I.1 is:

$$Lx_{i,m+1} = Vy_{i,m} + LX_i^B - VY_i^B \qquad \text{(I.1)}$$

Letting $\quad X_{\Delta i} = \dfrac{VY_i^B - LX_i^B}{\Delta}$ $\qquad$ **(I.2)**

and

$\Delta = V\text{-}L \quad$ where $\quad \Delta \neq 0$ $\qquad$ **(I.3)**

Substituting (I.2) and (I.3) into (I.1) yields :

$x_{i,m+1} = \dfrac{V}{L} y_{i,m} - \dfrac{\Delta}{L} X_{\Delta i}$ $\qquad$ **(I.4)**

Now letting $R_{\Delta} = \dfrac{L}{\Delta}$ we obtain

$x_{i,m+1} = \left(\dfrac{R_{\Delta}+1}{R_{\Delta}} \right) y_{i,m} - \left(\dfrac{1}{R_{\Delta}} \right) X_{\Delta i}$ $\qquad$ **(I.5)**

We can expand $x_{i,m+1}$ around m using a Taylor Series

$x_{i,m+1} = x_{i,m} + \left. \dfrac{dx_i}{dh} \right|_{h=m} (\Delta h) + \dfrac{1}{2} \left. \dfrac{d^2 x_i}{dh^2} \right|_{h=m} (\Delta h)^2 + \ldots$ $\qquad$ **(I.6)**

Where $\Delta h = (m+1) - m = 1.$

Substituting (I.6) into (I.5) we obtain,

$x_i + \dfrac{dx_i}{dh} + \dfrac{1}{2} \dfrac{d^2 x_i}{dh^2} + \ldots = \left(\dfrac{R_{\Delta}+1}{R_{\Delta}} \right) y_i - \left(\dfrac{1}{R_{\Delta}} \right) X_{\Delta i}$ $\qquad$ **(I.7)**

If we assume that only the first derivative is significant we can approximate (I.7) by,

$$x_i + \frac{dx_i}{dh} = \left(\frac{R_\Delta + 1}{R_\Delta}\right) y_i - \left(\frac{1}{R_\Delta}\right) X_{\Delta i} \tag{I.8}$$

Rearranging we obtain,

$$\begin{aligned}
\frac{dx_i}{dh} &= -x_i + \left(\frac{R_\Delta + 1}{R_\Delta}\right) y_i - \left(\frac{1}{R_\Delta}\right) X_{\Delta i} \\
&= -\left(\frac{R_\Delta + 1}{R_\Delta}\right) x_i + \left(\frac{1}{R_\Delta}\right) x_i + \left(\frac{R_\Delta + 1}{R_\Delta}\right) y_i - \left(\frac{1}{R_\Delta}\right) X_{\Delta i} \\
&= \left(\frac{R_\Delta + 1}{R_\Delta}\right) (y_i - x_i) + \left(\frac{1}{R_\Delta}\right) (x_i - X_{\Delta i})
\end{aligned} \tag{I.9}$$

This ordinary differential equation (I.9) is called the difference point equation (DPE) and can be solved with arbitrary boundary conditions; $x_i(h=1) = X_i^B$. It approximates the composition profile from the bottom of a column section upwards and becomes increasingly accurate as h→∞. At stationary/pinch points, where $\frac{dx_i}{dh} = 0$, the difference point equation (I.9) and the difference equation (I.1) are exactly equivalent. The difference point equation (I.9) approximation to the difference equation (I.1) is more accurate for difficult separations where the separation vector s is small (i.e. $s_i = x_i - y_i$ is small). It is exactly equivalent to (I.1) if solved using Euler integration with unit step size.

To obtain the composition profile from the top of a column section downwards we simply have to reverse the direction of integration. The ODE describing this compositional change down the column section is seen in (I.10) below.

$$\frac{dx_i}{dn} = \left(\frac{R_\Delta + 1}{R_\Delta}\right) (x_i - y_i) + \left(\frac{1}{R_\Delta}\right) (X_{\Delta i} - x_i) \tag{I.10}$$

Where $X_{\Delta i} = \dfrac{VY_i^B - LX_i^B}{\Delta} = \dfrac{VY_i^T - LX_i^T}{\Delta}$ **(I.11)**

In this case increasing values of n denote stages further down from the stage at which the boundary/initial value is chosen. In general the form of the difference point equation seen in (I.10) will be used and the stage count will be performed down a column section.

Appendix J: *Discussion: The Thermodynamic and Mathematical Consistency of Solutions Generated for Negative Compositions*

Are solutions generated using the difference point equation and various thermodynamic models consistent or even valid at all, in negative composition space? This issue can be addressed by separating the concepts of mathematical and thermodynamic consistency. For physical relevance and accuracy we, clearly, require the models we use to be thermodynamically consistent. This allows us confidence in the prediction of realistic vapour-liquid-equilibrium. Negative compositions are clearly physically impossible and unrealistic and thermodynamic models will, of course, be thermodynamically inconsistent when handling these compositions.

The question, then, is why should we bother tracking solutions outside the mass balance triangle (MBT)? The answer to this question is that they give additional mathematical/topological information about the system. If the models are mathematically consistent, the topology will be consistent. By consistent, we mean that the D.E is still differentiable over the composition range considered, trajectories are continuous across the MBT, they do not cross one another, and they originate at unstable nodes or infinity and terminate at stable nodes or infinity. If models are consistent close to the MBT and predict topological features (for a particular system) that behave in the same or similar ways upon variation of parameters, the process of tracking negative composition space solutions can be thought of as useful – from a practical perspective.

As an example of this practical usefulness, consider the case where a stable node is predicted outside the MBT for mathematically consistent models and this node moves into the MBT at some value of a varied parameter. The fore knowledge of the existence of the node gives us valuable information about the potential for a stable node in positive composition space. If we only plot the physically relevant solution we have no information about a) the rates of trajectories close to the

boundary of the MBT and b) the potential for a singularity upon small variations of the aforementioned parameter. This situation would be severely restricting.

The theoretical validity of solutions in negative composition space is clear; these solutions are theoretically invalid. However, recent work by Modise et al has confirmed the practical merits of generating these solutions. Modise et al (2005) generated column profile maps experimentally. Using mathematically consistent models, Modise et al (2005) were able to show that the qualitative form of topology (for the systems under investigation) was retained when comparing mathematically generated residue curve maps and experimentally generated column profile maps. In short, topology "predicted" in negative composition space was "transformed" and shifted into the MBT retaining topological features such as nodes and distillation boundaries. The experimentally generated column profile map also corresponded very well to the mathematically generated CPM.

This will not be true of all models or, indeed, all composition ranges and it is clear that not all models will be mathematically consistent or even defined in negative composition space. The Wilson liquid activity coefficient model, for instance, contains logarithms that are undefined for negative compositions and even the simplest models are not consistent for all compositional values; discontinuities can be produced.

In general, the topological predictions of the various models, throughout composition space, could be quite different. Even the number of nodes predicted could be different. However, in essence, all we require is mathematical/topological consistency close to the boundaries of the MBT. If this is satisfied our understanding of the system and potential changes to the topological structure, when parameters are varied, is increased and is therefore extremely useful.

References

Abdul Mutalib, M. I. and Smith, R., Operation and Control of Dividing Wall Distillation Columns Part1: Degrees of Freedom and Dynamic Simulation, *Trans IChemE*, 76, Part A, p308-318 (1998a).

Abdul Mutalib, M. I. and Smith, R., Operation and Control of Dividing Wall Distillation Columns Part2: Simulation and Pilot Plant Studies Using Temperature Control, *Trans IChemE*, 76, Part A, p319-334, (1998b).

Agrawal, R. and Fidkowski, Z.T., More Operable Arrangements of Fully Thermally Coupled Distillation Columns, *AIChE J*, 44(11), p2565-2568, (1998).

Akashah, S.A., Erbar, J.H., Maddox, R.N., *Chem. Eng. Commun.* 3, p461. (1979).

Amminudin, K. A.; Smith, R.; Thong, D. Y.-C. and Towler, G. P., Design and Optimization of Fully Thermally Coupled Distillation Columns, Part 1: Preliminary Design and Optimization Methodology, *Trans IChemE*, 76, Part A, p701-715, (2001).

Carlberg, N. A. and Westerberg, A. W. Temperature-Heat Diagrams for Complex Columns 3. Underwood's Method for the Petlyuk configuration, *Ind. Eng. Chem. Res.,* 28, p1386 (1989).

Castillo, F.J.L., Thong, D.Y.-C., & Towler, G.P., Homogeneous azeotropic distillation. 1. Design procedure for single-feed columns at non-total reflux. *Industrial and Engineering Chemistry Research,* 37(3), p987-997, (1998).

Christiansen, A. C. and Skogestad, S. Energy Savings in Complex Distillation Arrangements: Importance of Using the Preferred Separation. Paper 199d, *AIChE Meeting, Los Angeles* (1997).

Doherty, M.F., Perkins, J.D., On the Dynamics of Distillation Processes I. The Simple Distillation of Multicomponent Non-Reacting, Homogeneous Liquid Mixtures. *Chem. Eng. Sci.*, 33, p281-301, (1978a).

Doherty, M.F., Perkins, J.D., On the Dynamics of Distillation Processes II. The Simple Distillation of Model Solutions. *Chem. Eng. Sci.*, 33, p569-578, (1978b).

Doherty, M.F., Perkins, J.D., On the Dynamics of Distillation Processes III. The Topological Structure of Ternary Residue Curve Maps. *Chem. Eng. Sci.*, 34, p1401- 1414, (1979a).

Doukas, N. and Luyben W. L. Economics of Alternative Distillation Configurations for Separation of Ternary Mixtures*, Ind. Eng. Chem. Process Des. Dev.*, 17, 273 (1978).

Fenske, M.R., *Ind. Eng. Chem.,* 24, p482, (1932).

Fidkowski, Z. T.; Krolikowski, L. Minimum Energy Requirements of Thermally Coupled Distillation Systems. *AIChE J.*, 33, p643, (1987).

Finn, A. J., Rapid Assessment of Thermally Coupled Side-Columns. Gas Sep. Purif., 10(3), p169, (1996).

Fonyo, Z.; Szabo, J. and Foldes, P., Study of Thermally Coupled Distillation Columns, *Acta Chim*, 82, p235, (1974).

Franklin, N.L., Counterflow Cascades Part 1, *Chemical Engineering Research Design*, Vol. 64, p56-64, (1986).

Franklin, N.L., "The Theory of Countercurrent Cascades", *Chem. Eng. Res. Des.*, Vol. 66, (1988).

Glinos, K. A. and Malone, M. F., Optimality Regions for Complex Alternatives in Distillation Systems, *Chem. Eng. Res. Des.*, 66, p229, (1988).

Halvorsen, I. and Skogestad, S., Optimizing Control of Petlyuk Distillation: Understanding the Steady-State Behaviour, *Comp. Chem. Eng.*, 21, p249-254, (1997).

Halvorsen, I. and Skogestad, S., Optimal Operation of Petlyuk Distillation: Steady-State Behaviour, *J. Proc. Contr.,* 9, p407-424, (1999).

Halvorsen, I., Minimum Energy Requirements in Complex Distillation Arrangements, *PhD thesis,* (2001)

Hauan, S., Ciric, A., Westerberg, A.W., Lien, K.M., Difference Points in Extractive and Reactive Cascades I- Basic Properties and Analysis, *Submitted to Chem.Eng.Sci.*, (1998).

Hausen, H., Rektifikation idealer Dreistoff-Gemische. *Zeitschrift für angewandte Physik*, 4, p41-51, (1952).

Hendry, J. E.; Rudd, D. F. and Seader, J. D. Synthesis in the Design of Chemical Processes. *AIChE J.*, 19, 1 (1973).

Hengestebeck, R.J., "Distillation: Principles and Design Procedures" Reinheld, (1961).

Holland, S.T., Tapp M.; Hildebrandt, D., Glasser, D and Hausberger, B., Novel Separation System Design Using "Moving Triangles", *Comp. and Chem. Eng.,* 29, p181-189, (2004 a).

Holland, S.T., Tapp M.; Hildebrandt, D., Glasser, D and Hausberger, B., Column Profile Maps. 2. Derivation and Interpretation, *Ind. Eng. Chem. Res*., 43(14), p3590-3603, (2004 b).

Hoffmann, E.J., Azeotropic and Extractive distillation. *Wiley (Interscience)*, New York, (1964).

Kaibel, G., Distillation Column Arrangement with Low Energy Consumption, *IChemE Symposium Series*, no. 109, p43-59, (1988).

Kaibel, G. Innovation Award 1995: Split Wall for the Environment. Web page http://www.basf-ag.basf.de/basf/html/e/entwick/innov/trenn95.htm

Kirkbridge, C.G., Pet. Ref., 23, 87, (1944).

Kolbe, B. and Wenzel, S. Novel Distillation Concepts Using One-Shell Columns. *International Conference on Distillation and Absorption, Baden-Baden, Germany* September 30 – October 2, (2002).

Lestak, F.; Egenes, D. J.; Reay, D. Efficiency at Low Cost. AIChE Spring Meeting, Houstan, Texas; Paper 3c, (1999).

McCabe, W. L. and Thiele, E. W., Graphical Design of Fractionating Columns, *Ind. & Eng Chem*, 17, 6, p606-611, (1925).

Modise, T.S., Tapp M.; Hildebrandt, D. and Glasser, D, Can the Operating Leaves of a Distillation Column Really be Expanded?, *Ind. Eng. Chem. Res*., 44(19), p7511-7519, (2005).

Ognisty, T. P., Analyze Distillation Columns With Thermodynamics. *Chem. Eng. Prog.* pp 40-46, (1995).

Ostwald, W. Lehrbuch der Algemeinen Chemie. Verwandtschaftslehre. Erste Teil. *Verlag von Wilhelm Engelmann,* Leipzig, Germany, (1902).

Parkinson, G. Chementator. Chem. Eng. July, 21 and 22, (1998).

Petlyuk, F. B.; Platonov, V. M. and Slavinskii, D. M. Thermodynamically Optimal Method of Separating Multicomponent Mixtures, *Int. Chem. Eng*., 5 (3), p555, (1965).

Petlyuk, F.B., Danilov, R.Y., Theory of distillation trajectory bundles and its application to the optimal design of separation units: distillation trajectory bundles at infinite reflux, *Trans IChemE,* 79, PartA, p733-746, (2001).

Rische, E.A., Rektifikation idealer Dreistoffgemische unter der Voraussetzung, daβ der Widerstand des Stoffaustausches allein auf der Flüssigkeitsseite liegt. *Zeitschrift für angewandte Physik,* **7**, pp90-96, (1955).

Rudd, H., Thermal Coupling for Energy Efficiency, *Supplement to The Chem. Eng.*, S14, (1992).

Schreinemakers F.A.H., Einige Bemerkungen ueber Dampfdruecke Ternaerer Gemische. *Zeitschrift für Physikalische Chemie*, 43, p671-685, (1902).

Schultz, M. A.; Stewart, D. G.; Harris, J. M.; Rosenblum, S. P.; Shakur, M. S. and O'Brian, D. E. Reduce Costs with Dividing Wall Columns. *CEP Mag*. May (2002).

Serafimov, L.A., Separation Technology of Azeotropic Mixtures. Book: Azeotropy and Polyazeotropy, Section XXI. *Chemistry Publishing Co.,* Moscow, p 186-224, (1968a).

Serafimov, L.A., Theoretical Principles of Distillation Sequences Design and Synthesis for Nonideal Multicomponent Mixtures. *PhD Thesis. Lomonosov Institute of Fine Chemical Technology,* Moscow, (1968b).

Spadoni, G. and Stramigioli, C., Optimum Design of Thermally Coupled Distillation System, *3rd Int. Cong. Comp. and Chem. Eng, Paris,* p27-44, (1983).

Stichlmair, J., Distillation and rectification. *Ullmann's Encyclopaedia of Industrial Chemistry.* (5th ed.). Vol. B3, p4-1-4-94 VCH, Weinheim, (1987).

Stupin, W. J. and Lockhart, F. J. Thermally Coupled distillation - A Case History, *Chem. Eng. Prog.*, 68(10), p71, (1972).

Tapp, M., Holland, S.T., Hildebrandt, D., Glasser, D., Expanding the Operating Leaves in Distillation Column Sections by Distributed Feed Addition and Sidestream Withdrawal. *Accepted for publication in the proceedings of the PSE conference 2004,* Kumming, China, (2003).

Tapp, M., Holland, S.T., Hildebrandt, D., Glasser, D., Column Profile Maps. 1. Derivation and Interpretation, *Ind. Eng. Chem. Res.*, 43(2), p364-374, (2004).

Tedder, D. W. and Rudd, D. F., Parametric Studies in Industrial Distillation: Part 1. Design Comparisons, *AIChE J.*, 24, p303, (1978).

Triantafyllou, C. and Smith, R., The Design and Optimisation of Fully Thermally Coupled Distillation Columns, Trans. Inst Chem. Eng., 70, p118 (1992).

Underwood, A.J.V., Fractional Distillation of Multicomponent Mixtures. *Chem. Eng. Prog.,* 44(8), p603-614., 1948.

Van Dongen d.B., Dohery M.F., "Design and Synthesis of Homogeneous Azeotropic Distillations. 1. Problem Formulation for a Single Column." *Ind. Eng. Chem. Fundam.* 24, p454, (1985).

Vogelpohl A., "On the Relation between Ideal and Real Systems in Ternary Distillation." *TransIChemE.* 77, p487, (1999).

Widago, S., & Seider, W.D., Azeotropic distillation. *A.I.Ch.E. Journal,* 42(1), p96-130, (1996).

Wahnschafft O.M., Koehler J.W., Blass E., Westerberg A.W., The Product Composition Region of Single-Feed azeotropic distillation columns. *Industrial and Engineering Chemistry Research,* 31, p2345-2362, (1992).

Westerberg, A. W., The Synthesis of Distillation Based Separation Systems, *Comp. Chem. Eng*. 9(5), p421, (1985).

Westerberg , A. W. and Wahnschafft , O. Synthesis of Distillation Based Separation Systems, *Advances Chem. Eng. J. L. Anderson, ed.,* 23, p63-170 (1996).

Wolff, E. A. and Skogestad, S. Operation of Integrated Three-Product (Petlyuk) Distillation Columns, *Ind. Eng. Chem. Res*., 34, p2094, (1995)

Wright, R. O. Fractionation Apparatus. U.S. Patent 2471134, (1949).

Yoemanns, H., Grossmann, I.E., "A disjunctive programming method for the integration of heat integrated distillation sequences." *AIChE Annual Meeting, Miami.*, (1998b).

Zharov, V.T., Free Evaporation of Homogeneous Multicomponent Solutions. *Russ. J. Phys. Chem.* 41(11), p1539-1543, (1967).

Zharov, V.T., Phase Transformations (Distillation Lines) and Rectification of Multicomponent Solutions. *Russ. J. Appl. Chem.* 41(12), p2530-2536, (1968c).